DISSERTATION

THE SEDIMENT YIELD OF SOUTH KOREAN RIVERS

Submitted by

Chun-Yao Yang

Department of Civil and Environmental Engineering

In partial fulfillment of the requirements

For the Degree of Doctor of Philosophy

Colorado State University

Fort Collins, Colorado

Spring 2019

Doctoral Committee:

Advisor: Pierre Y. Julien

Robert Ettema
Peter Nelson
Sara L. Rathburn

ABSTRACT

THE SEDIMENT YIELD OF SOUTH KOREAN RIVERS

South Korea is experiencing increasing river sedimentation problems, which requires a reliable method to predict the sediment yield. With the recent field measurements at 35 gaging stations in South Korea provided by K-water, we quantified the sediment yield by using the flow duration curve and sediment rating curve. The current sediment yield models have large discrepancies between the predictions and measurements. The goal of this dissertation is to provide better understanding to the following questions: (1) How much of the total sediment load can be measured by the depth-integrated samplers? (2) Can we predict the sediment yield based only on watershed area? (3) Is there a parametric approach to estimate the mean annual sediment yield based on the flow duration curve and sediment rating curve?

With 1,962 sediment discharge measurements from the US D-74 sampler, the total sediment discharge is calculated by both the Modified Einstein Procedure (MEP) and the Series Expansion of the Modified Einstein Procedure (SEMEP). It is concluded that the SEMEP is more accurate because MEP occasionally computes suspended loads larger than total loads. In addition, SEMEP was able to calculate all samples while MEP could only compute 1,808 samples.

According to SEMEP, the ratio Q_m/Q_t of measured sediment discharge Q_m to total sediment discharge Q_t is a function of the Rouse number Ro, flow depth h, and the median grain size of the bed material d_{50}. In Korean sand and gravel bed rivers, the materials in suspension are fine (silt or clay) and Ro ≈ 0. The ratio Q_m/Q_t reduces to a function of flow depth h, and at least 90% of the total sediment load is measured when $h > 1$ m. More than 80% of the sediment load is measured when the discharge Q is larger than four times mean annual discharge $\bar{Q}$ ($Q/\bar{Q} > 4$).

The ratio Q_s/Q_t of suspended sediment discharge Q_s to total sediment discharge can be also analyzed with SEMEP and the result shows that Q_s/Q_t is a function of h/d_{50} and Ro. When Ro

≈ 0, the ratio Q_s/Q_t increases with h/d_{50}. The suspended load is more than 80% of the total sediment load when $h/d_{50} > 18$.

The relationship between specific sediment yield, SSY, and watershed area, A, is $SSY = 300A^{-0.24}$ with an average error of 75%. Besides the specific sediment yield, the mean annual discharge, the normalized flow duration curve, the sediment rating curve, the normalized cumulative distribution curve, and the half yield discharge vary with watershed area. From the normalized flow duration curve at an exceedance probability of 0.1%, small watersheds ($A < 500$ km^2) have $42 < Q/\bar{Q} < 63$, compared to large watersheds ($A > 5000$ km^2) which have $14 < Q/\bar{Q} < 33$. In terms of sediment rating curves, at a given discharge, the sediment load of small watersheds is one order of magnitude higher than for large watersheds. From the normalized cumulative distribution curves, the half yield (50% of the sediment transported) occurs when the discharge is at least 15 times the mean discharge. In comparison, the half yield for large watersheds corresponds to $Q/\bar{Q} < 15$.

The flow duration curve can be parameterized with $\hat{a}$ and $\hat{b}$ by using a double logarithmic fit to the flow duration curve. This parametric approach is tested with 35 Korean watersheds and 716 US watersheds. The value of $\hat{a}$ generally increases with watershed area. The values of $\hat{b}$ are consistently between 0.5 and 2.5 east of the Mississippi River and the Pacific Northwest. Large variability in $\hat{b}$ is found in the High Plains and in Southern California, which is attributed to the high flashiness index in these regions. A four-parameter model is defined when combining with the sediment rating curve. The four parameters are: $\hat{a}$ and $\hat{b}$ for the flow duration curve, and $\bar{a}$ and $\bar{b}$ for the sediment rating curve. The mean annual discharge $\bar{Q}_s$ is calculated by $\bar{Q}_s = \bar{a}\hat{a}^{\bar{b}}\Gamma(1+\hat{b}\bar{b})$. The model results are compared to the flow-duration/sediment-rating curve method. The average error of this four-parameter model is only 8.6%. The parameters can also be used to calculate the cumulative distribution curves for discharge and sediment load.

ACKNOWLEDGEMENTS

I would like to thank everyone who helped me both directly and indirectly with my dissertation. The support that I've received in both a scholarly sense and in my personal life has greatly helped me in my pursuit a PhD degree at Colorado State University.

I thank Dr. Pierre Julien for being an amazing advisor. You are always inspiring, encouraging, and patient. I learned A LOT from you. Thanks also to my committee members, Drs. Rob Ettema, Sara Rathburn, and Peter Nelson for their positive and helpful comments. I'd also like to give special thanks to Nick Grieco and Larry Thayer for their friendships and the helps on editing my dissertation.

Thanks to my coworkers from Dr. Julien's Dream team: Marcos Palu, Neil Andika, Weimin Li, Dr. Jai Hong Lee. Thanks to Woochul Kang for working with me on the Korean project. Thanks to Kristin LaForge and Sydney Doidge for working with me on the Middle Rio Grande project. It has been a pleasure working with all of you. I am grateful for the discussions in Friday seminars. They helped me improve my thinking and direct my thoughts.

A special thanks to Haw Yen for suggesting that I study at CSU. I also appreciate the friends I've met during my study at CSU: Irene Hsu, Alice Lin, Da-Wei Lu, Noriaki Hosoya, Yejian Huang, Yishu Zhang, Yangyang Wu, Dustin Lance, Sam Shih, Alan Li, Jordan Deshon, Ryan Rykhus, and Noah Gustavson. Life is much more joyful with your friendships and companionship. Thanks to Jen and Brian in Berkeley for their hospitality when I just arrived the US and taking me to explore the Sierra Nevada mountains. Shout out to Ching-Yu Wang and Randy Babcock. They are doing an amazing job helping international students like me adjusting to our new lives in the US.

Thanks to Dr. Mazdak Arabi, K-water, and US Bureau of Reclamation for providing the funding over the past four years. Thanks to the kind donors of the following scholarships: Whitney Borland Advanced Student Graduate Scholarship, Tipton-Kalmbach/Stantec Fellow, and Jeng Song Wang Memorial Scholarship.

I am also grateful to my friends and family in Taiwan. Thanks to Samuel Huang for visiting. Thanks to Jin Hsueh, Hung-ta Chien, Esther Chang and Ian Lin for checking on me every once in a while. Last, thanks to my dad and mom for their unconditional love and support.

TABLE OF CONTENTS

LIST OF TABLES

LIST OF FIGURES

Chapter 1

Introduction

1.1 Problem Statement

Sediment yield is the amount of sediment passing a watershed outlet in a certain time period. Estimates of sediment yield are essential in the design of hydraulic engineering and the management of water resources. Sediment yield is measured by continuous measurements of stream discharge and sediment concentration. With the flow and sediment records, sediment yield can be estimated by combining flow duration curve and sediment rating curve (Piest 1964; Strand and Pemberton 1982; Julien 2010). The factors influencing sediment yield can be categorized into seven groups: topography, climate, soil and lithology, hydrology, vegetation cover or land use, drainage network, and catchment morphology (de Vente et al. 2011). Based on the river data from 280 watersheds, Milliman and Syvitski (1992) found that those small mountainous watersheds in Asia tend to have largest sediment yield because of flashy floods and active tectonic activities.

The recent river measurements in South Korea provide us an unique opportunity to study the sediment yield in this region. South Korea located in the northeastern Asia margin and has frequent earthquake activities (Jin and Park 2007). In addition, more than three typhoons affect Korea every year on average (Jeong et al. 2007). The typhoons bring in heavy rainfall. The soil erosion in South Korea is mainly associated with the intense rainfall during typhoons (Kim et al. 2006; Lee and Heo 2011). Large scale erosion such as landslide can cause critical flood damage. The sedimentation followed by the erosion often have negative consequences too. For example, sedimentation in the reservoirs can impair their performance on flood control and water storage (Figure 1.1). The need for estimating sediment yield is becoming more important due to climate change and the recent change by the Four River Restoration Project (FRRP). The fluvial sediment monitoring in South Korea started in the 1990s. The monitoring program provides information on river stage and the concentration of suspended sediment.

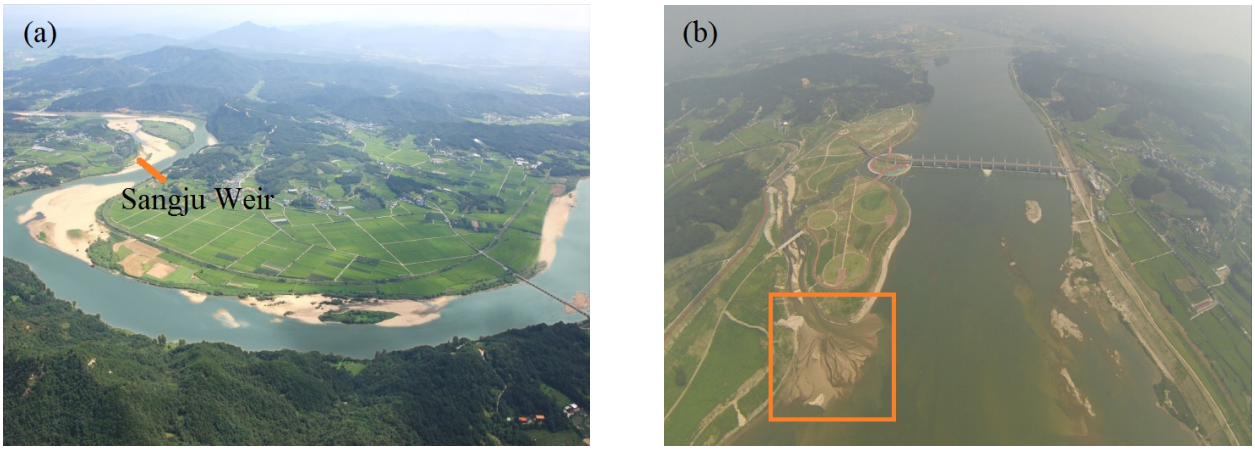

Figure 1.1: Examples of reservoir sedimentation; (a) sedimentation at Sangju Weir in Nakdong River; (b) sedimentation at Yeoju Weir in Han River (photos from Kim (2016))

To provide a comprehensive study the sediment yield in South Korea based on the river measurements, firstly, we need to figure out how much sediment is transported as bedload. The measurement of bedload is still facing numerous challenges (Morris and Fan 2009; Wohl et al. 2015). Bedload is generally estimated to be 10% to 20% of the total sediment load (Turowski et al. 2010). The ratio may be higher in small, mountainous streams (Laronne et al. 1993; Turowski et al. 2010; Ziegler et al. 2014). For example, Hayward (1980) found that up to 90% of sediment is transported in bedload in Torlesse stream. In South Korea, suspended sediment load is measured by the depth-integrating sampler US DH-48, US DH-74, or the point-integrating sampler US P-63. Methods to estimate the total sediment load have been developed (Colby et al. 1955; Toffaleti 1969; Holmquist-Johnson et al. 2009; Shah-Fairbank 2009). The case of Torlesse watershed shows the ratio of bedload can vary a lot in different watersheds. The bedload in South Korea is typically computed by the Modified Einstein Procedure. However, Julien et al. (2017) found that the calculation of sediment varies up to 80% by using different approaches to calculate the total sediment load from measured load. Therefore, a reliable method to estimate the total sediment load from the measurement would be necessary. In addition, the quantification of the ratio of measured to total sediment load, as well as the ratio of suspended to total sediment load would be helpful for the long term sediment management.

Secondly, a dependable equation with easily available parameters to evaluate the sediment yield can be helpful. Julien et al. (2017) tested the existing regression equations for the prediction of sediment yield in South Korea and found existing methods to be highly variable. The existing models includes the Korean Institute of Construction Technology (KICT) model and Yoon (2011). KICT (2005) proposed the sediment yield for watersheds range from 200 to 2,000 km^2 to be estimated as

$$SSY = 972 D^{1.039} d_s^{-0.825} \tag{1.1}$$

where SSY is the specific sediment yield in tons/km^2·year, D is the watershed density in km/km^2, and d_s is the bed material size in millimeter. The results show that changes in d_{50} might change the prediction of sediment yield by more than one order of magnitude (Figure 1.2a).

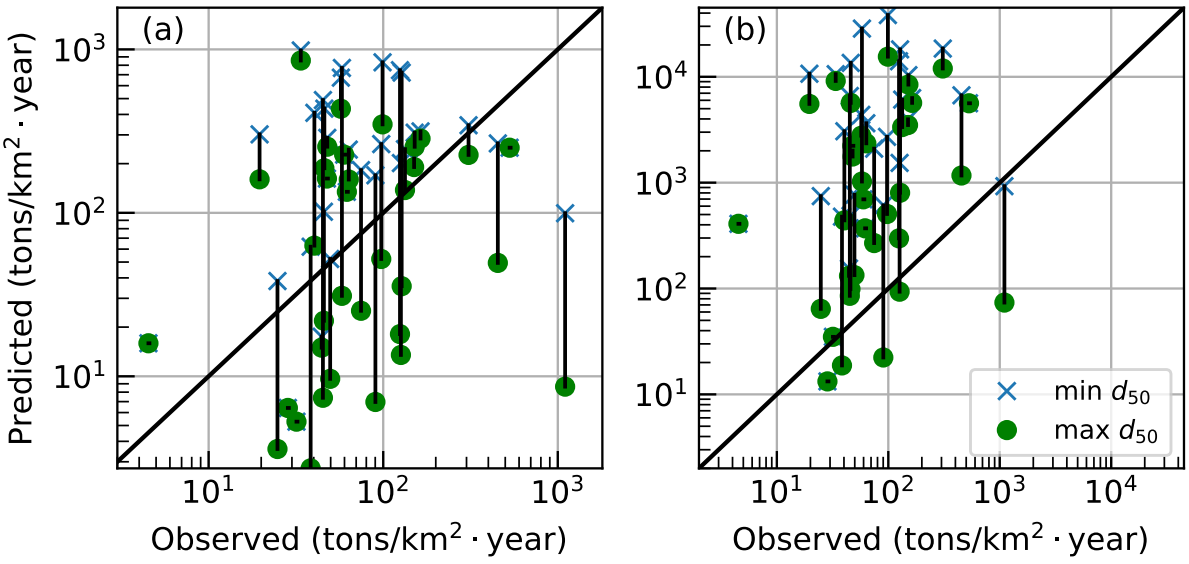

Figure 1.2: Testing of KICT model. Observed sediment yield is calculated from the total sediment load by the Modified Einstein Procedure

Yoon (2011) analyzed the measurements from reservoir surveys and suggested that the sediment yield be estimated by:

$$SSY = 4395 A^{0.464} S^{-2.0} d_s^{-0.855} \tag{1.2}$$

where SSY is the specific sediment yield in $m^3/km^2 \cdot$year, A is the watershed area in km^2, S is the river bed slope (%), and d_s is the bed material size d_{50} in mm. The results also show large variability due to inputted grain size. Furthermore, the Yoon's model tends to overpredict SSY (Figure 1.2b). The root mean squared error (RMSE) is 320 tons/$km^2 \cdot$year and 7500 tons/$km^2 \cdot$year for the KICT model and the Yoon's model, respectively. The mean absolute percentage error (MAPE) is 300% and 6500% for the KICT model and the Yoon's model. Since the current models produce huge prediction errors, I would like to develop a method with better accuracy.

Many studies have showed that the specific sediment yield (sediment yield per unit area) decreases as the drainage area increases (Gurnell et al. 1996; Higgitt and Lu 1996; Milliman and Syvitski 1992; Kane and Julien 2007; Vanmaercke et al. 2014). Milliman and Syvitski (1992) demonstrated the inverse relationship between specific sediment yield and drainage area with 280 watersheds around the world (Figure 1.3). On the other hand, the watershed area has been shown can be used as a predictor of flow or sediment variables such as annual discharge, mean annual sediment yield (e.g. Goodrich et al. 1997; Verstraeten and Poesen 2001; Syvitski et al. 2003; Galster 2007). Therefore, I would like to investigate the water discharge and sediment variables and relate them to watershed area.

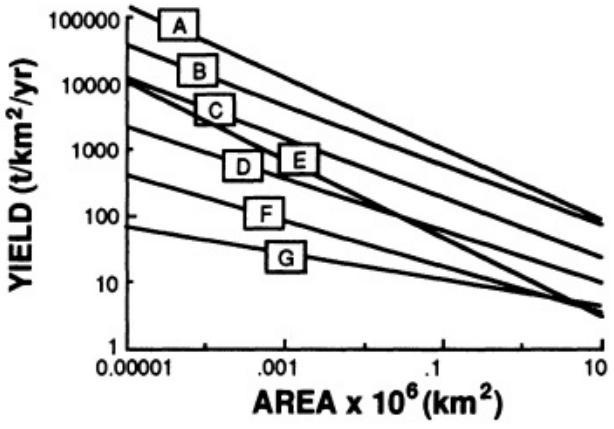

Figure 1.3: Regression models of specific sediment yield and basin area for seven topographic categories: A: high mountain (headwaters at elevations $>$ 3000 m), B: south Asia/Oceania (1000-3000 m), C: N/S America, Africa, and Alpine Europe (1000-3000 m), D: non-alpine Europe and high Arctic (1000-3000 m), E: upland (500-1000 m), F: lowland (100-500 m), and G: coastal plain ($<$ 100 m) from Milliman and Syvitski (1992)

Thirdly, the traditional method to calculate the sediment yield is to use the flow-duration, sediment rating curve method. The method uses a table to divide the flow duration curve into several slices. The median discharge of each slice is identified and the corresponding sediment discharge is calculated by the sediment rating curve. The method requires long-term flow discharge and sediment records. Is it possible to develop a method based on a few parameters describing the flow discharge and sediment rating curve to circumvent this empirical table approach?

1.2 Research Objectives

The overall research purpose is to quantify the magnitude and frequency of total sediment discharge in Korean Rivers. The specific research objectives are:

1. to estimate the total sediment load from the measured sediment load. In addition, the ratio of the measured to total sediment load and the ratio of the suspended to total sediment load will be examined.

2. to investigate the cumulative distribution functions of water and sediment yield, and define the water and sediment relationships with watershed area.

3. to develop and test a procedure to determine sediment load based on the parametric description of flow duration and sediment rating curves.

The dissertation consists of seven chapters. An introduction is provided in Chapter 1. Chapter 2 presents the literature review for methods of sediment measurement, estimate of total sediment load from measured load, and prediction for sediment yield. The background of the study site and available data are presented in Chapter 3. Chapter 4 details the calculation examples for total sediment load from measured load. Chapter 5 presents the flow duration curves, sediment rating curves, cumulative distribution curve of sediment discharge in South Korea. In Chapter 6, a new procedure to parameterize flow duration curve is proposed. Extensive application with examples in the USA is present in Chapter 7. Chapter 8 closes the dissertation with a summary, conclusions from the analysis.

Chapter 2

Literature Review

The determination of sediment yield relies on the continuous flow and sediment discharge measurements. This chapter provides a review of the techniques to determine sediment yield from the river measurements. The specific topics include: 1) the whole picture of how the sediment yield is computed based on river measurement; 2) the potential development of new technique for sediment yield calculation; and 3) summary of the existing sediment yield studies in South Korea. Section 2.1 provides information of total sediment load and Section 2.2 provides the techniques of computing total sediment discharge from measurement. Section 2.3 presents sediment rating curves to link sediment discharge with flow discharge. The methods to calculate long-term sediment yield are described in Section 2.4. Section 2.5 reviews the theory of transform method that can be used to develop a new method for sediment yield calculation. Section 2.6 summarizes existing sediment yield studies of South Korea.

2.1 Total Sediment Load

Julien (2010) showed that the total sediment load L_t in a river can be classified in three ways as shown in Figure 2.1:

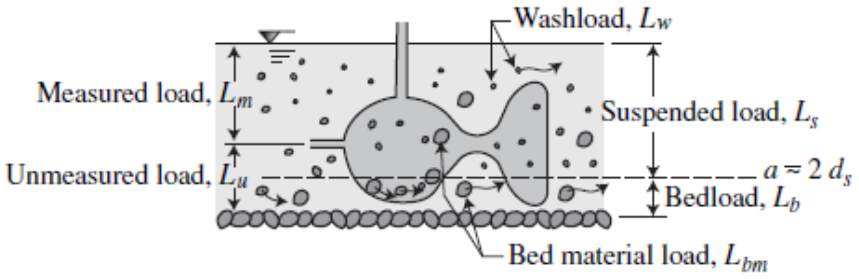

Figure 2.1: Sketch of ways to determine the total load (Julien 2010)

1. By the type of movement. The total sediment load consists of the bedload L_b and suspended load L_s. Bedload refers to the quantity of sediment that is moving in the bed layer, and suspended load refers to the sediment particles held in suspension.

$$L_t = L_b + L_s \tag{2.1}$$

Considering an experiment in a flume with sediment particles on the bed, as the flow discharge increases, the movement of sediment proceeds through the following stages. At the beginning, the velocity is small and all particles are static. As the flow increases, some of the particles on the bed surface slide, roll, or move in saltation. Following a further increase in discharge, some particles may be held in suspension by turbulent eddies. Figure 2.2 illustrates the patterns of sediment movement as discharge increases.

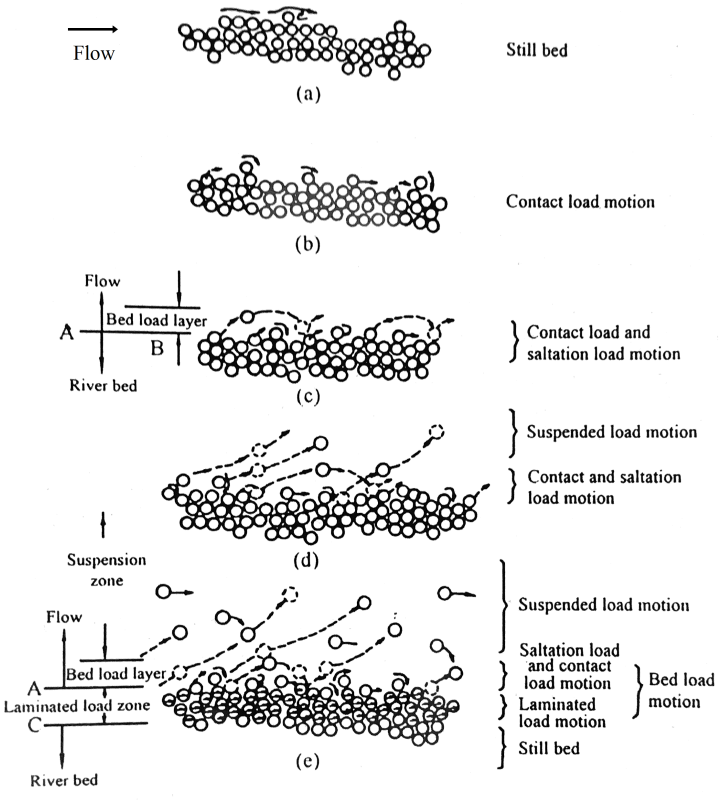

Figure 2.2: Patterns of sediment motion (Chien and Wan 1999)

By studying the data from European rivers, Kresser (1964) proposed a criterion, $\bar{u}^2/gD = 360$, to distinguish bed load and suspended load, where $\bar{u}$ is the mean flow velocity and D is the cutoff grain diameter between suspended load and bed load. However, the applications by Komar (1980) on Mississippi River and other regions showed that this equation tends to overpredict D.

2. By the method of measurement. The total sediment load is comprised of the measured load L_m and unmeasured load L_u. The point sampler or depth integrating sampler can only measure from the water surface to approximately 10 centimeters (4.1 inches) above the bed, so the measured sediment load is only part of the suspended load. The unmeasured sediment load consists of the entire bedload plus the fraction of the suspended load transported below the lowest sampling elevation.

$$L_t = L_m + L_u \tag{2.2}$$

3. By the source of sediment. In this case, total sediment load is made up of the washload load L_w and bed material load L_{bm}. Washload is the fine sediment fraction coming from upland watershed, and the coarser grain sizes from the channel bed of the upstream reach is the bed material load (Chien and Wan 1999). The 10^{th} percentile of the bed material (d_{10}) is commonly used to distinguish washload and bed material load.

$$L_t = L_w + L_{bm} \tag{2.3}$$

2.1.1 Measurement of Suspended Load

Theoretically, the unit suspended sediment discharge q_s past a river cross-section is

$$q_s = \int_0^h C(z)v_s(z)\mathrm{d}z \tag{2.4}$$

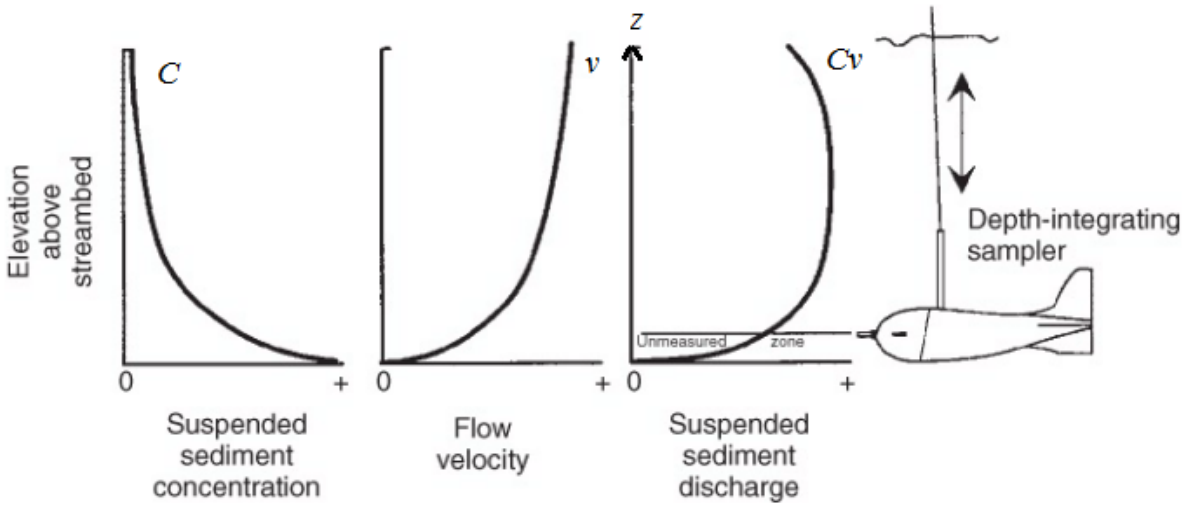

Figure 2.3: Vertical profiles of suspended sediment concentration C, flow velocity v and sediment discharge $C \cdot v$. If a depth-integrating sampler traverses at a constant rate, the samples collected are velocity-depth integrated. Only the zone lower than the nozzle is not sampled (Hicks and Gomez 2016).

where C and v_s are the concentration and downstream velocity of the suspended sediment, respectively, and C and v_s vary with the distance to bed z. Practically, v_s is assumed to be equal to the streamwise flow velocity v, i.e., $v_s = v$ (Hicks and Gomez 2016). With this assumption, equation (2.5) can be rewritten as follows:

$$q_s = \int_0^h C(z)v(z)\mathrm{d}z \tag{2.5}$$

In practice, the integral can be determined by two types of samplers, known as integrating samplers. The first is a depth-integrating sampler. It continuously collects water and sediment when the sampler traverses from the surface to the bed and back again (Figure 2.3). If the sampler traverses at a constant rate, the concentration measured is the averaged concentration of the vertical depth.

The second type is a point sampler. It is used to determine the mean sediment concentration at any given depth. It can also be used to collect samples over an increment of depth. This is useful when a stream is too deep for a depth-integrating sampler (Simons and Sentürk 1992). A list of depth-integrating samplers and point samplers can be found on USGS website (https://water.usgs.gov/fisp/catalog_index.html). Figure 2.4 provides a flowchart for the selection of a suspended sediment sampler.

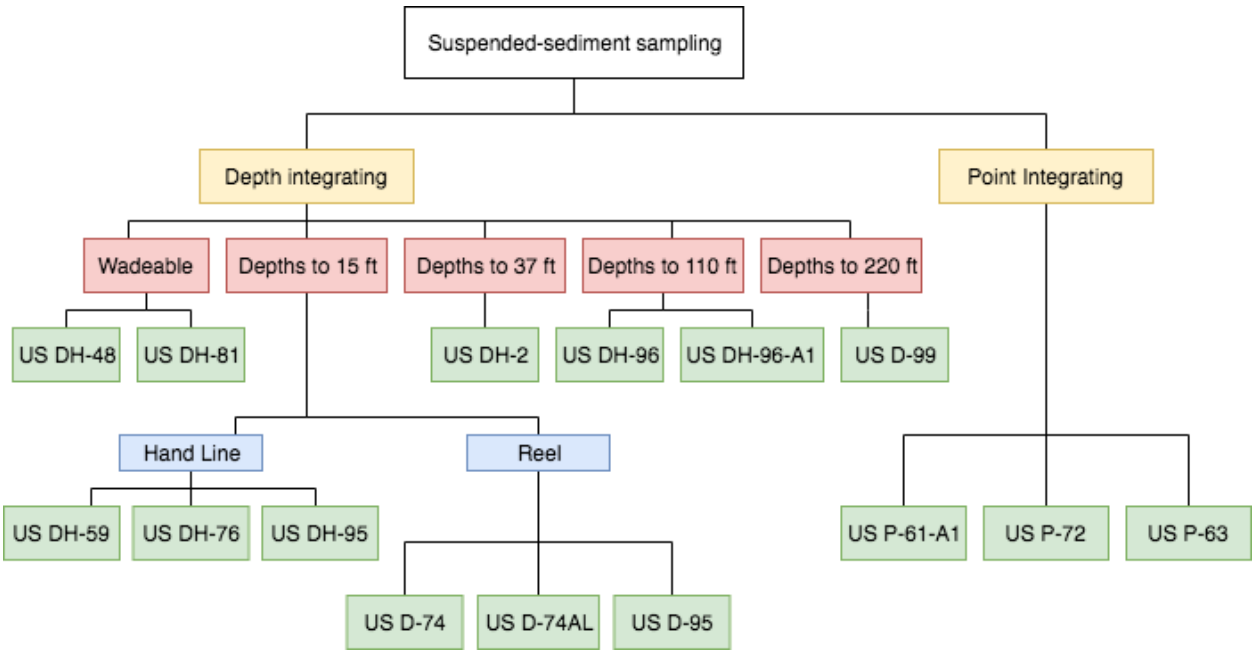

Figure 2.4: Selection of a suspended sediment sampler (from Davis 2005)

For both samplers, the zones that are lower than the nozzle of sampler can not be measured. The measured suspended sediment discharge q_m is calculated as

$$q_m = \int_{d_n}^{h} Cv\mathrm{d}z \tag{2.6}$$

where d_n is the height of the nozzle or the unmeasured depth.

2.1.2 Measurement of Bedload

In sand-bed rivers, direct measurement of bedload with bedload samplers can be problematic because the flow and bedload transport are disturbed when a sampler is placed on the bed. The flow disturbance in sand-bed rivers can cause further worsening of entrainment of sediment (Holmes Jr 2010). Indirect measurements of bedload such as bedform velocimetry are commonly used because bedload transport corresponds largely to the movement of bedform. But in general, bedload is small compared to suspended load (Julien 2010).

In gravel- and cobble-bed streams, common approaches for bedload sampling include various traps, tracers, and samplers. An example of bedload sampler is Helley-Smith (Figure 2.5) (Helley

and Smith ; Emmett 1979). It is a type of pressure-difference sampler. There are various sizes of the sampler in terms of its opening, body, and mesh size of sampler bag. The choice of the size depends upon the bed material being sampled.

Another type of bed sampler is the bedload trap (Bunte et al. 2004; Bunte et al. 2007). A bedload trap consists of an aluminum frame and a nylon net (Figure 2.6). A bedload trap collects all the sediment that enter into it until it is full. The advantage of bedload traps is that they collect a wider range of particle sizes or transport rate compared to the Helley-Smith samplers.

There are still several technical difficulties with bedload measurements that need to be overcome, such as samplers that can be used under a variability of flow conditions and bed topography, and reduces the interference to flow due to the sampler (Garcia et al. 2000). Examples of recent development of bedload techniques can be found in Møen et al. 2010, Rickenmann et al. 2014, Kociuba 2016, Rickenmann 2017, and etc.

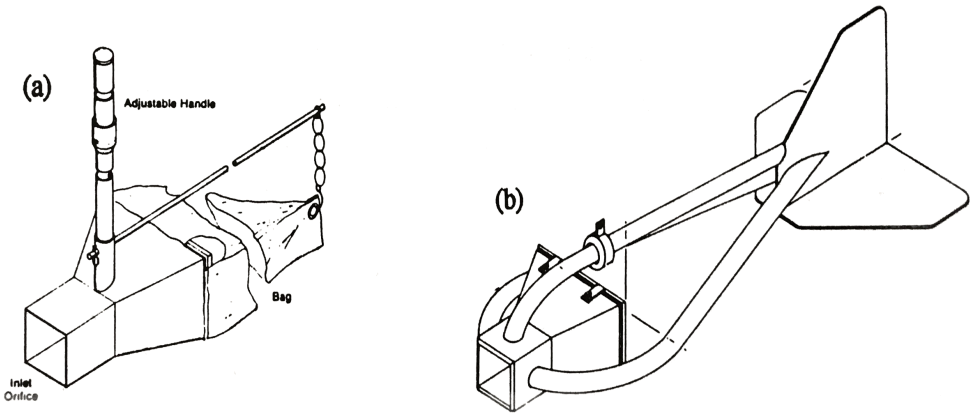

Figure 2.5: Helley-Smith samplers, (a) hand held and (b) cable suspended (from Simons and Sentürk 1992)

2.2 Estimating Total Load from Measurements

The methods to estimate the total sediment load from measured sediment load including empirical approaches, Toffaleti (1969) Method, Einstein method, Modified Einstein Procedure (MEP), Bureau of Reclamation Automated Modified Einstein Procedure (BORAMEP), Series Expansion

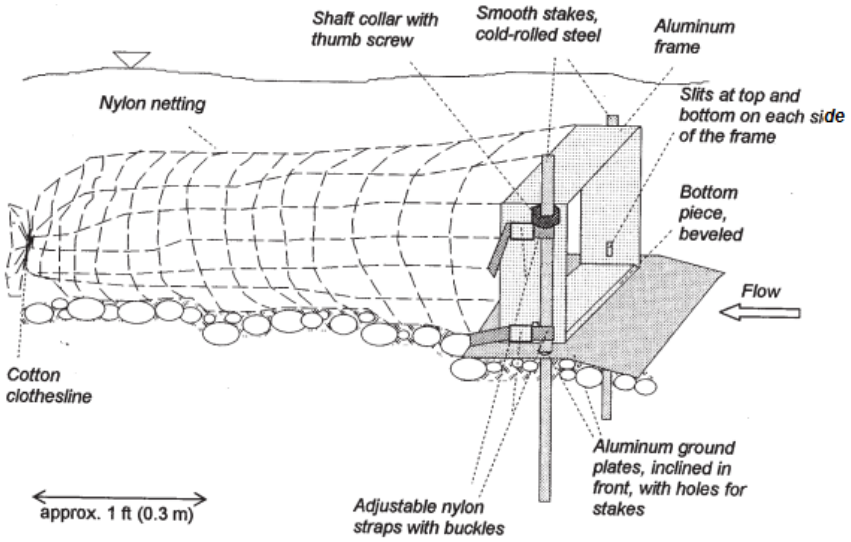

Figure 2.6: A bedload trap and its parts (from Bunte et al. 2007)

of the Modified Einstein Procedure (SEMEP), and Series Expansion of the Modified Einstein Point Procedure (SEMEPP). The Toffaleti (1969) Method and the SEMEPP are not the focus of this research and are not present in this section, but their descriptions and procedures can be found in the Appendix A.

2.2.1 Empirical Approaches

Based on reservoir survey data, U. S. Bureau of Reclamation devised a table for evaluating the unmeasured load (Lane and Borland 1951; Strand and Pemberton 1982). Turowski et al. (2010) compiled the sediment load measured by Williams and Rosgen (1989) and compared the result to Maddock and Borland (1950) and Lane and Borland (1951). The classification of suspended sediment concentration is based on Maddock and Borland (1950) and Lane and Borland (1951). The field measurement compares well with the sand-bed streams except for the high concentration, but large scatter is found in gravel-bed streams. Figure 2.7 shows the fraction of bedload versus suspended sediment concentration and suspended sediment discharge. Although there is a huge scatter, the bedload fraction generally decreases as the suspended sediment concentration/discharge increases. The fraction of bedload becomes less than 20% when the concentration is higher than 1,000 mg/l (suspended load 1,000 kg/s). Turowski et al. (2010) highlighted that the average bed-

load fraction for sand-bed and gravel-bed streams are alike when the suspended discharge is above 10 kg/s. A possible explanation may be that "around transport rates of 10 kg/s, all grain sizes are mobilized and the particle size distribution of the transported load approaches the size distribution on the bed".

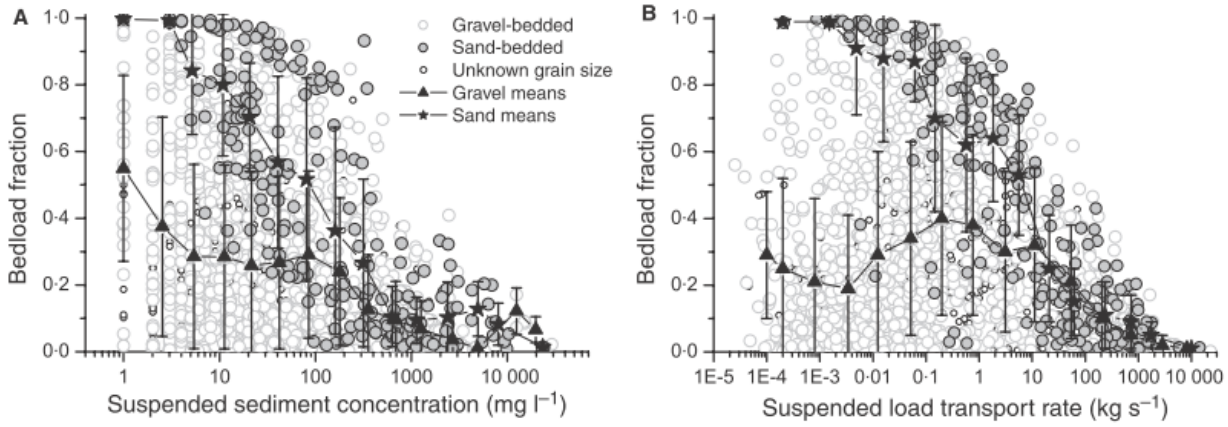

Figure 2.7: (A) Bedload fraction vs suspended sediment concentration; and (B) bedload fraction vs suspended load (Turowski et al. 2010)

Table 2.1: Bedload fraction based on suspended sediment concentration (Turowski et al. 2010)

Suspended sediment concentration (ppm)	Gravel bed				Sand bed			
	Maddock and Borland (1950)	Lane and Borland (1951)	Data mean	Data SD	Maddock and Borland (1950)	Lane and Borland (1951)	Data mean	Data SD
<1000	0.05	0.05 to 0.11	0.26	0.27	< 0.5	0.2 to 0.6	0.51	0.33
1000 to 7500	0.05 to 0.1	0.05 to 0.11	0.055	0.085	0.1 to 0.2	0.09 to 0.26	0.1	0.089
>7500	0.02 to 0.08	0.02 to 0.07	0.088	0.054	0.1 to 0.2	0.05 to 0.13	0.035	0.032

2.2.2 Einstein's Approach

Einstein (1950) combined the theory of bed load motion and the diffusion theory of suspended load, and proposed a method to calculate the total sediment load. The total sediment discharge per unit width q_t can be calculated from the sum of the unit bed sediment discharge q_b and the unit suspended sediment discharge q_s:

$$q_t = q_b + q_s = q_b + \int_a^h Cvdz \tag{2.7}$$

where a is the bed layer of thickness $a = 2d_s$ and h is the water depth. As sketched in Figure 2.8, this approach estimates the suspended load from bedload.

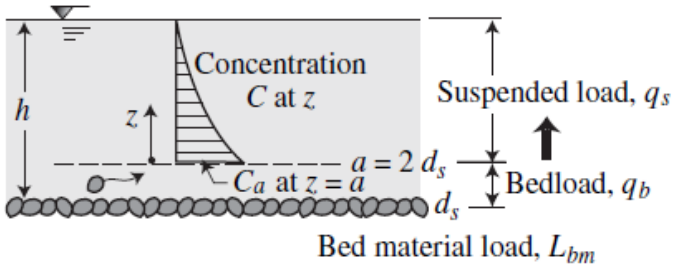

Figure 2.8: Sketch of the Einstein approach (Julien 2010)

The velocity profile for a hydraulically rough boundary, according to Keulegan (1938), can be calculated by following equations

$$\frac{v}{u_*} = \frac{1}{\kappa} \ln\left(\frac{z}{z_o}\right) \tag{2.8}$$

$$v = \frac{u_*}{\kappa} \ln\left(\frac{30z}{k_s'}\right) \tag{2.9}$$

where v is the velocity at a distance z above the river bed, u_* is the shear velocity, κ is the von Karman constant assumed equal to 0.4, and z_o is the vertical elevation where the velocity equals

to zero. By the pipe experiment on rough boundaries, the corresponding value of $z_o = k_s^{'}/30$, and the grain roughness height $k_s^{'}$ can be considered as d_s.

The sediment concentration profile is described by Rouse (1937). The relative concentration C/C_a

$$\frac{C}{C_a} = \left(\frac{h-z}{z}\frac{a}{h-a}\right)^{\frac{\omega}{\beta_s \kappa u_*}} \tag{2.10}$$

Figure 2.9 demonstrates suspended sediment concentration when $a/h = 0.05$.

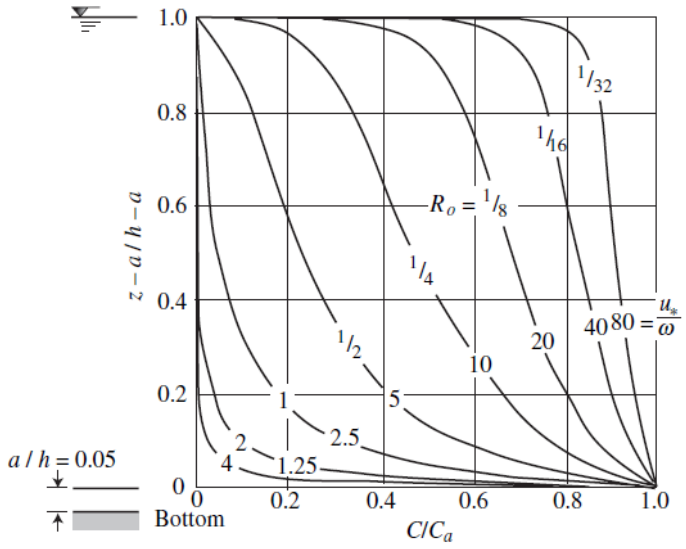

Figure 2.9: Relative concentration of suspended sediment with relative depth above the bed $z = 0.05h$ [from Julien (2010)]

By substituting C and v in Equation 2.7, it becomes

$$q_t = q_b + \int_a^h C_a \frac{u_*}{\kappa}\left(\frac{h-z}{z}\frac{a}{h-a}\right)^{\frac{\omega}{\beta_s \kappa u_*}} \ln\left(\frac{30z}{d_s}\right) dz \tag{2.11}$$

The reference concentration $C_a = q_b/av_a$ is calculated from the unit bed sediment discharge q_b transported in the bed layer of thickness $a = 2d_s$, given the velocity v_a at the top of the bed layer, $v_a = (u_*/\kappa)\ln(30a/d_s) = 4.09u_*/\kappa$, Einstein used $v_a = 11.6u_*$. Rewriting Equation 2.11 in dimensionless form with $z^* = z/h$, $E = 2d_s/h$ and $Ro = \omega/\beta_s\kappa u_*$ gives:

$$q_t = q_b \left[1 + I_1 \ln \frac{30h}{d_s} + I_2 \right] \tag{2.12}$$

where

$$I_1 = 0.216 \frac{E^{\text{Ro}-1}}{(1-E)^{\text{Ro}}} \underbrace{\int_E^1 \left[\frac{1-z^*}{z^*} \right]^{\text{Ro}} dz^*}_{J_1(\text{Ro})} \tag{2.13}$$

$$I_2 = 0.216 \frac{E^{\text{Ro}-1}}{(1-E)^{\text{Ro}}} \underbrace{\int_E^1 \left[\frac{1-z^*}{z^*} \right]^{\text{Ro}} \ln z^* dz^*}_{J_2(\text{Ro})} \tag{2.14}$$

In his paper, Einstein prepared nomographs to solve the two integrals I_1 and I_2.

2.2.3 Modified Einstein Procedure (MEP)

The Modified Einstein Procedure provides a tool to estimate the unmeasured load from measured load. It can be used for depth-integrated samples or point samples. Colby et al. (1955) reviewed several total load formulas including Einstein (1950), but none of the methods were consistent with the measurement from the sand-bed Niobrara River in Nebraska. Therefore, they developed a procedure based on the measured suspended load from depth-integrated samples. A particle size distribution was also collected for the bed from sieve analysis. The Rouse number (Ro) is determined by matching the total load determined based on the measured suspended sediment and the measured bed material. Ro is known for the given bin (particle size classes) when the total load matches and then Ro for the remaining bins can be determined by a power equation. With the Ro of each bin, the load for each bin can be determined too. The total load is the sum of them.

Several suggestions have been proposed over the years. Lara (1966) noticed that the approach for calculating Ro by Colby and Hembree was subjective and could lead to different answers based on the bin used. Lara proposed to use a least squares regression to determine Ro. An exponential relationship between Ro and settling velocity (ω) is determined by a minimum of two overlapping bins. Lara also found that the exponent is not always 0.7. Equation 2.15 is an example of the power

function.

$$\text{Ro} = C_1(\omega)^{C_2} \tag{2.15}$$

where C_1 and C_2 are constants determined from the regression analysis.

Burkham and Dawdy (1980) conducted a general study of the MEP in an attempt to develop a reliable method for measuring and computing sediment discharge. Their study led to three deviations from Colby et al. (1955). First, they determined a direct relationship between bed load transport and bed load intensity. Second, they used the roughness coefficient (k_s) as $5.5d_{65}$. Lastly, they showed that the calculated u_* tends to be higher and the Einstein correction factor tends to be lower than the values determined by Colby et al. (1955). Their approach is known as the Revised Modified Einstein Method.

Shen and Hung (1983) proposed two modifications of the MEP. First, Ro should be determined by the field data instead of the 0.7 power of the fall velocity. Second, they introduced an optimization procedure to minimize the difference between the measured loads and calculated suspended rates. Shen and Hung called their method Remodified Einstein Procedure.

2.2.4 Bureau of Reclamation Automated Modified Einstein Procedure (BORAMEP)

The BORAMEP was developed by Holmquist-Johnson at the Bureau of Reclamation. The development of BORAMEP provides a standardized procedure to compute the total sediment discharge based on MEP. The software and user manual are available at the website (https://www.usbr.gov/tsc/techreferences/computer%20software/models/boramep/index.html). The program is developed in Visual Basic. The software supports data input from a formatted spreadsheet to process several samplers at one time. It also allows manual data input.

The main features of the BORAMEP includes: (1) it provides numerical solutions for the parameters that were obtained from nomograms; and (2) the Rouse number (Ro) is determined by fitting a regression equation to relate Ro to fall velocity ω. The Ro value can be decided for all size

classes based on the regression equation. To enable this process, the program requires a minimum of two size classes in suspension and bed materials.

A step by step procedure for the BORAMEP is taken from the report *Bureau of Reclamation Automated Modified Einstein Procedure (BORAMEP) Program for Computing Total Sediment Discharge* (Holmquist-Johnson et al. 2009) and present as follows:

1. Compute the measured suspended load:

$$Q_m = 0.0027 Q C_m \text{ (tons/day)} \tag{2.16}$$

where $Q =$ discharge (ft^3/s) and $C_m =$ suspended sediment concentration (mg/l).

2. Compute the product of the hydraulic radius and friction slope assuming $x = 1$:

   (a) First, compute the value of $\sqrt{RS_f}$ using the equation given by Colby et al. (1955)

$$\sqrt{RS_f} = \frac{V}{5.75\sqrt{g}\log\left[12.27\frac{h}{k_s}x\right]} \tag{2.17}$$

   where V is the average stream velocity (ft/s), h is the flow depth (ft), x is a dimensionless parameter needed to be determined, g is the acceleration due to gravity (ft/s^2), and k_s is the effective roughness $k_s = d_{65}$ (ft).

   (b) Compute the shear velocity u_*:

$$u_* = \sqrt{gRS_f} \tag{2.18}$$

   (c) Compute the laminar sublayer thickness δ:

$$\delta = \frac{11.66\nu}{u_*} \tag{2.19}$$

   where ν is the kinematic viscosity of water (ft^2/s)

(d) Recheck x to make sure that the initial guess is valid by the following equation with Figure 2.10 (Einstein's Plate #3). An equation is developed to relate the parameter s to $\frac{k_s}{\delta}$.

$$x = \frac{-9.95 + 75.30\sqrt{\frac{k_s}{\delta}} - 201.73\frac{k_s}{\delta} + 288.37\left(\frac{k_s}{\delta}\right)^{1.5} - 195.25\left(\frac{k_s}{\delta}\right)^{2} + 57.6\left(\frac{k_s}{\delta}\right)^{2.5}}{1 + 33.96\sqrt{\frac{k_s}{\delta}} - 139.12\frac{k_s}{\delta} + 237.35\left(\frac{k_s}{\delta}\right)^{1.5} - 181\left(\frac{k_s}{\delta}\right)^{2} + 56.7\left(\frac{k_s}{\delta}\right)^{2.5}} \tag{2.20}$$

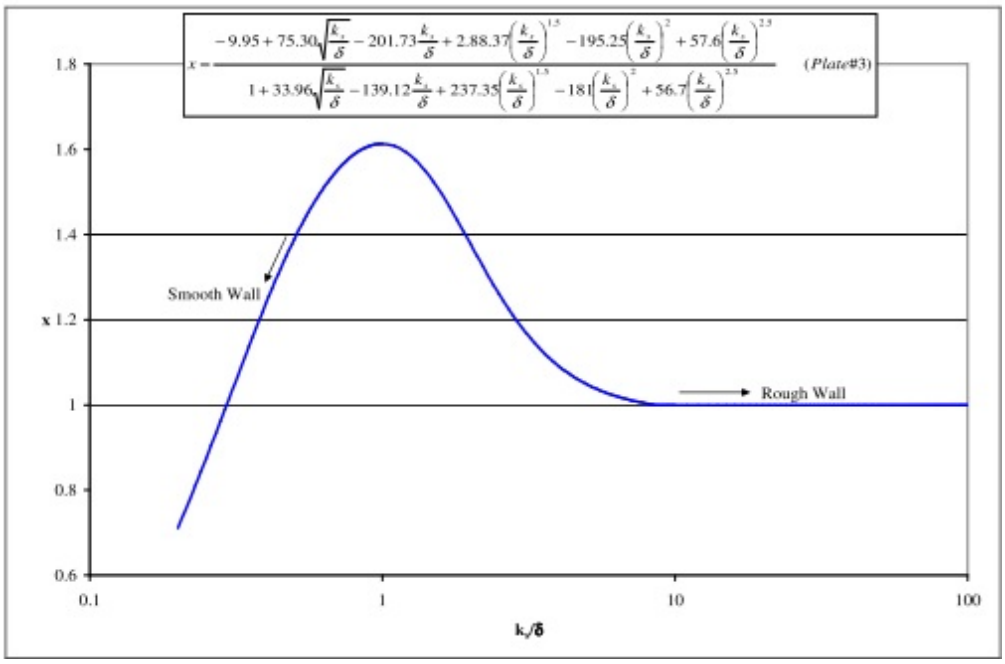

Figure 2.10: Einstein's multiplication factor x (from Shah-Fairbank 2006)

3. Compute the value of P:

$$P = 2.303 \log\left[30.2\frac{hx}{k_s}\right] \tag{2.21}$$

4. Compute the fraction of the flow depth not sampled A:

$$A = \frac{d_n}{h}$$

where d_n is the vertical distance not sampled = nozzle height (ft)

5. Compute the sediment discharge $Q_s{}'$ for each fraction:

$$Q_s{}' = i_s Q_m \times \%_{sampled}$$

where $\%_{sampled}$ is computed by choosing the equations below based on a P value closest to the computed P value from above.

For P = 4,

$$\%_{sampled} = \frac{100 - 2941.79A^2 + 265357.48A^4 + 64219.08A^6 - 325482.24A^8}{1 - 29.38A^2 + 2621.48A^4 + 5407.23A^6 + 157.44A^8 + 1272.32A^{10}} \quad (2.22)$$

For P = 8,

$$\%_{sampled} = \frac{100 + 30991.16A^2 + 21184.18A^4 + 211800.14A^6 - 263775.36A^8}{1 + 336.12A^2 + 444.29A^4 + 15662.05A^6 + 5759.38A^8 - 2976.45A^{10}} \quad (2.23)$$

For P = 11,

$$\%_{sampled} = \frac{100.19 + 31425.83A^2 - 54359.86A^4 + 1566703.2A^6 - 1543898.1A^8}{1 + 336.12A^2 + 444.29A^4 + 15662.05A^6 + 18936.5A^8 - 5820.32A^{10}} \quad (2.24)$$

For P = 14,

$$\%_{sampled} = \frac{100.31 + 45744.98A^2 103307.39A^4 + 635604.51A^6 - 784215.44A^8}{1 + 485A^2 + 2934.57A^4 + 7640.27A^6 + 11737.99A^8 - 3015.81A^{10}} \quad (2.25)$$

6. Compute the bedload for each size fraction:

   (a) Calculate the shear intensity ψ for all particle sizes in the analysis. ψ is calculated using the greater of the following two equations.

$$\psi = 1.65 \left(\frac{d_{35}}{RS_f} \right) \text{ or } 0.66 \left(\frac{d_i}{RS_f} \right) \quad (2.26)$$

where d_{35} is the particle size at which 35% of the bed material by weight is finer (ft) and d_i is the geometric mean for each size class (ft).

(b) Compute the intensity of bedload transport ϕ_*.

$$\phi_* = \frac{0.023p}{(1-p)} \tag{2.27}$$

where p is the probability that a sediment particle is entrained in the flow and is calculated using the following version of Error Function (Yang 1996):

$$p = 1 - \frac{1}{\sqrt{\pi}} \int_a^b e^{-t^2} dt \tag{2.28}$$

where $a = -B_*\psi - \frac{1}{\eta_0}$, $b = B_*\psi - \frac{1}{\eta_0}$, B_* is equal to 0.143 and η_0 is equal to 0.5.

(c) Compute the unit bed-load for each size fraction:

$$i_B q_B = 1200 d_i^{3/2} i_B \frac{\phi_*}{2}$$

where i_B is the fraction of bed material in a given size range.

(d) Compute the bedload for each size fraction in tons/day.

$$i_B Q_B = i_B q_B (43.2W) \tag{2.29}$$

where W is the channel width (ft).

7. Compute the theoretical exponent for vertical distribution of sediment (Ro).

(a) Compute the ratio $\frac{Q_s{}'}{i_B Q_B}$ for all size classes with suspended transport.

(b) Size classes of calculated values for the ratio of the suspended load to the bedload are used as the reference ranges for computation for values of Ro. The ratio of suspended load to bedload is set equal to a function with the parameters I_1, J_1, J_1', and J_2' as the

following:

$$\frac{Q_s{}'}{i_B Q_B} = \frac{I_1}{J_1}\left(PJ_1' + J_2'\right) \tag{2.30}$$

For each size class an initial value of Ro is assumed by using the following equation:

$$\text{Ro} = -0.1465 \ln\left(\frac{Qs'}{i_B Q_B}\right) + 1.0844 \tag{2.31}$$

(c) Once the Ro is determined for the overlapping suspended and bed material size classes, a log-log plot is made of the relationship between Ro and the fall velocity ω for each size class. A power function equation is then developed such that Ro $= a\omega^b$. The remaining values of Ro for the bedload are computed using this relationship. The fall velocity is computed using the following equation (Rubey 1933):

$$\omega = \left(\sqrt{\frac{2}{3} + \frac{36\nu^2}{(G-1)gd_i^3}} - \sqrt{\frac{36\nu^2}{(G-1)gd_i^3}}\right)\sqrt{(G-1)gd_i} \tag{2.32}$$

where G is the specific gravity of sediment.

8. Compute the total sediment load. The total sediment for a size fraction is calculated as

$$i_T Q_T = Q_{si}{}'\frac{(PJ_1 + J_2)}{(PJ_1' + J_2')} \text{ for fine sediment;} \tag{2.33}$$

$$i_T Q_T = i_B Q_B(PI_1 + I_2 + 1) \text{ for coarse sediment} \tag{2.34}$$

Eq. (2.33) is most accurate and applicable for the ranges of fine particle sizes or when Ro is small; Eq. (2.34) is accurate for the ranges of coarse particle sizes or when Ro is large (Simons and Sentürk 1992).

Figure 2.11 provides a schematic flow diagram to show how the BORAMEP works. Shah-Fairbank (2006) tested the BORAMEP with the data collected on the Low Flow Conveyance Channel (LFCC) in Rio Grande. She analyzed the error messages generated by the BORAMEP when

it terminated the total sediment load computation. The main errors and limitations of BORAMEP are: (1) Ro could not be calculated because there is a minimum of two overlapping bins required. However, particles in the measured zone not found in the bed have been seen in practice; (2) Negative values of Ro can be generated when fitting regression equations to Ro and ω. However, negative Ro is physically impossible because it implies that the sediment concentration is higher at the free surface than the bed; (3) Total sediment load calculated by BORAMEP is sometimes lower than the measured load, which is also physically impossible. It happens when the BORAMEP could not determine the total load when the program is stopped due to an error message. In this case, the total load is calculated using a suspended sediment load equation. Sometimes it is unclear why an error message occurred, according to Shah-Fairbank (2006).

2.2.5 Series Expansion of the Modified Einstein Procedure (SEMEP)

To remove most of the empiricism found in the existing MEP, Shah-Fairbank (2009) calculated the Rouse number, Ro, from the median particle size measured in suspension d_{50ss}. The measured unit sediment discharge q_m is evaluated by integrating the product of flow velocity and sediment concentration from the nozzle height d_n to the free surface at $z = h$. Recall the equation of measured load Eq. (2.6):

$$q_m = \int_{d_n}^{h} Cv dz$$

Replacing the C and v by Eq. (2.9) and Eq. (2.10) with $C_a = \dfrac{q_b}{11.6 u_* a}$, the equation becomes

$$q_m = 0.216 q_b \frac{E^{\text{Ro}-1}}{(1-E)^{\text{Ro}}} \left\{ \ln\left(\frac{60}{E}\right) J_1' + J_2' \right\} \tag{2.35}$$

$$J_1' = \int_A^1 \left(\frac{1-z^*}{z^*}\right)^{\text{Ro}} dz^* \tag{2.36}$$

$$J_2' = \int_A^1 \ln z^* \left(\frac{1-z^*}{z^*}\right)^{\text{Ro}} dz^* \tag{2.37}$$

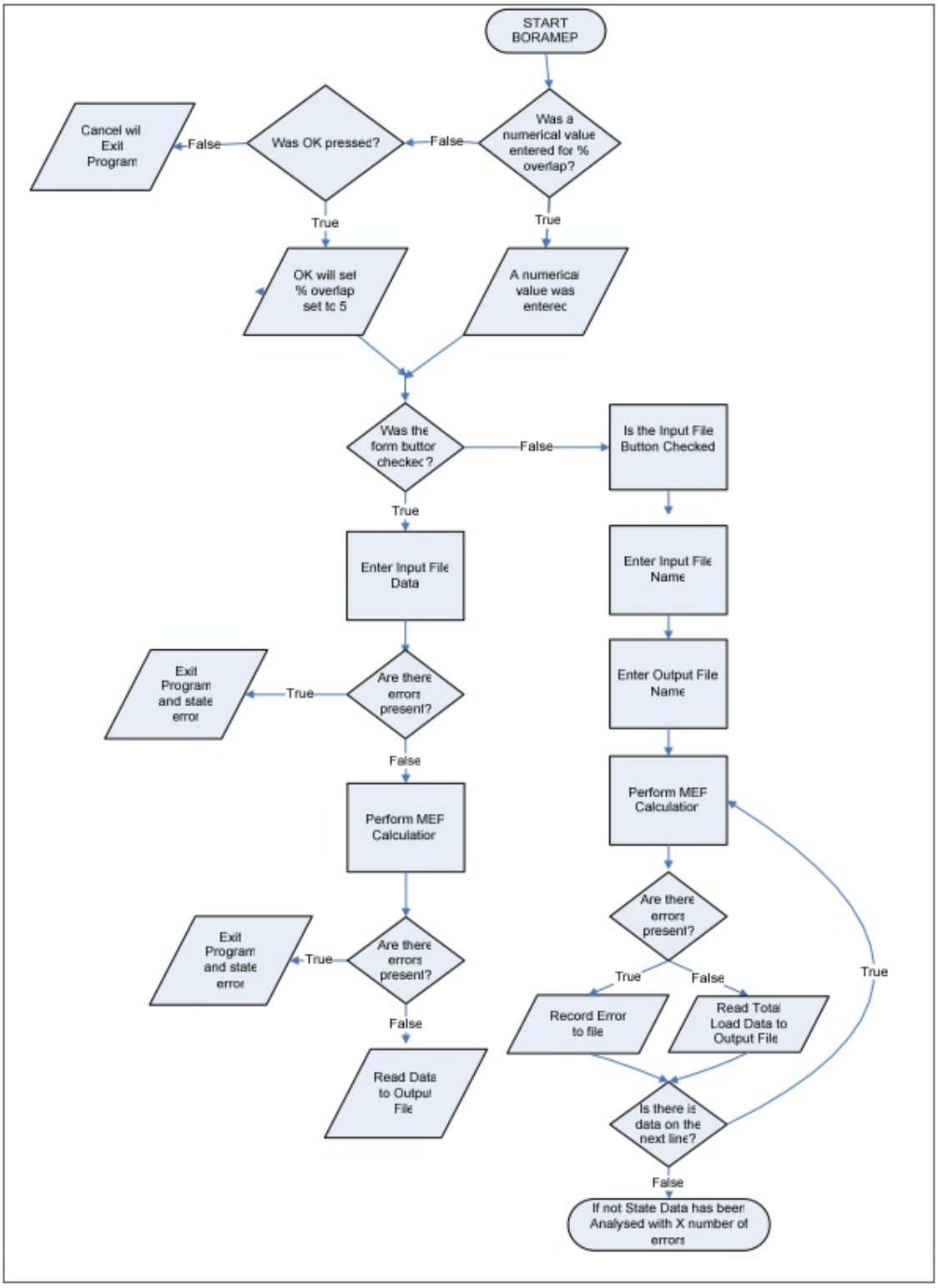

Figure 2.11: Flowchart of BORAMEP (from Shah-Fairbank 2006)

where $A = d_n/h$, $\omega =$ settling velocity of the median suspended particle d_{50ss},

$$\omega = \frac{8\nu}{d_{50ss}} \left[\left(1 + 0.0139 d_*^3\right)^{0.5} - 1 \right] \tag{2.38}$$

$$d_* = d_{50ss} \left[\frac{(G-1)g}{\nu^2} \right]^{\frac{1}{3}} \tag{2.39}$$

, where $d_* =$ dimensionless grain size, $G =$ specific weight of sediment, $\nu =$ kinematic viscosity of water, $g =$ gravitational acceleration, and $d_{50ss} =$ the median size of suspended material.

In SEMEP, the Rouse number, Ro, is directly evaluated from the suspended material by using the following equation

$$\text{Ro} = \frac{\omega}{\beta_s \kappa u_*} \tag{2.40}$$

where $\beta_s =$ the ratio of the turbulent mixing coefficient of sediment to the momentum exchange coefficient and β_s has been found equal to 1 for most practical applications; $\kappa =$ von Karman constant usually close to 0.4, and $u_* =$ shear velocity $\approx \sqrt{ghS}$ (h = flow depth, and S = river bed slope).

J_1' and J_2' are the modified Einstein integrals. Shah-Fairbank adopted the numerical solution developed by Guo and Julien (2004) to solve the modified Einstein integrals. The unit bedload q_b can be solved from the above equation when the measured sediment discharge is known

$$q_b = \frac{q_m}{0.216} \frac{(1-E)^{\text{Ro}}}{E^{\text{Ro}-1}} \frac{1}{\ln(60/E) J_1' + J_2'} \tag{2.41}$$

The unit suspended sediment discharge q_s can be calculated when q_b is solved,

$$q_s = \int_a^h Cv \mathrm{d}z \tag{2.42}$$

$$= 0.216 q_b \frac{E^{\text{Ro}-1}}{(1-E)^{\text{Ro}}} \left\{ \ln\left(\frac{60}{E}\right) J_1 + J_2 \right\} \tag{2.43}$$

$$J_1 = \int_E^1 \left(\frac{1-z_*}{z_*} \right)^{\text{Ro}} \mathrm{d}z_* \tag{2.44}$$

$$J_2 = \int_E^1 \ln z_* \left(\frac{1-z_*}{z_*} \right)^{\text{Ro}} \mathrm{d}z_* \tag{2.45}$$

The total sediment load can be calculated by the following equation:

$$q_t = q_b + q_s = q_b + 0.216 q_b \frac{E^{\mathrm{Ro}-1}}{(1-E)^{\mathrm{Ro}}} \left\{ \ln\left(\frac{60}{E}\right) J_1 + J_2 \right\} \tag{2.46}$$

Figure 2.12 summarized the procedures of total sediment discharge calculation by SEMEP. SEMEP was tested on several laboratory and sand-bed river data from the Niobrara to the Mississippi River. Julien (2010) summarized the main advantages of SEMEP as:

1. based on median grain diameter (d_{50}) in suspension no bins are required;
2. bedload calculated based on measured load, no need to arbitrarily divide the Einstein bedload equation by 2;
3. calculate Ro directly from settling equation, no need to fit based on power function;
4. calculate total load even when there are not enough overlapping bins between suspended and bed material; and
5. calculated total load cannot be less than measured load.

The relationship between u_*/ω and mode of transport and recommended sediment transport procedure is presented in Shah-Fairbank et al. (2011), where $u_*/\omega = 2.5/\mathrm{Ro},$.

Baird and Varyu (2011) used the sediment measurements from Rio Grande Low Flow Conveyance Channel (LFCC), Niobrara River, and San Acacia Floodway Gage to evaluate the performance of SEMEP. The results of SEMEP are compared to the measured total sediment load and the calculated total load by BORAMEP. They found that both methods yield comparable results to the measurements, while SEMEP is able to calculate all the data because it does not require overlapping bins between suspended and bed materials.

Dehghani et al. (2014) performed a case study in the Chelichay watershed in northeastern Iran using MEP and SEMEP. The Chelichay watershed consists of one sand bed river and four gravel bed rivers. Their result showed that in sand bed river, SEMEP fitted the measurements well, but MEP had a tendency to overestimate the total load. For the gravel bed rivers, three rivers got the

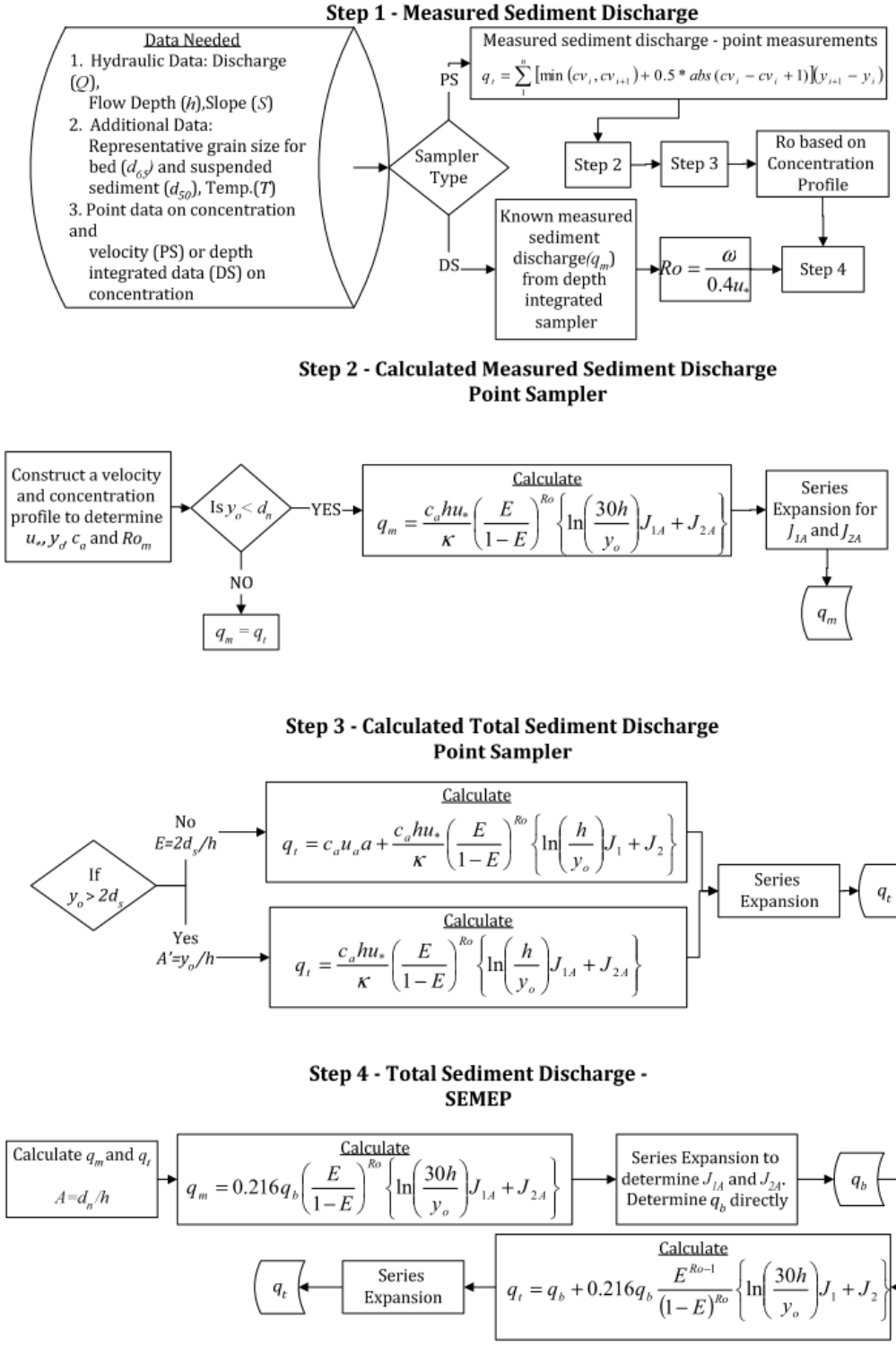

Figure 2.12: Flowchart of total sediment discharge calculation by SEMEP and SEMEPP (from Shah-Fairbank et al. 2011)

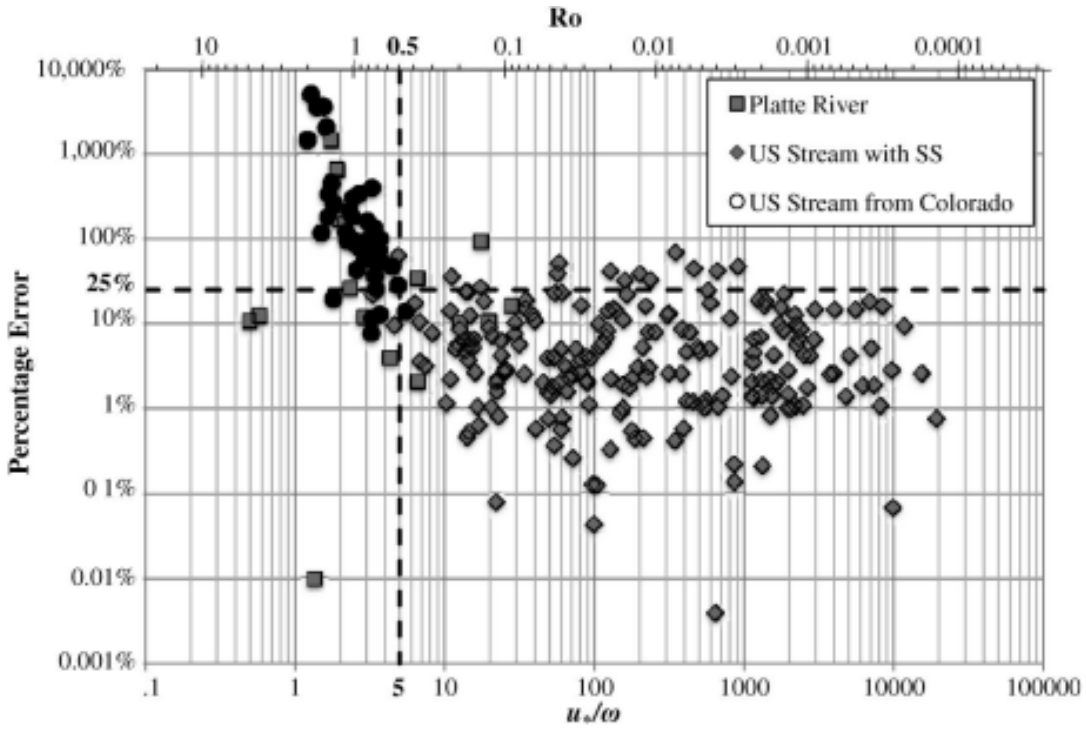

Figure 2.13: SEMEP performance as a function of u_*/ω (Shah-Fairbank et al. 2011)

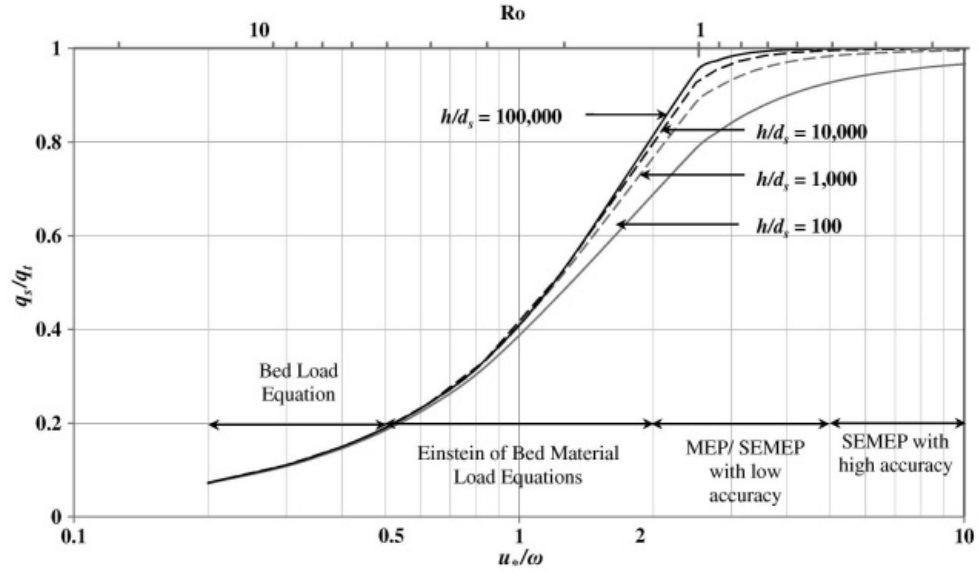

Figure 2.14: Mode of sediment transport and recommended calculated procedure (Shah-Fairbank et al. 2011)

better result with SEMEP. Overall, they suggested SEMEP to be a more comprehensive method in calculating the total sediment load.

2.3 Sediment Rating Curves

Sediment concentration and discharge, for both suspended load and bedload, are usually displayed as a flow discharge on log-log graphs (e.g., Batalla et al. 2005; Bunte et al. 2014; Sholtes 2015; Warrick 2015). Such relationship between flow and sediment is known as a sediment rating curve. Although exhibiting scatter, rating curves demonstrate that the sediment concentration, or sediment discharge, appears to be independent of discharge. This allows the mean sediment yield to be determined based on the discharge history. Sediment rating curves are typically constructed on the basis of instantaneous concentration-discharge data pairs, but can also be concentration-discharge data that are averaged over daily, monthly, or other time periods (Morris and Fan 2009).

The log-log relationship between sediment concentration (or discharge) and flow discharge can be presented mathematically in a linear form:

$$\log C = \bar{a} + \bar{b} \log Q \tag{2.47}$$

or

$$C = \bar{a} Q^{\bar{b}} \tag{2.48}$$

where $\bar{a}$ and $\bar{b}$ are empirical coefficients and they can be determined either by visual curve fitting or by regression. The linear relationship is generally true for the streams with capacity-limited sediment transport. For the streams with supply-limited sediment transport, the sediment load can vary a lot for a given discharge because it does not depend solely on discharge. In this case, concentration-discharge data pairs may be split by season or month and fit the sediment rating curve for an individual subset (e.g.Kao and Milliman 2008; Julien 2010, p. 335). Sediment discharge displays higher correlation to flow discharge compared to sediment concentration because sediment discharge is the product of flow discharge and sediment concentration.

2.4 Computing the Sediment Load

2.4.1 Time-Series Summation Method

The daily sediment load can be computed if a reliable rating relationship between the sediment concentration and discharge is available. The daily sediment discharge Q_s is computed as one of the following equations:

Metric units:

$$Q_s = 0.0864CQ \tag{2.49}$$

where Q_s is in metric tons/day, suspended sediment concentration C is in mg/l, and Q is in m^3/s.

U.S. customary units:

$$Q_s = 0.002446CQ \tag{2.50}$$

where Q_s is in metric tons/day, C is in mg/l, and Q is in ft^3/s.

Sediment yield is obtained by summing daily sediment discharge over a long period of time. Notice that the time unit should be consistent for discharge data and rating curves (Morris and Fan 2009). For example, to compute the sediment load from a daily flow series, one should use a sediment rating curve that is constructed based on mean daily discharge and daily sediment load. Only if the concentration does not change rapidly in a day, a rating curve based on instantaneous C-Q relationship can be applied to mean daily discharge, else the concentration and discharge should be divided into hourly increments.

The summation can also be used to construct mass curves and double mass curves. Mass curves plot the cumulative sediment load as a function of time in years. Double mass curves present the cumulative sediment load as a function of the cumulative water discharge. Both curves are particularly useful to detect changes in flow regimes. Figure 2.15 provides an example of double mass curve to illustrate how the sediment yield change before and after highway construction. Following extensive highway construction in 1963, the sediment yield during 1960 to 1963 is nearly 10 times higher compared to the sediment yield before the construction.

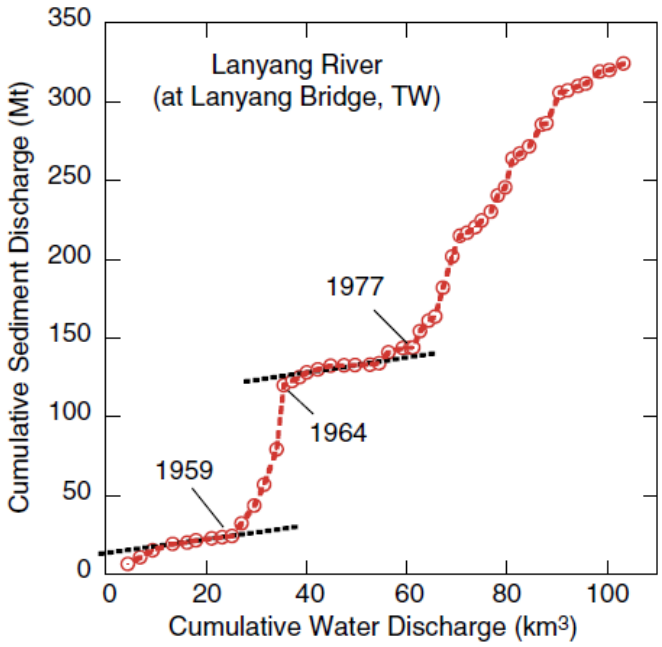

Figure 2.15: Double mass curve for Lanyang River, Taiwan, 1950-2000 (Milliman and Farnsworth 2013)

2.4.2 The Flow-Duration/Sediment-Rating Curve Approach

The flow-duration/sediment-rating curve (FDSRC) method combines a flow duration curve and sediment rating curve. Flow duration curve is an output of frequency analysis of flow discharge. Flow duration curve plots discharge as a function of the percentage of time a given flow discharge is equalled or exceeded (Bui 2014). The flow duration curve is divided into intervals and the average discharge for each class is calculated as the mean discharge at the midpoint of the interval. The sediment load is then calculated by the sediment rating curve. The mean annual sediment yield is the sum of all the production of sediment discharge and the interval width of each class. Julien (2010) states that the method is most reliable under three conditions: (1) long period of recording; (2) sufficient sediment concentration measurement at high flows is available; and (3) widely scattered sediment rating curve.

2.5 Parametric Analysis of Runoff and Sediment Transport

Julien (1996) developed a method to transform the flow and sediment duration curves. The transform is useful for determination of the mean annual discharge and mean annual sediment

yield. Moreover, the method can be used to estimate the expected values and exceedance probability at a given value. For a random variable X and its possible value x, the cumulative distribution function (cdf) $F(x)$ is the probability that X will take a value less than or equal to x:

$$F(x) = P(X \leq x) \tag{2.51}$$

The probability density function (pdf) $f(x)$ is derived from the cdf

$$f(x) = \frac{\mathrm{d}F(x)}{\mathrm{d}x} \tag{2.52}$$

The probability of exceedance $E(x)$:

$$E(x) = 1 - F(x) \tag{2.53}$$

Julien (1996) showed that rainfall intensity is exponentially distributed, and we define $\Psi = i/\bar{i}$, where i is the rainfall intensity, and $\bar{i}$ is the mean rainfall intensity as shown in Figure 2.16. The pdf of Ψ is

$$f(\Psi) = e^{-\Psi} \tag{2.54}$$

An interesting property of an exponential distribution is that the exceedance probability and pdf are identical,

$$E(\Psi) = f(\Psi) = e^{-\Psi} \tag{2.55}$$

We assume that a variable x can be expressed as a power function of an exponential distribution of Ψ:

$$x = \hat{a}\Psi^{\hat{b}} \tag{2.56a}$$

$$\text{or inversely, } \Psi = ax^b \tag{2.56b}$$

where

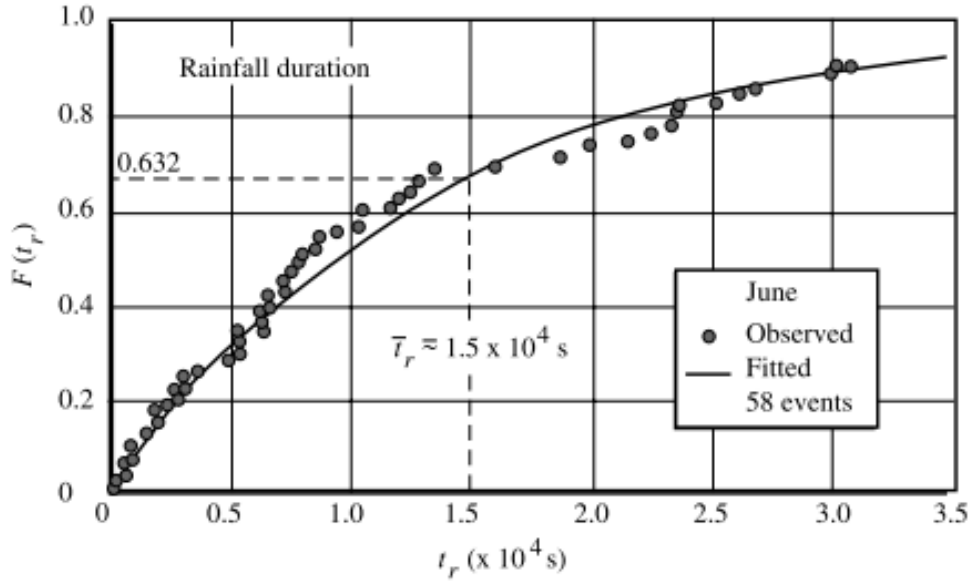

(a) Cumulative distribution curve of rainfall duration

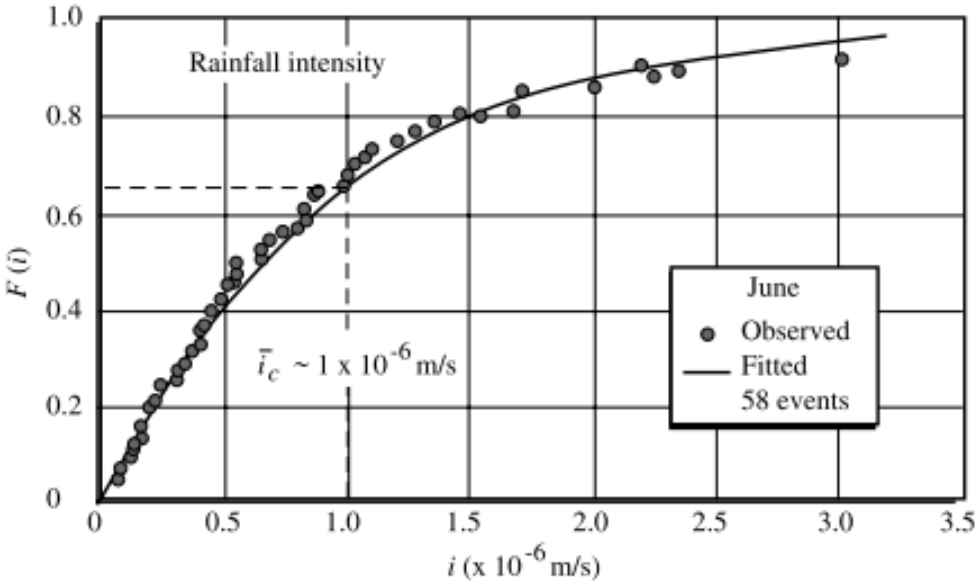

(b) Cumulative distribution curve of rainfall intensity

Figure 2.16: Observed rainfall intensity and duration compared to exponential distribution (from Julien 2018)

$$\hat{a} = (1/a)^{1/b} \tag{2.57a}$$

$$\hat{b} = 1/b \tag{2.57b}$$

The pdf of x, $f(x)$, is calculated from Eqs. (2.52) and (2.56a):

$$f(x) = abx^{b-1}e^{-ax^b} = ab\left(\frac{\Psi}{a}\right)^{\frac{b-1}{b}} e^{-\Psi} \tag{2.58}$$

From the definition $\Psi = ax^b$ we obtain

$$\mathrm{d}\Psi = abx^{b-1}\mathrm{d}x \tag{2.59}$$

From Eqs. (2.55) and (2.56b), we obtain:

$$f(\Psi)\mathrm{d}\Psi = e^{-\Psi}(abx^{b-1}\mathrm{d}x) = abx^{b-1}e^{-ax^b}\mathrm{d}x = f(x)\mathrm{d}x \tag{2.60}$$

There are two methods to evaluate the values of $\hat{a}$, $\hat{b}$: (1) a graphical method, and (2) the method of moments.

2.5.1 Graphical Method

By taking natural logarithm on both sides of Eq. (2.55) twice, one gets

$$-\ln E(\Psi) = \Psi = ax^b \tag{2.61}$$

$$\Pi = \ln\left[-\ln E(\bar{\Psi})\right] = \ln\bar{\Psi} = \ln a + b\ln x \tag{2.62}$$

As shown in Figure 2.17, the transform parameters a and b are evaluated by plotting the values of Π and $\ln x$. The points on the graph often form a straight line, and the slope of the line gives the exponent b. In practice, the linearity is usually found for higher values of $\ln x$ and Π. A linear regression line is fitted to the higher values of $\ln x$ and Π, and the regression coefficient and exponent are $\ln a$ and b, respectively.

2.5.2 Method of Moments

The transform parameters $\hat{a}$ and $\hat{b}$ can also be evaluated from the first and second moment. The first moment M_1 is the mean, and it is defined as

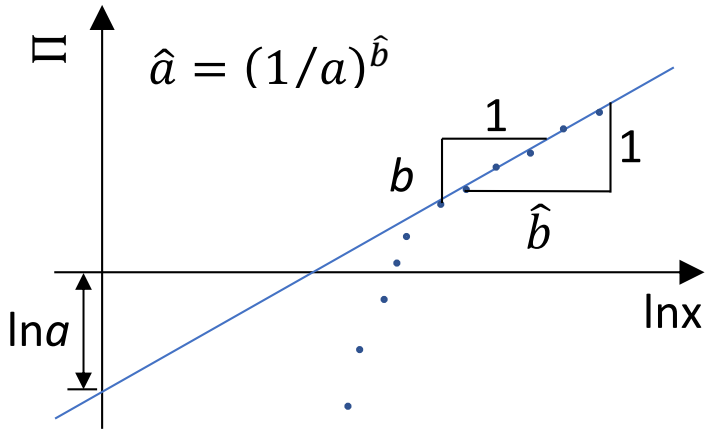

Figure 2.17: Graphical illustration of the values of a and b

$$\begin{aligned} M_1 &= \bar{x} \\ &= \int_0^\infty x f(x) \mathrm{d}x \\ &= \hat{a} \int_0^\infty \Psi^{\hat{b}} e^{-\Psi} \mathrm{d}\Psi \\ &= \hat{a}\Gamma(1+\hat{b}) \end{aligned} \tag{2.63}$$

where Γ is the gamma function and $\Gamma(\hat{b}) = \int_0^\infty \Psi^{\hat{b}-1} e^{-\Psi} \mathrm{d}\Psi$.

The second moment M_2 is the mean of x^2,

$$\begin{aligned} M_2 = \overline{x^2} &= \int_0^\infty x^2 f(x) \mathrm{d}x \\ &= \int_0^\infty (\hat{a}\Psi^{\hat{b}})^2 f(\Psi) \mathrm{d}\Psi \\ &= \hat{a}^2 \int_0^\infty \Psi^{2\hat{b}} e^{-\Psi} \mathrm{d}\Psi \\ &= \hat{a}^2 \Gamma(1+2\hat{b}) \end{aligned} \tag{2.64}$$

By dividing Eq. (2.64) by the square of Eq. (2.63), one gets

$$\frac{\Gamma(1+2\hat{b})}{\left[\Gamma\left(1+\hat{b}\right)\right]^2} = \frac{\overline{x^2}}{\bar{x}^2} \tag{2.65}$$

The values of $\overline{x^2}$ and $\bar{x}^2$ are calculated from the sample, and the value of $\hat{b}$ can be evaluated from the above equation. The value of $\hat{a}$ can then be solved from Eq. (2.63) as

$$\hat{a} = \frac{\bar{x}}{\Gamma(1+\hat{b})} \tag{2.66}$$

2.5.3 Interpretation of the Exponent Parameter $\hat{b}$

Julien (1996) tested this procedure for runoff and sediment transport. Two examples are shown for the flow discharge and sediment discharge of the Rio Grande, as shown in Figure 2.18.

2.6 Statistical Analysis

The degree of accuracy of a proposed method is evaluated through a statistical analysis. Four parameters are examined: (1) the root mean squared error (RMSE) (2) the Mean Absolute Percentage Error (MAPE); (3) the coefficient of determination R^2; (4) the concordance correlation coefficient; (5) Kolmogorov-Smirnov ; and (6) 1-Wasserstein distance.

The RMSE represents the standard deviation of the differences between predicted and observed values:

$$\text{RMSE} = \sqrt{\frac{1}{n}\sum_{i=1}^{n}(X_i - Y_i)^2} \tag{2.67}$$

where X_i = observed value, in this case is measured sediment yield, Y_i = predicted value, and n = number of samples.

The MAPE measures the size of the error relative the size of observation:

$$\text{MAPE} = \frac{1}{n}\sum_{i=1}^{n}\frac{|X_i - Y_i|}{X_i} \tag{2.68}$$

the MAPE shows the deviation of the prediction from the actual measurement.

The coefficient of determination, denoted R^2, is a measurement of the variation between the predicted values and observed values.

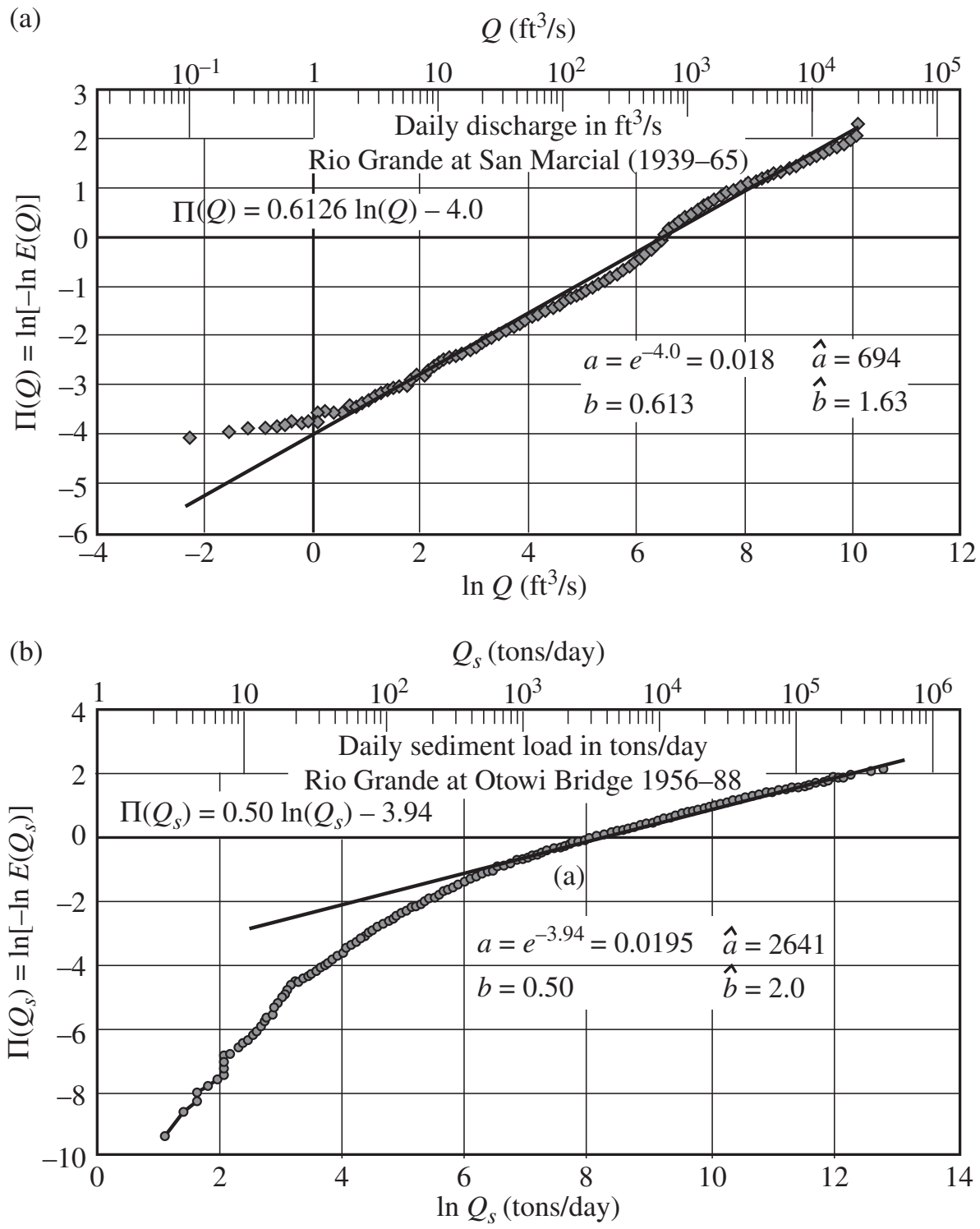

Figure 2.18: Examples of (a) flow and (b) sediment discharge duration curves from Julien (2018)

$$R^2 = \left(\frac{\sum_{i=1}^{n}(X_i - \bar{X})(Y_i - \bar{Y})}{\sqrt{\sum_{i=1}^{n}(X_i - \bar{X})^2 \sum_{i=1}^{n}(Y_i - \bar{Y})^2}} \right)^2 \tag{2.69}$$

where $\bar{X}$ = the mean of observed value and $\bar{Y}$ = the mean of predicted value. The variation between observation and prediction reduces as the value of R^2 approaches 1.

The concordance correlation coefficient, denoted ρ_c, measures how closely the predicted and the observed values fall on the 45 degree line from the origin (Lin 1989):

$$\rho_c = \frac{2s_{xy}}{s_x^2 + s_y^2 + (\bar{X} - \bar{Y})^2} \tag{2.70}$$

$$s_{xy} = \frac{\sum_1^n (X_i - \bar{X})(Y_i - \bar{Y})}{n-1} \tag{2.71}$$

$$s_x^2 = \frac{\sum_1^n (X_i - \bar{X})^2}{n-1} \tag{2.72}$$

$$s_y^2 = \frac{\sum_1^n (Y_i - \bar{Y})^2}{n-1} \tag{2.73}$$

The best possible value of ρ_c is 1, meaning the observation and prediction have perfect agreement.

The performance of the analytical solution of cumulative distribution functions is evaluated by the Kolmogorov-Smirnov statistic and the 1-Wasserstein distance.

Kolmogorov-Smirnov statistic quantifies the maximum distance between two curves (Figure 2.19a):

$$D = \max |F(x) - G(x)| \tag{2.74}$$

where $F(x)$ is the cumulative curve of discharge or sediment and $G(x)$ is the theoretical cumulative distribution curve.

The 1-Wasserstein distance measures the area between two curves (Figure 2.19b) and is defined as:

$$W = \int_{x=-\infty}^{\infty} |F(x) - G(x)| \, \mathrm{d}x \tag{2.75}$$

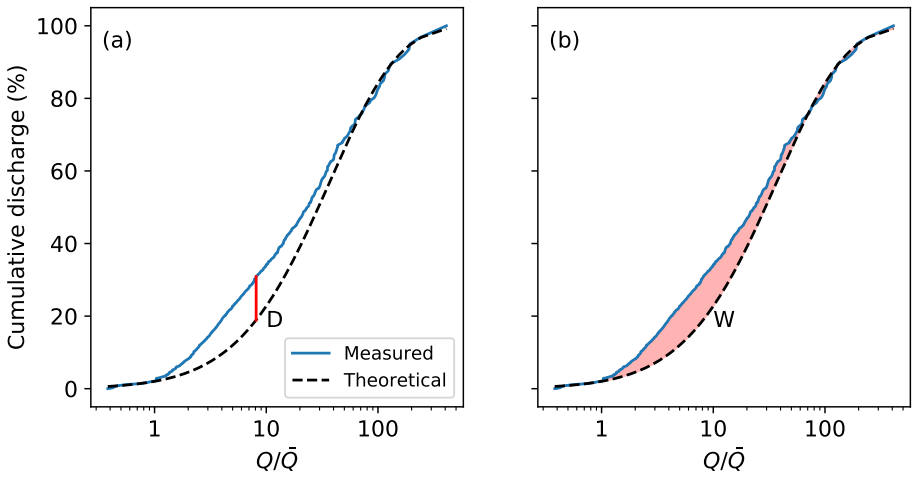

Figure 2.19: Graphical illustrations of (a) the Kolmogorov-Smirnow distance, and (b) the 1-Wassertein distance

Chapter 3

Sediment Yield in South Korea

We performed the research project "Multivariate Regression Analysis and Model Development for the Estimation of Sediment Yield from Ungauged Watershed in the Republic of Korea", sponsored by K-water, during May, 2016 to February, 2017 (Julien et al. 2017). Flow and sediment measurements along with watershed attributes were provided to study the mean annual sediment yield. This gave us the opportunity to further the studies on the sediment regimes in South Korea. The following sections detail the study site and the given data.

3.1 Study Site

South Korea is located in East Asia, on the southern half of the Korean Peninsula. The population is 57.5 millions (The World Bank 2017). The topography of Korea Peninsula features on ridge hill masses and wide flat valley plains (Yoon and Woo 2000). The studied watersheds includes the five Korean rivers, Han River, Nakdong River, Geum River, Yeongsan River, and Seomjin River. The location of the stations are presented in Figure 3.1. The five river basins occupy 85% of the total South Korea land area of 99,828 km^2. Studied watersheds range from 128 to 20,381 km^2. The attributes of the stations are present in Table 3.1. The climate is classified as humid continental and humid subtropical. The mean annual precipitation ranges from 1000 mm to 1400 mm (Figure 3.2). The rainfall is associated with the monsoons and typhoons, and about two-thirds of the rainfall occurs between June and September. A geologic map of the Korean Peninsula is provided in Figure 3.3. The geology of South Korea is relatively old and the erosion rate is low (Yoon and Woo 2000; Song et al. 2010). The land cover is classified into seven types: urban, agriculture, forest, wetland, pasture, water, and bare land. The land use percentage of each watershed is shown in Figure 3.4. The study watersheds are not highly urbanized (1.9% to 15.0%). For most of the watersheds, the land use are mainly forest (23.0% to 79.8%) or agriculture (10.3% to 48.0%). Julien

et al. (2017) provides more detailed information on the watershed attributes, including drainage density, soil type, etc.

3.2 Previous Sediment Yield Studies in South Korea

Walling and Webb (1983) is one of the earliest studies of the sediment yield in Korean Peninsula. They analyzed the river monitoring stations and estimated the sediment yield to be 500 to 750 tons/year·km^2. But Lvovich et al. (1991) suggested the range to be 1,000 - 5,000 tons/year·km^2. A more recent dataset (Milliman and Farnsworth 2013) on the major rivers in Korea shows the range is between about 75 to 400 tons/year·km^2 (Table 3.2). Several studies used the Universal Soil Loss Equation (USLE) or Revised Universal Soil Loss Equation (RUSLE) for regional studies. The soil loss of the entire country except the surrounding islands was quantified by Park et al. (2011) using RUSLE. The average amounts of soil lost in 1985, 1995, and 2005 were 1,710, 1,740, and 2,000 tons/year·km^2, respectively. From their finding, Tamjin River watershed has the highest soil erosion, 3,830 tons/year·km^2. However, the largest increase of soil erosion happened in Seomjin River, from 1,360 tons/year·km^2 in 1985 to 1990 tons/year·km^2 in 2005, 46.3% of increment in 20 years. Jang et al. (2015) also conducted a national scale assessment by USLE with a finer resolution, 10 m, of digital elevation model (DEM). The average soil loss is estimated to be 3,456 tons/year·km^2 and up to 1,500,000 tons/year·km^2. Nonetheless, quantification of sediment yield was beyond the goals of the two studies, the required information to calculate sediment yield, such as sediment delivery ratio, was not available. Kim et al. (2012) evaluated the sediment loss of mine tailing dumps at the Samgwang mine in Chungcheongnam province. Kim (2006) applied RUSLE to predict the soil loss of Imha watershed which is located at the upstream of Nakdong River. The mean annual gross soil erosion is predicted to be 3,450 tons/year·km^2. The erosion by a typhoon event, Maemi typhoon, is also computed. The soil loss by Maemi typhoon account for 39% of the annual erosion. Some calculated the soil erosion by USLE/RUSLE but estimated the sediment yield from field measurements. Lee and Choi (2010) compared the sediment deposit in Bosung reservoir and compared it to the results of USLE to study the scale effect of (DEM). Lee and Lee

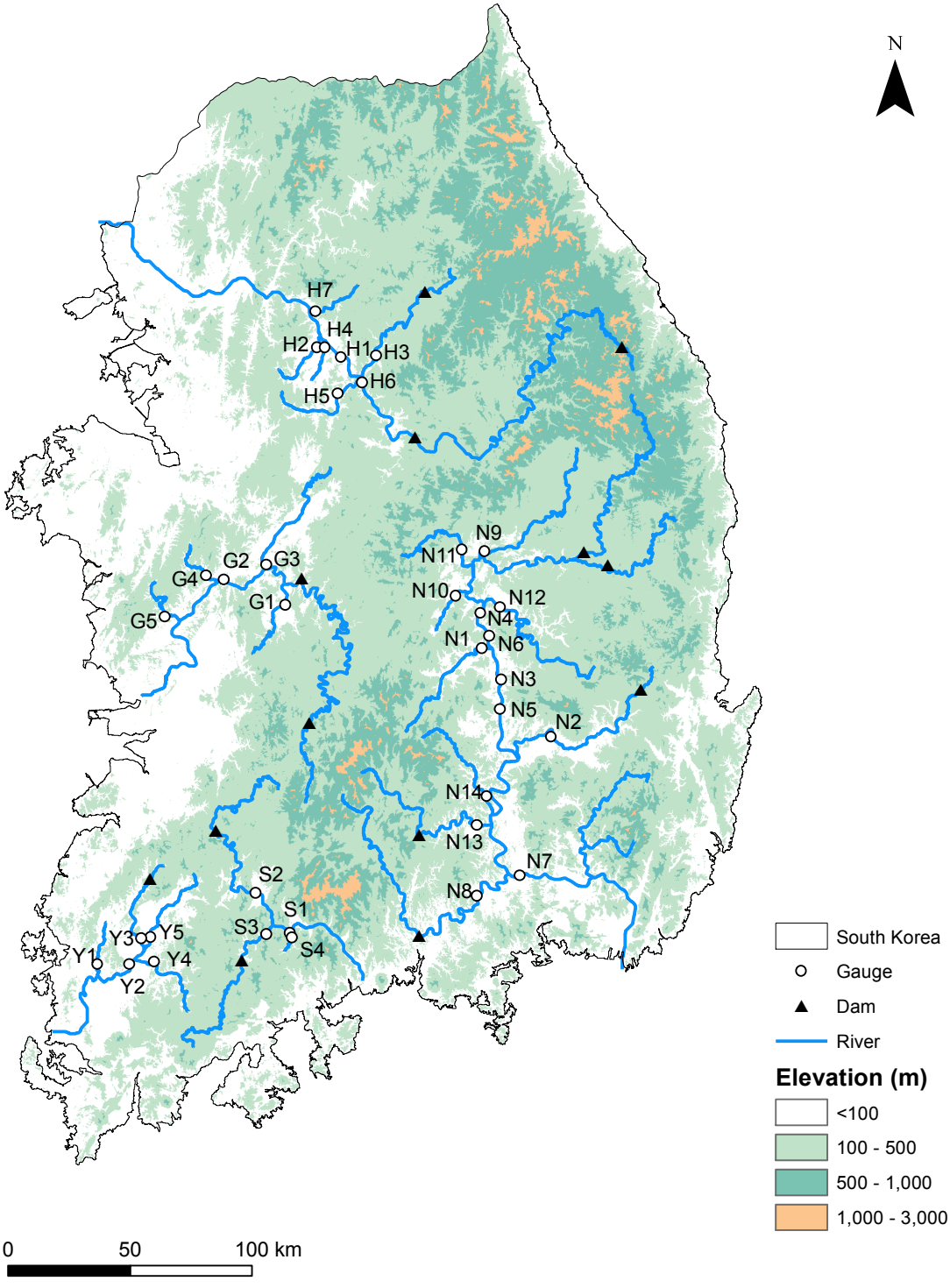

Figure 3.1: Study gages and watersheds (Elevation data: ASTER Global DEM)

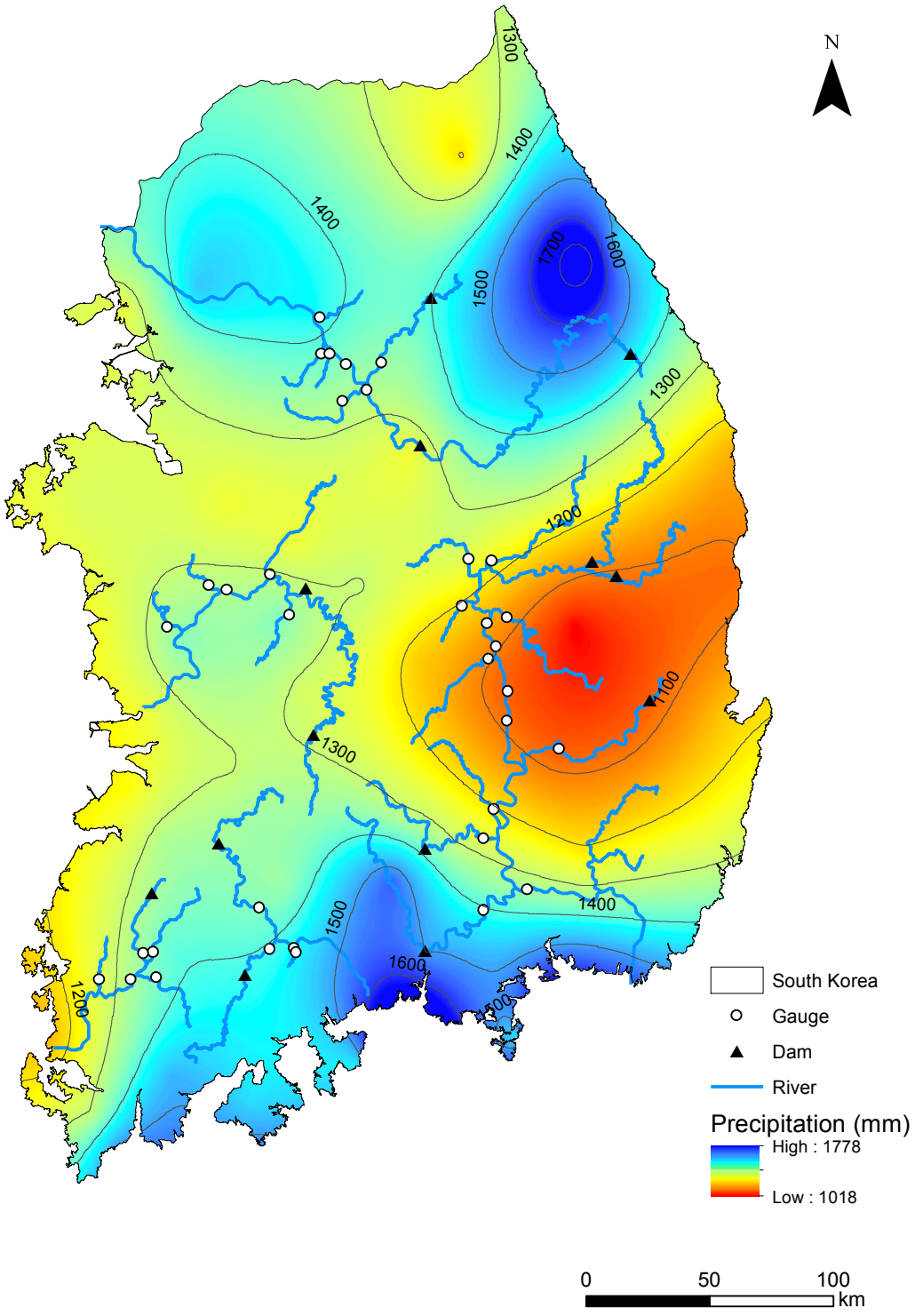

Figure 3.2: Annual precipitation of South Korea (data source: Korea Meteorological Administration)

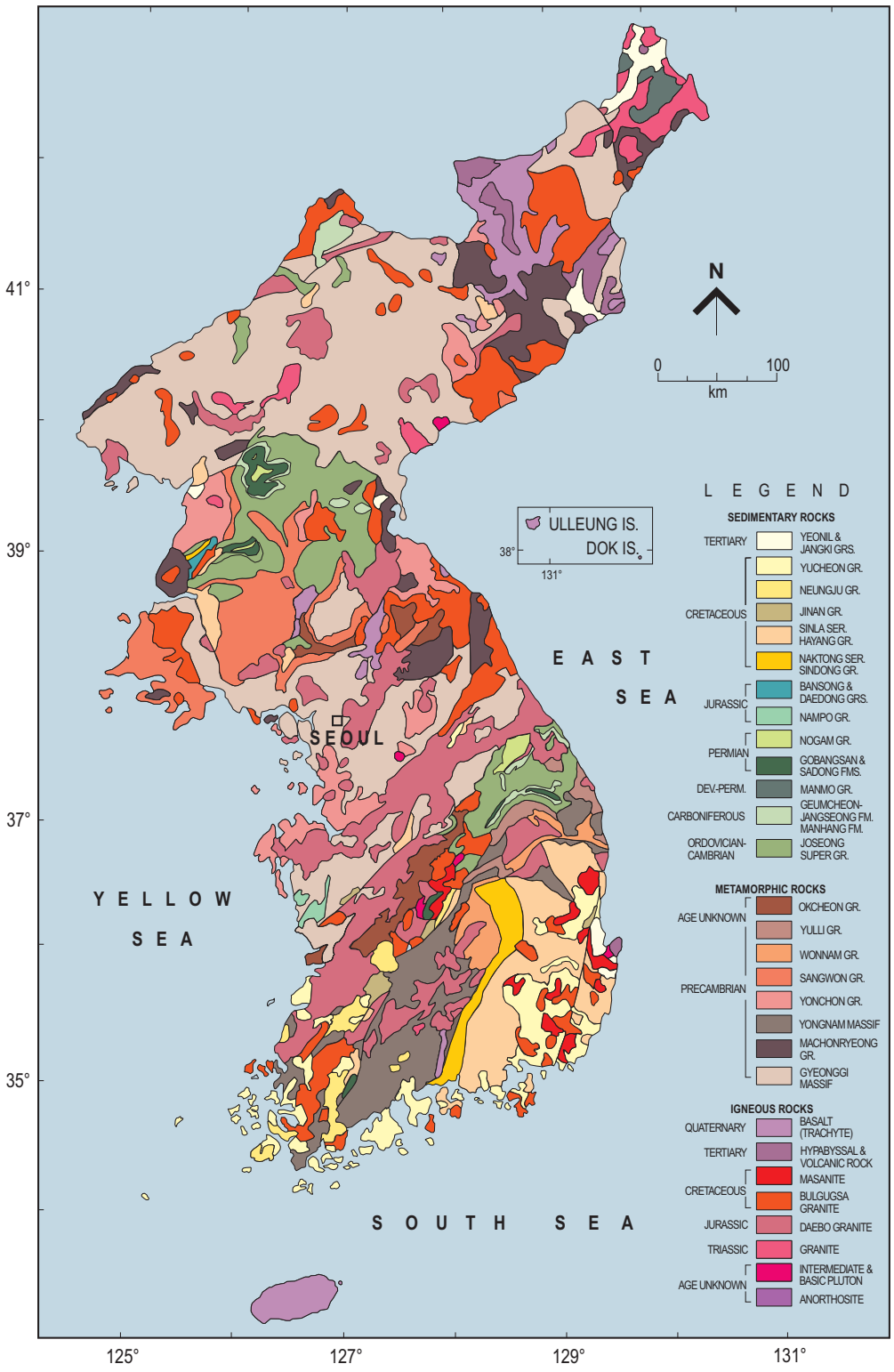

Figure 3.3: Geologic map of the Korean Peninsula (figure source: Chough (2013)

Table 3.1: Watershed attributes (data source: Ministry of Land, Infrastructure and Transport, Korea)

Station	Area (km^2)	Avg. Slope (%)	Channel Width (m)	Outlet Elevation (m)	Mean annual precipitation (mm)	Relief (m)	Main Channel Length (km)	Relief Ratio (m/m)
H1	11,074	44.4	475	35	1,409	1,534	340	0.013
H2	283	16.6	258	42	1,370	554	31	0.023
H3	1,346	43.0	491	53	1,387	1,210	82	0.022
H4	173	10.0	185	42	1,353	390	26	0.016
H5	519	20.0	238	57	1,315	604	44	0.019
H6	8,823	46.8	390	42	1,420	1,527	321	0.013
H7	307	42.8	143	23	1,397	1,124	37	0.037
N1	979	36.7	279	36	1,163	1,265	64	0.024
N2	1,541	34.1	168	28	1,081	1,146	74	0.018
N3	10,913	37.7	515	30	1,167	1,534	300	0.011
N4	9,407	38.6	468	40	1,172	1,524	265	0.013
N5	11,101	37.5	463	17	1,165	1,547	314	0.011
N6	9,533	40.3	602	34	1,171	1,530	278	0.013
N7	20,381	35.3	557	3	1,219	1,895	426	0.009
N8	2,999	39.4	286	7	1,464	1,899	155	0.025
N9	1,512	34.4	222	62	1,275	1,362	102	0.022
N10	175	28.0	131	52	1,178	731	20	0.032
N11	614	47.1	230	66	1,282	1,030	51	0.033
N12	1,318	36.3	380	43	1,046	1,136	103	0.022
N13	1,239	41.3	263	9	1,306	1,474	103	0.025
N14	750	43.0	320	17	1,207	1,393	63	0.034
G1	606	33.3	328	32	1,337	814	48	0.026
G2	6,275	34.4	570	8	1,279	1,596	266	0.017
G3	1,850	24.0	272	15	1,270	632	81	0.010
G4	258	41.6	167	22	1,301	610	31	0.027
G5	208	34.3	224	11	1,309	582	43	0.028
Y1	190	21.3	180	18	1,275	561	30	0.021
Y2	2,039	27.9	628	9	1,365	1,167	69	0.021
Y3	668	23.8	330	16	1,372	1,160	40	0.029
Y4	580	36.7	245	15	1,405	903	45	0.030
Y5	552	31.4	356	13	1,321	789	55	0.020
S1	1,269	37.8	211	41	1,419	1,137	113	0.018
S2	1,788	34.9	376	51	1,348	1,091	138	0.019
S3	3,818	36.5	242	25	1,376	1,329	165	0.018
S4	128	43.7	81	31	1,430	814	16	0.057

Relief: The different between the highest elevation in the watershed to the outlet; Relief ratio = Relief/Basin Length. Basin length = length in a straight line from the outlet of a stream to the farthest point on the drainage divide of its basin.

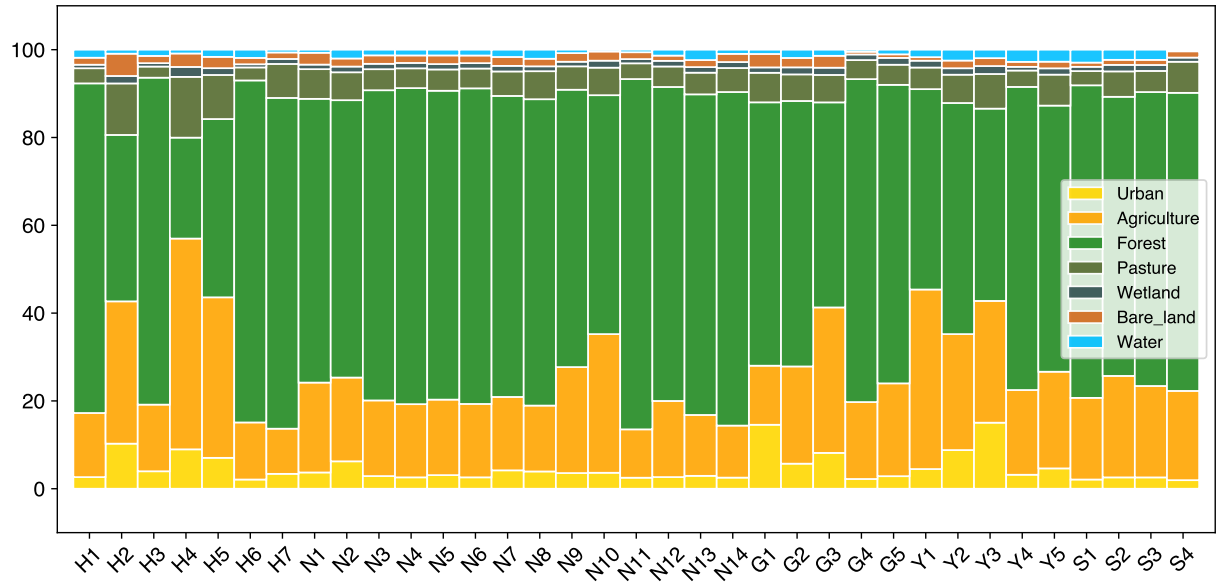

Figure 3.4: Land cover percentage of the 35 stations (source: Ministry of Land, Infrastructure and Transport, Korea)

(2010) and Lee and Kang (2013) used discharge records and sediment rating curves to calculate the sediment yields of Cheoncheon, Donghyang, Chungju, Yeaju, Whakwon, Sunsan, Kongju and Kurea watersheds. Kim (2016) simulated the daily discharge at Sangju Weir using the TANK rainfall runoff model. Based on the flow-duration/sediment rating curve method, the sediment yield of Sangju weir was estimated to be 57 tons/year·km^2. Table 3.2 summarizes the sediment yield in South Korea.

Table 3.2: Published sediment yield studies of South Korea

Site	A (km^2)	Rainfall (mm)	Max Elev	Low Elev	Sediment yield (tons/yr· km^2)	Method	Refs
Samgwang mine	21	1257	480	65	1.9 - 8.8	USLE	1
Imha	1361	1037	1215	80	890	RUSLE	2
Donghyang	165		1589	205	145	Rating curve	3
Cheoncheon	287				71	Rating curve	3
Yeoju	11114				41	Rating curve	4
Waegwan	11104				39	Rating curve	4
Gongju	7213				20	Rating curve	4
Chungju	6648				208	Rating curve	4
Gurye 2	3980				92	Rating curve	4
Seonsan	433				171	Rating curve	4
Bosung	273	1495	794	121	314	Reservoir survey	5
Han	25000				400		6
Geum	9900				222		6
Mankyong	1600				400		6
Nakdong	24000				342		6
Sapgyo	1700				76		6
Seomjin	4900				408		6
Yeongsan	2800				250		6
Sangju	7407				57	FDSRC	7
Maeho	8.1				293	RUSLE	8

References: 1. Kim et al. (2012); 2. Kim (2006); 3. Lee and Lee (2010); 4. Lee and Kang (2013); 5. Lee and Choi (2010); 6. Milliman and Farnsworth (2013); 7. Kim (2016); 8. Lee and Kang (2018)

3.3 Available Data for this Study

3.3.1 River Data in South Korea

The daily discharge includes daily average stage and daily average discharge from 2005/1/1 to 2014/12/31. Figure 3.5a presents an example of river gage at Hyangseok station in the Nakdong River. The sediment concentrations were measured by using the depth-integrating D-74, or in some cases by using the point sampling P-61A (Figure 3.5b). In addition, the grain size distribution of bed material and suspended material were provided. Bed materials were sampled by the US BM-54 bed material sampler, the 60L Van Veen Grab sampler or by grid sampling. Suspended material grain sizes were determined by laser diffraction. The depth-integrating samples were used in this study. The lengths of record are summarized in Figure 3.6.

(a) Hyangseok station (N9)

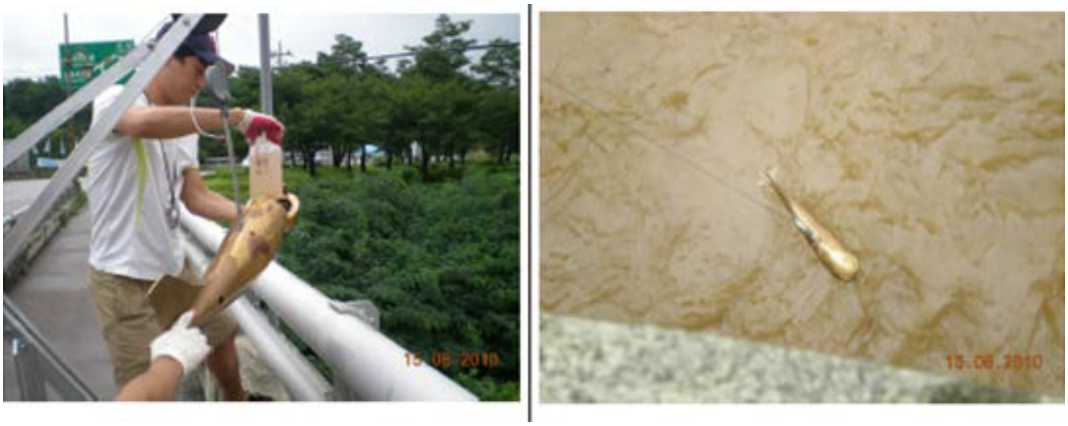

(b) Suspended load sample collection (P-61 sampler)

Figure 3.5: Example of gaging station and sediment sample collection (source: Kim (2016))

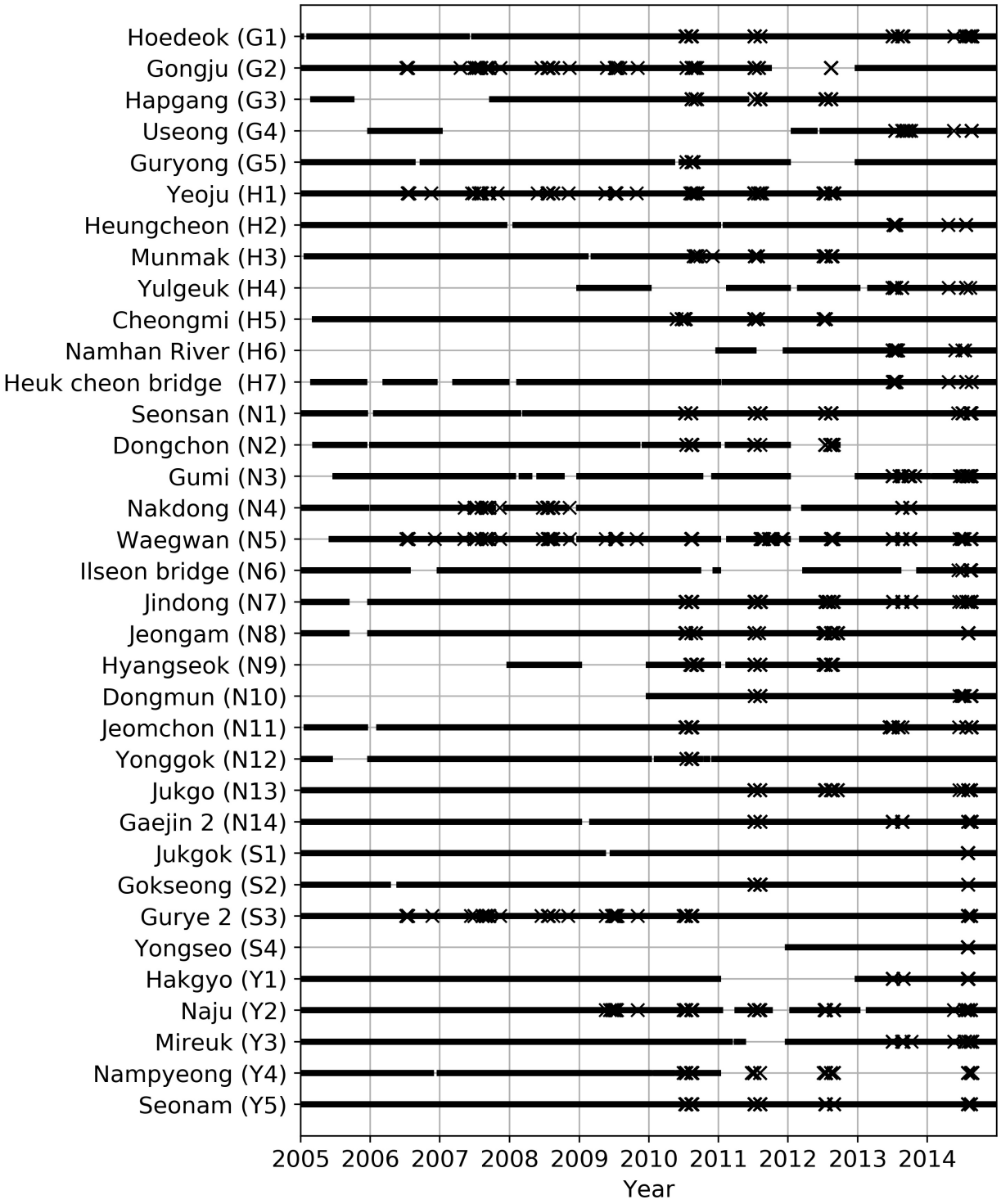

Figure 3.6: Available average daily discharges (line) and sediment surveys (×) (data source: K-water)

Chapter 4

The Ratio of Measured to Total Sediment Load

The Series Expansion of the Modified Einstein Procedure (SEMEP) the latest developments of the Modified Einstein Procedure. It is used to compare with the results of total sediment discharge calculations by the Modified Einstein Procedure with the measurements from South Korea. Addressed next is the question of how to determine the ratio of measured to total sediment discharge and the ratio of suspended to total sediment discharge. These ratios depend on flow conditions and sediment particle-size distribution. A calculation example and comprehensive comparison of SEMEP and MEP is provided in Section 4.1, followed by the theoretical approach to calculate the ratio of measured to total sediment discharge (Section 4.2) and the ratio of suspended to total sediment discharge (Section 4.3).

4.1 MEP vs SEMEP

Total sediment load is provided by K-water with the suspended load measurements. The provided total sediment load is calculated a version of MEP that is similar to the BORAMEP. I developed a SEMEP program in Python for this study by following the procedure detailed in Shah-Fairbank (2009) (Figure 2.12). The only difference is that the Einstein Integrals in the original SEMEP program by Shah-Fairbank (2009) are calculated by using the series-based scheme by Guo and Julien. In this study, I use the scipy.integrate.quad method in Python. A review for different algorithms for the Einstein Integrals is available (Zamani et al. 2017). The detailed procedures of BORMEP and SEMEP can be found in Section 2.2.4 and 2.2.5. A comparison of the total sediment loads by the MEP and the SEMEP is present in the following subsections.

The following demonstrates a single sample that is calculated using both the MEP and the SEMEP. Table 4.1 provides the flow condition and channel geometry, and Table 4.2 provides the grain size distributions for suspended and bed materials.

Table 4.1: Hydraulic data and properties for sample data

Site: H1 Measurement date: 2012/07/06		
Discharge (Q)	= 2337 m^3/s	= 82525 ft^3/s
Mean velocity (V)	1.8 m/s	5.8 ft/s
Mean water depth (h)	5.0 m	16.2 ft
Channel width (W)	265 m	868 m
Water temperature (T)	20.6 °C	69.1 °F
Cross section area (A)	1310 m^2	14099 ft^2
Nozzle height (d_n)	10 cm	0.3 ft
Water surface slope (S_f)	0.000538	
Suspended sediment concentration (C_m)	594.6 mg/l	

Table 4.2: Sediment size fractions for sample data

Size fraction (mm)	Geometric mean D_i (mm)	(ft)	i_s (%)	i_B (%)	Fall velocity (ft/s)
0.001 - 0.062	0.0079	0.000026	94.8	1.1	0.00018
0.062 - 0.125	0.0884	0.00029	4.7	0.5	0.02180
0.125 - 0.25	0.1768	0.00058	0.3	3.7	0.0671
0.25 - 0.5	0.3536	0.00116	0.2	4.5	0.154
0.5 - 1	0.7071	0.00232	0	34.6	0.259
1.0 - 2.0	1.4142	0.00464	0	19.1	0.391
2.0 - 4.0	2.8284	0.00928	0	11.2	0.565
4 - 8	5.6569	0.01855	0	9.2	0.805
8 - 16	11.3137	0.03711	0	16.0	1.14
16 - 32	22.6274	0.07422	0	0	1.62

d_{65} = 2.24 mm; d_{50} = 1.24 mm
d_{35} = 0.87 mm; $d_{50_{ss}}$ = 0.0222 mm

4.1.1 MEP Computation Example

For the sample in Table 4.1 and Table 4.2, by following the steps in Section 2.2.4, the calculation of the total sediment load by MEP is summarized below:

1. $Q_m = 2.446 \times 10^{-3} C_{mg/l} Q = 2.446 \times 10^{-3} \times 594.6 \times 82524.7 \, \dfrac{\mathrm{ft}^3}{\mathrm{s}} = 120,023$ tons/day.

2. $x = 0.989$ is solved by trial and error. $\sqrt{RS_f} = \dfrac{V}{5.75\sqrt{g}\log\left[12.27\dfrac{h}{k_s}x\right]} = 0.0404\,(\mathrm{ft})^{1/2}$.

3. $P = 2.303 \log \left[30.2 \dfrac{hx}{k_s}\right] = 2.303 \log \left[30.2 \dfrac{16.24 \text{ ft} \times 0.989}{2.24 \text{ mm} \times 0.00328 \dfrac{\text{ft}}{\text{mm}}}\right] = 11.1.$

4. The fraction of the flow depth not sampled $A = \dfrac{d_n}{h} = \dfrac{0.3 \text{ ft}}{16.24 \text{ ft}} = 0.018.$

5. For A = 0.018 and P = 11.1, $\%_{sampled} = 99.4\%$ by using Eq. (2.24). The suspended load of each size fraction is shown in Table 4.4.

6. The bedload for each size fraction is calculated in Table 4.3.

7. Although Holmquist-Johnson et al. (2009) suggested that the size range less than 0.0625 mm should not be used, the suspended materials in South Korea are often silt and the size range less than 0.0625 mm are still used here. By trial and error, Ro are determined to be 0.863 for size class 0.125 mm to 0.25 mm, and 1.086 for size class 0.25 mm to 0.5 mm, respectively. Figure 4.1 is the plot of the two suspended load points indicating the power function regression Ro $= a\omega^b$ and the resulting Ro that were calculated using the regression equation; where $a = 1.874$ and $b = 0.291$. The regressed Ro are shown in the fourth column in Table 4.4.

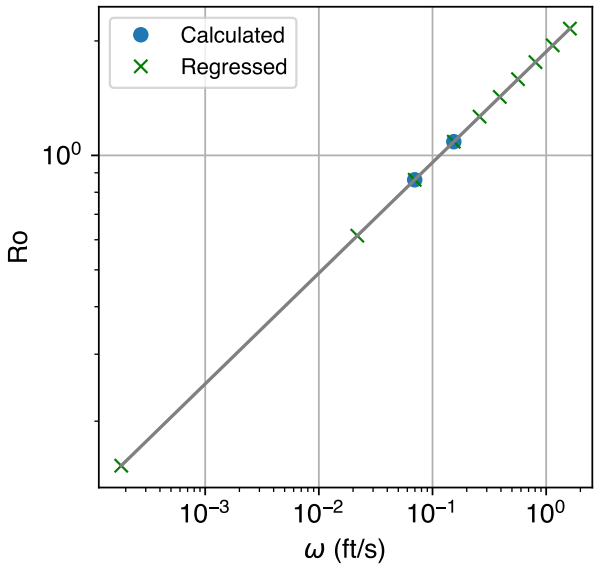

Figure 4.1: Ro regression analysis

8. Compute the total sediment load. The total sediment for a size fraction is calculated as

$$i_T Q_T = Q_{si}{}' \frac{(PJ_1 + J_2)}{(PJ_1' + J_2')} \text{ for fine sediment;}$$

$$i_T Q_T = i_B Q_B (PI_1 + I_2 + 1) \text{ for coarse sediment}$$

The suspended load was calculated for size class smaller than 0.25 mm (the first three rows of Table 4.4). The suspended load was calculated to be 120,738 tons/day. The bedload was calculated for the larger size classes. The bedload was calculated to be 13,364 tons/day. The total load computed was 134,102 tons/day.

Table 4.3: Unit bedload of each size fraction

D_i (mm)	i_B	ψ	ϕ_*	$i_B q_B$	$i_B Q_B$
0.0079	1.1	2.869	1.901	0.0000016	0.062
0.0884	0.5	2.869	1.901	0.000028	1.06
0.1768	3.7	2.869	1.901	0.000585	22.09
0.3536	4.5	2.869	1.901	0.00201	76.00
0.7071	34.6	2.869	1.901	0.0441	1,652.74
1.4142	19.1	2.869	1.901	0.0688	2,580.51
2.8284	11.2	3.731	1.901	0.0718	2,691.78
5.6569	9.2	7.463	0.223	0.0311	1,166.07
11.3137	16	14.926	0.017	0.0116	436.87
22.6274	0	0	0	0	0

Table 4.4: Total sediment discharge computation by MEP

i_s	$Q_s{}'$	E	Ro	J_1'	$-J_2'$	J_1	$-J_2$	$\frac{PJ_1+J_2}{PJ_1'+J_2'}$	I_1	$-I_2$	PI_1+I_2+1	i_TQ_T
94.8	113,145	0.0000032	0.01	0.98	0.915	1	1	1.01	1436			114462
4.7	5,610	0.0000357	0.27	1.05	1.356	1	2	1.04	162			5835
0.3	358	0.000071	0.67	1.64	3.097	2.325	7	1.23	9			441
0.2	239	0.000143	1.26						1	4.40	4.45	338
0	0	0.000286	1.9						0.23	1.83	1.94	3205
0	0	0.000571	2.7						0.13	1.07	1.55	4000
0	0	0.001143	4						0.08	0.71	1.40	3756
0	0	0.002285	5						0.06	0.50	1.30	1521
0	0	0.004570	6						0.04	0.36	1.24	542
0	0	0.009140	8						0.03	0.26	0.00	0
100												134102

4.1.2 SEMEP Computation Example

The computation of SEMEP is summarized in Table 4.5. See the following for explanation of symbols in Table 4.5, row by row:

Table 4.5: Total sediment discharge computation

Variable	Value	Unit
q_m	5.25	m^2/s
T	20.6	°C
ν	1.004×10^{-6}	m^2/s
d_*	0.56	-
ω	0.000442	m/s
u_*	0.1617	m/s
Ro	0.00683	-
u_*/ω	366	-
E	0.000501	-
A	0.0202	-
J_1'	0.98	-
J_2'	-0.91	-
I_1	409.15	-
I_2	-412.12	-
q_b	0.001288	kg/ms
q_t	5.32	kg/ms
Q_t	121,624	tons/day

1. Unit measured sediment discharge q_m $(\mathrm{m}^2/\mathrm{s})$:

$$\begin{aligned} q_m &= C_m \times Q/W \\ &= \frac{594.6 \times 2336.84\,\mathrm{m}^3/\mathrm{s}}{264.53m} = 5.25\,\mathrm{m}^2/\mathrm{s} \end{aligned}$$

2. An empirical equation of kinematic viscosity of water ν is used (García 2008):

$$\begin{aligned} \nu &= \frac{1.79 \times 10^{-6}}{1 + 0.03368T + 0.00021T^2}\ (\mathrm{m}^2/\mathrm{s}) \\ &= \frac{1.79 \times 10^{-6}}{1 + 0.03368(20.6) + 0.00021(20.6)^2} = 1.004 \times 10^{-6}\ \mathrm{m}^2/\mathrm{s} \end{aligned} \tag{4.1}$$

where $T =$ temperature of water in degrees centigrade ($^\circ$C)

3. Dimensionless particle diameter d_*

$$\begin{aligned} d_* &= d_{50}\left(\frac{(G-1)g}{\nu^2}\right)^{1/3} \\ &= \frac{0.0222\text{ mm}}{1000\,\text{m/mm}}\left(\frac{(2.65-1)\times 9.81}{(1.004\times 10^{-6})^2}\right) = 0.56 \end{aligned} \tag{4.2}$$

4. Fall velocity ω (m/s):

$$\begin{aligned} \omega &= \frac{8\nu}{d_s}\left((1+0.0139d_*^3)^{0.5}-1\right) \\ &= \frac{8\times 1.004\times 10^{-6}}{0.0222\times 10^{-3}\text{ m}}\left((1+0.0139\times 0.56^3)^{0.5}-1\right) \\ &= 0.000441\text{ m/s} \end{aligned} \tag{4.3}$$

5. Shear velocity $u_* = \sqrt{gRS} \approx \sqrt{ghS} = \sqrt{9.81\times 4.95\times 0.000538} = 0.1617$ m/s

6. Rouse number Ro:

$$\begin{aligned} \text{Ro} &= \frac{\omega}{\beta_s \kappa u_*} \\ &= \frac{0.000442}{1\times 0.4\times 0.1617} = 0.00683 \end{aligned} \tag{4.4}$$

where κ is the von Kármán constant = 0.4; β_s is the momentum correction factor for the sediment and is assumed as 1.

7. $u_*/\omega = 2.5/\text{Ro} = 2.5/0.00683 = 366$

8. $E = 2d_s/h = 2\times 1.24/1000/4.95 = 0.000501$

9. $A = d_n/h = 10/100/4.95 = 0.0202$

10. J_1', given by Eq. (2.36).

11. J_2', given by Eq. (2.37).

12. I_1, given by Eq. (2.13).

13. I_2, given by Eq. (2.14).

14. Unit bedload discharge q_b (kg/ms) using Eq. (2.35).

15. Unit total sediment discharge q_t (kg/ms):

$$q_t = q_b \left[1 + I_1 \ln \frac{30h}{d_s} + I_2 \right] \tag{4.5}$$

16. Total sediment discharge Q_t (tons/day):

$$Q_t = q_t W \times 86.4 = 121,624 \text{ tons/day} \tag{4.6}$$

The total sediment load computed in SEMEP was 121,624 tons/day which is comparable to the computation in MEP, 134,102 tons/day (Table 4.6).

Table 4.6: Summary of MEP and SEMEP results

Unit (tons/day)	MEP	SEMEP
Measured load	120,052	120,052
Suspended load	120,738	121,595
Bedload	13,364	29
Total load	134,102	121,624

4.1.3 All Korean Data

This study calculated the total sediment load from the suspended load measurements for a total of 2036 records for 35 stations. MEP and SEMEP are used and compared.

I first compared the total sediment discharge Q_t calculation by MEP and SEMEP. The total sediment load of 1,962 out of 2,036 suspended load samples was calculated by SEMEP. Using MEP, 1808 samples were calculated.

Figure 4.2 presents the ratio Q_m/Q_t for all samples computed by MEP and SEMEP. The measured sediment discharge Q_m is calculated as the product of discharge Q and measured concentration C in both cases. In Figure 4.2a, the predicted total sediment load is compared to the measured load. The predictions from SEMEP are close to measured, while the predictions from MEP tend to be slightly higher on average, with scatter larger than 2 orders of magnitude. Figure 4.2b shows that the values of u_*/ω range from 15 to 1853. The Q_m/Q_t of MEP range from 8×10^{-8} to 26. The Q_m/Q_t of SEMEP range from 0.5 to 0.995. According to Julien (2010), the primary mode of transport should be suspended load when $u_*/\omega > 5$. Therefore, Q_m/Q_t is expected to be close to 1. This is true for sand-bed rivers, but deviations are noticeable for cobble and gravel-bed streams. Also Q_m/Q_t should always be lower than 1 because the total load cannot be less than measured load. The results of MEP do not always satisfy this requirement. A total of 29 samples out of 1,808 resulted in $Q_m > Q_t$ when using the MEP. It is physically impossible for the total load to be smaller than the measured load. Additionally, in the case of $Q_m/Q_t = 8 \times 10^{-8}$, where $Q_m = 400$ tons/day and $Q_t = 9 \times 10^9$ tons/day, such high sediment load in the unmeasured zone is also very unlikely. Other known issues with MEP are reported by Shah-Fairbank (2009). For instance, MEP requires at least two overlapping bins between suspended material and bed material to determine Ro. In addition, Ro for the remaining bins are determined by regression analysis when overlapping bins exist, and sometimes a negative Ro exponent can be generated, which erroneously implies that the sediment concentration increases towards the free surface. Therefore, SEMEP is considered more accurate and is used for the rest of analysis.

4.2 Ratio of Measured to Total Load Q_m/Q_t

In Fig. 4.3, I investigated the relationships between the ratio of the measured to total sediment discharge Q_m/Q_t and (a) u_*/ω, (b) concentration C, (c) discharge Q, and (d) normalized discharge

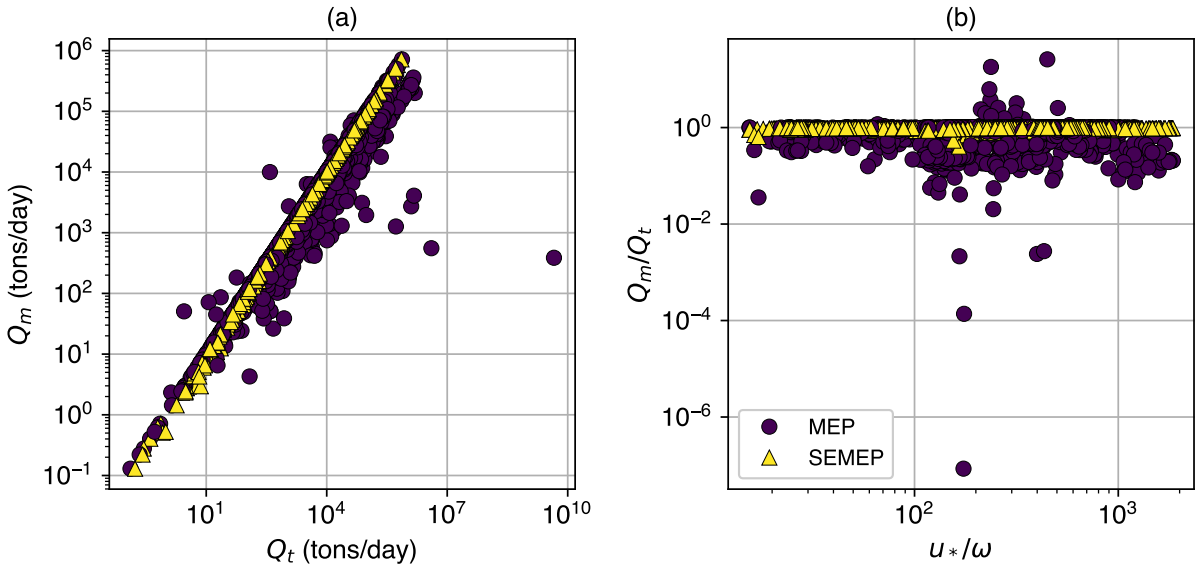

Figure 4.2: MEP and SEMEP comparison: (a) calculated total sediment discharge vs measured load, (b) Q_s/Q_t vs u_*/ω

$Q/\bar{Q}$. In Fig. 4.3a, b, c, and d, the difference among various bed materials are subtle. Overall, the measurement contains over 80% of the sediment load (1,936 out of 1,962 samples). In Fig. 4.3d, it can be seen that more than 80% of the sediment load is measured when $Q/\bar{Q} > 10$.

According to the SEMEP, the ratio of measured to total sediment discharge can be shown as:

$$\begin{aligned}\frac{q_m}{q_t} &= \frac{0.216 q_b \dfrac{E^{\mathrm{Ro}-1}}{(1-E)^{\mathrm{Ro}}}\left\{\ln\left(\dfrac{30h}{d_s}\right)J_1' + J_2'\right\}}{q_b + 0.216 q_b \dfrac{E^{\mathrm{Ro}-1}}{(1-E)^{\mathrm{Ro}}}\left\{\ln\left(\dfrac{30h}{d_s}\right)J_1 + J_2\right\}} \\ &= \frac{0.216 \dfrac{E^{\mathrm{Ro}-1}}{(1-E)^{\mathrm{Ro}}}\left\{\ln\left(\dfrac{30h}{d_s}\right)J_1' + J_2'\right\}}{1 + 0.216 \dfrac{E^{\mathrm{Ro}-1}}{(1-E)^{\mathrm{Ro}}}\left\{\ln\left(\dfrac{30h}{d_s}\right)J_1 + J_2\right\}}\end{aligned} \tag{4.7}$$

As can be seen from the above equation, q_m/q_t is a function of Ro, h/d_s, and $A = d_n/h$. But since d_n is fixed with the same sampler, q_m/q_t becomes a function of Ro, h, and d_s.

$$q_m/q_t = f'(\mathrm{Ro}, h, d_s) \tag{4.8}$$

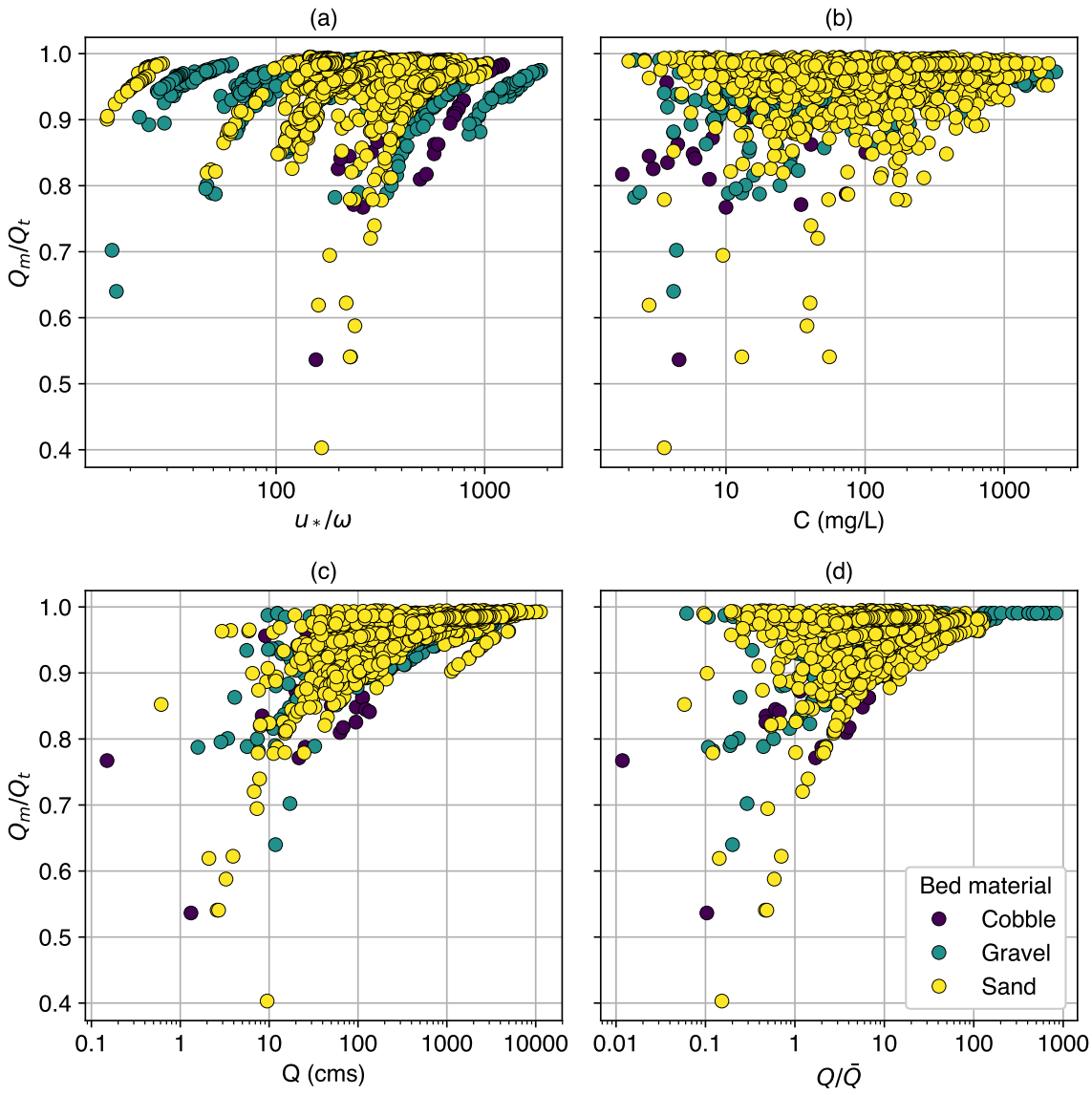

Figure 4.3: Relationships between Q_m/Q_t and (a) u_*/ω, (b) concentration C, (c) discharge Q, and (d) $Q/\bar{Q}$

Fig. 4.4 plots values of the ratio Q_m/Q_t by varying the value of water depth as a function of d_s. The flow depth h is varied from 0.15 to 15 m. The ratio Q_m/Q_t increases with flow depth h, but decreases when Ro increases (or when u_*/ω decreases). When Ro is close to 0, d_s becomes insignificant to Q_m/Q_t, and the measured sediment discharge is more than 90% of the total sediment discharge when depth $h > 1$ meter. When Ro > 2 (or $u_*/\omega < 1.2$), measured load is negligible. It indicates most of the sediment is transported below the nozzle.

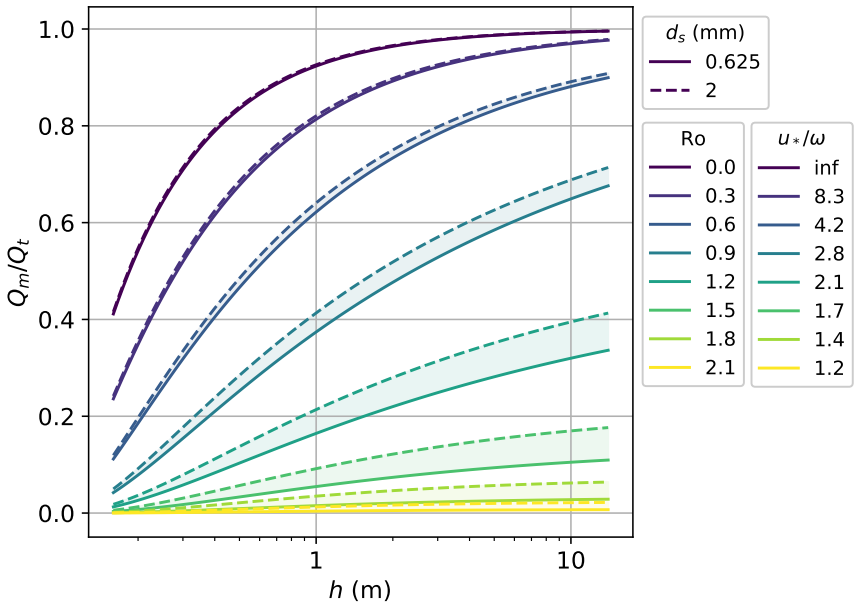

Figure 4.4: Theoretical solution of Q_m/Q_t as a function of h, Ro for sands for SEMEP

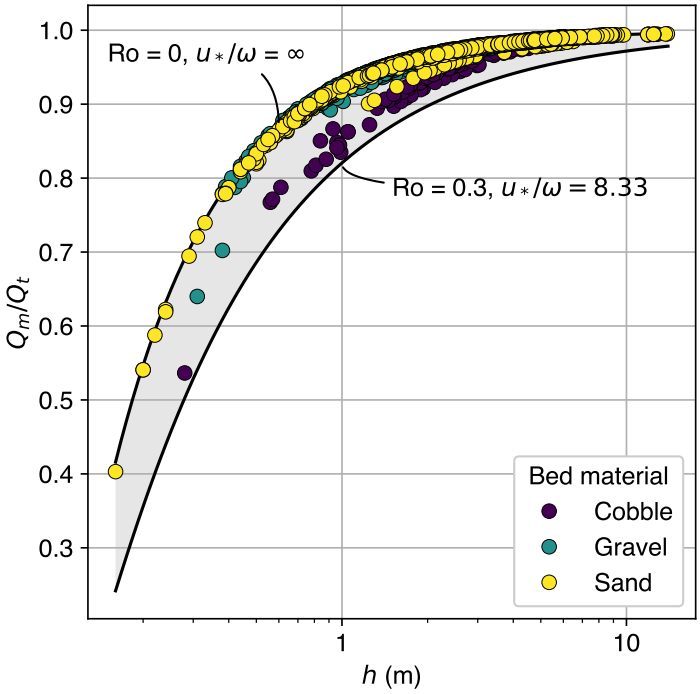

Figure 4.5: All Korean measurements (1,962 points) with the theoretical solution of Q_m/Q_t with Ro = 0 and Ro = 0.3 for $d_s = 2$ mm

Figure 4.5 plots the ratio Q_m/Q_t for all the Korean samples with the theoretical solution as a function of flow depth. The values of Ro of the Korean samples range from 0.001 to 0.16 ($15 < u_*/\omega < 1853$). The low Ro is because the median grain size of the sediment in suspension is silt at all 35 stations (average $d_{50ss} = 0.023$ mm). When Ro and d_s are small and the nozzle height is fixed, Q_m/Q_t becomes only a function of water depth h, and the ratio Q_m/Q_t increases with the flow depth h. Figure 4.5 shows that 90% of the total sediment load is measured when $h > 1$ m in sand and gravel bed rivers.

4.3 Ratio of Suspended to Total Load Q_s/Q_t

Similar to Figure 4.3 I investigated the relation of ratio Q_s/Q_t to (a) u_*/ω, (b) sediment concentration C, (c) flow discharge Q, and (d) the ratio of flow discharge to mean annual discharge $Q/\bar{Q}$ (Figure 4.6). Because the median grain sizes of suspended material are silt at all the stations, the values u_*/ω are generally high. Q_s/Q_t is close to 1 and averages 0.99 in sand bed rivers (Figure 4.6a). For gravel bed and cobble bed rivers, Q_s/Q_t increases as Q, C, or $Q/\bar{Q}$ increases (Figure 4.6b, Figure 4.6c, and Figure 4.6d). The same trend was also observed in Turowski et al. (2010). Furthermore, Q_s/Q_t reduces when the grain size is greater for a given discharge, u_*/ω, or concentration. For gravel bed rivers, Q_s/Q_t varies from 0.871 to 0.999; for cobble bed rivers, Q_s/Q_t ranges from 0.232 to 0.971. Figure 4.6d shows that during high flows ($Q/\bar{Q} > 1$), over 90% of the sediment is transported in suspension for gravel bed and sand bed rivers. This analysis clearly indicates that the predominant mode of sediment transport in Korean rivers is in suspension.

Figure 4.7 shows the ratio of Q_b/Q_t as functions of suspended sediment concentration and suspended load to provide a comparison to Figure 2.7. The commons is that the ratio transported as bedload decreases both with increasing sediment concentration and load. In addition, the ratio becomes similar when the sediment discharge is high ($Q_s > 100$ kg/s).

The total sediment load Q_t is obtained by multiplying the unit sediment discharge q_t by the channel width W. The measured and suspended sediment discharge are obtained in similar fashion. Therefore, the ratio $Q_s/Q_t = q_s/q_t$. Since the unit total sediment discharge $q_t = q_b + q_s$, the ratio

of suspended to total sediment discharge can be derived as follows:

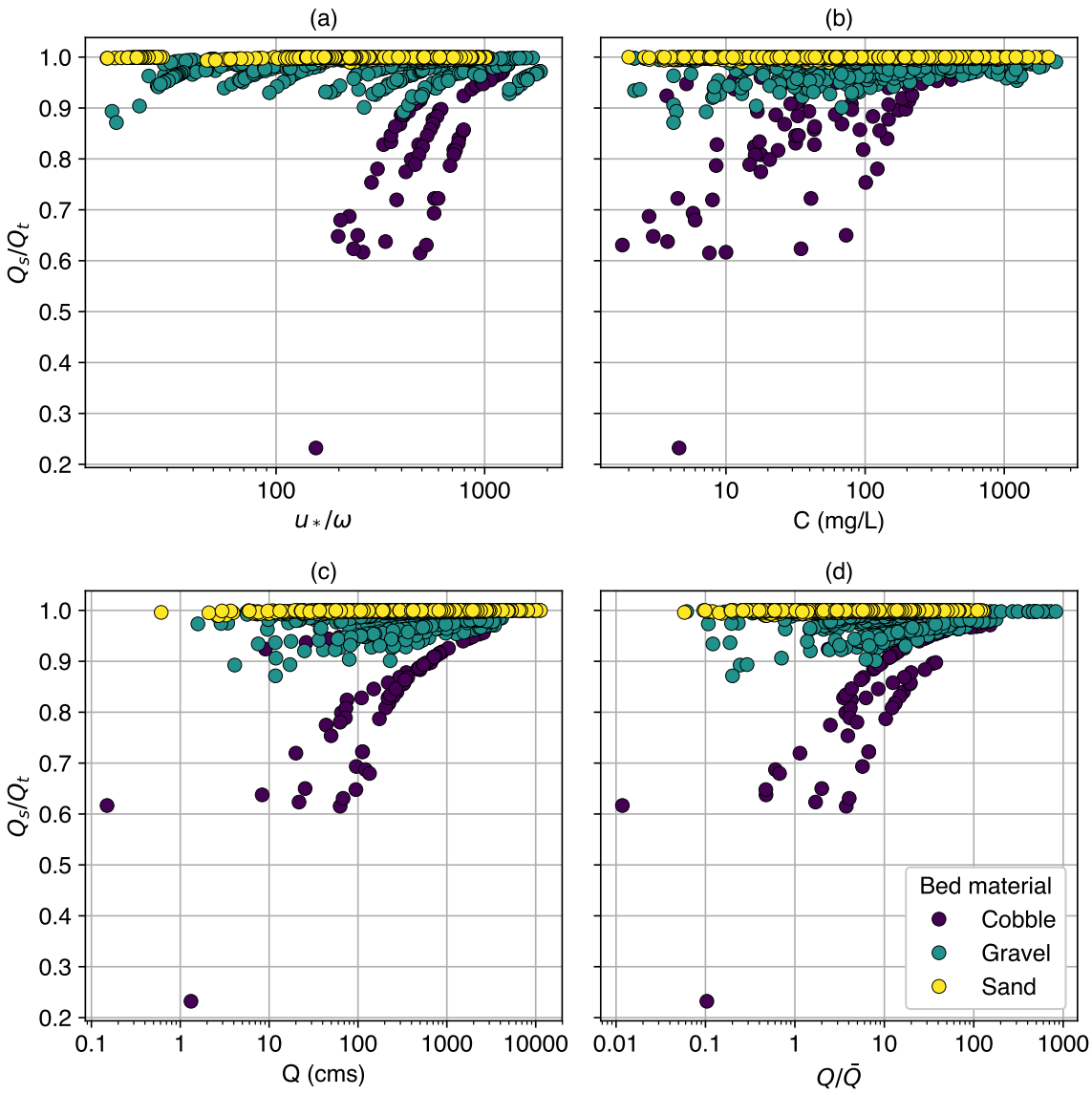

Figure 4.6: Relationships between Q_s/Q_t and (a) u_*/ω, (b) concentration C, (c) discharge Q, and (d) $Q/\bar{Q}$

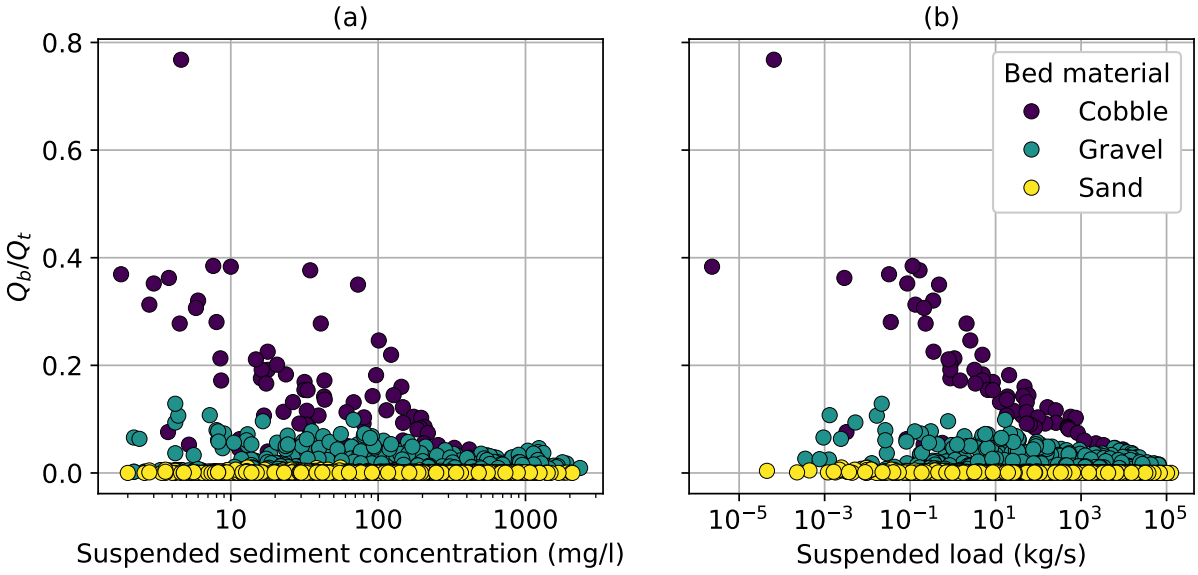

Figure 4.7: The ratio of bedload to total sediment load plotted as a function of: (a) suspended sediment concentration; and (b) suspended sediment transport rate

$$\begin{aligned}\frac{q_s}{q_t} &= \frac{q_s}{q_b + q_s} \\ &= \frac{0.216 q_b \dfrac{E^{\mathrm{Ro}-1}}{(1-E)^{\mathrm{Ro}}} \left\{ \ln\left(\dfrac{30h}{d_s}\right) J_1 + J_2 \right\}}{q_b + 0.216 q_b \dfrac{E^{\mathrm{Ro}-1}}{(1-E)^{\mathrm{Ro}}} \left\{ \ln\left(\dfrac{30h}{d_s}\right) J_1 + J_2 \right\}} \\ &= \frac{0.216 \dfrac{E^{\mathrm{Ro}-1}}{(1-E)^{\mathrm{Ro}}} \left\{ \ln\left(\dfrac{30h}{d_s}\right) J_1 + J_2 \right\}}{1 + 0.216 \dfrac{E^{\mathrm{Ro}-1}}{(1-E)^{\mathrm{Ro}}} \left\{ \ln\left(\dfrac{30h}{d_s}\right) J_1 + J_2 \right\}}\end{aligned} \tag{4.9}$$

It is interesting to observe that the ratio of suspended to total load q_s/q_t only changes with two variables now, e.g. h/d_s and Ro:

$$q_s/q_t = f(h/d_s, \mathrm{Ro}) \tag{4.10}$$

As Eq. (4.9) shown that the ratio of suspended to total sediment discharge Q_s/Q_t is only a function of h/d_s and Ro. The analytical solution of Eq. (4.9) is plotted in Fig. 4.8. Fig. 4.8 shows the ratio Q_s/Q_t at constant values of Ro while varying the value of h/d_s. The ratio of Q_s/Q_t increases when the values of Ro decrease.

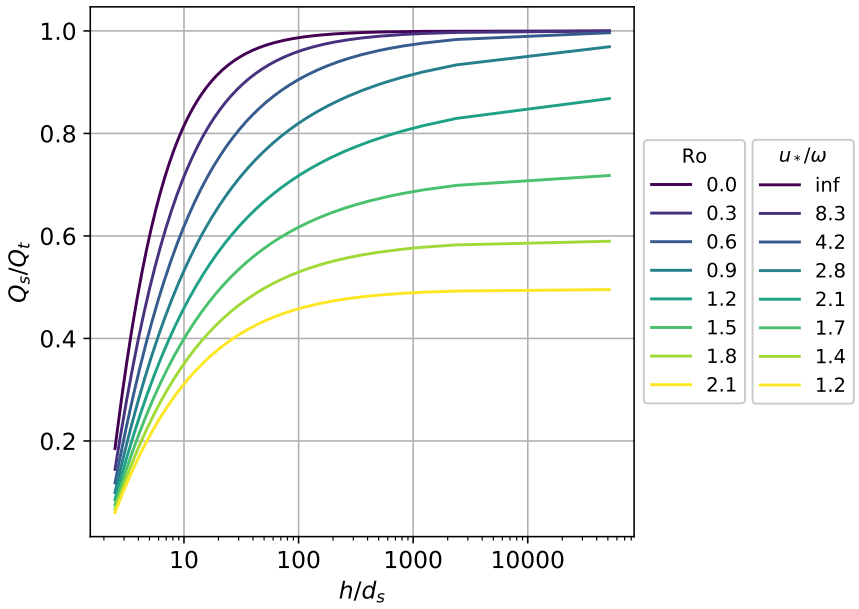

Figure 4.8: Theoretical solution of Q_s/Q_t as a function of h/d_s and Ro for SEMEP

Fig. 4.9 plots the analytical solution of Q_s/Q_t with the measurements. Due to the materials in suspension being fine, the values of Ro are small (Ro < 0.16) and therefore the change of Ro only results in little change in Q_s/Q_t. All of the measurements in South Korea are within the theoretical solution Ro = 0 and Ro = 0.3. The suspended load is more the 80% of the total sediment load when $h/d_s > 18$.

4.4 Discussion and Conclusion

1. SEMEP outperformed MEP in terms of stability, consistency, and accuracy. SEMEP managed to calculate bedloads from 1,962 measurements, while MEP calculated 1,808 of measurements. The original MEP method requires at least two overlapping bins between suspended materials and bed materials. Errors sometimes occurred when creating the power relationship between the Rouse number and fall velocity. Instead of overlapping bins, the Rouse number for the SEMEP is estimated by the median grain size of the bed material. With values of u_*/ω in the range between 10 and 2,000, the results showed that the ratio between suspended load and total load calculated by MEP varied from 10^{-7} to 20. In reality,

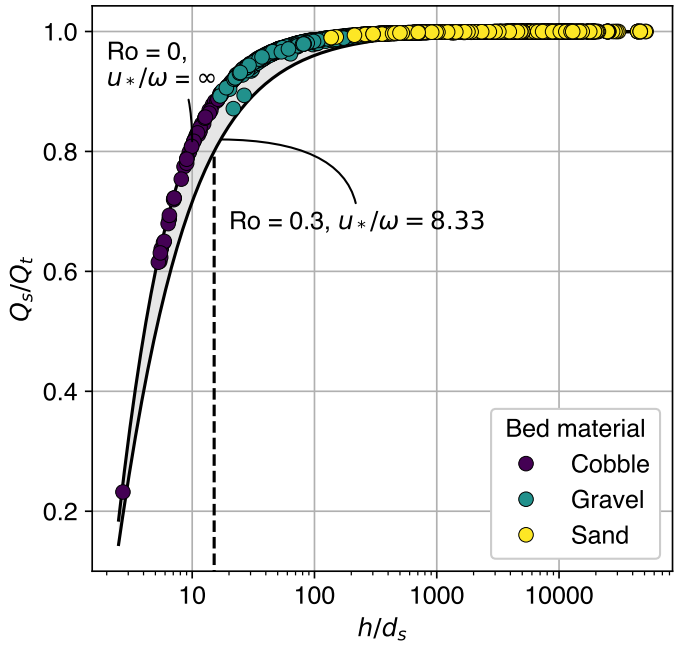

Figure 4.9: All Korean measurements (1,962 points) with the theoretical solution of Q_s/Q_t with Ro = 0 and Ro = 0.3

this ratio should never be greater than 1, which raises suspicion regarding the accuracy of the original MEP method. On the other hand, Figure 2.13 the error of the SEMEP is less than 25% when $u_*/\omega > 5$ (Ro < 0.5). For this reason, the SEMEP calculations are considered more versatile and more accurate.

2. The ratio of measured sediment discharge is greater than 80% when $Q/\bar{Q} > 4$. Based on the theoretical analysis, the ratio of measured to total load is a function of flow depth, grain size and Rouse number. The ratio increases as the flow depth increases but decreases when the Rouse number increases. At the same Rouse number and same flow depth, larger bed material has a higher measured ratio. This relationship has practical applications: because of the fine suspended materials in South Korea and the corresponding low Rouse number ($Ro < 0.16$), the measured sediment load is more than 90% of the total sediment load when $h > 1$ m for sand and gravel bed rivers.

3. The results of SEMEP calculations showed the suspended load accounts for 99% of the total sediment load in sand bed rivers in South Korea. For gravel and sand bed rivers, over 90% of the sediment is in suspension when $Q/\bar{Q} > 10$. The theoretical analysis shows that Q_s/Q_t is a function of h/d_s and Ro. The value of Q_s/Q_t increases when h/d_s increases, but decreases when Ro increases. Because the values of Ro are low in the Korean rivers, the ratio Q_s/Q_t becomes a function of only h/d_s. The suspended load is more the 80% of the total sediment load when $h/d_s > 18$. For 2 mm sand, this corresponds to $h > 3.6$ cm.

Chapter 5

Sediment Yield and Watershed Area

To explore the patterns of river flow and sediment discharge, I use the river measurements in Section 3.3. Discharge and sediment measurements from 35 gaging stations are used to quantify the magnitude and frequency of the annual amounts of flow and sediment discharge across South Korea. Flow duration curves and sediment rating curves are used to define the flow-exceedance probability relationship and the flow-sediment load relationship. Using the product of flow duration curve and sediment rating curve, the mean annual sediment yield as well as the discharge-cumulative sediment yield can be calculated. The role of watershed area in river flow and sediment transport is also explored.

5.1 Flow-Duration/Sediment-Rating Curve Method

5.1.1 Flow Duration Curve

The daily discharge from 2005 to 2014 are provided. To obtain the flow duration curve, the discharge values are sorted from the largest to the smallest. Next, I assigned each discharge value a rank (m), starting with 1 for the largest discharge value. The exceedance probability (P) can be calculated as follows:

$$P = 100[m/(N+1)] \tag{5.1}$$

in which P is the probability that a given flow will be equalled or exceeded (% of time), m is the ranked position on the listing, and N is the number of events for period of record.

5.1.2 Sediment-Rating Curve

In last chapter, I calculated the total sediment discharges from the suspended load measurements by SEMEP for 1,962 records for 35 stations. The total sediment discharges are used to construct the discharge-total sediment discharge relationship for each station. There are more than

20 different methods for fitting sediment rating curves, the most commonly used sediment rating curve is a power function (Walling 1978; Asselman 2000; Lee and Lee 2010; Julien 2010):

$$Q_t = \bar{a}Q^{\bar{b}} \tag{5.2}$$

where Q_t is the total sediment discharge in tons/day, Q is flow discharge in m^3/s, $\bar{a}$ and $\bar{b}$ are the regression coefficients. The ordinary least squares regression is used to estimate the parameters $\bar{a}$ and $\bar{b}$. As many authors have pointed out, the R^2 statistic overestimates the linear association between these variables because Q_t is a product of Q and suspended sediment concentration. Despite this difficulty, sediment rating curves are still commonly used in engineering and resource planning.

5.1.3 Flow-Duration/Sediment-Rating Curve Method

Integration of sediment rating curve and flow duration curve gives an average of sediment yield. Because the flow records are usually available over longer periods than sediment records, this method allows the expansion of a relatively small amount of sediment data to the longer period of discharge (Sheppard 1965). Table 5.1 provides an example of the use of the flow-duration-sediment-rating curve method. The flow duration curve is divided into bins as shown in column (1). Column (2) is the midpoint of each bin and column (3) is the interval of each bin. The discharge of each midpoint can be interpolated from the flow duration curve (column 4), and the sediment discharge is determined from the sediment rating curve (column 5). In this example, we have the sediment rating curve of H1 as $Q_t = 0.011Q^{1.92}$. Column (6) is the product of column (3) and column (4) and the sum of it is the mean annual discharge in m^3/s. Similarly, column (7) is the product of column (3) and column (5) and the sum of it is the mean annual sediment yield in tons/day. The calculated mean discharge, sediment yield, and specific sediment yield for each station are presented in Table 5.2.

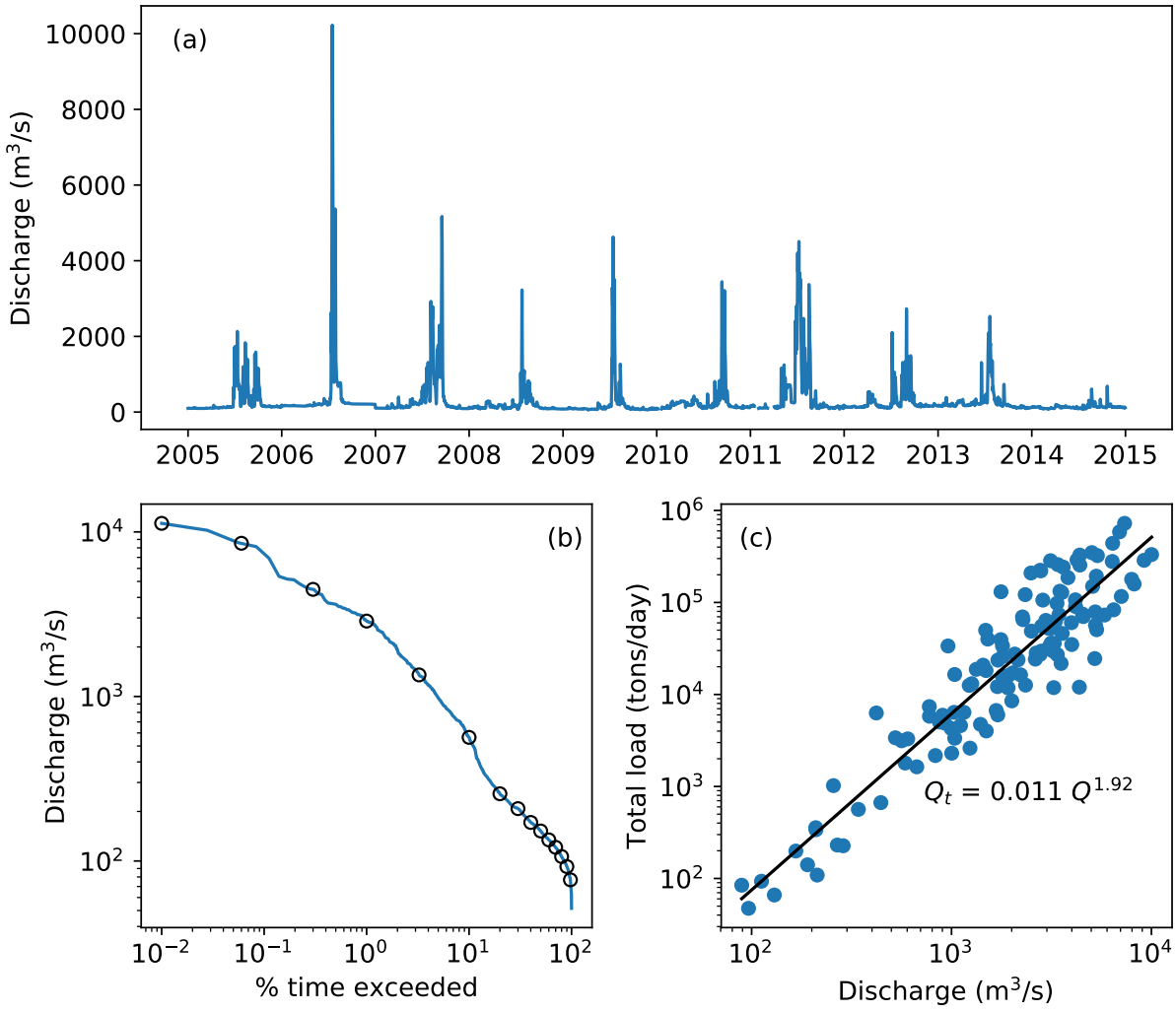

Figure 5.1: (a) Daily mean discharge from 2005/1/1 to 2014/12/31, (b) flow duration curve, and (c) sediment rating curve of Yeoju station (H1)

Table 5.1: Total sediment load and specific sediment yield at station H1 based on SEMEP

Time intervals (%) (1)	Interval midpoint (%) (2)	Interval ΔP (%) (3)	Discharge Q (m^3/s) (4)	Q_t (tons/day) (5)	$Q \times \Delta P$ (m^3/s) (6)	$Q_t \times \Delta P$ (tons/day) (7)
$0 \sim 0.02$	0.01	0.02	11,272	641,949	2.3	128
$0.02 \sim 0.1$	0.06	0.08	8,529	376,168	6.8	301
$0.1 \sim 0.5$	0.3	0.4	4,475	109,317	17.9	437
$0.5 \sim 1.5$	1	1	2,871	46,705	28.7	467
$1.5 \sim 5$	3.25	3.5	1,352	11,020	47.3	386
$5 \sim 15$	10	10	564	2,064	56.4	206
$15 \sim 25$	20	10	256	455	25.6	45
$25 \sim 35$	30	10	208	305	20.8	31
$35 \sim 45$	40	10	172	211	17.2	21
$45 \sim 55$	50	10	152	168	15.2	17
$55 \sim 65$	60	10	134	132	13.4	13
$65 \sim 75$	70	10	121	108	12.1	11
$75 \sim 85$	80	10	106	85	10.6	8
$85 \sim 95$	90	10	92	65	9.2	6
$95 \sim 100$	97.5	5	77	45	3.8	2
Total		100			287	2,080

Table 5.2: Mean discharge, sediment yield, and specific sediment yield for the 35 watersheds

Watershed	Area (km)	Mean discharge (m^3/s)	Sediment yield (tons/year)	Specific sediment yield (tons/km^2·year)
H1	11,074	287	760,009	69
H2	283	10	130,545	461
H3	1,346	48	317,545	236
H4	173	5.6	47,970	277
H5	519	14	94,309	182
H6	8,823	200	191,949	22
H7	307	13	29,825	97
N1	979	15	44,775	46
N2	1,541	26	45,866	30
N3	10,913	196	200,824	18
N4	9,407	155	388,567	41
N5	11,101	201	518,131	47
N6	9,533	129	45,044	4.7
N7	20,381	369	1,029,480	51
N8	2,999	70	87,757	29
N9	1,512	24	84,472	56
N10	175	3.0	7,033	40
N11	614	17	19,923	32
N12	1,318	17	34,998	27
N13	1,239	31	64,178	52
N14	750	15	31,459	42
G1	606	15	59,891	99
G2	6,275	141	573,746	91
G3	1,850	40	210,827	114
G4	258	6.1	12,598	49
G5	208	4.6	13,970	67
S1	1,269	18	42,222	33
S2	1,788	29	84,320	47
S3	3,818	62	138,235	36
S4	128	3.9	3,727	29
Y1	190	6.5	15,905	84
Y2	2,039	59	197,210	97
Y3	668	22	99,040	148
Y4	580	13	22,224	38
Y5	552	12	16,885	31

5.2 Water and Sediment Discharge

5.2.1 Water Discharge

The mean annual discharge, or annual discharge (Q_a) is calculated as the sum of the product of column (3) and column (4) in Table 5.1. The annual Runoff (R) is defined as annual discharge normalized by watershed area: $R = Q_a/A$. The mean discharge ($\bar{Q}$) is the mean value of the daily discharge. Runoff is found inversely related to watershed area (Figure 5.2a). The runoff of the stations in Han River are higher for a given area compared to other watersheds. The mean discharge equivalent to the annual discharge (correlation coefficient 0.99). The mean annual discharge generally increases with watershed area (Figure 5.2b). The annual discharge Q_a and mean discharge $\bar{Q}$ can be, therefore, expressed as functions of watershed area:

$$Q_a = 3.75 \times 10^{-4} A^{0.9} \tag{5.3}$$

$$\bar{Q} = 0.045 A^{0.9} \tag{5.4}$$

$$R = 0.376 A^{-0.1} \tag{5.5}$$

where Q_a is in km^3/year, $\bar{Q}$ is in m^3/s, R is in mm/year, and A is watershed area in km^2. The slope 0.9 is close to what is reported in Syvitski and Milliman (2007), who found the slope = 0.8 for the global database of 488 rivers.

By dividing the discharge by the mean discharge $\bar{Q}$, the dimensionless parameter $Q^* = Q/\bar{Q}$ is used for the comparison of the flow duration curves between different watersheds. There were no significant differences in the five major river watersheds. Instead, difference between small watersheds and large watersheds is found. Figure 5.3 shows the normalized flow duration curves. The watersheds that are smaller than 500 km^2 or larger than 5,000 km^2 are highlighted. The small watersheds are G4, G5, H2, H4, H7, N10, and Y1, and large watersheds are G2, H1, H2, N4, N5, N6, and N7. The small watersheds have higher Q^* for the high flow , and have lower Q^* for low flow. The result demonstrates that watershed size is one of the key factors for the shape of flow duration curve, even though the topography and land use might be quite different among

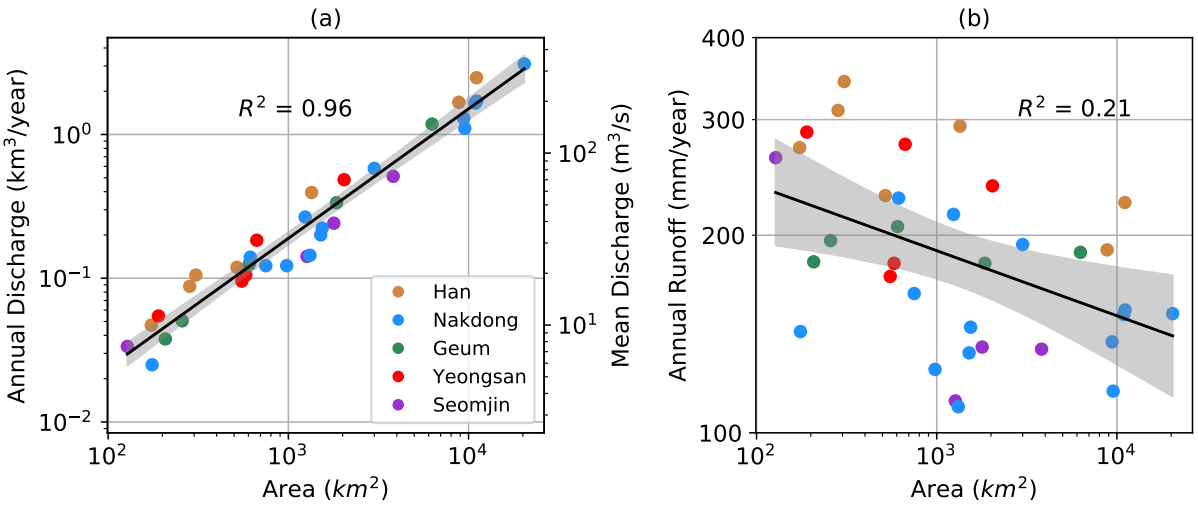

Figure 5.2: (a) Watershed area vs annual runoff (b) watershed area versus annual discharge and mean discharge

watersheds with similar sizes. H4 is a fairly mild small watershed (relief ratio 14.9 m/km) and the land use is mainly agriculture (48%). It has a flow duration curve shape resembling that of S4, which is a steep, relatively pristine watershed (67% forest). Figure 5.4 shows the relationships of watershed area with Q^* at P = 0.1% and 50% ($Q^*_{0.1}$ and Q^*_{50}). $Q^*_{0.1}$ generally decreases when area increases (log-linear Pearson correlation r = -0.50). The values of $Q^*_{0.1}$ for small watersheds range from 44 to 62, compared to the range of large watersheds, 14 to 32. On the other hand, Q^*_{50} show positive relationship with watershed area (log-linear Pearson r = 0.53). The slope, defined as the absolute difference of Q^* between P=1% and P=10%, flow duration curve also indicates the time of watershed responses to precipitation inputs. The steeper the slope implies storm runoff enters the channel more quickly (Yadav et al. 2007; Wohl 2014). This reflects that the hydrographs of small watersheds are sharper and have shorter lag time between hyetograph and hydrograph. As the river goes downstream, the floodwave attenuates. The hydrographs expect to have attenuated peak and longer lag time.

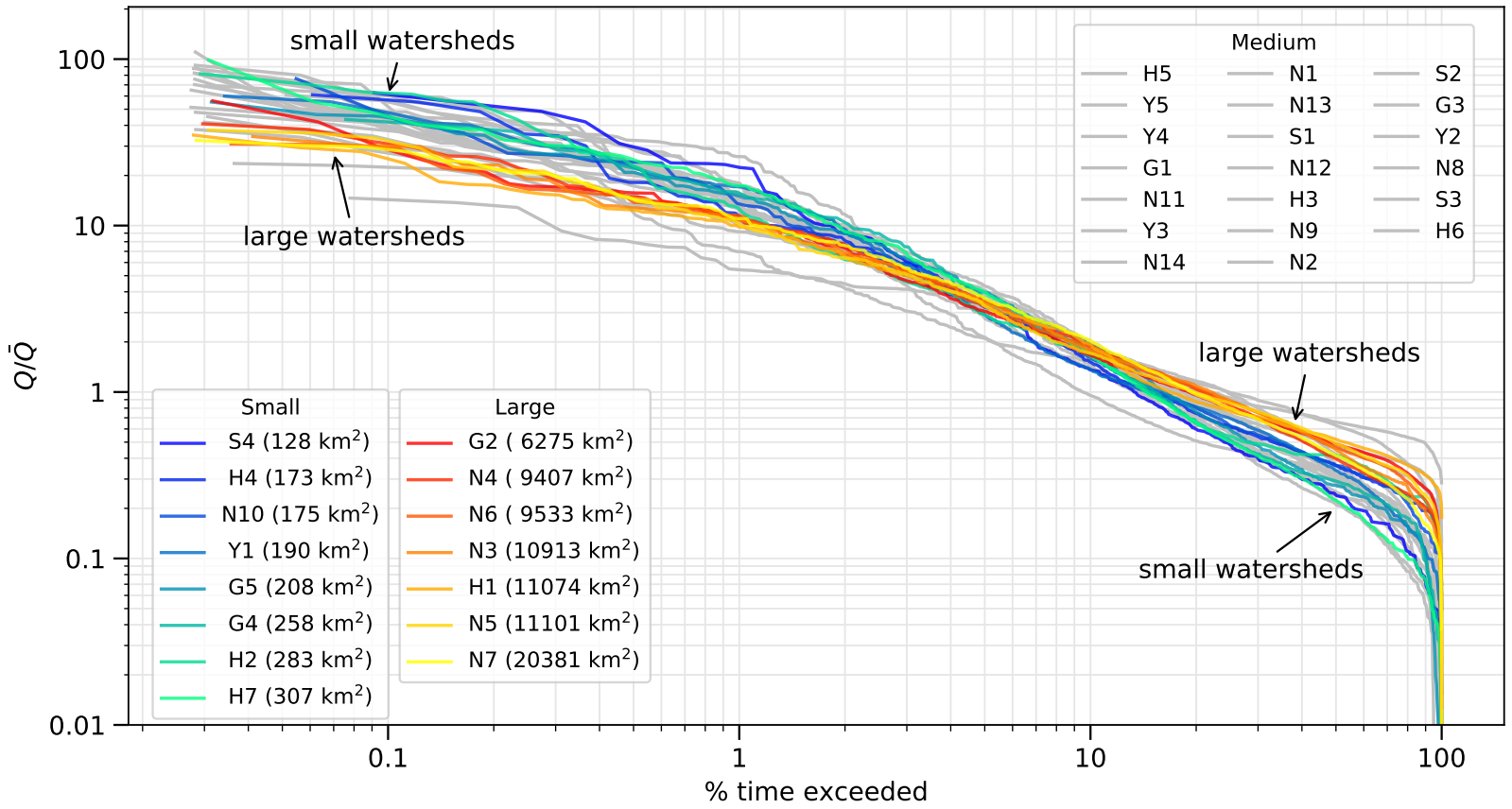

Figure 5.3: Normalized flow duration curves derived from daily discharges at the gauging stations in South Korea. The blue-ish lines are watersheds smaller than 500 km^2, red-ish lines are watersheds larger than 5,000 km^2, and gray lines are watershed sizes between 500 and 5,000 km^2

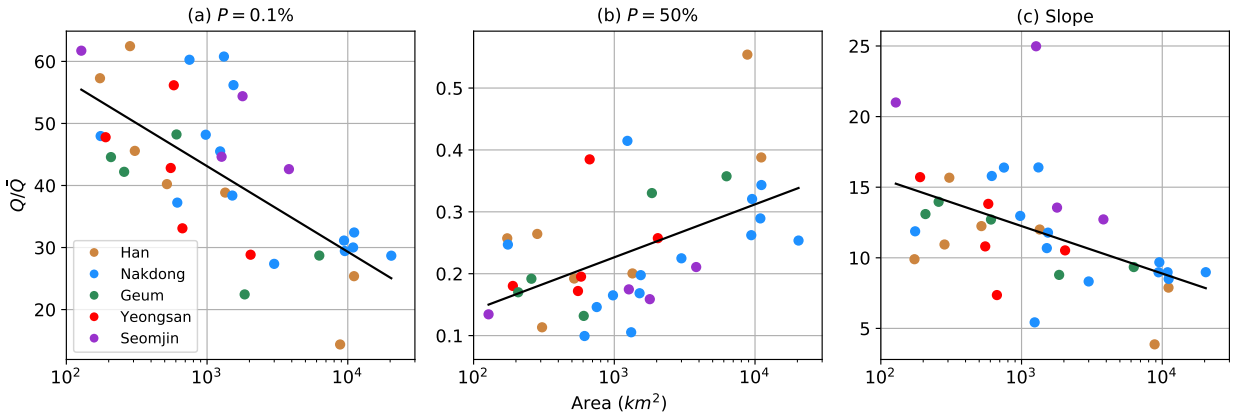

Figure 5.4: $Q^*_{0.1}$ and Q^*_{50} vs watershed area

5.2.2 Sediment Rating Curve for Total Load

Total sediment discharge is calculated by SEMEP. Total sediment discharge Q_t showed a positive and statistically significant relation with discharge Q ($p < 0.01$). Table 5.3 lists the coefficient of sediment rating curves for each station. The exponent $\hat{b}$ ranges from 0.83 to 2.88, with an average of 1.73. The exponent of G5 is especially high. Although the coefficient of determination R^2 is quite high, 95%, there are 7 samples of sediment measurement available. More samples are needed to justify that the sediment content of G5 is higher than other regions. R^2 of N10 and G3 are relatively low. Large scatter between sediment concentration C and discharge Q before and after 2012 was found for N10, which is the year of Four Rivers Restoration Project was implemented. The sediment concentration of N4 and N6 also reduced after 2012.

Figure 5.6 shows the relationship between the coefficients and area. $\bar{a}$ generally decreases with the increase of watershed area, though $\bar{b}$ is fairly constant in the range of 1.5 to 2.0. The average is 1.72. It indicates that at a given discharge, the sediment discharge reduces when watershed area goes up, and the difference is up to 2 orders of magnitude for the smallest and largest watersheds. A similar trend can also be seen in Figure 5.5. The small watersheds are at the left side of the figure and large watersheds are at the right side. The coefficient $\bar{a}$ is often interpreted as an index of erosive severity. A high value of $\bar{a}$ indicates abundance of weathered materials. The exponent $\bar{b}$

represents the erosive and transport power of the channel (Asselman 2000; Atieh et al. 2015). This may reflect that the small watersheds have more available sediment to be transported or higher sediment delivery ratio. The small watersheds S4, G5, G4, H2 are steep, mountainous watersheds, and H4 and Y1 are highly developed into agriculture, 48% of area are used by agriculture in H4 and 40% for Y1.

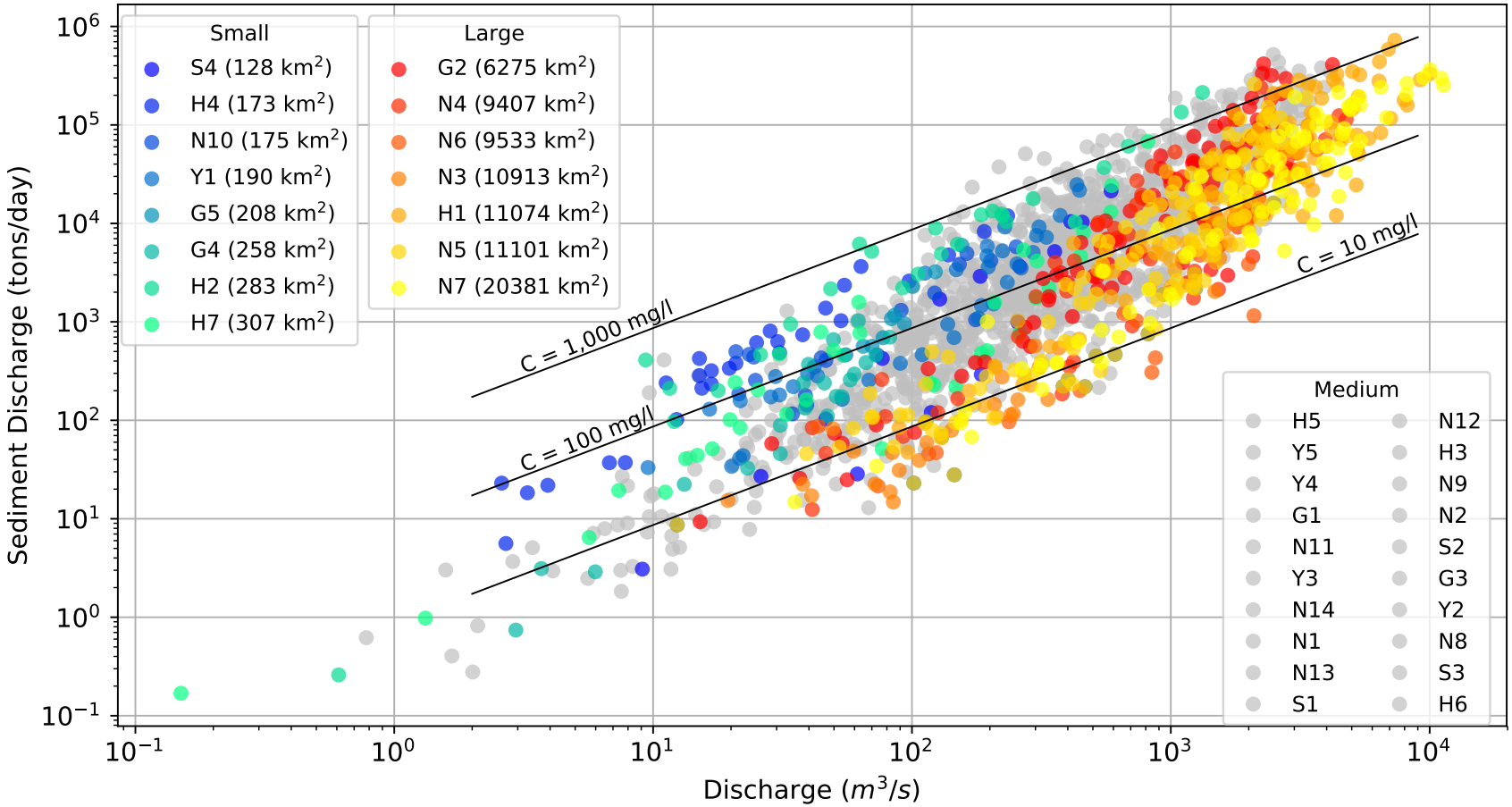

Figure 5.5: Sediment rating curves for small and large watershed areas

Table 5.3: Coefficient and Exponent for sediment rating curve

Station	Area (km^2)	$\bar{a}$	$\bar{b}$	R^2	Sample #	Sampled Year
S4	128	0.022	2.097	0.89	15	1
H4	173	2.921	1.567	0.96	29	2
N10	175	9.317	0.832	0.49	41	2
Y1	190	0.525	1.643	0.90	40	2
G5	208	0.003	2.889	0.95	15	1
G4	258	0.120	1.954	0.93	22	2
H2	283	2.479	1.593	0.95	26	2
H7	307	1.217	1.371	0.88	37	2
H5	519	0.362	1.815	0.86	51	3
Y5	552	0.038	2.001	0.93	75	4
Y4	580	0.065	1.886	0.93	89	4
G1	606	0.308	1.739	0.91	65	4
N11	614	0.085	1.740	0.87	57	3
Y3	668	1.225	1.545	0.85	37	2
N14	750	0.121	1.740	0.83	57	3
N1	979	0.341	1.644	0.87	68	4
N13	1239	2.147	1.225	0.63	70	3
S1	1269	0.049	1.875	0.99	15	1
N12	1318	0.730	1.400	0.87	28	1
H3	1346	0.013	2.111	0.85	54	3
N9	1512	1.151	1.441	0.77	66	3
N2	1541	0.116	1.666	0.87	57	3
S2	1788	0.046	1.880	0.94	29	2
G3	1850	5.475	1.218	0.41	51	3
Y2	2039	0.269	1.632	0.83	119	5
N8	2999	0.579	1.341	0.69	91	4
S3	3818	0.068	1.742	0.91	124	6
G2	6275	0.029	1.896	0.86	137	7
H6	8823	0.004	2.065	0.84	30	2
N4	9407	0.041	1.778	0.80	58	3
N6	9533	0.068	1.442	0.79	16	1
N3	10913	0.020	1.739	0.93	33	2
H1	11074	0.011	1.916	0.86	123	7
N5	11101	0.013	1.917	0.84	169	9
N7	20381	0.007	1.937	0.91	88	5

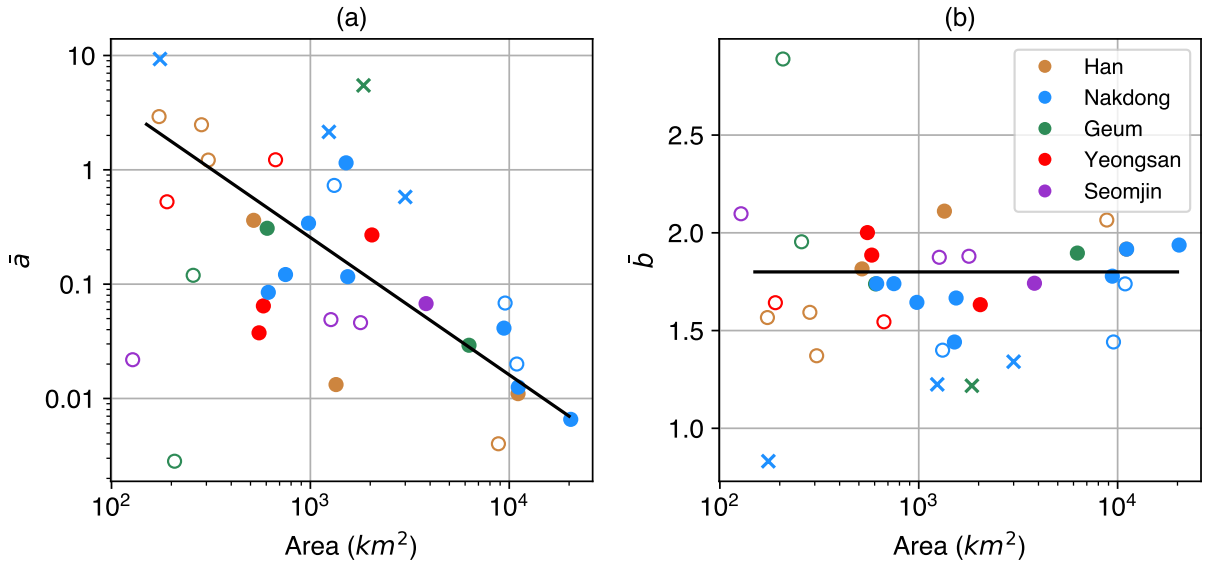

Figure 5.6: (a) $\bar{a}$ vs Area, (b) $\bar{b}$ vs Area (Open circle: record of measurement is less than 3 years; Solid circle: record of measurement equal or more than 3 years; $\times$: $R^2 < 0.7$)

5.2.3 Sediment Yield

The annual sediment yield is estimated by flow-duration-sediment-rating curve method (Table 5.2). The sediment yield ranges from 3,727 (S4) to 1,029,480 (N7) tons/year, generally increasing with watershed area (Figure 5.7). The SSY varies from 5 tons/km^2·year to 461 tons/km^2·year. H2 watershed has the highest SSY. This might be due to the fact that H2 has the highest percentage of bare land (5%) among all watersheds. The sediment yield at N6 and N3 are significantly lower than the stations N4 and N5. Because N4 located at the upstream of N6 and N3, and N5 is at the downstream of N6 and N3, it is reasonable to believe the SSY at N6 and N3 are underestimated. Another reason is that N3 and N6 have few sediment samples. In addition, the samples of N3 and N6 are only available after 2012. In fact, the sediment concentrations are found decreasing after 2012 for some stations in Nakdong River (i.e., N4, N5, and N10).

Figure 5.7 shows the relationships between sediment yield, SSY and watershed area. Though highly scattered, a negative trend between SSY and drainage area is found. The sediment yield are functions of watershed area as shown below:

$$SY = 300A^{0.76}, R^2 = 0.66 \tag{5.6}$$

$$SSY = 300A^{-0.24}, R^2 = 0.16 \tag{5.7}$$

The RMSE of the regression of SSY is 86 tons/km^2·year. The MAPE is 75.2% We found significant improvement in the prediction of the SSY by using watershed area as the predictor variable.

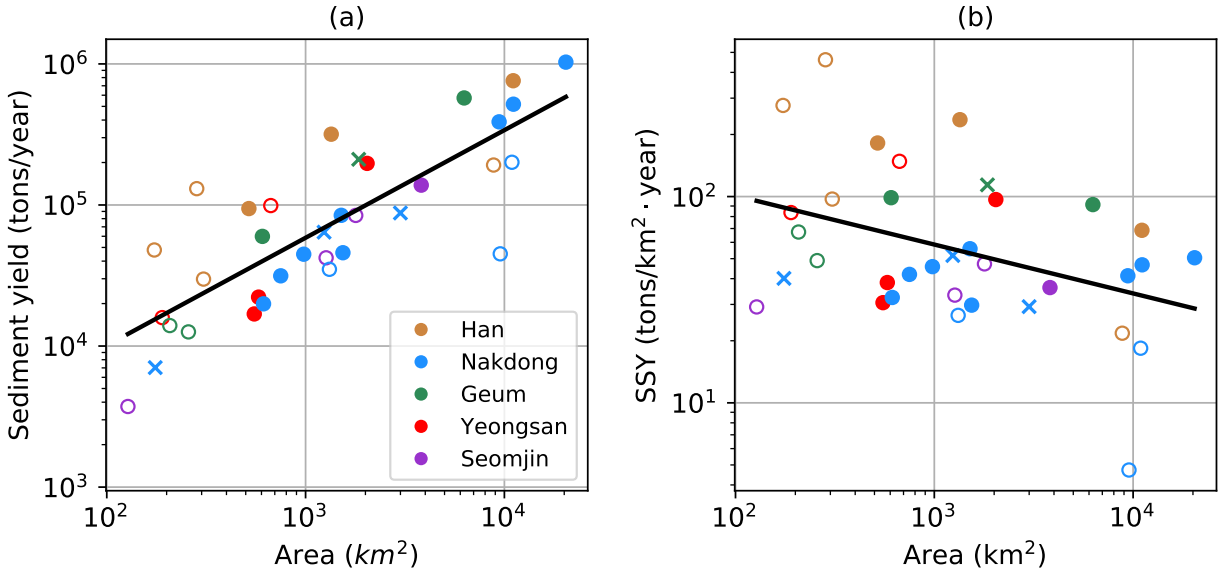

Figure 5.7: Regression between specific sediment yield and watershed area (Open circle: record of measurement is less than 3 years; Solid circle: record of measurement equal or more than 3 years; ×: $R^2 < 0.7$)

5.2.4 Cumulative Distribution Curves for Flow and Sediment

Figure 5.8 plots the cumulative distribution functions of the sediment load at these stations. According to the analysis in Chapter 4, most of the sediment is measured when $Q/\bar{Q} > 1$, so the results here should be fairly accurate. The figure highlights most sediment is transported during short periods of time. Only 2% to 15% of sediment is transported with the flow smaller than the mean discharge. A noticeable trend is small watersheds have higher half yield discharge ($Q^*_{s50} = Q_{s50}/\bar{Q}$), i.e., discharge of 50% of the sediment yield transported. Half of the annual

sediment yield is transported at discharges 4.4 times to 44 times the mean discharge. For the small watersheds, half of the sediment yield is generated during the flow larger than at least 15 times the mean discharge. In comparison, for large watersheds, the half yield discharges less than 15 times the mean discharge. Figure 5.10 plots the discharges that transport 25%, 50%, and 75% of annual sediment load (denoted by Q^*_{s25}, Q^*_{s50}, and Q^*_{s75}, respectively) against watershed area. It emphasizes the role of flood in the transport sediment load, especially for the smaller watersheds. The flow at H6 is regulated by the reservoir, and the influence of dams on sediment transport can be observed in Figure 5.8 and Figure 5.10. Alternatively, the frequency of sediment yield can be examined with flow duration curve Figure 5.9. For small watersheds, 80% of total load was carried in the time ranges between 0.5% to 4.5%, and for large watersheds, 80% of total load was carried in the time ranges between 2.6% to 15.1%.

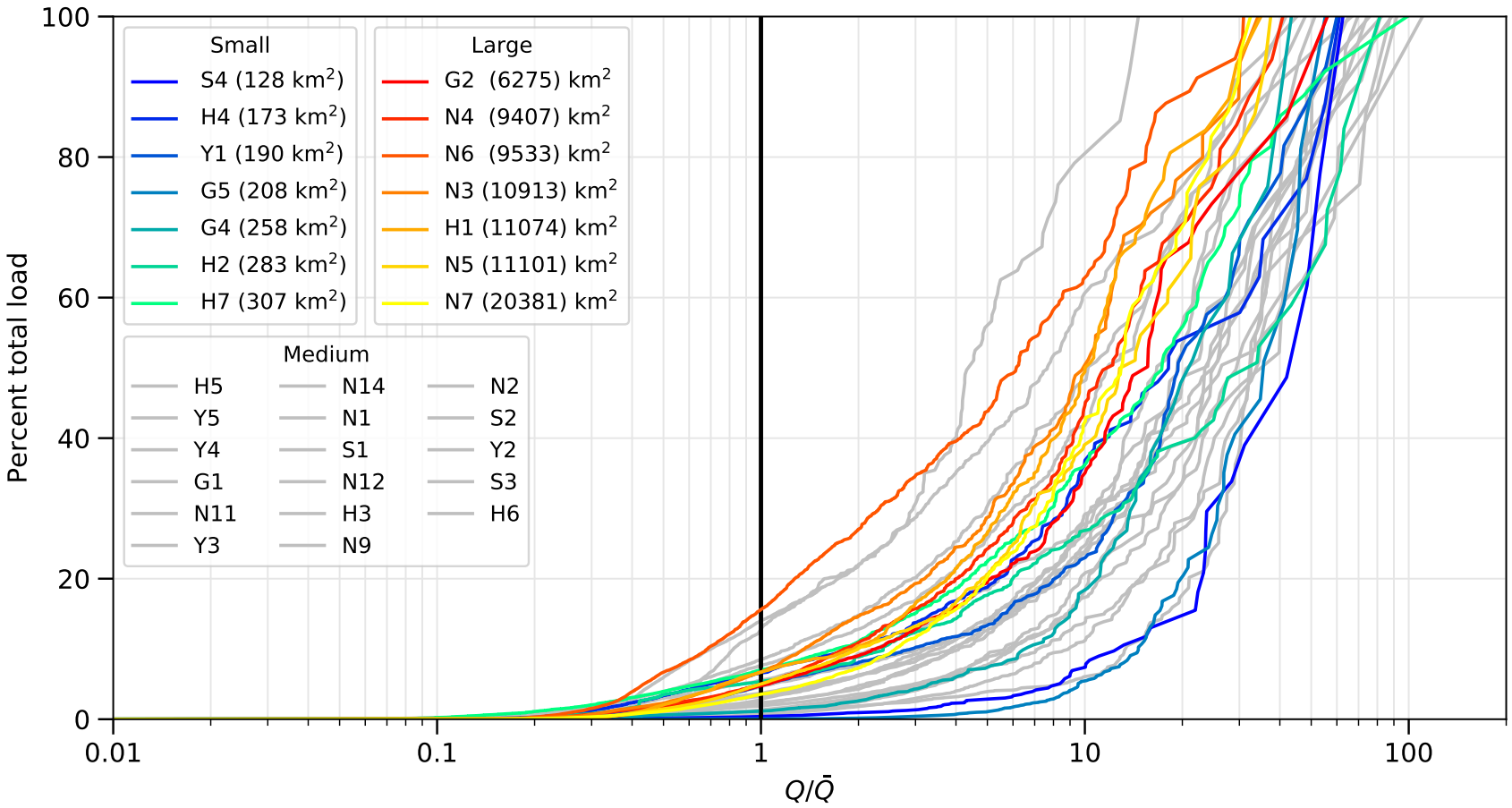

Figure 5.8: Cumulative distribution function of sediment load (only sediment rating curve $R^2 > 0.7$ are shown)

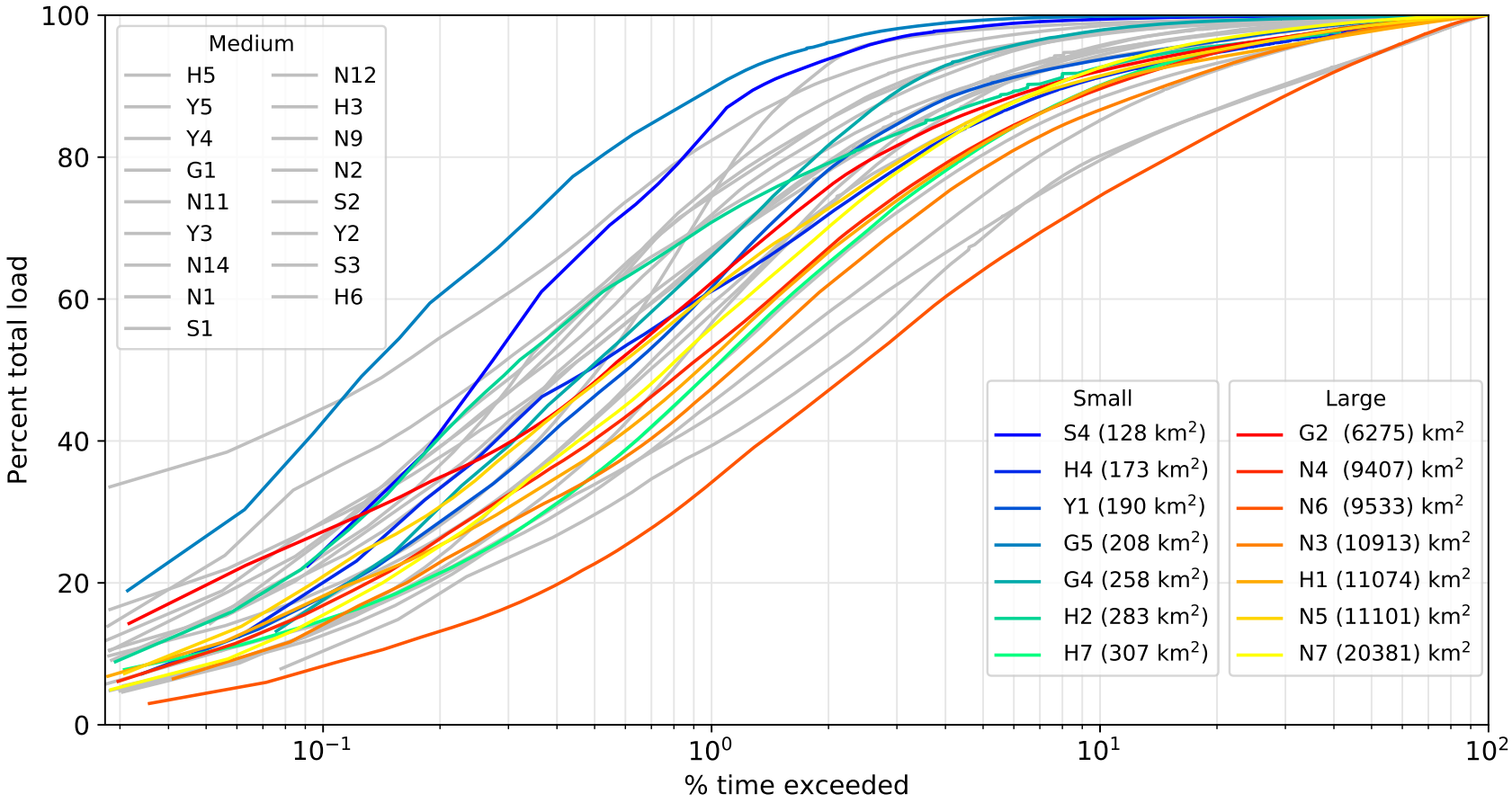

Figure 5.9: Cumulative distribution function of sediment load (only sediment rating curve $R^2 > 0.7$ are shown)

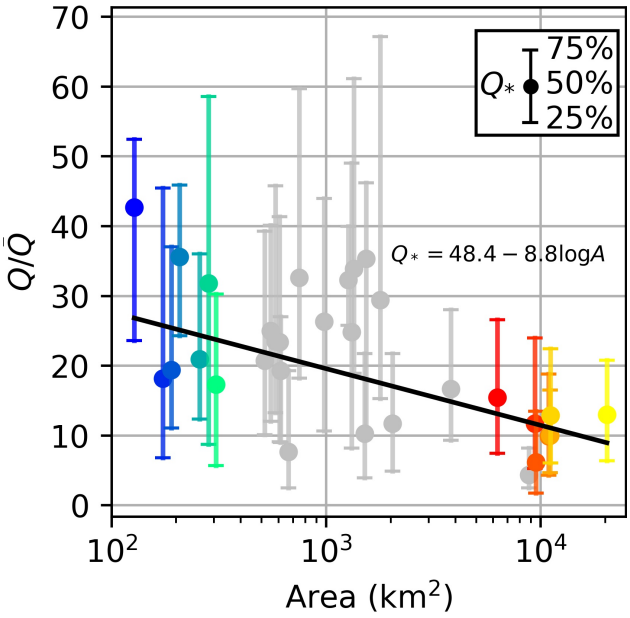

Figure 5.10: Relationships of Q^*_{s25}, Q^*_{s50}, and Q^*_{s75} with watershed area.

5.3 Discussion and Conclusion

Several hydrological variables (i.e., mean annual flow, mean daily flow, sediment yield, and specific sediment yield) correlate with watershed area. The watershed areas of studied watersheds range from 128 to 20,381 km^2. The differences between the watersheds less than 500 km^2 and larger than 5,000 km^2 are highlighted. For normalized flow duration curves, $Q/\bar{Q}$ decreases from 60 to 25 when watershed area increases from 100 to 21,000 km^2 at exceedance probability equals 0.1%. The opposite trend is found for more frequent flows. At exceedance probability equals 50%, $Q/\bar{Q}$ decreases from 15 to 8 as watershed area increases from 100 to 21,000 km^2. This indicates that the discharges in small watersheds increase dramatically during events. The flood attenuates as it goes downstream.

At a given discharge, the sediment discharge of a small watershed is one order of magnitude larger than for a large watershed on average. The analysis of cumulative distribution curves for sediment shows that sediment is mostly transported during floods, especially for small watersheds.

The value of $Q/\bar{Q}$ for the half yield discharge (half of the sediment transported) decreases from 26 to 9 when the watershed area increases from 100 to 21,000 km^2.

The specific sediment yield can be predicted as a function of watershed area: $SSY = 300A^{-0.24}$. The prediction errors are significant less than the KICT model and Yoon's model (RMSE = 86 tons/km^2·year and MAPE = 75%). The inverse relationship between the specific sediment yield and drainage area agree with previous studies (Gurnell et al. 1996; Higgitt and Lu 1996; Milliman and Syvitski 1992; Kane and Julien 2007; Vanmaercke et al. 2014). The common explanation of this inverse relationship is because sediment is more likely to be deposited as it goes downstream into a milder slope and a wider floodplain (Walling and Webb 1983). Figure 5.11 compares the sediment yields of Korean rivers to the results of Milliman and Syvitski (1992). The studied watersheds are classified by the maximum elevation of the watershed followed the classification by Milliman and Syvitski (1992). The specific sediment yields of studied watersheds are lower than the headwater watersheds studied by Milliman and Syvitski (1992). This shows that Korea has lower sediment yield compared to the rest of the Asia and it may be because of dams.

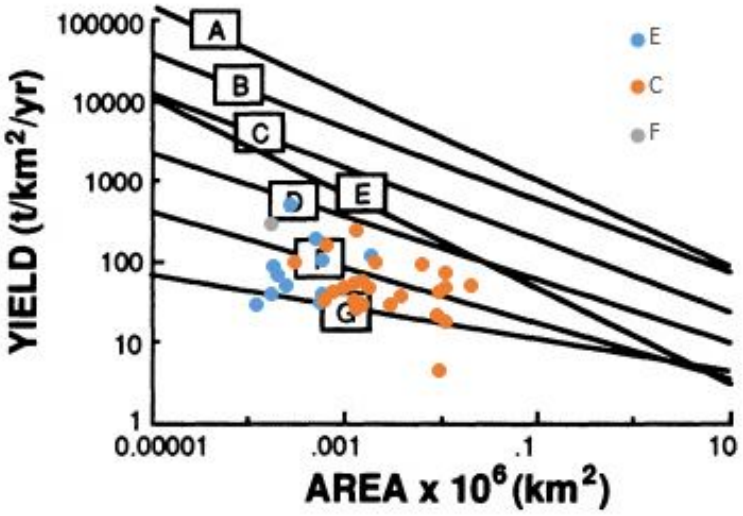

Figure 5.11: Korean sediment yields with the results of Milliman and Syvitski (1992)

Chapter 6

Parametric Analysis of the Sediment Yield

In Chapter 5, I show that half of the sediment is transported by the flow that is at least 4.4 times the mean discharge in South Korea. The parametric analysis of this chapter uses a logarithmic transform on the exceedance probability function to define two parameters describing the flow duration curve: a coefficient and an exponent. The new method works well when a straight line can be fitted to this double log plot at high discharges. When combined with the two parameters defining the sediment curve, I develop a procedure based on four parameters: two defining the flow duration curve and two defining the sediment rating curve.

This parametric approach allows the estimate of the long-term mean values of the runoff or sediment yield. The proposed four-parameter method is then applied to stations in South Korea. The calculation results of the proposed method are compared to the traditional method, i.e., flow-duration/sediment-rating curve method.

6.1 Parametric Analysis

6.1.1 Definition of the Four Parameters

The discharge record of station N9 in South Korea is used as an example to illustrate the methods to parameterize the flow duration curve. Figure 6.1 provides the daily discharge from January 1, 2008 to December 31, 2014 and the sediment rating curve at N9. The graphical method and the method of moments are both used to evaluate the parameters $\hat{a}$ and $\hat{b}$ to define the flow duration curve. The parameters $\bar{a}$ and $\bar{b}$ are used to define the sediment rating curve.

Graphical method

The exceedance probability for a given discharge is calculated by Eq (5.1). Figure 6.1b and Figure 6.1d present an example of the transform on the flow duration curve at N9 station in South Korea. A linear relationship between the higher values of $\ln Q$ and transformed exceedance proba-

bility $\Pi = \ln(-\ln E)$ can be found. The transform parameters are determined by using a graphical approach. A straight line is fitted by ordinary least squares in the zone of interest, i.e., the higher values of $\ln Q$. The higher values of $\ln Q$ is defined as a discharge larger than 1.5 times the mean daily discharge. The result of ordinary least squares gives $\Pi(Q) = -0.60 + 0.37 \ln Q$. The values $\hat{b} = 1/0.37 = 2.68$ and $\hat{a} = (1/e^{-0.60})^{0.37} = 5.02$.

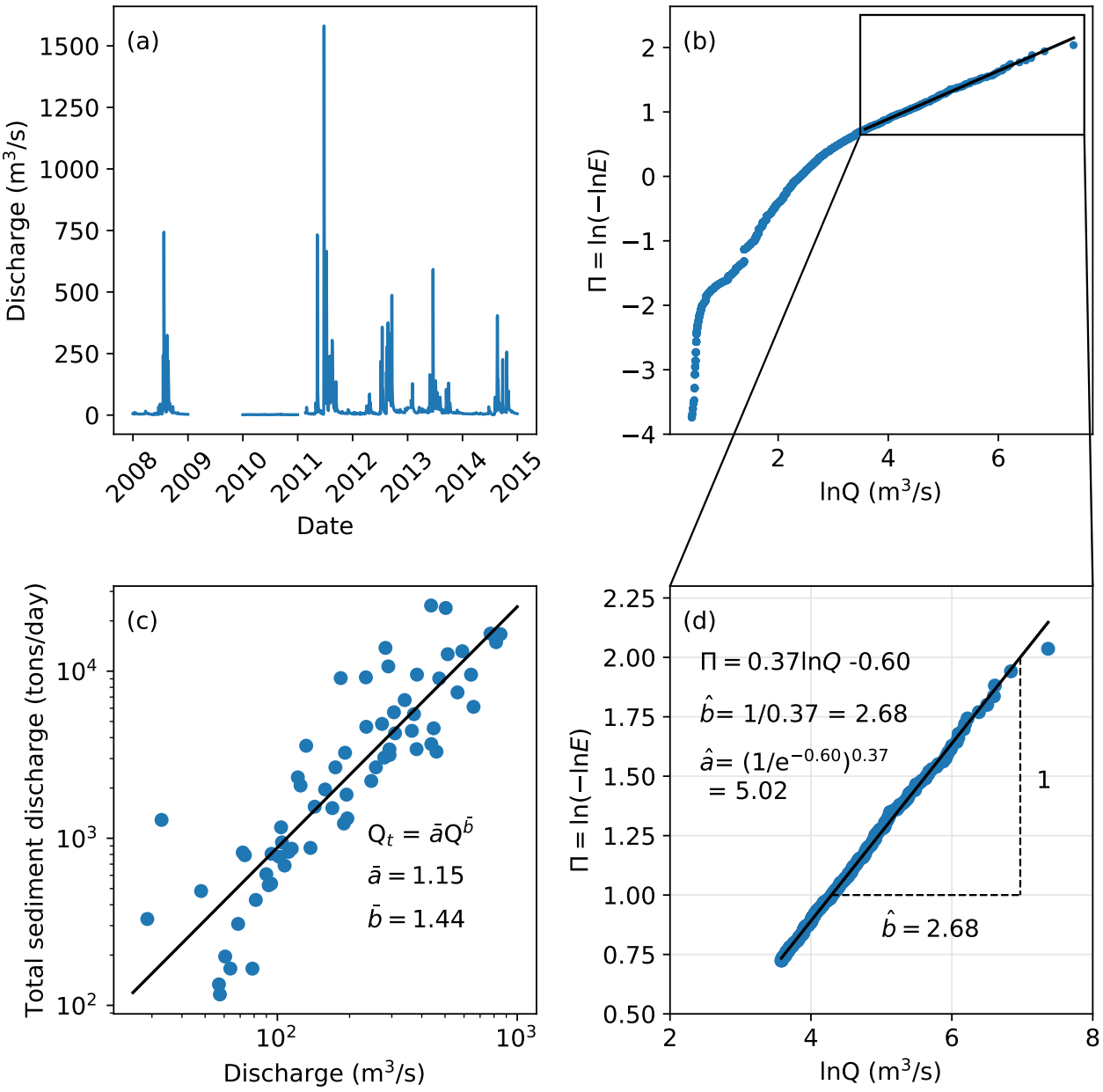

Figure 6.1: (a) Mean daily discharge from 2008 to 2014, (b) transformed flow duration curve, (c) sediment rating curve, and (d) close-up for the high discharges of Hyangseok station (N9). Graphically we can show that the value of $\hat{b}$ is the inverse of the slope of the linear function

Method of moments

The average discharge $\bar{Q} = 23.7$ m^3/s. The average value of $\overline{Q^2} = 5111.6$ m^6/s^2. When substituting discharge Q for x, the value of $\hat{b}$ can be solved from Eq. (2.65):

$$(\overline{Q^2}/\bar{Q}^2) = \frac{\Gamma(1+2\hat{b})}{\left[\Gamma\left(1+\hat{b}\right)\right]^2} = 5111.6/23.7^2 = 10.91$$

The value of $\hat{b} = 2.35$.

From Eq. (2.66):

$$\hat{a} = \frac{\bar{x}}{\Gamma(1+\hat{b})} = 8.37 \tag{6.1}$$

6.1.2 Mean Annual Flow and Sediment Yield

With reference to the analysis in Section 2.5, we now consider that variable x is the daily flow discharge Q. The main discharge is obtained from Eq. (2.63) as

$$\bar{Q} = \hat{a}\Gamma(1+\hat{b}) \tag{6.2}$$

Because sediment discharge and flow discharge generally follow power laws (for example, sediment rating curve relates the flow discharge to sediment discharge as $Q_s = \bar{a}Q^{\bar{b}}$), the mean annual sediment discharge of a river can be estimated as follows:

$$\begin{aligned}
\bar{Q}_s &= \int_0^\infty Q_s f(Q_s)\mathrm{d}Q_s \\
&= \int_0^\infty \bar{a}Q^{\bar{b}} f(Q)\mathrm{d}Q \\
&= \int_0^\infty \bar{a}\left(\hat{a}\Psi^{\hat{b}}\right)^{\bar{b}} f(\Psi)\mathrm{d}\Psi \\
&= \bar{a}\hat{a}^{\bar{b}}\int_0^\infty \Psi^{\bar{b}\hat{b}}e^{-\Psi}\mathrm{d}\Psi \\
\bar{Q}_s &= \bar{a}\hat{a}^{\bar{b}}\Gamma(1+\bar{b}\hat{b})
\end{aligned} \tag{6.3}$$

6.1.3 Cumulative Distribution Curves

The cumulative distribution curve calculates the cumulative quantity of discharge/sediment discharge passing through a gage for a given discharge. Values of discharge are sorted from the smallest to the largest. The cumulative percent passing is computed as:

$$\%_{pass} = \frac{W_{passed}}{W_{total}} \times 100\% \tag{6.4}$$

where W_{passed} = the total mass of the discharge smaller than or equal the current discharge; W_{total} = the total mass of the discharge in the record.

Distribution of river flows usually follow a gamma distribution (Botter et al. 2013; Markovic 1965). By using the proposed method, we can also show the cumulative discharge function as an incomplete gamma function:

$$\begin{aligned} Q_\Psi &= \int_0^\Psi Q f(Q) \mathrm{d}Q \\ &= \int_0^\Psi Q f(\Psi) \mathrm{d}\Psi \\ &= \hat{a} \int_0^\Psi \Psi^{\hat{b}} e^{-\Psi} \mathrm{d}\Psi \\ &= \hat{a}\gamma(1+\hat{b}, \Psi) \end{aligned} \tag{6.5}$$

, where γ is the incomplete gamma function $\gamma(\hat{b}, \Psi) = \int_0^\Psi x^{\hat{b}-1} e^{-\Psi} \mathrm{d}\Psi$.

By dividing the above function by the mean discharge, the function of normalized cumulative discharge can be shown as a cumulative distribution function P for gamma variables with a shape parameter $1 + \hat{b}$:

$$\frac{Q_\Psi}{\bar{Q}} = \frac{\gamma(1+\hat{b}, \Psi)}{\Gamma(1+\hat{b})} = P(1+\hat{b}, \Psi) \tag{6.6}$$

Similarly, the cumulative function of sediment discharge is

$$\frac{Q_{s\Psi}}{\bar{Q}_s} = \frac{\gamma(1+\bar{b}\hat{b}, \Psi)}{\Gamma(1+\bar{b}\hat{b})} = P(1+\bar{b}\hat{b}, \Psi) \tag{6.7}$$

Alternatively:

$$Q/\bar{Q} = \frac{\hat{a}\Psi^{\hat{b}}}{\hat{a}\Gamma(1+\hat{b})} = \frac{\Psi^{\hat{b}}}{\Gamma(1+\hat{b})} \tag{6.8}$$

$$Q_s/\bar{Q}_s = \frac{\bar{a}(\hat{a}\Psi^{\hat{b}})^{\bar{b}}}{\bar{a}\hat{a}^{\bar{b}}\Gamma(1+\bar{b}\hat{b})} = \frac{\Psi^{\hat{b}\bar{b}}}{\Gamma(1+\hat{b}\bar{b})} \tag{6.9}$$

6.2 Application of the Parametric Method

6.2.1 Mean Annual Sediment Yield

The mean annual sediment load can be calculated when the coefficient and exponent $\bar{a}$ and $\bar{b}$ of the sediment rating curve and the transformed parameters $\hat{a}$ and $\hat{b}$ are known. For instance, $\bar{a}$ and $\bar{b}$ of N9 can be found in Table 5.3. The mean annual sediment load can be estimated by equation Eq. (6.3). The sediment yield calculated by the graphical method and the moment method are 84,000 and 89,924 tons/year, respectively. The results show good agreement with the 84,472 tons/year calculated by the FDSRC method.

Table 6.1: Sediment yield calculated from different methods

Method	$\hat{a}$	$\hat{b}$	$\bar{a}$	$\bar{b}$	$\bar{Q}_s$ (tons/year)
Graphic	5.02	2.68	1.15	1.44	84,005
Moments	8.37	2.35	1.15	1.44	89,924
FDSRC	-	-	1.15	1.44	84,472

6.2.2 Cumulative Distribution Curves

The theoretical solution of the cumulative distribution curve for discharge $P(1+\hat{b}, \Psi)$ and sediment load $P(1+\hat{b}\bar{b}, \Psi)$ from Eqs. (6.6) and (6.7) and plotted in Figure 6.2. The values of Ψ is calculated from Eq. (2.56a): $\Psi = \sqrt[\hat{b}]{Q/\hat{a}}$. Figure 6.3 provides an comparison of the measured and theoretical cumulative distribution curves of N9. The values of $\hat{a}$ and $\hat{b}$ are 8.37 and 2.35 by the method of moments.

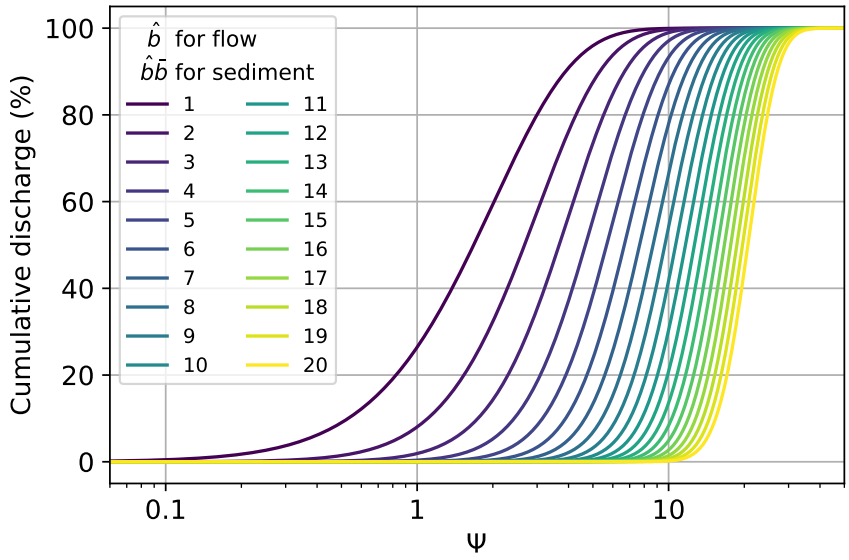

Figure 6.2: Analytical solution of cumulative distribution curves for flow and sediment

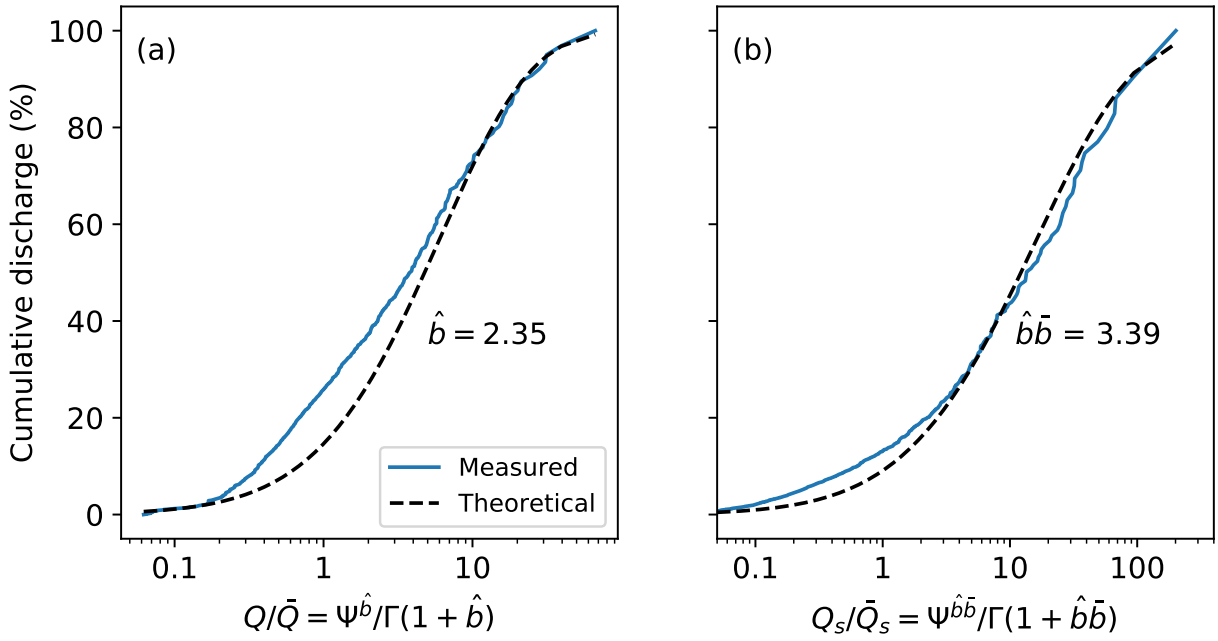

Figure 6.3: Comparison between theoretical solutions and observation. (a) Water, and (b) sediment of Hyangseok station (N9). The value of $\hat{b}$ is 2.35, and $\bar{b}$ is 1.44

It is clear that the theoretical cumulative distribution curves are fairly close to the measurements. In this study, the incomplete gamma function and the complete gamma function are calculated by an extension of python, *scipy.stat.gamma*.

6.3 Testing of the Parametric Method in South Korea

6.3.1 Graphical Method vs Method of Moments

The flow and sediment records from 35 stations in South Korea are used here. The exceedance probability of a given discharge is calculated as described previously in Section 5.1.1. The sediment rating curve is also required to estimate the mean annual sediment load. The same sediment rating curves of Chapter 5 are used here. The values of $\hat{a}$ and $\hat{b}$ are evaluated by both the graphical method and the method of moments. The results are summarized in Table 6.2. The values of $\hat{b}$ vary in the range of 1.14 and 2.89 by the method of moments. The graphical method gives the range of $\hat{b}$ from 1.90 and 4.90. Figure 6.4 shows that the distribution of $\hat{b}$ against $\hat{a}$. The value of $\hat{b}$ decreases as $\hat{a}$ increases for both methods.

Next, the sediment yield is calculated by Eq. (6.3) and compared to the sediment yield from the FDSRC (Figure 6.5a). Both methods have good agreement to the FDSRC method. The method of moments has the absolute percent difference between 1.2% and 22% (mean difference = 8%); the graphical method has the absolute percent difference between 0.5% and 846% (mean difference = 59%). The cumulative distributions of the absolute percent difference are plotted in Figure 6.5b.

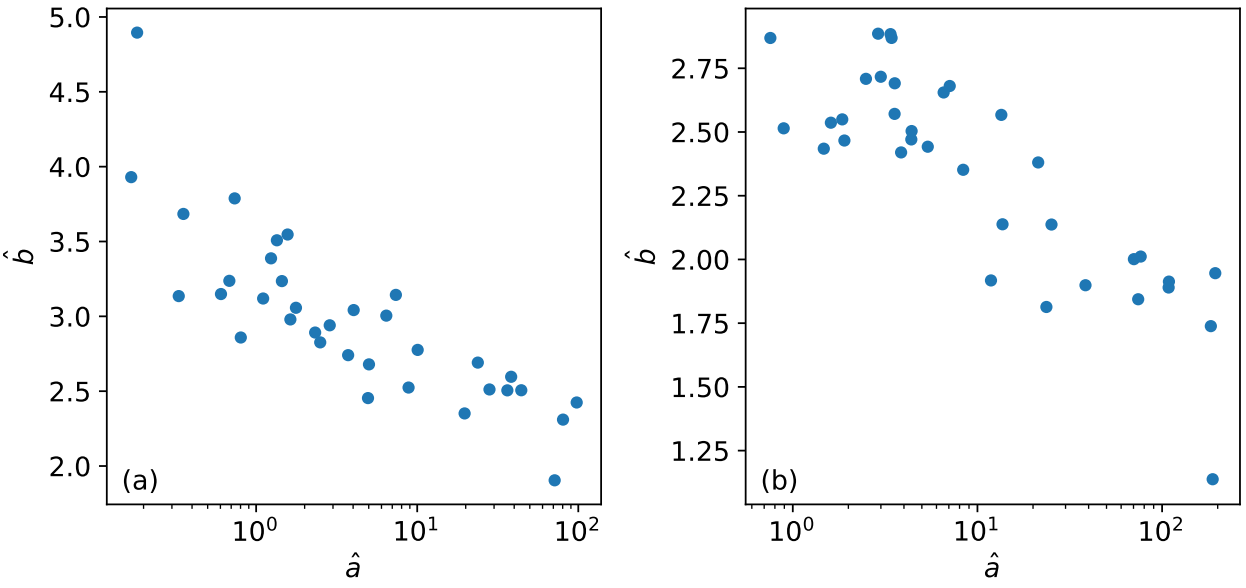

Figure 6.4: $\hat{a}$ vs $\hat{b}$: (a) Graphical method, and (b) method of moments

Table 6.2: Values of $\hat{a}$, $\hat{b}$, and $\bar{Q}_s$ by graphical method and the method of moments

Site	$\bar{a}$	$\bar{b}$	Moments			Graphic		
			$\hat{a}$	$\hat{b}$	$\bar{Q}_s$ (Mkg/yr)	$\hat{a}$	$\hat{b}$	$\bar{Q}_s$ (Mkg/yr)
H1	0.011	1.92	183.64	1.74	811	80.40	2.31	840
H2	2.479	1.59	2.49	2.71	151	1.11	3.12	121
H3	0.013	2.11	13.47	2.57	291	6.43	3.00	339
H4	2.921	1.57	1.61	2.54	52	0.60	3.15	52
H5	0.362	1.82	4.38	2.47	99	2.50	2.83	105
H6	0.004	2.07	187.87	1.14	206	71.34	1.90	214
H7	1.217	1.37	3.00	2.72	32	1.45	3.24	35
N1	0.341	1.64	3.57	2.69	47	1.24	3.39	58
N2	0.116	1.67	6.56	2.66	45	1.57	3.55	55
N3	0.020	1.74	108.49	1.89	220	44.27	2.51	222
N4	0.041	1.78	76.57	2.01	437	36.27	2.51	435
N5	0.013	1.92	108.88	1.91	541	38.30	2.60	572
N6	0.068	1.44	74.22	1.84	49	28.10	2.51	42
N7	0.007	1.94	194.05	1.95	1109	97.74	2.42	1241
N8	0.579	1.34	38.47	1.90	99	19.69	2.35	84
N9	1.151	1.44	8.37	2.35	90	5.02	2.68	84
N10	9.317	0.83	0.89	2.51	7	0.33	3.14	5
N11	0.085	1.74	5.38	2.44	20	2.86	2.94	28
N12	0.730	1.40	3.43	2.87	37	1.35	3.51	42
N13	2.147	1.22	13.67	2.14	73	3.73	2.74	38
N14	0.121	1.74	2.90	2.89	35	0.74	3.79	58
G1	0.308	1.74	4.40	2.50	61	2.32	2.89	61
G2	0.029	1.90	70.35	2.00	602	23.78	2.69	622
G3	5.475	1.22	23.63	1.81	230	8.84	2.52	187
G4	0.120	1.95	1.90	2.47	14	0.68	3.24	28
G5	0.003	2.89	1.47	2.43	17	0.80	2.86	39
Y1	0.525	1.64	1.85	2.55	17	0.35	3.68	28
Y2	0.269	1.63	25.18	2.14	218	10.07	2.78	235
Y3	1.225	1.54	11.84	1.92	117	4.95	2.45	93
Y4	0.065	1.89	3.56	2.57	24	1.77	3.06	32
Y5	0.038	2.00	3.86	2.42	19	1.63	2.98	24
S1	0.049	1.87	3.38	2.88	43	0.18	4.90	400
S2	0.046	1.88	7.08	2.68	86	4.03	3.04	99
S3	0.068	1.74	21.33	2.38	153	7.37	3.14	221
S4	0.022	2.10	0.76	2.87	3	0.17	3.93	13

Eighty percent of the samples have difference less than 12% for the method of moments, while 57% for the graphical method. For the graphical method, the high error is associated with the high value of $\hat{b}$. If $\hat{b} > 3.5$, it is better to recheck the linearity at high discharges when using the graphical method.

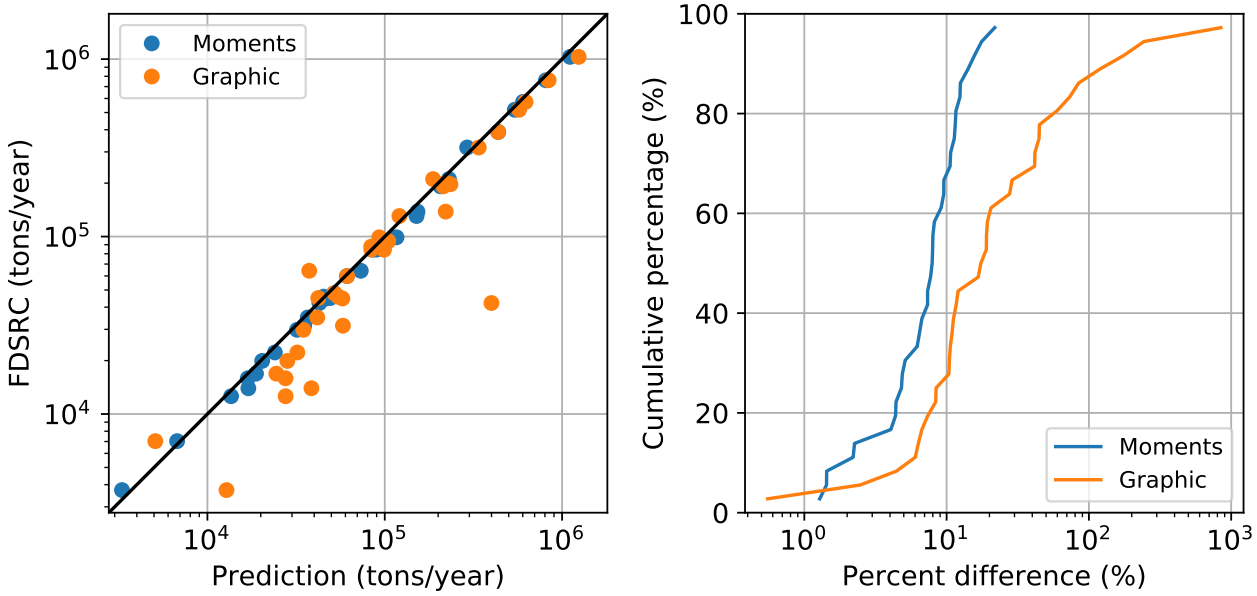

Figure 6.5: (a) Predictions of sediment discharge by the graphical method and the method of moments compared to the FDSRC; and (b) cumulative distribution of the difference

The degree of accuracy is further evaluated by using the statistical parameter including RMSE, R^2, and ρ_c. The results are listed in Table 6.3. The RMSE of the moments method is 28% of the graphical method. The R^2 and ρ_c of the moments method are close to 1, indicating that the calculations are very close to the FDSRC. All the statistical parameters shows the method of moments is better and more consistent.

Table 6.3: Statistical comparison between the graphical method and the method of moments

Method	MAPE (%)	RMSE (tons/yr)	R^2 (%)	ρ_c (%)
Moments	8	21,285	99.9	99.6
Graphic	59	75,536	97.1	95.4

The cumulative distribution curves of flow and sediment are calculated by Eqs. (6.6) and (6.7) and compared to the measurements. The agreement between the theoretical solution and the stream measurement is measured by the Kolmogorov-Smirnov distance D and the 1-Wasserstein distance W. The average Kolmogorov-Smirnov distance of discharge is 16.6% for the method of moments and 19.0% for the graphical method. The distances of the sediment curves are generally higher. The average Kolmogorov-Smirnov distance of sediment discharge is 17.3% for the method of moments and 29.7% for the graphical method. Figure 6.6 plots the cumulative distribution of errors. For discharge, the Kolmogorov-Smirnov distance of the graphical method is 17% higher than the method of moments on average and the 1-Wasserstein distance is 149% higher; for sediment, the Kolmogorov-Smirnov distance of the graphical method is 72% higher than the method of moments and the 1-Wasserstein distance is 149% higher.

To sum up, parameter evaluation by the method of moments gives more accurate predictions of both the sediment yield and the cumulative distribution curves. The parameters can be evaluated by the method of moments directly with computers and the result is not subjective, therefore the method of moments is used for the rest of the study.

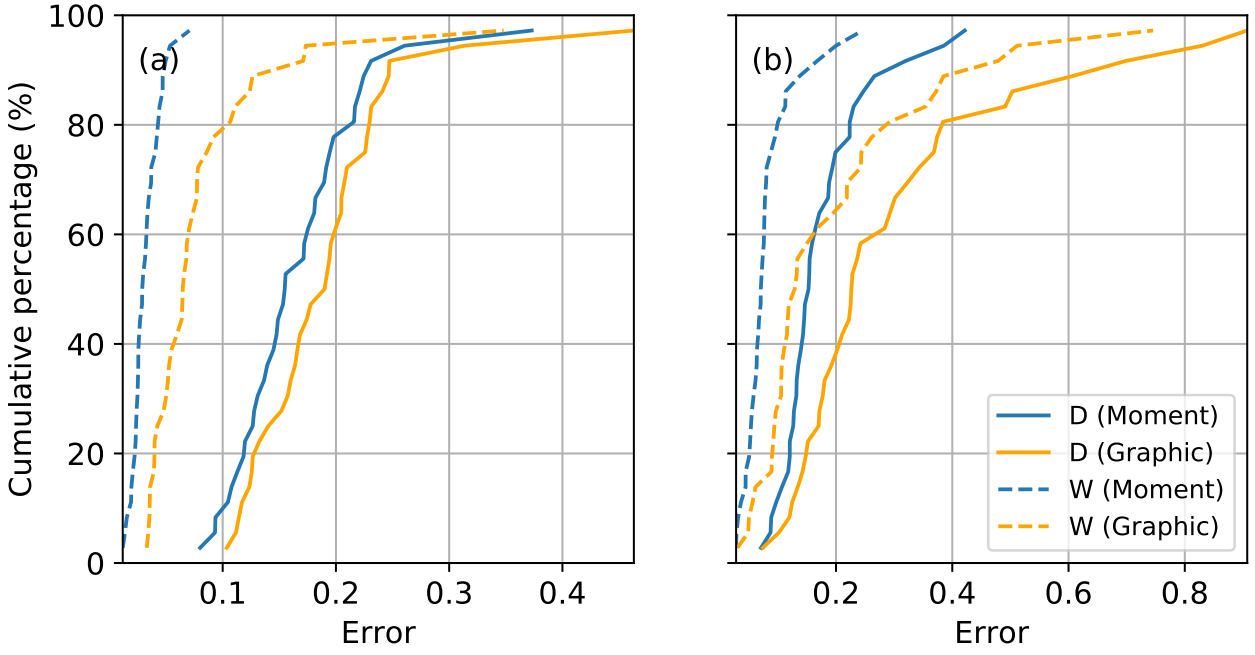

Figure 6.6: Statistical results for the parametric approach (a) flow and (b) sediment

Table 6.4: The Kolmogorov-Smirnov distance, D, and the 1-Wasserstein distance, W, by the graphical method and the method of moments

Site	Moments				Graphic			
	Flow		Sediment		Flow		Sediment	
	D	W	D	W	D	W	D	W
G1	0.13	0.03	0.13	0.07	0.14	0.03	0.17	0.11
G2	0.22	0.02	0.19	0.07	0.23	0.05	0.18	0.12
G3	0.19	0.04	0.14	0.05	0.20	0.09	0.17	0.11
G4	0.12	0.03	0.23	0.08	0.16	0.13	0.61	0.38
G5	0.10	0.02	0.42	0.25	0.11	0.05	0.70	0.48
H1	0.23	0.03	0.19	0.08	0.23	0.05	0.13	0.09
H2	0.20	0.05	0.19	0.11	0.19	0.04	0.15	0.09
H3	0.16	0.01	0.11	0.07	0.16	0.04	0.21	0.20
H4	0.19	0.04	0.17	0.10	0.20	0.07	0.24	0.10
H5	0.13	0.01	0.09	0.04	0.13	0.03	0.12	0.11
H6	0.26	0.04	0.25	0.14	0.25	0.07	0.20	0.11
H7	0.09	0.02	0.09	0.04	0.11	0.07	0.19	0.13
N1	0.15	0.03	0.16	0.06	0.18	0.09	0.30	0.22
N2	0.22	0.04	0.22	0.10	0.25	0.11	0.37	0.24
N3	0.18	0.03	0.13	0.08	0.20	0.06	0.18	0.12
N4	0.15	0.03	0.12	0.06	0.17	0.05	0.15	0.09
N5	0.22	0.04	0.20	0.11	0.23	0.06	0.22	0.12
N6	0.19	0.03	0.13	0.06	0.21	0.07	0.14	0.09
N7	0.15	0.03	0.14	0.07	0.15	0.05	0.23	0.13
N8	0.15	0.02	0.10	0.03	0.16	0.04	0.12	0.05
N9	0.12	0.02	0.07	0.03	0.12	0.04	0.07	0.06
N10	0.18	0.02	0.22	0.03	0.20	0.07	0.23	0.06
N11	0.08	0.03	0.14	0.09	0.10	0.08	0.34	0.26
N12	0.09	0.05	0.13	0.08	0.13	0.08	0.29	0.15
N13	0.37	0.05	0.32	0.06	0.31	0.04	0.28	0.05
N14	0.14	0.03	0.15	0.08	0.19	0.12	0.49	0.35
S1	0.17	0.07	0.27	0.20	0.46	0.35	0.91	0.75
S2	0.11	0.02	0.12	0.07	0.12	0.04	0.24	0.13
S3	0.14	0.03	0.12	0.04	0.17	0.11	0.38	0.29
S4	0.13	0.05	0.39	0.17	0.23	0.17	0.83	0.51
Y1	0.18	0.03	0.15	0.06	0.24	0.17	0.50	0.37
Y2	0.17	0.03	0.15	0.05	0.19	0.08	0.23	0.17
Y3	0.22	0.04	0.15	0.08	0.21	0.04	0.10	0.03
Y4	0.11	0.02	0.16	0.05	0.13	0.06	0.37	0.22
Y5	0.14	0.02	0.15	0.07	0.17	0.06	0.32	0.24

6.3.2 One-Parameter Prediction of Sediment Yield in South Korea

The values of $\hat{a}$ and $\hat{b}$ by using the method of moments are listed in Table 6.2. The correlations between the four parameters $\hat{a}$, $\hat{b}$, $\bar{a}$, and $\bar{b}$ and watershed area are found. For $\hat{a}$ and $\hat{b}$, stations H6 and N13 were removed from the regression analysis because the flow are regulated by dams. For $\bar{a}$ and $\bar{b}$, stations G5, S4, N10, N13, G3, and N8 were removed because of low R-squared. The following are the functions of $\hat{a}$, $\hat{b}$, $\bar{a}$, and $\bar{b}$ with watershed area:

$$\hat{a} = 0.0045A^{1.07},\ R^2 = 0.92 \tag{6.10}$$

$$\hat{b} = 3.60 - 0.17 \ln A,\ R^2 = 0.48 \tag{6.11}$$

$$\bar{a} = 123.2A^{-0.96},\ R^2 = 0.56 \tag{6.12}$$

$$\bar{b} = 1.45 + 0.04 \ln A,\ R^2 = 0.08 \tag{6.13}$$

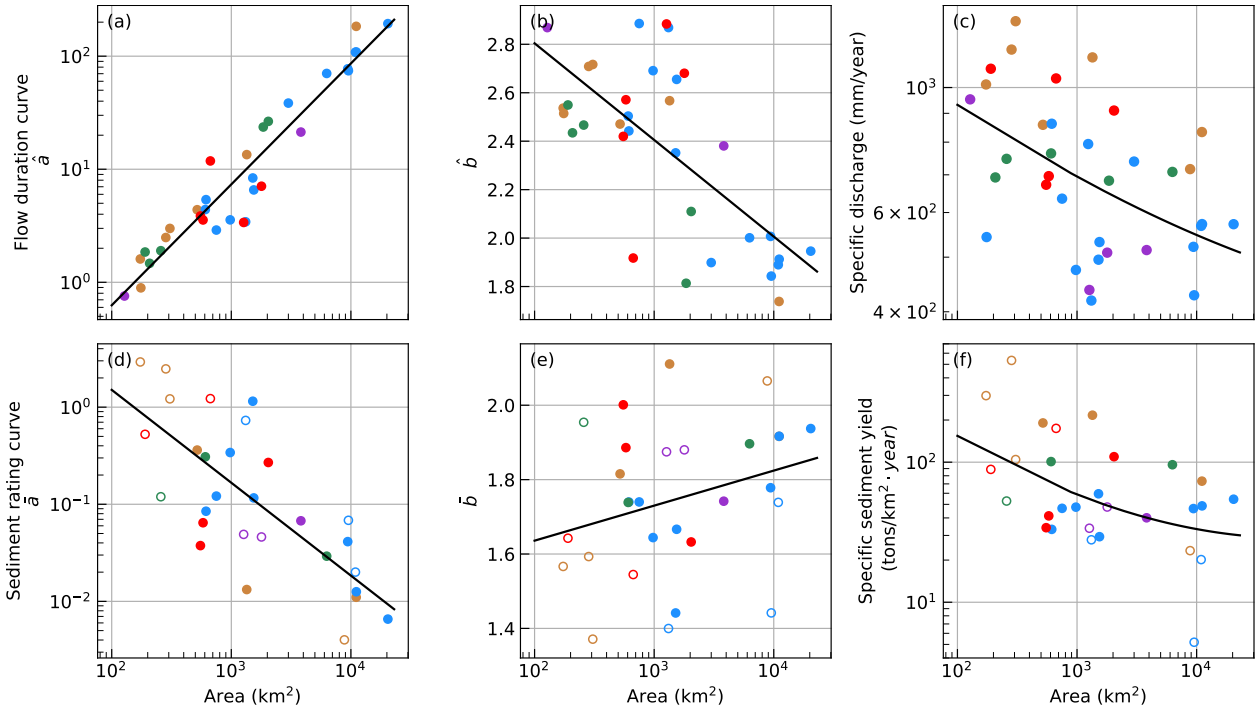

Figure 6.7: Four parameters $\hat{a}$, $\hat{b}$, $\bar{a}$, and $\bar{b}$ vs watershed area. The black lines are the regression line

With these relations, the annual discharge and sediment discharge can be estimated as a sole function of watershed area. This approach is called the one-parameter model because all four parameters are defined as a function of drainage area. For a given area, the values of $\hat{a}$, $\hat{b}$, $\bar{a}$, and $\bar{b}$ are evaluated from Eqs. (6.10), (6.11), (6.12), and (6.13) shown respectively in Figure 6.7a, b, d, and e. Therefore, the mean annual discharge and sediment discharge become functions of watershed area and can be next calculated using Eqs. (6.2) and (6.3), respectively. In Figure 6.7c and f, the annual runoff and specific sediment yield are plotted as functions of area. Figure 6.8 compares the one-parameter model with the four-parameter model, i.e., $\hat{a}$, $\hat{b}$, $\bar{a}$, and $\bar{b}$ evaluated directly from the measurements. The RMSE is 15 tons/km^2·year and 85 tons/km^2·year for the four-parameter and one-parameter models respectively. The MAPE is 8% and 83% for the four-parameter and one-parameter models respectively.

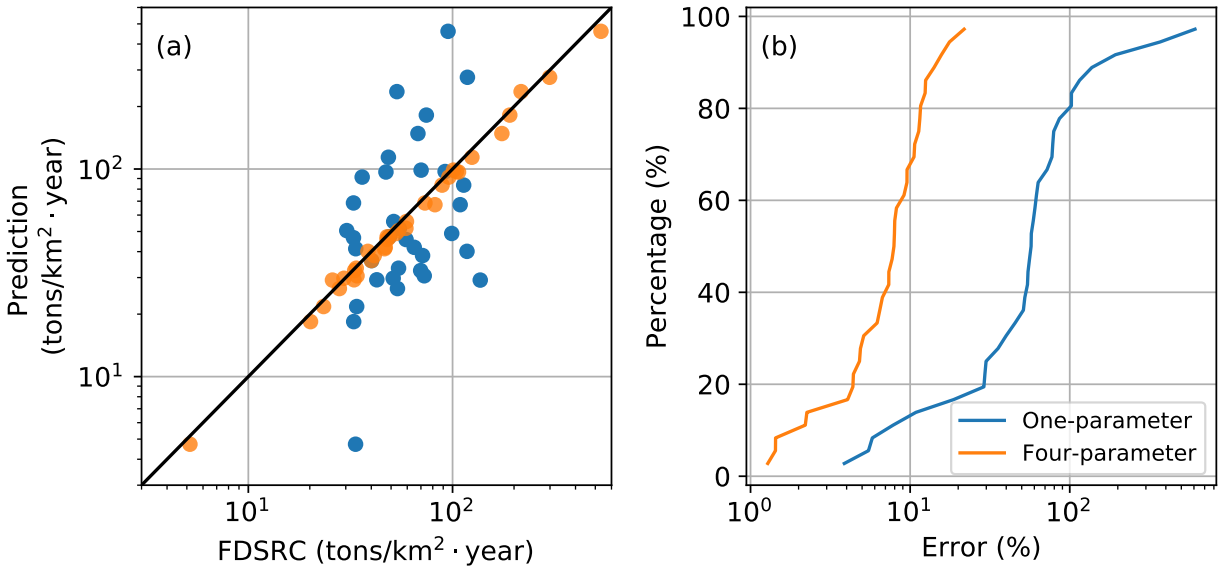

Figure 6.8: Comparison between the regression model, the four-parameter model, and the FDSRC

6.3.3 Validation

Four additional stations with daily discharge and suspended sediment measurements in South Korea became available for validation: Socheon, Sancheong, Cheoncheon, and Cheongseong.

Daily discharge is available from 2006 to 2015. Samples of sediment concentration were taken during 2009 to 2013. The watershed areas, flow duration curves, and sediment rating curves of the validation sites are listed in Table 6.5. Note that the sediment rating curves of the validation sites are only suspended discharge-flow relationships ($Q_s - Q$). There is no information of bed material at these sites so SEMEP is not used. The prediction from the one-parameter and four-parameter models are shown in Table 6.5. Overall, the four-parameter model has the better performance (MAPE = 7% compared to 65% for the one-parameter model).

Table 6.5: Validation data and result

Site	Area (km^2)	$\hat{a}$	$\hat{b}$	$\bar{a}$	$\bar{b}$	Specific sediment yield[1]		
						FDSRC	4-param.	1-param.
Socheon	697	5.92	2.25	0.17	1.74	39	40	67
Sancheong	1130	7.95	2.51	0.16	1.68	50	56	56
CheonCheon	291	1.92	2.37	0.56	1.67	42	47	94
Cheongseong	490	2.23	2.72	0.14	1.82	50	51	76

[1] tons/km^2·year

Table 6.6: Statistical performance for the validation data

Model	MAPE (%)	RMSE (t/km^2·yr)	R^2 (%)	ρ_c (%)
One-parameter	65	32	-28	-5
Four-Parameter	7	3.9	91	81

6.4 Discussion and Conclusion

According to the new method, the mean annual discharge can be calculated as $\bar{Q} = \hat{a}\Gamma(1+\hat{b})$, and the mean annual sediment yield can be computed as $\bar{Q}_s = \bar{a}\hat{a}^{\bar{b}}\Gamma(1+\bar{b}\hat{b})$. The cumulative distribution curves for sediment can be estimated as $Q_{sx}/\bar{Q}_s = P(1+\bar{b}\hat{b})$ where $P(1+\bar{b}\hat{b})$ is the cumulative distribution function for gamma variables with a shape parameter $1+\hat{b}$ (for flow $\bar{b} = 1$).

The method of moments is preferred as all the statistical parameters show it has better accuracy (MAPE = 8%, RMSE = 21,000 tons/year, $R^2 = 99.9\%$, $\rho_c = 99.6\%$, the average $D = 17.3\%$, and the average $W = 3.1\%$ for flow). Additionally, the method of moments is direct and not subjective and can be programmed easily. But the graphical method still provides visual information, which can be useful to detect abnormalities in the data, such as when the flow record is not stationary. The values of $\hat{a}$, $\hat{b}$, $\bar{a}$, and $\bar{b}$ are found to be functions of watershed area. The following relations are proposed: $\hat{a} = 0.0045A^{1.07}$, $\hat{b} = 3.6 - 0.17 \ln A$, $\bar{a} = 123.2A^{-0.96}$, $\bar{b} = 1.45 + 0.04 \ln A$, where A is watershed area in km^2. Therefore, the sediment yield can also be predicted with only one parameter, watershed area.

These proposed models are compared to the multiple-regression model proposed by Julien et al. (2017) (Appendix B). Julien's model is defined as follows:

$$SSY = 1.34 \times 10^{-9} A^{-0.016} P^{2.587} \%U^{0.735} Sand^{1.810} S^{-0.380} \tag{6.14}$$

where A is the watershed area in km^2, P is the mean annual precipitation in mm, $\%U$ is the percentage of urban, $Sand$ is the percentage of sand at 0 - 50 cm, and S is the watershed average slope (%). Table 6.7 shows the statistical measurements of errors. The parametric approach can bring significant improvement to the prediction of sediment yield.

Table 6.7: Statistical performances for the available models

Model	RMSE (t/km^{2}yr)	MAPE (%) (%)	ρ_c (%)	R^2 (%)
Four-parameter model	15	8	99	100
One-parameter model	85	83	18	31
Multiple-regression model	72	80	74	77

Chapter 7

Extensive Validation of the Parametric Sediment Yield Method

The goal of this chapter is to illustrate the generality and versatility of the parametric method. The proposed method is applied to the gages in the U.S. The values of $\hat{a}$ and $\hat{b}$ are obtained by the method of moments. The theoretical solution cumulative distribution curve is also applied to many gages in the U.S. because of the availability of long-term records. A summary of the results from Korea and the U.S. is also presented at the end of the present study.

7.1 Additional Data

Daily flow and sediment discharge data of the United States are available on the USGS Sediment Data Portal (https://cida.usgs.gov/sediment/). The mean daily discharge, daily suspended discharge, and information on sediment-sampling site for the period to 2016 were retrieved from the website. The earliest daily flow record track dates back to 1861. I removed sites with less than 20 years of complete stream flow or less than 500 sediment measurements. A total of 716 sites remained for testing the proposed new method. The analyses at all gages were based on the years with fewer than 30 days missing from the flow discharge record. The number of discharge data points for the 718 gages varies between 7,558 and 57,235 mean daily values, and 506 and 21,914 mean daily sediment discharge. A detail description of how the sediment data were collected and processed are documented in Lee and Glysson (2013).

The sediment rating curves are obtained by dividing the discharges into small intervals and taking the average value of each interval because the sediment discharges of American gages are extensive and widely dispersed. The intervals are spaced so that they are equal on a log-log plot. The ranges are typically as follows: 1-10, 10-20, 20-40, 40-80, 80-160, 160-320, 320-640, 640-1280, and so on.

The selected sites cover a wide range of climatic condition in the United States and drainage areas ranging from approximately 2.5 to 1,800,000 km^2 (Figure 7.1). Watersheds were chosen such that a wide range of flow regimes would be analyzed, including flashy and non-flashy, and stationary and non-stationary systems. Summary information for sites used in the present study can be found in Appendix C.

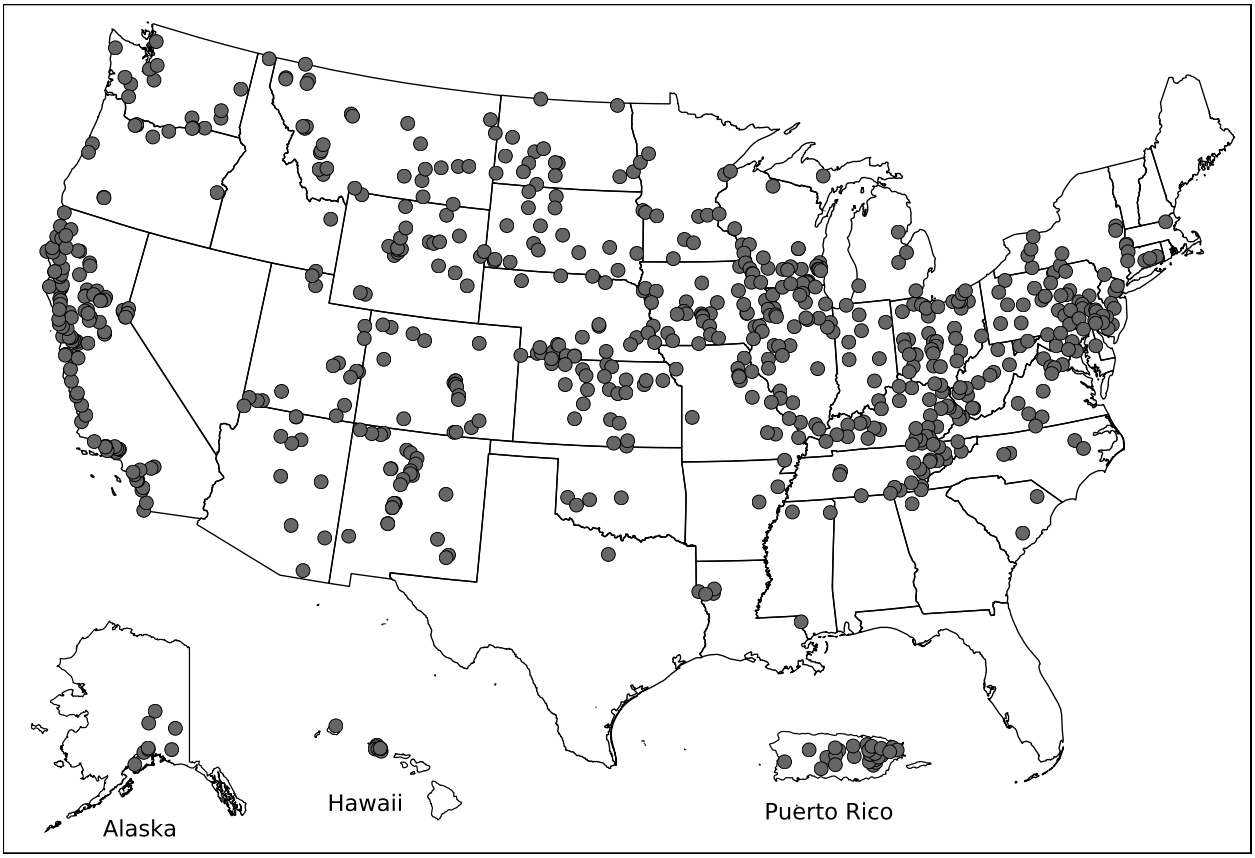

Figure 7.1: Map of US stations used in this study

7.2 Results

7.2.1 Sediment Yield Parameters in the USA

The parametric method is applied to all the 716 stations across the US. The method of moments is used to obtain the values of $\hat{a}$ and $\hat{b}$. The sediment rating curves are defined by the daily discharge and the daily sediment load for the values of $\bar{a}$ and $\bar{b}$. The results of parametric analysis

are listed in Appendix D. Estimated sediment yields range from 3 to 96,000,000 tons/year. The specific sediment yields vary six order of magnitudes (0.24 to 42,000 tons/km^2·year), with higher yields tending to occur in smaller basins (Figure 7.2). The negative trend between basin area was also found by Kane (2003) Renwick (1996), Renwick et al. (2005b), and Renwick et al. (2005a). However, the causes of the variability are beyond the scope of this study. A map of the specific sediment yield is provided in Figure 7.3.

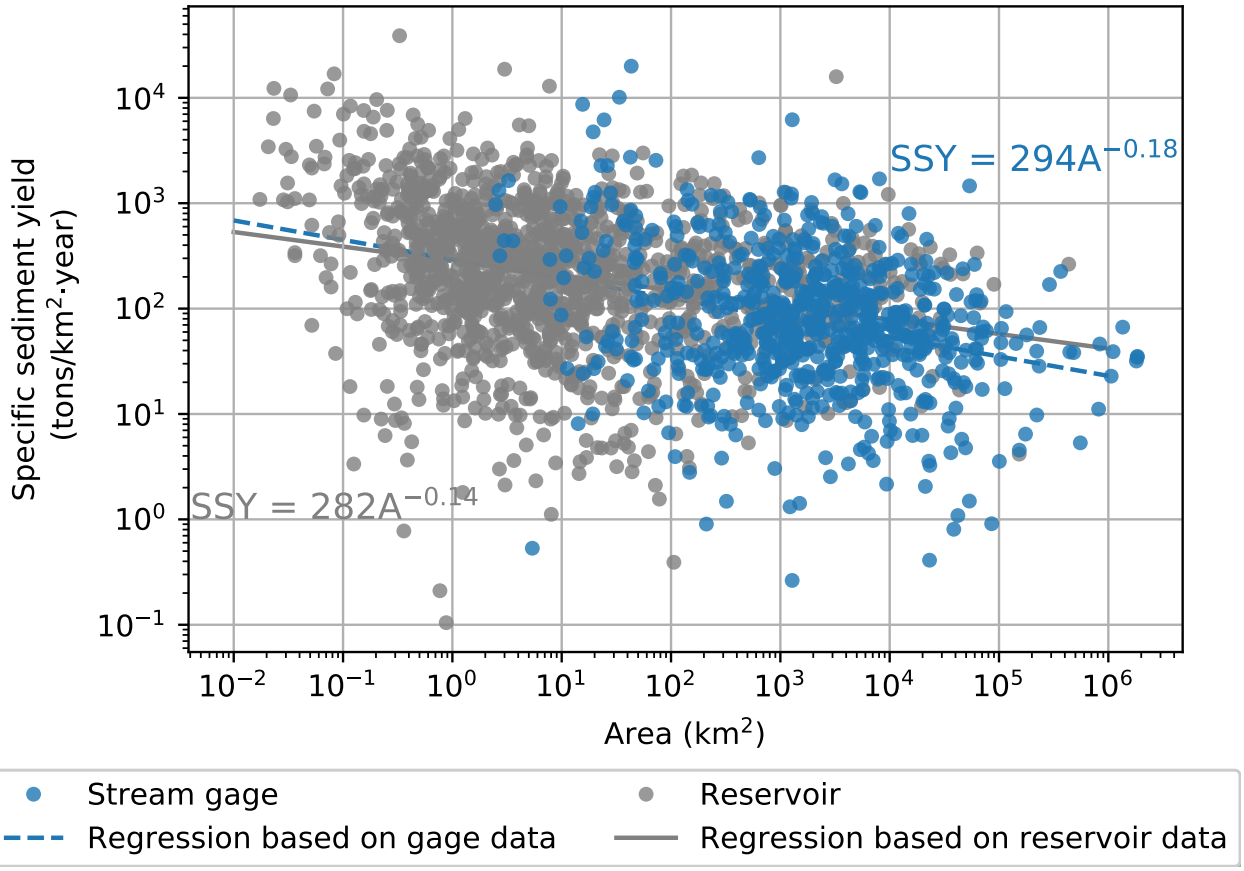

Figure 7.2: Relationship between specific sediment yield and watershed area. The specific sediment yields from river gages are compared to 1,374 reservoir sedimentation surveys (data source of the reservoir data: the Reservoir Sedimentation (RESSED) Database)

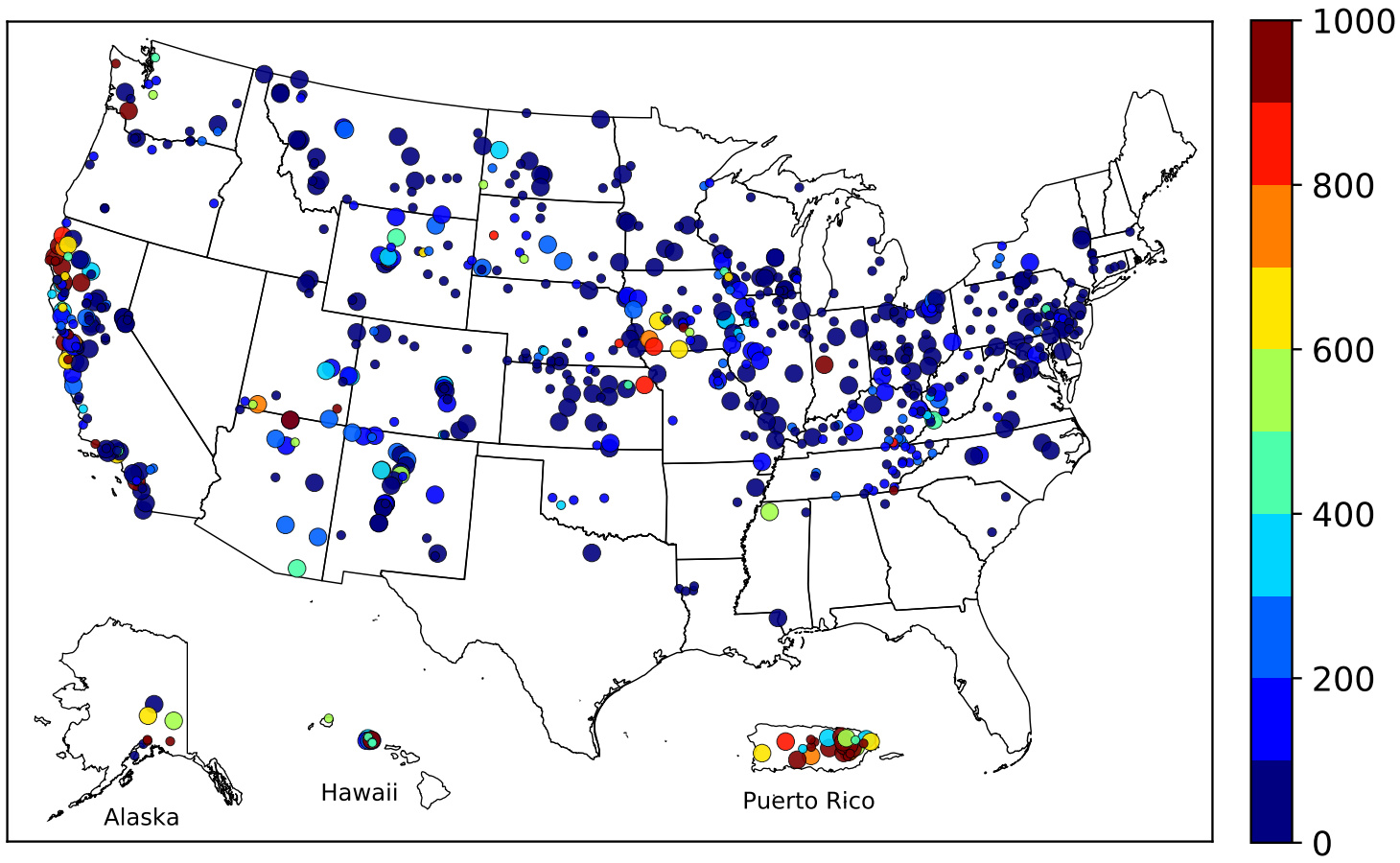

Figure 7.3: Map of specific sediment yields (unit: tons/km^2·year). Large circles are for the gages with daily suspended sediment discharge with more than 10 years collected, and small circles are for gages with less than 10 years of measured daily suspended sediment discharge

The values of $\hat{a}$ and $\hat{b}$ are plotted against drainage area (Figure 7.4). The values of $\hat{a}$ vary up to eight orders of magnitude. The parameter $\hat{a}$ increases from 1 to 100,000 as the drainage area increases from 10 km^2 to 1,000,000 km^2. Similar to South Korea, the value of $\hat{a}$ increases with drainage area, while the value of $\hat{b}$ is the opposite.

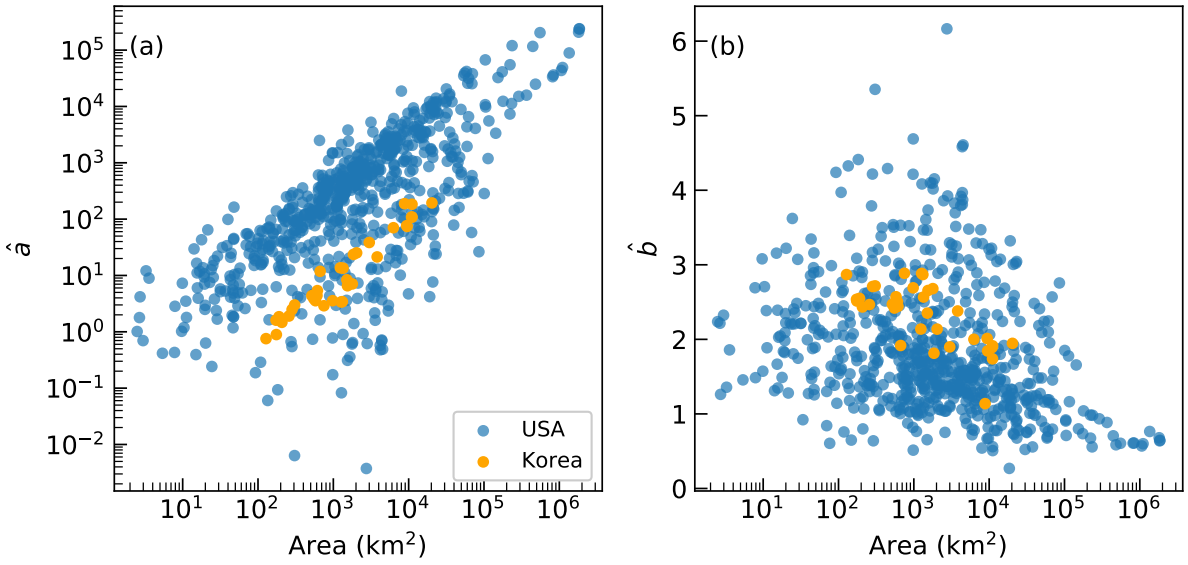

Figure 7.4: Watershed area vs (a) $\hat{a}$ and (b) $\hat{b}$

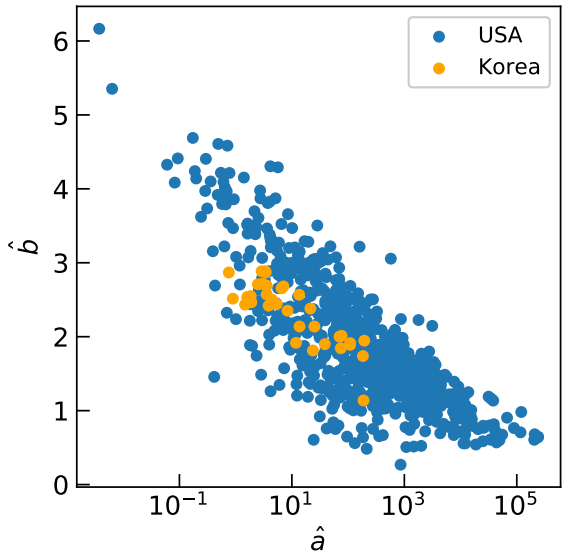

Figure 7.5: Values of $\hat{a}$ vs $\hat{b}$

The parameter $\hat{b}$ is a measure of the nonlinearity in rain-runoff response. The values of $\hat{b}$ of the US stations vary from 0.27 to 6.27. The US stations have greater variability because wide range of climatic conditions of the gages. Contrarily, because the climatic condition in South Korea is relatively homogeneous, the values of $\hat{b}$ have a narrower range in between 1.13 and 2.89. Overall, the typical values of $\hat{b}$ range between 1.2 and 3.5. Seventy-three percent of the watersheds are within the range.

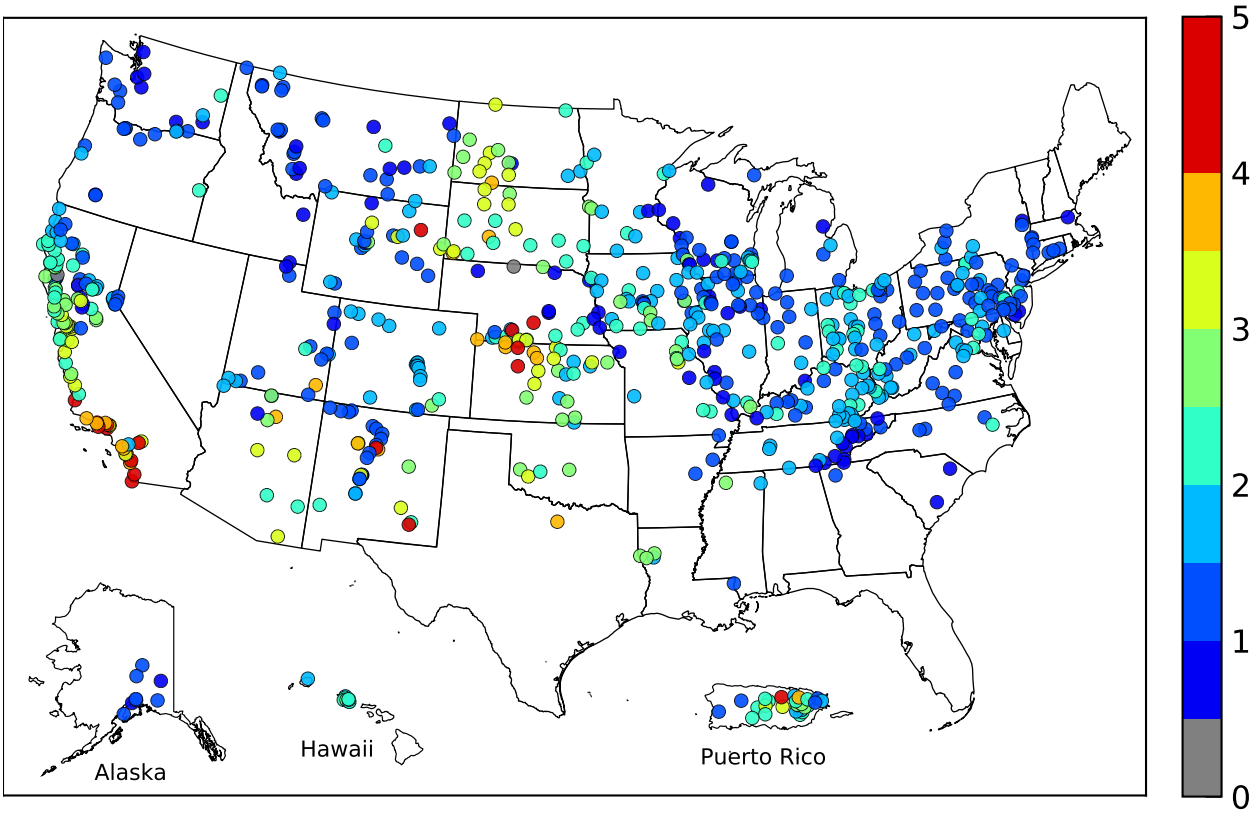

Figure 7.6: Map of $\hat{b}$

The spatial distribution of $\hat{b}$ is plotted in Figure 7.6. I found regionality in the value of $\hat{b}$. The values of $\hat{b}$ are remarkably consistent east of Mississippi River and the Pacific Northwest. The values of $\hat{b}$ in these regions are consistently in between 0.5 and 2.5. The variability of $\hat{b}$ is greater in the High Plains and South California. The variability is likely to attributed to the arid and hydrologically flashy climate in these regions. Flashiness can be quantified by the Richards-Baker

flashiness index (Baker et al. 2004):

$$RB = \frac{\sum_{i=1}^{n} |q_i - q_{i-1}|}{\sum_{i=1}^{n} q_i} \tag{7.1}$$

where RB is the Richards-Baker flashiness index, q_i is the daily mean discharge on day i, and n is the total number of days in the flow record. It is the ratio of daily fluctuations in discharge to the total discharge. The RB index is high for the watersheds which have high interdaily variation in discharge. A watershed is considered flashy when $RB > 0.4$ (Rosburg et al. 2016). The values of $\hat{b}$ is found increasing with the value of flashiness index (Figure 7.7a). Small streams are commonly known to be more flashy than large streams and therefore decreasing $\hat{b}$ value with increasing watershed size is expected (Baker et al. 2004) (Figure 7.7b). This helps explain why small watersheds tend to have high $\hat{b}$ values.

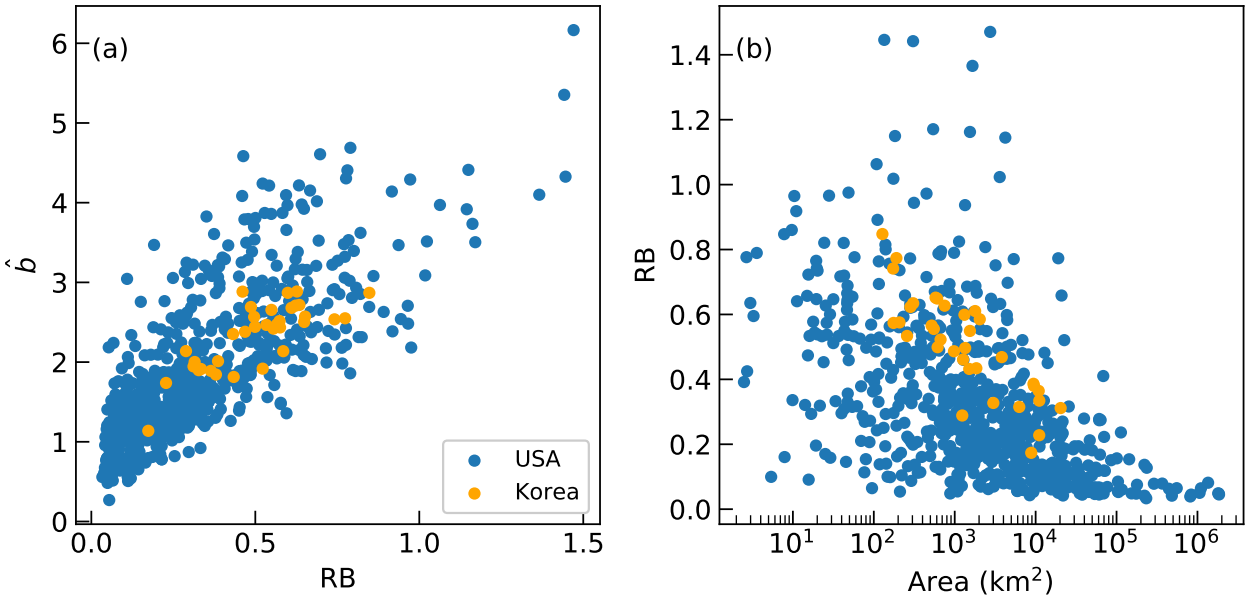

Figure 7.7: (a) The flashiness index, RB, vs $\hat{b}$; and (b) Watershed area vs RB

Figure 7.8a compares the sediment discharge calculated by the parametric method to the FD-SRC. The difference of calculated sediment loads varies between 0.14% and 83.6%, and 95% of them are less than 20% (Figure 7.8b). As can be seen in Table 7.1, the MAPE = 8%, $R^2 = 99.9$,

and $\rho_c = 99.8$. These statistical parameters show that we have excellent agreement between the proposed method to the traditional method. The cause of this difference is mainly due to extreme events and nonstationarity of the flow regime. Appendix E shows an example with the largest difference from Arikaree River at Haigler, Nebraska (USGS 06821500). The sediment load estimated by the FDSRC is 39,000 tons/year but by the parametric method gives 71,000 tons/year. The single extreme event in May 31, 1935 with the mean daily discharge 17,000 ft/s was the four times higher than the second largest event. The sediment load from the extreme event like this cannot be reflected in the FDSRC method.

Table 7.1: Statistical performance for the US stations

MAPE (%)	RMSE (tons/yr)	R^2 (%)	ρ_c (%)
8.6	457523	99.9	99.8

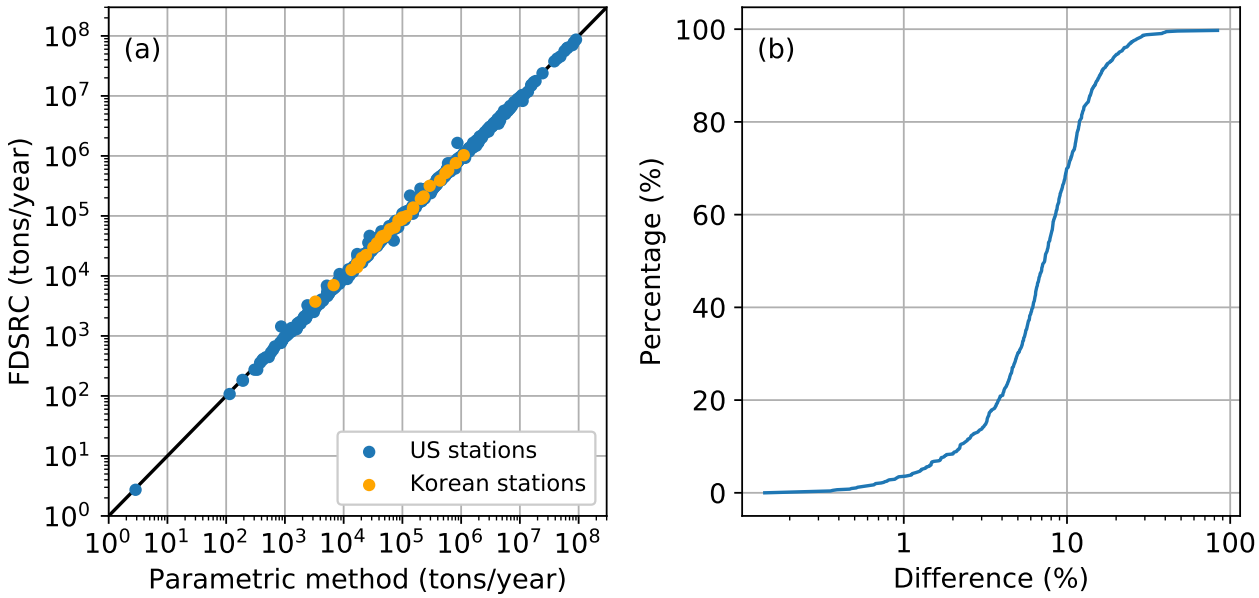

Figure 7.8: (a) Comparison of the computed annual sediment load. X-axis is flow-duration-sediment-rating curve method, and Y-axis is the double-log transform method. (b) Cumulative distribution of the difference between the sediment load estimated by the parametric method and the FDSRC method

7.2.2 Cumulative Distribution Curves for Flow and Sediment Discharge

The cumulative distribution curves of flow and sediment are also calculated and compared to the measurements. Figure 7.9 shows that the error generally decreases with longer record, especially for sediment load. In Figure 7.9d we can see that the 1-Wasserstein distance, W, is less than 20% when the record is longer than 40 years.

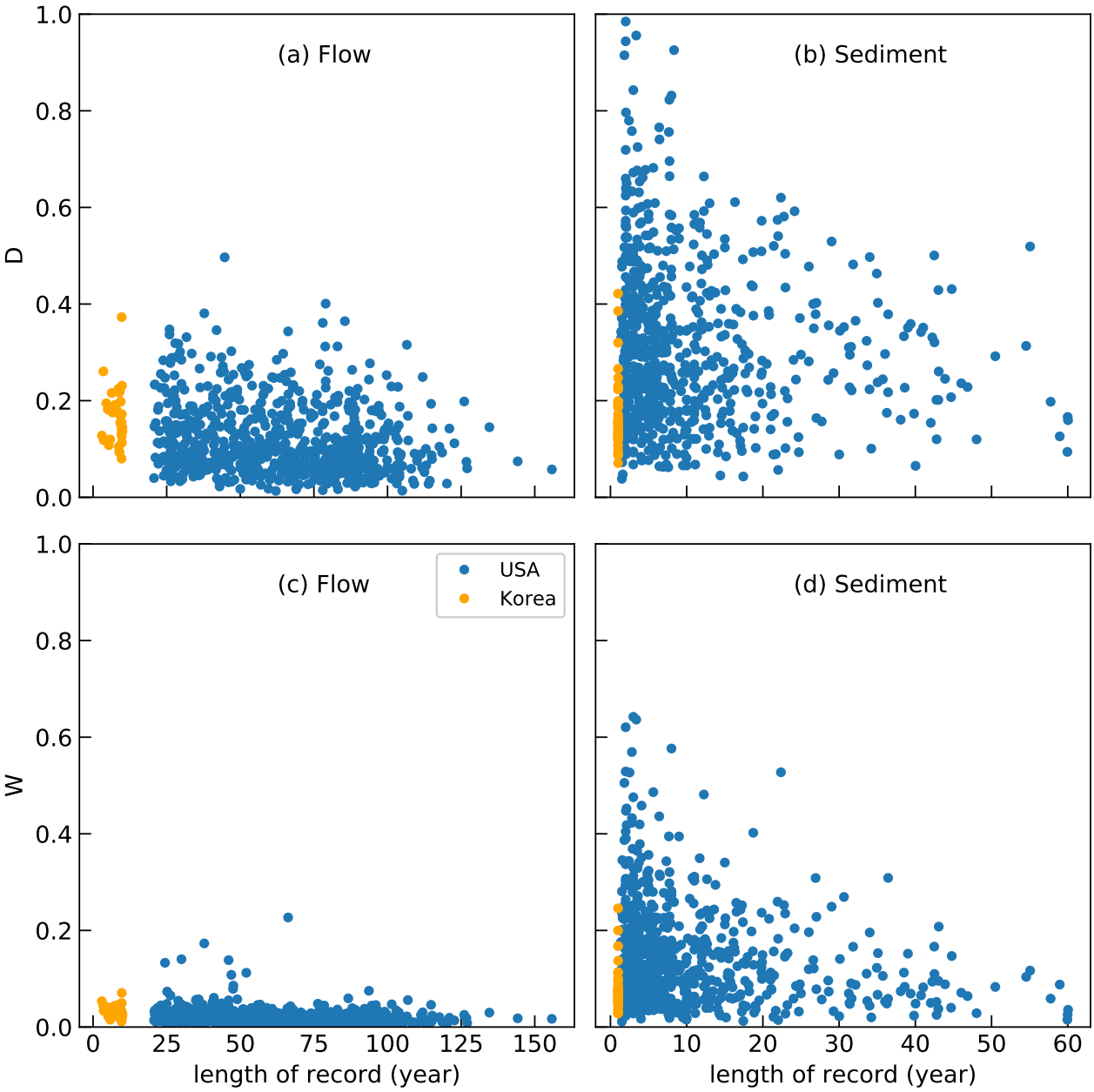

Figure 7.9: (a) Length record for flow vs D from CDF of Q, (b) length record for sediment vs D from CDF of Q_s, (c) length record for flow vs W from CDF of Q, and (d) length record for flow vs D from CDF of Q_s

7.3 Conclusion

A proposed new method to parameterize the flow duration curve is developed and extensively tested on 35 gages in South Korea and 716 gages in the US. The prediction of sediment yield using the proposed method has excellent agreement to the flow-duration/sediment rating curve method with an average difference only 8.6%. The parameters can be used to estimate the cumulative distribution curves for flow and sediment discharge. The prediction of cumulative distribution curve for flow has an average Kolmogorov-Smirnov distance of 11%. While the prediction for sediment discharge has higher error, the error reduces with the length of record. The value of $\hat{b}$ describes the nonlinearity between rainfall and runoff processes. The typical values of $\hat{b}$ range between 1.2 and 3.5. The values of $\hat{b}$ are consistently between 0.5 and 2.5 in the east of Mississippi River and the Pacific Northwest. Large variability in $\hat{b}$ is found in the regions in High Plains and southern California. The variability is attributed to the high flashiness index in these regions.

Chapter 8

Conclusions

In this study, first, 1,962 sediment measurements at 35 stations in five South Korean rivers were used to estimate the total sediment load. The total sediment load is quantified by the Series Expansion of the Modified Einstein Procedure (SEMEP). The ratio of measured sediment load to total sediment load, as well as the ratio of suspended load to total sediment load are investigated.

Second, the streamflow data at these stations are used to generate flow duration curves. With the flow duration curves and sediment rating curves, the sediment yield is calculated as a function of drainage area. In order to compare the flow duration curves and sediment cumulative curves across different watersheds, these curves are normalized by dividing the discharge by mean discharge.

Last, I developed a parametric method to define the flow duration curve. The parameters $\hat{a}$ and $\hat{b}$ are obtained by the method of moments, and are combined with parameters $\bar{a}$ and $\bar{b}$ from the sediment rating curve to calculate the mean annual values and cumulative distribution curves of discharge and sediment load.

The conclusions are summarized as follows:

1. **Objective 1: (a) to estimate the total sediment load from the measured sediment load; (b) to examine the ratio of the measured to total sediment load; and (c) to examine the ratio of the suspended to total sediment load.**

   1a) SEMEP can calculate bedload from all 1,962 measurements, while MEP calculated only 1,808 of them. The ratio between the suspended and total load calculated by SEMEP correctly ranges from 0.2 to 1, and 97% of the ratios are greater than 0.9. For this reason, the SEMEP calculations are considered better and more accurate.

   1b) The ratio of measured sediment discharge is greater than 80% when $Q/\bar{Q} > 1$. Because the fine suspended materials in South Korea, the Rouse number Ro < 0.16, and the measured

sediment load is more than 90% of the total sediment load when $h > 1$ m for sand and gravel bed rivers.

1c) The results of SEMEP showed the suspended load consists over 99% of the total sediment load in sand bed rivers in South Korea. For gravel and sand bed rivers, over 90% of the sediment is in suspension when $Q/\bar{Q}$. Because the values of Ro is low in the Korean rivers, the ratio Q_s/Q_t becomes only a function of h/d_s. The suspended load is more the 80% of the total sediment load when $h/d_s > 18$.

2. **Objective 2: to investigate the cumulative distribution functions of water and sediment yield, and define the water and sediment relationships with watershed area.**

   Several hydrological variables (i.e., mean annual discharge, sediment yield, specific sediment yield) correlate with watershed area. For normalized flow duration curves, $Q/\bar{Q}$ decreases from 60 to 25 when watershed area increases from 128 to 20,381 km^2 at an exceedance probability equal to 0.1%. At a given discharge, the sediment load of a small watershed is one order of magnitude larger than for a large watershed. The cumulative distribution curves for sediment show that sediment is mostly transported during floods, especially for small watersheds. The value of $Q/\bar{Q}$ for the half yield discharge (half of the sediment transported) decreases from 26 to 9 when the watershed area increases from 128 to 20,381 km^2. The specific sediment yield can be predicted as a function of watershed area: $SSY = 300A^{-0.24}$. The RMSE = 86 tons/km^2·year and MAPE = 75% are significant less than the KICT and Yoon's model (RMSE = 320 and 7500 tons/km^2·year, respectively).

3. **Objective 3: to develop and test a procedure to determine sediment load based on the parametric description of flow duration and sediment rating curves.**

   A proposed new method to parameterize the flow duration curve is developed and extensively tested on 35 gages in South Korea and 716 gages in the US. According to the new method, the mean annual discharge can be calculated as $\bar{Q} = \hat{a}\Gamma(1+\hat{b})$, and the mean annual sediment yield can be computed as $\bar{Q}_s = \bar{a}\hat{a}^{\bar{b}}\Gamma(1 + \bar{b}\hat{b})$. The prediction of sediment yield using the

proposed method has excellent agreement to the flow-duration/sediment rating curve method with an average difference only 8.6%. The cumulative distribution curves for sediment can be estimated as $Q_{sx}/\bar{Q}_s = P(1+\bar{b}\hat{b})$ where $P(1+\bar{b}\hat{b})$ is the cumulative distribution function for gamma variables (for flow $\bar{b} = 1$). The values of $\hat{a}$ and $\hat{b}$ are found to be functions of watershed area. In South Korea, $\hat{a} = 0.0045A^{1.07}$, $\hat{b} = 3.6 - 0.17 \ln A$, $\bar{a} = 123.2A^{-0.96}$, $\bar{b} = 1.45 + 0.04 \ln A$, where A is watershed area in km^2. The values of $\hat{b}$ are consistently between 0.5 and 2.5 east of Mississippi River and the Pacific Northwest. Large variability in $\hat{b}$ is found in High Plains and Southern California, which is attributed to the high flashiness index in these regions.

The data and Python scripts for this study are available at https://github.com/chunyaoyang/dissertation.

Bibliography

Asselman, N. (2000). "Fitting and interpretation of sediment rating curves." *Journal of Hydrology*, 234(3-4), 228–248.

Atieh, M., Mehltretter, S. L., Gharabaghi, B., and Rudra, R. (2015). "Integrative neural networks model for prediction of sediment rating curve parameters for ungauged basins." *Journal of Hydrology*, 531, 1095–1107.

Baird, D. C. and Varyu, D. (2011). *Initial Evaluation of the Series Expansion of the Modified Einstein Procedure (SEMEP) for Computing Total Sediment Load*. Bureau of Reclamation, Technical Service Center, Denver, CO.

Baker, D. B., Richards, R. P., Loftus, T. T., and Kramer, J. W. (2004). "A new flashiness index: characteristics and applications to midwestern rivers and streams." *Journal of the American Water Resources Association*, 40(2), 503–522.

Batalla, R. J., Garcia, C., and Rovira, A. (2005). "A decade of sediment transport measurements in a large Mediterranean river (the Tordera, Catalan Ranges, NE Spain)." *Catchment dynamics and river processes : Mediterranean and other climate regions*, C. Garcia and R. J. Batalla, eds., Elsevier Science, 1 edition, Chapter 8, 117–140.

Botter, G., Basso, S., Rodriguez-Iturbe, I., and Rinaldo, A. (2013). "Resilience of river flow regimes." *Proceedings of the National Academy of Sciences*, 110(32), 12925–12930.

Bui, C. (2014). "Flow Duration Curve Analysis from Cochiti Dam to Elephant Butte Reservoir." *Report*, U.S. Department of Interior, Bureau of Reclamation, Albuquerque, New Mexico.

Bunte, K., Abt, S. R., Potyondy, J. P., and Ryan, S. E. (2004). "Measurement of coarse gravel and cobble transport using portable bedload traps." *Journal of Hydraulic Engineering*, 130(9), 879–893.

Bunte, K., Abt, S. R., Swingle, K. W., and Cenderelli, D. A. (2014). "Effective discharge in rocky mountain headwater streams." *Journal of hydrology*, 519, 2136–2147.

Bunte, K., Swingle, K. W., and Abt, S. R. (2007). *Guidelines for using bedload traps in coarse-bedded mountain streams: construction, installation, operation, and sample processing*, Vol. 191. US Department of Agriculture, Forest Service, Rocky Mountain Research Station.

Burkham, D. and Dawdy, D. R. (1980). "General study of the modified Einstein method of computing total sediment discharge." *Water Supply Paper*.

Chien, N. and Wan, Z. (1999). *Mechanics of Sediment Transport*. American Society of Civil Engineers, Reston, VA (jun).

Chough, S. K. (2013). *Geology and sedimentology of the Korean Peninsula*. Elsevier Science Direct E-books. Elsevier Science, Amsterdam ; Burlington.

Colby, B. R., Hembree, C. H., et al. (1955). *Computations of total sediment discharge, Niobrara River near Cody, Nebraska*. US Geological Survey Washington, DC.

Davis, B. E. (2005). "A guide to the proper selection and use of federally approved sediment and water-quality samplers." *Report*, US Geological Society.

de Vente, J., Verduyn, R., Verstraeten, G., Vanmaercke, M., and Poesen, J. (2011). "Factors controlling sediment yield at the catchment scale in NW Mediterranean geoecosystems." *Journal of Soils and Sediments*, 11(4), 690–707.

Dehghani, A. A., Haddadchi, A., Omid, M. H., and Movahedi, N. (2014). "Applicability of MEP and SEMEP for computing total sediment load (Case Study: Chelichay Catchment in Golestan Province)." *KSCE Journal of Civil Engineering*, 18(6), 1912–1919.

Einstein, H. A. (1950). "The bed-load function for sediment transportation in open channel flows.

Einstein, H. A. and Chien, N. (1953). *Transport of sediment mixtures with large ranges of grain sizes*, Vol. 47. University of California, Institute of Engineering Research.

Emmett, W. W. (1979). *A field calibration of the sediment-trapping characteristics of the Helley-Smith bedload sampler*, Vol. 1139. US Government Printing Office.

Galster, J. C. (2007). "Natural and anthropogenic influences on the scaling of discharge with drainage area for multiple watersheds." *Geosphere*, 3(4), 260–271.

Garcia, C., Laronne, J. B., and Sala, M. (2000). "Continuous monitoring of bedload flux in a mountain gravel-bed river." *Geomorphology*, 34(1-2), 23–31.

García, M. H. (2008). "Sediment Transport and Morphodynamics." *Sedimentation Engineering*, American Society of Civil Engineers, Reston, VA, 21–163.

Goodrich, D. C., Lane, L. J., Shillito, R. M., Miller, S. N., Syed, K. H., and Woolhiser, D. A. (1997). "Linearity of basin response as a function of scale in a semiarid watershed." *Water Resources Research*, 33(12), 2951–2965.

Guo, J. and Julien, P. Y. (2004). "Efficient Algorithm for Computing Einstein Integrals." *Journal of Hydraulic Engineering*, 130(12), 1198–1201.

Gurnell, A., Hannah, D., and Lawler, D. (1996). "Suspended sediment yield from glacier basins." *Erosion and Sediment Yield: Global and Regional Perspectives*, D. E. Walling and B. W. Webb, eds., International Association of Hydrological Sciences, Wallingford, UK, 586.

Hayward, J. A. (1980). "Hydrology and Stream Sediments in a Mountain Catchment." Ph.D. dissertation, Ph.D. dissertation.

Helley, E. J. and Smith, W. "Development and calibration of a pressure-difference bedload sampler." *Open-File Report 73-108*.

Hicks, M. and Gomez, B. (2016). "Sediment Transport." *Tools in Fluvial Geomorphology*, M. G. Kondolf and H. Piégay, eds., John Wiley & Sons, Chapter 15, 1156.

Higgitt, D. L. and Lu, X. (1996). "Patterns of sediment yield in the upper Yangtze basin, China." *Erosion and Sediment Yield: Global and Regional Perspectives*, D. E. Walling and B. W. Webb, eds., International Association of Hydrological Sciences, Wallingford, UK, 586.

Holmes Jr, R. R. (2010). "Measurement of bedload transport in sand-bed rivers: a look at two indirect sampling methods." *US Geological Survey Scientific Investigations Report*, 5091, 236–252.

Holmquist-Johnson, C., Raff, D. A., and Russell, K. (2009). "Bureau of Reclamation Automated Modified Einstein Procedure (BORAMEP) program for computing total sediment discharge." *Report*.

Jang, C., Shin, Y., Kum, D., Kim, R., Yang, J. E., Kim, S. C., Hwang, S. I., Lim, K. J., Yoon, J.-K., Park, Y. S., and Jung, Y. (2015). "Assessment of soil loss in South Korea based on land-cover type." *Stochastic Environmental Research and Risk Assessment*, 29(8), 2127–2141.

Jeong, K.-S., Kim, D.-K., and Joo, G.-J. (2007). "Delayed influence of dam storage and discharge on the determination of seasonal proliferations of Microcystis aeruginosa and Stephanodiscus hantzschii in a regulated river system of the lower Nakdong river (South Korea)." *Water Research*, 41(6), 1269–1279.

Jin, S. and Park, P.-H. (2007). "Tectonic activities and deformation in south korea constrained by gps observations." *International Journal of Geology*, 2, 11–15.

Julien, P. Y. (1996). "Transforms for Runoff and Sediment Transport." *Journal of Hydrologic Engineering*, 1(3), 114–122.

Julien, P. Y. (2010). *Erosion and sedimentation*. Cambridge University Press, 2 edition.

Julien, P. Y. (2018). *River mechanics.* Cambridge University Press, 2 edition.

Julien, P. Y., Kang, W., and Yang, C.-Y. (2017). "Multivariate Regression Analysis and Model Development for the Estimation of Sediment Yield from Ungauged Watershed in the Republic of Korea." *Report*, Colorado State University, Fort Collins.

Kane, B. (2003). "Specific Degradation as Function of Watershed Characteristics and Climatic Parameters." Ph.D. dissertation, Colorado State University, Fort Collins, CO.

Kane, B. and Julien, P. Y. (2007). "Specific Degradation of Watersheds." *International Journal of Sediment Research*, 22(2), 114–119.

Kao, S. and Milliman, J. (2008). "Water and sediment discharge from small mountainous rivers, taiwan: the roles of lithology, episodic events, and human activities." *The Journal of Geology*, 116(5), 431–448.

Keulegan, G. H. (1938). *Laws of turbulent flow in open channels*, Vol. 21. National Bureau of Standards US.

Kim, H. S. (2006). "Soil Erosion Modeling Using RUSLE and GIS on the Imha Watershed, South Korea." M.S. thesis, Colorado State University, Colorado State University.

Kim, H. Y. (2016). "Optimization of Sangju Weir Operations To Mitigate Sedimentation Problems." Ph.D. dissertation, Colorado State University, Fort Collins, CO.

Kim, J.-H., Ho, C.-H., Lee, M.-H., Jeong, J.-H., and Chen, D. (2006). "Large increase in heavy rainfall associated with tropical cyclone landfalls in korea after the late 1970s." *Geophysical Research Letters*, 33(18).

Kim, S.-M., Choi, Y., Suh, J., Oh, S., Park, H.-D., and Yoon, S.-H. (2012). "Estimation of soil erosion and sediment yield from mine tailing dumps using gis: a case study at the samgwang mine, korea." *Geosystem Engineering*, 15(1), 2–9.

Kociuba, W. (2016). "Effective method for continuous measurement of bedload transport rates by means of river bedload trap (rbt) in a small glacial high arctic gravel-bed river." *Hydrodynamic and Mass Transport at Freshwater Aquatic Interfaces*, Springer, 279–292.

Komar, P. D. (1980). "Modes of sediment transport in channelized water flows with ramifications to the erosion of the Martian outflow channels." *Icarus*, 42(3), 317–329.

Korean Institute of Construction Technology (2005). "Korean Dam Design Criteria and Manual." *Report*, Korean Institute of Construction Technology, Goyang, South Korea.

Kresser, W. (1964). "Gedanken zur geschiebe-und schwebstoffführung der gewässer." *Österreichische Wasserwirtschaft*, 16(1/2), 6–11.

Lane, E. W. and Borland, W. M. (1951). "Estimating bed load." *Eos, Transactions American Geophysical Union*, 32(1), 121–123.

Lara, J. M. (1966). *Computation of" Z's" for Use in the Modified Einstein Procedure*. Department of the Interior, Bureau of Reclamation, Division of Project Investigations, Hydrology Branch, Sedimentation Section.

Laronne, J. B. et al. (1993). "Very high rates of bedload sediment transport by ephemeral desert rivers." *Nature*, 366(6451), 148.

Lee, C. J. and Glysson, G. D. (2013). "Compilation, quality control, analysis, and summary of discrete suspended-sediment and ancillary data in the united states, 1901-2010." *U.S. Geological Survey Data Series 776*, US Geological Survey.

Lee, G. S. and Choi, I. H. (2010). "Scaling effect for the quantification of soil loss using GIS spatial analysis." *KSCE Journal of Civil Engineering*, 14(6), 897–904.

Lee, G.-S. and Lee, K.-H. (2010). "Determining the Sediment Delivery Ratio Using the Sediment-Rating Curve and a Geographic Information System Embedded Soil Erosion Model on a Basin Scale." *Journal of Hydrologic Engineering*, 15(10), 834–843.

Lee, J.-H. and Heo, J.-H. (2011). "Evaluation of estimation methods for rainfall erosivity based on annual precipitation in Korea." *Journal of Hydrology*, 409(1), 30–48.

Lee, S. and Kang, S. (2018). "Estimating magnitude of suspended sediment transport in ungauged east coastal zone." *Journal of Korea Water Resources Association*, 51(2), 175–182.

Lee, S. E. and Kang, S. H. (2013). "Estimating the GIS-based soil loss and sediment delivery ratio to the sea for four major basins in South Korea." *Water Science & Technology*, 68(1), 124.

Lin, L. I.-K. (1989). "A Concordance Correlation Coefficient to Evaluate Reproducibility." *Biometrics*, 45(1), 255.

Lvovich, M., Karasik, G. Y., Bratseva, N., Medvedeva, G., and Maleshko, A. (1991). "Contemporary intensity of the world land intracontinental erosion." *USSR Academy of Sciences, Moscow*.

Maddock, T. and Borland, W. M. (1950). *Sedimentation Studies for the Planning of Reservoirs by the Bureau of Reclamation*. Bureau of Reclamation, Hydrology Division.

Markovic, R. D. (1965). "Probability functions of best fit to distributions of annual precipitation and runoff." *Hydrology papers (Colorado State University); no. 8*.

Milliman, J. D. and Farnsworth, K. L. (2013). *River discharge to the coastal ocean: a global synthesis*. Cambridge University Press.

Milliman, J. D. and Syvitski, J. P. M. (1992). "Geomorphic/Tectonic Control of Sediment Discharge to the Ocean: The Importance of Small Mountainous Rivers." *The Journal of Geology*, 100(5), 525–544.

Møen, K. M., Bogen, J., Zuta, J. F., Ade, P. K., and Esbensen, K. (2010). "Bedload measurement in rivers using passive acoustic sensors." *US Geological Survey Scientific Investigations Report*, 5091, 336–351.

Morris, G. L. and Fan, J. (2009). *Reservoir Sedimentation Handbook*. McGraw-Hill Book Co., New York.

Park, S., Oh, C., Jeon, S., Jung, H., and Choi, C. (2011). "Soil erosion risk in Korean watersheds, assessed using the revised universal soil loss equation." *Journal of hydrology*, 399(3-4), 263–273.

Piest, R. F. (1964). "Long term sediment yields from small watersheds." *International Association of Hydrological Sciences*, 65, 121–140.

Renwick, W., Carlson, K., and Hayes-Bohanan, J. (2005a). "Trends in recent reservoir sedimentation rates in southwestern Ohio." *Journal of Soil and Water Conservation*, 60(2), 72–79.

Renwick, W. H. (1996). "Continent-scale reservoir sedimentation patterns in the United States." *Erosion and Sediment Yield: Global and Regional Perspectives*, D. E. Walling and B. W. Webb, eds.

Renwick, W. H., Smith, S., Bartley, J., and Buddemeier, R. (2005b). "The role of impoundments in the sediment budget of the conterminous United States." *Geomorphology*, 71(1-2), 99–111.

Rickenmann, D. (2017). "Bedload transport measurements with geophones, hydrophones, and underwater microphones (passive acoustic methods)." *Gravel-Bed Rivers: Processes and Disasters*, 185–208.

Rickenmann, D., Turowski, J. M., Fritschi, B., Wyss, C., Laronne, J., Barzilai, R., Reid, I., Kreisler, A., Aigner, J., Seitz, H., et al. (2014). "Bedload transport measurements with impact plate geophones: comparison of sensor calibration in different gravel-bed streams." *Earth Surface Processes and Landforms*, 39(7), 928–942.

Rosburg, T. T., Nelson, P. A., Sholtes, J. S., and Bledsoe, B. P. (2016). "The effect of flow data resolution on sediment yield estimation and channel design." *Journal of Hydrology*, 538, 429–439.

Rouse, H. (1937). "Modern Conceptions of the Mechanics or Fluid Turbulence." *Transactions of the American Society of Civil Engineers*, 102(1), 463–505.

Rubey, W. W. (1933). "Settling velocity of gravel, sand, and silt particles." *American Journal of Science*, (148), 325–338.

Shah-Fairbank, S. C. (2006). "Variability in Total Sediment Load Using BORAMEP on the Rio Grande Low Flow Conveyance Channel." M.S. thesis, Colorado State University, Fort Collins, CO.

Shah-Fairbank, S. C. (2009). "Series expansion of the modified Einstein Procedure." Ph.D. dissertation, Colorado State University, Fort Collins, CO.

Shah-Fairbank, S. C. and Julien, P. Y. (2015). "Sediment load calculations from point measurements in sand-bed rivers." *International Journal of Sediment Research*, 30(1), 1–12.

Shah-Fairbank, S. C., Julien, P. Y., and Baird, D. C. (2011). "Total Sediment Load from SEMEP Using Depth-Integrated Concentration Measurements." *Journal of Hydraulic Engineering*, 137(12), 1606–1614.

Shen, H. W. and Hung, C. S. (1983). "Remodified Einstein procedure for sediment load." *Journal of Hydraulic Engineering*, 109(4), 565–578.

Sheppard, J. R. (1965). "Methods and Their Suitability for Determining Total Sediment Quantities." *Proceedings of the Federal Inter-agency Sedimentation Conference 1963*, U.S. Department of Agriculture, Agricultural Research Service, ed., Washington, D.C.

Sholtes, J. S. (2015). "On the magnitude and frequency of sediment transport in rivers." Ph.D. dissertation, Colorado State University, Fort Collins, CO.

Simons, D. B. and Sentürk, F. (1992). *Sediment transport technology: water and sediment dynamics*. Water Resources Publication.

Song, Y., Kim, H.-C., and Lee, T. J. (2010). "Geothermal development in korea: Country update 2005-2009." *World Geothermal Congress*, 25–29.

Strand, R. I. and Pemberton, E. L. (1982). "Reservoir Sedimentation." *Technical Guideline for Bureau of Reclamation*, U.S. Department of Interior Bureau of Reclamation, Denver.

Syvitski, J. P., Peckham, S. D., Hilberman, R., and Mulder, T. (2003). "Predicting the terrestrial flux of sediment to the global ocean: a planetary perspective." *Sedimentary Geology*, 162(1-2), 5–24.

Syvitski, J. P. M. and Milliman, J. D. (2007). "Geology, Geography, and Humans Battle for Dominance over the Delivery of Fluvial Sediment to the Coastal Ocean." *The Journal of Geology*, 115(1), 1–19.

The World Bank (2017). "Republic of Korea", <https://data.worldbank.org/country/korea-rep> (January, 2019).

Toffaleti, F. B. (1969). "Definitive computation of sand discharge in rivers." *Journal of the Hydraulics Division*, 95(1), 225–248.

Turowski, J. M., Rickenmann, D., and Dadson, S. J. (2010). "The partitioning of the total sediment load of a river into suspended load and bedload: a review of empirical data." *Sedimentology*, 57(4), 1126–1146.

Vanmaercke, M., Poesen, J., Broeckx, J., and Nyssen, J. (2014). "Sediment yield in Africa." *Earth-Science Reviews*, 136, 350–368.

Verstraeten, G. and Poesen, J. (2001). "Factors controlling sediment yield from small intensively cultivated catchments in a temperate humid climate." *Geomorphology*, 40(1), 123–144.

Walling, D. (1978). "Suspended sediment and solute response characteristics of the river exe, devon, england." *Research in fluvial systems*, 169–197.

Walling, D. E. and Webb, B. W. (1983). "Patterns of sediment yield." *Background to Palaeohydrology. A Perspective., 1983,*, 69–100.

Warrick, J. A. (2015). "Trend analyses with river sediment rating curves." *Hydrological processes*, 29(6), 936–949.

Williams, G. and Rosgen, D. (1989). "Measured total sediment loads (suspended loads and bedloads) for 93 United States streams." *Open-File Report 89-67*, US Geological Survey, Denver, CO.

Wohl, E. (2014). *Rivers in the landscape: science and management*. John Wiley & Sons.

Wohl, E., Lane, S. N., and Wilcox, A. C. (2015). "The science and practice of river restoration." *Water Resources Research*, 51(8), 5974–5997.

Yadav, M., Wagener, T., and Gupta, H. (2007). "Regionalization of constraints on expected watershed response behavior for improved predictions in ungauged basins." *Advances in Water Resources*, 30(8), 1756–1774.

Yang, C. T. (1996). *Sediment transport: theory and practice*. Krieger Pub Co.

Yoon, B. and Woo, H. (2000). "Sediment problems in Korea." *Journal of Hydraulic Engineering*, 126(7), 486–491.

Yoon, Y. J. (2011). "Development of Prediction Formulae for Sedimentation Rate of Multipurpose Dams." Ph.D. dissertation, Incheon National University, Incheon, South Korea.

Zamani, K., Bombardelli, F. A., and Kamrani-Moghaddam, B. (2017). "Comparison of Current Methods for the Evaluation of Einstein's Integrals." *Journal of Hydraulic Engineering*, 143(4), 06016026.

Ziegler, A. D., Sidle, R. C., Phang, V. X., Wood, S. H., and Tantasirin, C. (2014). "Bedload transport in SE Asian streams - uncertainties and implications for reservoir management." *Geomorphology*, 227, 31–48.

Appendix A

Total sediment discharge from measurements

A.1 The Toffaleti (1969) Method

Based on the concepts of Einstein (1950) and Einstein and Chien (1953), Toffaleti (1969) developed a procedure to calculate the total sediment load.

The flow depth is divided into four zones: "(1) the bed zone of the relative thickness $2d_i/h$ where d is the size of sediment and h is the depth of water; (2) the lower zone extending from $z/h = 2d_i/h$ to $z/h = 1/11.24$; (3) the middle zone extending from $z/h = 1/11.24$ to $z/h = 1/2.5$; and (4) the upper zone extending from $z/h = 1/2.5$ to the stream surface" (Simons and Sentürk 1992). Each zone has its concentration function (Figure A.1). The complete procedures to calculate the total sediment discharge by Toffaleti's method can be found in Simons and Sentürk (1992).

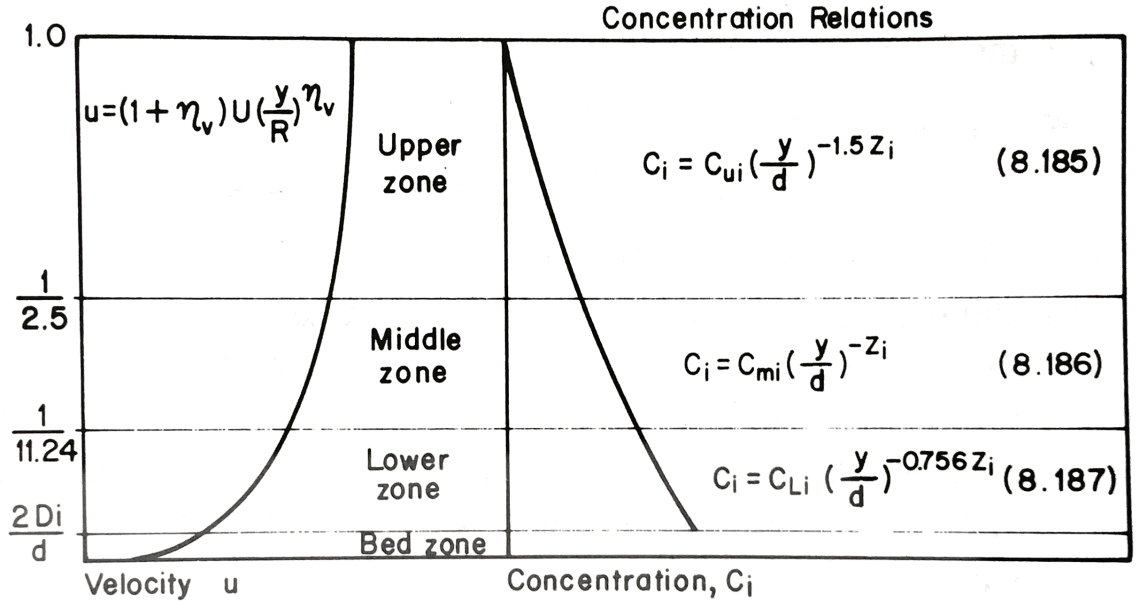

Figure A.1: Toffaleti's (1969) velocity and concentration profiles (from Simons and Sentürk 1992)

A.2 Series Expansion of the Modified Einstein Point Procedure (SEMEPP)

Point measurements can also be used to measure the suspended load. Point measurements are more accurate than the depth-integrating method because of the larger sampling volume. It is especially greater for deep sand-bed channels (Shah-Fairbank and Julien 2015).

Shah-Fairbank and Julien (2015) developed a procedure to calculate the total sediment load based on point velocity and sediment concentration measurements. Equation A.1 is derived from the logarithmic fit to the measured velocity profile, and the Rouse number, Ro, is obtained by fitting the power function to the concentration measurements.

$$v = \frac{u_*}{\kappa} \ln\left(\frac{z}{z_o}\right) \tag{A.1}$$

$$C = C_a \left(\frac{h-z}{z}\frac{a}{h-a}\right)^{\text{Ro}} \tag{A.2}$$

, where v is the velocity, u_* is the shear velocity, κ is the von Kármán constant of 0.4, z is the flow depth, z_o is the depth of flow where v is zero, C is the concentration, C_a is the reference concentration, h is the flow depth, a is the reference depth and Ro is the Rouse number. The values of u_*, z_o (depth of zero velocity), C_a and Ro are constants determined by the regression analysis.

The measured load and the total load can be calculated as follows:

$$q_m = \frac{C_a h u_*}{\kappa}\left(\frac{E}{1-E}\right)^{\text{Ro}}\left[\ln\left(\frac{h}{z_o}\right)J_{1A} + J_{2A}\right] \tag{A.3}$$

$$J_{1A} = \int_A^1 \left(\frac{1-z_*}{z_*}\right)^{\text{Ro}} dz_* \tag{A.4}$$

$$J_{2A} = \int_A^1 \ln z_* \left(\frac{1-z_*}{z_*}\right)^{\text{Ro}} dz_* \tag{A.5}$$

$$q_t = C_a v_a a + \frac{C_a h u_*}{\kappa} \left(\frac{E}{1-E} \right)^{\text{Ro}} \left[\ln \left(\frac{h}{z_o} \right) J_{1E} + J_{2E} \right] \tag{A.6}$$

$$J_{1E} = \int_E^1 \left(\frac{1-z_*}{z_*} \right)^{\text{Ro}} dz_* \tag{A.7}$$

$$J_{2E} = \int_E^1 \ln z_* \left(\frac{1-z_*}{z_*} \right)^{\text{Ro}} dz_* \tag{A.8}$$

Appendix B

Multivariate Regression Analysis and Model Development for the Estimation of Sediment Yield from Ungauged Watershed in the Republic of Korea

This appendix presents the summary of the result of Julien et al. (2017). The relationships between specific sediment yield and 34 watershed parameters are examined. These parameters are classified into 5 groups following the Universal Soil Loss Equation (USLE) as shown in Table B.1.

Table B.1: Parameter classification

Group	Factors
Watershed characteristics	Watershed area, watershed perimeter, main stream length, tributary length, total stream length, drainage density , channel width, elevation, minimum d_{50}, maximum d_{50}, mean d_{50}
Mean annual precipitation	Mean annual precipitation (1986 to 2015)
Land use	Percentage of urban, percentage of agriculture, percentage of forest, percentage of wetland, percentage of bare land, percentage of water
Soil type	Clay (0 10cm), clay (10 30cm), clay (30 50cm), clay (0 50cm), silt (0 10cm), silt (10 30cm), silt (30 50cm), silt (0 50cm), sand (0 10cm), sand (10 30cm), sand (30 50cm), sand (0 50cm)
Slope	Watershed average slope, slope at station, river slope

Based on the analyses, a five-parameter model is proposed:

$$SSY = 1.34 \times 10^{-9} A^{-0.016} P^{2.587} \%U^{0.735} Sand^{1.810} S^{-0.380} \tag{B.1}$$

where A is the watershed area in km^2, P is the mean annual precipitation in mm, $\%U$ is the percentage of urban, $Sand$ is the percentage of sand at 0 - 50 cm, and S is the watershed average slope ($\%$).

Appendix C

List of the US stations

Table C.1: The list of the US Stations used in this study

Station ID	Name	Latitude	Longitude	Area
1100000	MERRIMACK RIVER BL CONCORD RIVER AT LOWELL, MA	42.646	-71.298	12005
1127500	YANTIC RIVER AT YANTIC, CT	41.559	-72.121	231
1192883	COGINCHAUG RIVER AT MIDDLEFIELD, CT	41.520	-72.707	77
1193500	SALMON RIVER NEAR EAST HAMPTON, CT	41.552	-72.449	259
1197500	HOUSATONIC RIVER NEAR GREAT BARRINGTON, MA	42.232	-73.355	730
1198000	GREEN RIVER NEAR GREAT BARRINGTON, MA	42.193	-73.391	132
1199000	HOUSATONIC RIVER AT FALLS VILLAGE, CT	41.957	-73.369	1642
1200500	HOUSATONIC RIVER AT GAYLORDSVILLE, CT	41.653	-73.490	2580
1331095	HUDSON RIVER AT STILLWATER NY	42.936	-73.652	9772
1357500	MOHAWK RIVER AT COHOES NY	42.785	-73.708	8936
1379500	PASSAIC RIVER NEAR CHATHAM NJ	40.726	-74.390	259
1389500	PASSAIC RIVER AT LITTLE FALLS NJ	40.885	-74.226	1974
1401000	STONY BROOK AT PRINCETON NJ	40.333	-74.682	115
1411000	GREAT EGG HARBOR RIVER AT FOLSOM NJ	39.595	-74.852	148
1411500	MAURICE RIVER AT NORMA NJ	39.496	-75.077	290
1434000	DELAWARE RIVER AT PORT JERVIS, NY	41.371	-74.697	7967
1451000	LEHIGH RIVER AT WALNUTPORT, PA	40.757	-75.603	2303
1464500	CROSSWICKS CREEK AT EXTONVILLE NJ	40.137	-74.600	211
1467150	COOPER RIVER AT HADDONFIELD NJ	39.903	-75.021	44
1468500	SCHUYLKILL RIVER AT LANDINGVILLE, PA	40.629	-76.125	344
1470500	SCHUYLKILL RIVER AT BERNE, PA	40.523	-75.998	919
1470960	TULPEHOCKEN CR AT BLUE MARSH DAMSITE NEAR READING	40.371	-76.025	453
1472000	SCHUYLKILL RIVER AT POTTSTOWN, PA	40.242	-75.652	2971
1473000	PERKIOMEN CREEK AT GRATERFORD, PA	40.230	-75.452	723
1473120	SKIPPACK CREEK NEAR COLLEGEVILLE, PA	40.165	-75.433	139
1474500	SCHUYLKILL RIVER AT PHILADELPHIA, PA	39.968	-75.189	4903
1477120	RACCOON CREEK NEAR SWEDESBORO NJ	39.741	-75.259	70
1481000	BRANDYWINE CREEK AT CHADDS FORD, PA	39.870	-75.593	743
1481500	BRANDYWINE CREEK AT WILMINGTON, DE	39.770	-75.577	813
1491000	CHOPTANK RIVER NEAR GREENSBORO, MD	38.997	-75.786	293
1516500	COREY CREEK NEAR MAINESBURG, PA	41.791	-77.015	32
1517000	ELK RUN NEAR MAINESBURG, PA	41.815	-76.965	26
1531000	CHEMUNG RIVER AT CHEMUNG, NY	42.002	-76.635	6491

Table C.1 – continued from previous page

Station ID	Name	Latitude	Longitude	Area
1531500	SUSQUEHANNA RIVER AT TOWANDA, PA	41.765	-76.441	20194
1539000	FISHING CREEK NEAR BLOOMSBURG, PA	41.078	-76.431	710
1540500	SUSQUEHANNA RIVER AT DANVILLE, PA	40.958	-76.619	29060
1541000	WEST BRANCH SUSQUEHANNA RIVER AT BOWER, PA	40.897	-78.677	816
1544000	FIRST FORK SINNEMAHONING CR NEAR SINNEMAHONING, PA	41.402	-78.024	635
1547200	BALD EAGLE CREEK BL SPRING CREEK AT MILESBURG, PA	40.943	-77.786	686
1547500	BALD EAGLE CREEK AT BLANCHARD, PA	41.052	-77.604	878
1547700	MARSH CREEK AT BLANCHARD, PA	41.060	-77.606	114
1549500	BLOCKHOUSE CREEK NEAR ENGLISH CENTER, PA	41.474	-77.231	98
1553500	WEST BRANCH SUSQUEHANNA RIVER AT LEWISBURG, PA	40.968	-76.876	17734
1567000	JUNIATA RIVER AT NEWPORT, PA	40.478	-77.129	8687
1570500	SUSQUEHANNA RIVER AT HARRISBURG, PA	40.255	-76.886	62419
1573000	SWATARA CREEK AT HARPER TAVERN, PA	40.403	-76.577	873
1575000	SOUTH BRANCH CODORUS CREEK NEAR YORK, PA	39.921	-76.749	303
1576500	CONESTOGA RIVER AT LANCASTER, PA	40.050	-76.277	839
1578310	SUSQUEHANNA RIVER AT CONOWINGO, MD	39.658	-76.174	70189
1589000	PATAPSCO RIVER AT HOLLOFIELD, MD	39.310	-76.792	738
1594440	PATUXENT RIVER NEAR BOWIE, MD	38.956	-76.694	901
1597000	CRABTREE CREEK NEAR SWANTON, MD	39.501	-79.159	43
1603000	NORTH BRANCH POTOMAC RIVER NEAR CUMBERLAND, MD	39.622	-78.773	2271
1614500	CONOCOCHEAGUE CREEK AT FAIRVIEW, MD	39.716	-77.825	1279
1631000	S F SHENANDOAH RIVER AT FRONT ROYAL, VA	38.914	-78.211	4232
1638500	POTOMAC RIVER AT U.S. HWY 15 AT POINT OF ROCKS, MD	39.274	-77.543	
1639000	MONOCACY RIVER AT BRIDGEPORT, MD	39.679	-77.235	448
1650500	NORTHWEST BRANCH ANACOSTIA RIVER NR COLESVILLE, MD	39.066	-77.029	54
1658500	S F QUANTICO CREEK NEAR INDEPENDENT HILL, VA	38.587	-77.429	20
1663500	HAZEL RIVER AT RIXEYVILLE, VA	38.592	-77.965	738
1664000	RAPPAHANNOCK RIVER AT REMINGTON, VA	38.531	-77.814	1603
1667500	RAPIDAN RIVER NEAR CULPEPER, VA	38.350	-77.975	1212
2019500	JAMES RIVER AT BUCHANAN, VA	37.531	-79.679	5369
2029000	JAMES RIVER AT SCOTTSVILLE, VA	37.797	-78.491	11865
2060500	ROANOKE RIVER AT ALTAVISTA, VA	37.105	-79.295	4615
2066000	ROANOKE (STAUNTON) RIVER AT RANDOLPH, VA	36.915	-78.741	7682
2075500	DAN RIVER AT PACES, VA	36.642	-79.089	6700
2083500	TAR RIVER AT TARBORO, NC	35.894	-77.533	5654
2084160	CHICOD CR AT SR1760 NEAR SIMPSON, NC	35.562	-77.231	117
2116500	YADKIN RIVER AT YADKIN COLLEGE, NC	35.857	-80.387	5905
2118000	SOUTH YADKIN RIVER NEAR MOCKSVILLE, NC	35.845	-80.659	793

Table C.1 – continued from previous page

Station ID	Name	Latitude	Longitude	Area
2131000	PEE DEE RIVER AT PEEDEE, SC	34.204	-79.548	22870
2175000	EDISTO RIVER NR GIVHANS, SC	33.028	-80.391	7071
2383500	COOSAWATTEE RIVER NEAR PINE CHAPEL, GA	34.564	-84.833	2152
2430000	MACKEYS CREEK NR DENNIS, MS	34.526	-88.323	173
2489500	PEARL R NR BOGALUSA, LA	30.793	-89.821	17024
3015500	BROKENSTRAW CREEK AT YOUNGSVILLE, PA	41.853	-79.317	831
3020500	OIL CREEK AT ROUSEVILLE, PA	41.482	-79.695	733
3032500	REDBANK CREEK AT ST. CHARLES, PA	40.995	-79.394	1368
3040000	STONYCREEK RIVER AT FERNDALE, PA	40.286	-78.921	1168
3061500	BUFFALO CREEK AT BARRACKVILLE, WV	39.504	-80.172	300
3068800	SHAVERS FORK BELOW BOWDEN, WV	38.913	-79.770	391
3085000	MONONGAHELA RIVER AT BRADDOCK, PA	40.391	-79.858	19003
3111548	WHEELING CREEK BELOW BLAINE OH	40.067	-80.808	253
3139000	KILLBUCK CREEK AT KILLBUCK OH	40.481	-81.986	1202
3144500	MUSKINGUM RIVER AT DRESDEN OH	40.120	-82.000	15522
3150000	MUSKINGUM RIVER AT MCCONNELSVILLE OH	39.645	-81.850	19223
3151400	LITTLE KANAWHA RIVER NR WILDCAT, WV	38.743	-80.525	290
3159500	HOCKING RIVER AT ATHENS OH	39.329	-82.088	2442
3195500	ELK RIVER AT SUTTON, WV	38.663	-80.710	1404
3197000	ELK RIVER AT QUEEN SHOALS, WV	38.471	-81.284	2966
3199000	LITTLE COAL RIVER AT DANVILLE, WV	38.080	-81.836	697
3200500	COAL RIVER AT TORNADO, WV	38.339	-81.842	2233
3202400	GUYANDOTTE RIVER NEAR BAILEYSVILLE, WV	37.604	-81.645	793
3202750	CLEAR FORK AT CLEAR FORK, WV	37.623	-81.707	326
3204000	GUYANDOTTE RIVER AT BRANCHLAND, WV	38.221	-82.203	3170
3204500	MUD RIVER NEAR MILTON, WV	38.388	-82.113	663
3207800	LEVISA FORK AT BIG ROCK, VA	37.354	-82.196	769
3207965	GRAPEVINE CREEK NEAR PHYLLIS, KY	37.433	-82.354	16
3209300	RUSSELL FORK AT ELKHORN CITY, KY	37.304	-82.343	1435
3210000	JOHNS CREEK NEAR META KY	37.567	-82.458	146
3211500	JOHNS CREEK NEAR VAN LEAR, KY	37.744	-82.724	534
3212500	LEVISA FORK AT PAINTSVILLE, KY	37.815	-82.792	5553
3216500	LITTLE SANDY RIVER AT GRAYSON, KY	38.330	-82.939	1036
3217000	TYGARTS CREEK NEAR GREENUP, KY	38.564	-82.952	627
3219500	SCIOTO RIVER NEAR PROSPECT OH	40.420	-83.197	1469
3226800	OLENTANGY RIVER NEAR WORTHINGTON OH	40.110	-83.032	1287
3228500	BIG WALNUT CREEK AT CENTRAL COLLEGE OH	40.104	-82.884	492
3229000	ALUM CREEK AT COLUMBUS OH	39.945	-82.941	490

Table C.1 – continued from previous page

Station ID	Name	Latitude	Longitude	Area
3230450	HELLBRANCH RUN NEAR HARRISBURG OH	39.848	-83.157	93
3230500	BIG DARBY CREEK AT DARBYVILLE OH	39.701	-83.110	1383
3234000	PAINT CREEK NEAR BOURNEVILLE OH	39.264	-83.167	2090
3234500	SCIOTO RIVER AT HIGBY OH	39.212	-82.864	13289
3237280	UPPER TWIN CREEK AT MCGAW OH	38.644	-83.216	32
3240000	LITTLE MIAMI RIVER NEAR OLDTOWN OH	39.748	-83.931	334
3241500	MASSIES CREEK AT WILBERFORCE OH	39.722	-83.882	164
3244000	TODD FORK NEAR ROACHESTER OH	39.335	-84.087	567
3245500	LITTLE MIAMI RIVER AT MILFORD OH	39.171	-84.298	3116
3248500	LICKING RIVER NEAR SALYERSVILLE, KY	37.751	-83.084	363
3249500	LICKING RIVER AT FARMERS, KY	38.115	-83.543	2142
3251500	LICKING RIVER AT MCKINNEYSBURG, KY	38.600	-84.266	6024
3261500	GREAT MIAMI RIVER AT SIDNEY OH	40.287	-84.150	1401
3261950	LORAMIE CREEK NEAR NEWPORT OH	40.307	-84.384	394
3265000	STILLWATER RIVER AT PLEASANT HILL OH	40.058	-84.356	1303
3270500	GREAT MIAMI RIVER AT DAYTON OH	39.765	-84.197	6503
3280600	MIDDLE FORK KENTUCKY RIVER NEAR HYDEN, KY	37.137	-83.371	523
3281000	MIDDLE FORK KENTUCKY RIVER AT TALLEGA, KY	37.555	-83.594	1391
3281100	GOOSE CREEK AT MANCHESTER, KY	37.152	-83.760	422
3287500	KENTUCKY RIVER AT LOCK 4 AT FRANKFORT, KY	38.202	-84.882	14014
3291500	EAGLE CREEK AT GLENCOE, KY	38.705	-84.824	1132
3294500	OHIO RIVER AT LOUISVILLE, KY	38.280	-85.799	236130
3298500	SALT RIVER AT SHEPHERDSVILLE, KY	37.985	-85.717	3100
3308500	GREEN RIVER AT MUNFORDVILLE, KY	37.269	-85.888	4333
3310500	NOLIN RIVER AT WAX, KY	37.345	-86.122	1554
3314500	BARREN RIVER AT BOWLING GREEN, KY	37.003	-86.433	4789
3318500	ROUGH RIVER AT FALLS OF ROUGH, KY	37.589	-86.551	1305
3319000	ROUGH RIVER NEAR DUNDEE, KY	37.548	-86.722	1961
3320000	GREEN RIVER AT LOCK 2 AT CALHOUN, KY	37.534	-87.264	19596
3320500	POND RIVER NEAR APEX, KY	37.122	-87.319	502
3328500	EEL RIVER NEAR LOGANSPORT, IN	40.782	-86.264	2044
3335500	WABASH RIVER AT LAFAYETTE, IN	40.425	-86.897	18822
3340800	BIG RACCOON CREEK NEAR FINCASTLE, IN	39.813	-86.954	360
3361000	BIG BLUE RIVER AT CARTHAGE, IN	39.744	-85.576	477
3365500	EAST FORK WHITE RIVER AT SEYMOUR, IN	38.983	-85.899	6063
3382100	SOUTH FORK SALINE RIVER NR CARRIER MILLS, IL	37.638	-88.678	381
3383000	TRADEWATER RIVER AT OLNEY, KY	37.224	-87.781	660
3384450	LUSK CREEK NEAR EDDYVILLE, IL	37.473	-88.548	111

Table C.1 – continued from previous page

Station ID	Name	Latitude	Longitude	Area
3402000	YELLOW CREEK NEAR MIDDLESBORO, KY	36.668	-83.689	157
3403000	CUMBERLAND RIVER NEAR PINEVILLE, KY	36.813	-83.766	2095
3403500	CUMBERLAND RIVER AT BARBOURVILLE, KY	36.862	-83.887	2486
3403910	CLEAR FORK AT SAXTON, KY	36.634	-84.112	857
3404000	CUMBERLAND RIVER AT WILLIAMSBURG, KY	36.743	-84.156	4162
3404500	CUMBERLAND RIVER AT CUMBERLAND FALLS, KY	36.837	-84.343	5120
3406500	ROCKCASTLE RIVER AT BILLOWS, KY	37.171	-84.296	1564
3410500	SOUTH FORK CUMBERLAND RIVER NEAR STEARNS, KY	36.627	-84.533	2471
3455000	FRENCH BROAD RIVER NEAR NEWPORT, TN	35.982	-83.161	4812
3465500	NOLICHUCKY RIVER AT EMBREEVILLE, TN	36.176	-82.457	2085
3467500	NOLICHUCKY RIVER NEAR MORRISTOWN, TENN.	36.180	-83.175	4349
3469000	FRENCH BROAD RIVER BELOW DOUGLAS DAM, TN	35.952	-83.551	11766
3487500	SOUTH FORK HOLSTON RIVER AT KINGSPORT, TENN	36.523	-82.546	5012
3495500	HOLSTON RIVER NEAR KNOXVILLE, TN	36.016	-83.832	9705
3497000	TENNESSEE RIVER AT KNOXVILLE, TENNESSEE	35.955	-83.862	23139
3519500	LITTLE TENNESSEE RIVER AT MCGHEE, TENN	35.604	-84.212	6327
3520000	TENNESSEE RIVER AT LOUDON, TENN.	35.743	-84.332	31650
3528000	CLINCH RIVER NEAR TAZEWELL (LONE MOUNTAIN), TN	36.425	-83.398	3820
3532000	POWELL RIVER ABOVE U.S. HWY 25E NEAR ARTHUR, TN	36.542	-83.630	1777
3540500	EMORY RIVER AT OAKDALE, TN	35.983	-84.558	1979
3556000	TURTLETOWN CREEK AT TURTLETOWN, TN	35.133	-84.343	70
3561000	NORTH POTATO CREEK NEAR DUCKTOWN, TENN.	35.015	-84.383	34
3566000	HIWASSEE RIVER AT CHARLESTON, TN	35.295	-84.760	5952
3568000	TENNESSEE RIVER AT CHATTANOOGA, TN	35.087	-85.278	55426
3571000	SEQUATCHIE RIVER NEAR WHITWELL, TN	35.207	-85.497	1041
3571850	TENNESSEE RIVER AT SOUTH PITTSBURG, TN	35.011	-85.697	58638
3584500	ELK RIVER NEAR PROSPECT, TN	35.028	-86.948	4621
3603000	DUCK RIVER ABOVE HURRICANE MILLS, TN	35.930	-87.743	6623
3604500	BUFFALO RIVER NEAR LOBELVILLE, TN	35.813	-87.798	1831
3609500	TENNESSEE RIVER NEAR PADUCAH, KY	37.020	-88.281	104118
4024098	DEER CREEK NEAR HOLYOKE, MN	46.525	-92.389	20
4024430	NEMADJI RIVER NEAR SOUTH SUPERIOR, WI	46.633	-92.094	1088
4058500	EAST BRANCH ESCANABA RIVER AT GWINN, MI	46.282	-87.435	321
4073462	WHITE CREEK AT SPRING GROVE ROAD NR GREEN LAKE, WI	43.816	-88.928	8
4073468	GREEN LAKE INLET AT CT HIGHWAY A NR GREEN LAKE, WI	43.824	-88.927	139
4086600	MILWAUKEE RIVER NEAR CEDARBURG, WI	43.280	-87.943	1572
4087000	MILWAUKEE RIVER AT MILWAUKEE, WI	43.100	-87.909	1803
4087030	MENOMONEE RIVER AT MENOMONEE FALLS, WI	43.173	-88.104	90

Table C.1 – continued from previous page

Station ID	Name	Latitude	Longitude	Area
4087088	UNDERWOOD CREEK AT WAUWATOSA, WI	43.055	-88.046	47
4087120	MENOMONEE RIVER AT WAUWATOSA, WI	43.046	-88.000	319
4087159	KINNICKINNIC RIVER @ S. 11TH STREET @ MILWAUKEE,WI	42.998	-87.926	49
4095300	TRAIL CREEK AT MICHIGAN CITY, IN	41.717	-86.860	140
4102700	SOUTH BRANCH BLACK RIVER NEAR BANGOR, MI	42.354	-86.188	217
4142000	RIFLE RIVER NEAR STERLING, MI	44.073	-84.020	829
4144500	SHIAWASSEE RIVER AT OWOSSO, MI	43.015	-84.180	1393
4151500	CASS RIVER AT FRANKENMUTH, MI	43.328	-83.748	2178
4176500	RIVER RAISIN NEAR MONROE, MI	41.961	-83.531	2699
4182000	ST. MARYS RIVER NEAR FORT WAYNE, IN	40.988	-85.112	1974
4192500	MAUMEE RIVER NEAR DEFIANCE OH	41.292	-84.281	14362
4193500	MAUMEE RIVER AT WATERVILLE OH	41.500	-83.713	16395
4195500	PORTAGE RIVER AT WOODVILLE OH	41.449	-83.361	1109
4197100	HONEY CREEK AT MELMORE OH	41.022	-83.110	386
4198000	SANDUSKY RIVER NEAR FREMONT OH	41.308	-83.159	3240
4199000	HURON RIVER AT MILAN OH	41.301	-82.608	961
4201500	ROCKY RIVER NEAR BEREA OH	41.407	-81.887	692
4202000	CUYAHOGA RIVER AT HIRAM RAPIDS OH	41.341	-81.167	391
4206000	CUYAHOGA RIVER AT OLD PORTAGE OH	41.136	-81.547	1046
4207200	TINKERS CREEK AT BEDFORD OH	41.384	-81.527	217
4208000	CUYAHOGA RIVER AT INDEPENDENCE OH	41.395	-81.630	1831
4209000	CHAGRIN RIVER AT WILLOUGHBY OH	41.631	-81.403	637
4212100	GRAND RIVER NEAR PAINESVILLE OH	41.719	-81.228	1774
4221000	GENESEE RIVER AT WELLSVILLE, NY	42.122	-77.957	746
4223000	GENESEE RIVER AT PORTAGEVILLE NY	42.570	-78.042	2549
4227500	GENESEE RIVER NEAR MOUNT MORRIS NY	42.767	-77.839	3688
4232000	GENESEE RIVER AT ROCHESTER NY	43.181	-77.628	6428
4233300	SIXMILE CREEK AT BETHEL GROVE NY	42.403	-76.435	101
5058700	SHEYENNE RIVER AT LISBON, ND	46.447	-97.679	21212
5059000	SHEYENNE RIVER NEAR KINDRED, ND	46.632	-97.001	22792
5062000	BUFFALO RIVER NR DILWORTH, MN	46.961	-96.661	
5062500	WILD RICE RIVER AT TWIN VALLEY, MN	47.266	-96.248	2419
5099600	PEMBINA RIVER AT WALHALLA, ND	48.913	-97.917	8677
5114000	SOURIS RIVER NR SHERWOOD, ND	48.990	-101.958	23155
5280000	CROW RIVER AT ROCKFORD, MN	45.087	-93.734	6838
5288500	MISSISSIPPI RIVER AT HWY 610 IN BROOKLYN PARK, MN	45.127	-93.297	49469
5291000	WHETSTONE RIVER NEAR BIG STONE CITY, SD	45.292	-96.488	1052
5293000	YELLOW BANK RIVER NEAR ODESSA, MN	45.227	-96.354	1189

Table C.1 – continued from previous page

Station ID	Name	Latitude	Longitude	Area
5304500	CHIPPEWA RIVER NEAR MILAN, MN	45.108	-95.799	4869
5317000	COTTONWOOD RIVER NEAR NEW ULM, MN	44.289	-94.440	3367
5325000	MINNESOTA RIVER AT MANKATO, MN	44.169	-94.003	38591
5341500	APPLE RIVER NEAR SOMERSET, WI	45.158	-92.716	1500
5357335	BEAR RIVER NEAR MANITOWISH WATERS, WI	46.049	-89.985	211
5369500	CHIPPEWA RIVER AT DURAND, WI	44.631	-91.971	23336
5378500	MISSISSIPPI RIVER AT WINONA, MN	44.056	-91.638	153328
5382000	BLACK RIVER NEAR GALESVILLE, WI	44.060	-91.287	5387
5385000	ROOT RIVER NEAR HOUSTON, MN	43.769	-91.570	3238
5387500	UPPER IOWA RIVER AT DECORAH, IA	43.305	-91.796	1323
5388250	UPPER IOWA RIVER NEAR DORCHESTER, IA	43.421	-91.509	1994
5388500	PAINT CREEK AT WATERVILLE, IA	43.210	-91.306	111
5389400	BLOODY RUN CREEK NEAR MARQUETTE, IA	43.041	-91.207	88
5389500	MISSISSIPPI RIVER AT MCGREGOR, IA	43.027	-91.173	174825
5406500	BLACK EARTH CREEK AT BLACK EARTH, WI	43.134	-89.732	118
5407000	WISCONSIN RIVER AT MUSCODA, WI	43.198	-90.441	
5408000	KICKAPOO RIVER AT LA FARGE, WI	43.574	-90.643	689
5412500	TURKEY RIVER AT GARBER, IA	42.740	-91.262	4002
5413500	GRANT RIVER AT BURTON, WI	42.720	-90.819	697
5418500	MAQUOKETA RIVER NEAR MAQUOKETA, IA	42.083	-90.633	4022
5419000	APPLE RIVER NEAR HANOVER, IL	42.258	-90.285	637
5420500	MISSISSIPPI RIVER AT CLINTON, IA	41.781	-90.252	221704
5421000	WAPSIPINICON RIVER AT INDEPENDENCE, IA	42.464	-91.895	2714
5422000	WAPSIPINICON RIVER NEAR DE WITT, IA	41.767	-90.535	6050
5422470	CROW CREEK AT BETTENDORF, IA	41.551	-90.455	46
5426000	CRAWFISH RIVER AT MILFORD, WI	43.100	-88.849	1974
5427718	YAHARA RIVER AT WINDSOR, WI	43.209	-89.353	191
5427948	PHEASANT BRANCH AT MIDDLETON, WI	43.103	-89.512	47
5431017	DELAVAN LAKE INLET AT STATE HWY 50 AT LAKE LAWN,WI	42.621	-88.583	56
5431022	DELAVAN LAKE OUTLET AT BORG ROAD NEAR DELAVAN, WI	42.615	-88.625	109
5431486	TURTLE CREEK AT CARVERS ROCK ROAD NEAR CLINTON, WI	42.597	-88.829	515
5434500	PECATONICA RIVER AT MARTINTOWN, WI	42.510	-89.801	2678
5436500	SUGAR RIVER NEAR BRODHEAD, WI	42.612	-89.398	1355
5438500	KISHWAUKEE RIVER AT BELVIDERE, IL	42.256	-88.863	1393
5439000	SOUTH BRANCH KISHWAUKEE RIVER AT DEKALB, IL	41.931	-88.760	201
5440000	KISHWAUKEE RIVER NEAR PERRYVILLE, IL	42.194	-88.999	2846
5446500	ROCK RIVER NEAR JOSLIN, IL	41.556	-90.185	24732
5447500	GREEN RIVER NEAR GENESEO, IL	41.489	-90.158	2598

Table C.1 – continued from previous page

Station ID	Name	Latitude	Longitude	Area
5449500	IOWA RIVER NEAR ROWAN, IA	42.760	-93.622	1111
5451500	IOWA RIVER AT MARSHALLTOWN, IA	42.066	-92.908	3968
5454500	IOWA RIVER AT IOWA CITY, IA	41.657	-91.541	8472
5455000	RALSTON CREEK AT IOWA CITY, IA	41.664	-91.514	8
5464500	CEDAR RIVER AT CEDAR RAPIDS, IA	41.972	-91.667	16861
5465500	IOWA RIVER AT WAPELLO, IA	41.178	-91.182	32375
5466500	EDWARDS RIVER NEAR NEW BOSTON, IL	41.187	-90.967	1153
5469000	HENDERSON CREEK NEAR OQUAWKA, IL	41.001	-90.854	1119
5471050	SOUTH SKUNK RIVER AT COLFAX, IA	41.681	-93.247	2080
5474000	SKUNK RIVER AT AUGUSTA, IA	40.754	-91.277	11168
5476000	DES MOINES RIVER AT JACKSON, MN	43.618	-94.985	3238
5481650	DES MOINES RIVER NEAR SAYLORVILLE, IA	41.681	-93.668	15128
5482000	DES MOINES RIVER AT 2ND AVENUE AT DES MOINES, IA	41.612	-93.621	16175
5483000	EAST FORK HARDIN CREEK NEAR CHURDAN, IA	42.107	-94.370	62
5483450	MIDDLE RACCOON RIVER NEAR BAYARD, IA	41.779	-94.493	971
5483600	MIDDLE RACCOON RIVER AT PANORA, IA	41.687	-94.371	1140
5485500	DES MOINES RIVER BLW RACCOON RIV AT DES MOINES, IA	41.578	-93.605	25587
5486490	MIDDLE RIVER NEAR INDIANOLA, IA	41.424	-93.587	1268
5487980	WHITE BREAST CREEK NEAR DALLAS, IA	41.247	-93.290	862
5498000	MIDDLE FABIUS RIVER NEAR MONTICELLO, MO	40.094	-91.736	1018
5502500	NORTH FORK SALT RIVER NEAR SHELBINA, MO	39.741	-92.041	1246
5506000	YOUNGS CREEK NEAR MEXICO, MO	39.314	-91.947	175
5506500	MIDDLE FORK SALT RIVER AT PARIS, MO	39.484	-92.014	922
5507000	ELK FORK SALT RIVER NEAR PARIS, MO	39.443	-92.002	679
5508000	SALT RIVER NEAR NEW LONDON, MO	39.612	-91.407	6423
5516500	YELLOW RIVER AT PLYMOUTH, IND.	41.340	-86.304	761
5520500	KANKAKEE RIVER AT MOMENCE, IL	41.160	-87.669	5941
5525000	IROQUOIS RIVER AT IROQUOIS, IL	40.823	-87.581	1777
5526000	IROQUOIS RIVER NEAR CHEBANSE, IL	41.009	-87.823	5416
5527500	KANKAKEE RIVER NEAR WILMINGTON, IL	41.347	-88.186	13339
5532500	DES PLAINES RIVER AT RIVERSIDE, IL	41.822	-87.822	1632
5543500	ILLINOIS RIVER AT MARSEILLES, IL	41.327	-88.718	21391
5548280	NIPPERSINK CREEK NEAR SPRING GROVE, IL	42.443	-88.248	497
5552500	FOX RIVER AT DAYTON, IL	41.384	-88.789	6843
5558300	ILLINOIS RIVER AT HENRY, IL	41.107	-89.356	35079
5568000	MACKINAW RIVER NEAR GREEN VALLEY, IL	40.454	-89.606	2779
5570000	SPOON RIVER AT SEVILLE, IL	40.490	-90.340	4237
5570370	BIG CREEK NEAR BRYANT, IL	40.459	-90.133	107

Table C.1 – continued from previous page

Station ID	Name	Latitude	Longitude	Area
5583000	SANGAMON RIVER NEAR OAKFORD, IL	40.124	-89.985	13191
5585000	LA MOINE RIVER AT RIPLEY, IL	40.025	-90.632	3349
5586100	ILLINOIS RIVER AT VALLEY CITY, IL	39.703	-90.645	69264
5587500	MISSISSIPPI RIVER AT ALTON, IL	38.885	-90.181	444185
5591200	KASKASKIA RIVER AT COOKS MILLS, IL	39.583	-88.413	1225
5594100	KASKASKIA RIVER NEAR VENEDY STATION, IL	38.451	-89.628	11378
5599500	BIG MUDDY RIVER AT MURPHYSBORO, IL	37.748	-89.347	5618
6018500	BEAVERHEAD RIVER NEAR TWIN BRIDGES MT	45.383	-112.453	9371
6025500	BIG HOLE RIVER NEAR MELROSE MT	45.527	-112.702	6402
6026500	JEFFERSON RIVER NEAR TWIN BRIDGES MT	45.613	-112.329	19725
6088300	MUDDY CREEK NEAR VAUGHN MT	47.625	-111.635	580
6088500	MUDDY CREEK AT VAUGHN MT	47.561	-111.542	663
6115200	MISSOURI RIVER NEAR LANDUSKY MT	47.631	-108.688	105281
6130500	MUSSELSHELL RIVER AT MOSBY MT	46.995	-107.889	20161
6185500	MISSOURI RIVER NEAR CULBERTSON MT	48.124	-104.473	232732
6188000	LAMAR RIVER NR TOWER FALLS RANGER STATION, YNP	44.928	-110.394	1709
6191500	YELLOWSTONE RIVER AT CORWIN SPRINGS, MT	45.112	-110.794	6783
6214500	YELLOWSTONE RIVER AT BILLINGS MT	45.800	-108.467	30575
6228000	WIND RIVER AT RIVERTON, WY	43.011	-108.377	5980
6236100	WIND RIVER AB BOYSEN RESERVOIR, NR SHOSHONI, WY	43.129	-108.225	11370
6244500	FIVEMILE CREEK AB WYOMING CANAL, NR PAVILLION, WY	43.301	-108.703	306
6253000	FIVEMILE CREEK NEAR SHOSHONI, WY	43.222	-108.220	1083
6257000	BADWATER CREEK AT BONNEVILLE, WYO.	43.269	-108.080	2093
6258000	MUDDY CREEK NEAR SHOSHONI, WY	43.286	-108.276	860
6259500	BIGHORN RIVER AT THERMOPOLIS, WYO.	43.646	-108.203	20772
6268500	FIFTEEN MILE CREEK NEAR WORLAND, WY	44.021	-108.014	1342
6279500	BIGHORN RIVER AT KANE, WY	44.759	-108.181	40824
6290500	LITTLE BIGHORN R BL PASS CREEK, NR WYOLA, MT	45.177	-107.395	1109
6294000	LITTLE BIGHORN RIVER NEAR HARDIN MT	45.736	-107.557	3351
6294700	BIGHORN RIVER AT BIGHORN MT	46.147	-107.467	59283
6295000	YELLOWSTONE RIVER AT FORSYTH, MT.	46.266	-106.691	103978
6308500	TONGUE RIVER AT MILES CITY, MT	46.385	-105.846	13996
6309500	MIDDLE FORK POWDER RIVER ABOVE KAYCEE, WY	43.647	-106.809	1166
6313000	SOUTH FORK POWDER RIVER NEAR KAYCEE, WY	43.619	-106.577	2979
6313500	POWDER RIVER AT SUSSEX, WY	43.697	-106.306	8003
6317000	POWDER RIVER AT ARVADA, WY	44.650	-106.128	15670
6324500	POWDER RIVER AT MOORHEAD, MT	45.058	-105.878	20948
6326500	POWDER RIVER NEAR LOCATE, MT.	46.430	-105.310	33846

Table C.1 – continued from previous page

Station ID	Name	Latitude	Longitude	Area
6329500	YELLOWSTONE RIVER NEAR SIDNEY, MT.	47.678	-104.157	178925
6335500	LITTLE MISSOURI RIVER AT MARMARTH, ND	46.298	-103.918	12018
6336000	LITTLE MISSOURI RIVER AT MEDORA, ND	46.919	-103.528	16032
6337000	LITTLE MISSOURI RIVER NR WATFORD CITY, ND	47.590	-103.252	21523
6339500	KNIFE RIVER NR GOLDEN VALLEY, ND	47.154	-102.060	3186
6340500	KNIFE RIVER AT HAZEN, ND	47.285	-101.622	5802
6342500	MISSOURI RIVER AT BISMARCK, ND	46.814	-100.821	482776
6345500	HEART RIVER NR RICHARDTON, ND	46.746	-102.308	3212
6349000	HEART RIVER NR MANDAN, ND	46.834	-100.975	8573
6350000	CANNONBALL RIVER AT REGENT, ND	46.427	-102.552	1502
6352500	CEDAR CREEK NR PRETTY ROCK, ND	46.032	-101.832	3471
6354000	CANNONBALL RIVER AT BREIEN, ND	46.376	-100.934	10619
6357500	GRAND R AT SHADEHILL SD	45.756	-102.196	7747
6357800	GRAND R AT LITTLE EAGLE,SD	45.658	-100.818	13768
6359500	MOREAU R NEAR FAITH,SD	45.198	-102.157	6713
6360500	MOREAU R NEAR WHITEHORSE,SD	45.256	-100.843	12663
6386000	LANCE CREEK NEAR RIVERVIEW, WY	43.355	-104.271	5361
6394000	BEAVER CREEK NEAR NEWCASTLE, WYO.	43.535	-104.118	3419
6400000	HAT CR NEAR EDGEMONT,SD	43.240	-103.588	2484
6400500	CHEYENNE R NEAR HOT SPRINGS SD	43.305	-103.562	22582
6425720	BELLE FOURCHE R BL RATTLESNAKE C, NR PINEY, WY	43.984	-105.388	1282
6437000	BELLE FOURCHE R NEAR STURGIS,SD	44.513	-103.137	15017
6439300	CHEYENNE RIVER AT CHERRY CREEK,SD	44.600	-101.498	61041
6440200	SOUTH FORK BAD R NEAR COTTONWOOD,SD	43.969	-101.767	666
6441500	BAD R NEAR FORT PIERRE,SD	44.327	-100.384	8151
6446000	WHITE R NEAR OGLALA SD	43.255	-102.827	5584
6447000	WHITE R NEAR KADOKA,SD	43.752	-101.525	12846
6452000	WHITE R NEAR OACOMA,SD	43.748	-99.556	25680
6453500	PONCA CREEK AT ANOKA, NEBR.	42.943	-98.841	1308
6457500	NIOBRARA RIVER NEAR GORDON, NEBR.	42.640	-102.211	11111
6461500	NIOBRARA RIVER NEAR SPARKS, NEBR.	42.902	-100.362	18519
6465500	NIOBRARA RIVER NEAR VERDEL, NEBR.	42.740	-98.223	29992
6477000	JAMES R NEAR FORESTBURG,SD	43.974	-98.071	45618
6478500	JAMES R NEAR SCOTLAND,SD	43.186	-97.636	53540
6481000	BIG SIOUX R NEAR DELL RAPIDS,SD	43.790	-96.746	10171
6486000	MISSOURI RIVER AT SIOUX CITY, IA	42.486	-96.414	814814
6600500	FLOYD RIVER AT JAMES, IA	42.577	-96.311	2295
6606600	LITTLE SIOUX RIVER AT CORRECTIONVILLE, IA	42.482	-95.793	6475

Table C.1 – continued from previous page

Station ID	Name	Latitude	Longitude	Area
6606700	LITTLE SIOUX RIVER NEAR KENNEBEC, IA	42.081	-96.014	7091
6610000	MISSOURI RIVER AT OMAHA, NE	41.259	-95.923	836052
6645000	NORTH PLATTE RIVER BELOW CASPER, WY	42.859	-106.211	32567
6650000	NORTH PLATTE RIVER NEAR DOUGLAS, WY	42.683	-105.391	47495
6656000	NORTH PLATTE RIVER BELOW GUERNSEY RESERVOIR, WY	42.281	-104.755	42054
6758500	SOUTH PLATTE RIVER NEAR WELDONA, CO	40.321	-103.920	34201
6771000	WOOD RIVER NEAR RIVERDALE, NEBR.	40.799	-99.197	982
6785000	MIDDLE LOUP RIVER AT SAINT PAUL, NEBR.	41.204	-98.446	20914
6790500	NORTH LOUP RIVER NEAR SAINT PAUL, NEBR.	41.263	-98.449	11142
6803500	SALT CREEK AT LINCOLN, NEBR.	40.847	-96.682	1774
6805500	PLATTE RIVER AT LOUISVILLE, NEBR.	41.015	-96.158	221108
6807000	MISSOURI RIVER AT NEBRASKA CITY, NE	40.682	-95.847	1061900
6809000	DAVIDS CREEK NEAR HAMLIN, IA	41.674	-94.806	67
6809500	EAST NISHNABOTNA RIVER AT RED OAK, IA	41.009	-95.242	2315
6817000	NODAWAY RIVER AT CLARINDA, IA	40.743	-95.014	1974
6818000	MISSOURI RIVER AT ST. JOSEPH, MO	39.753	-94.857	1104635
6821500	ARIKAREE RIVER AT HAIGLER, NEBR.	40.029	-101.968	4403
6828500	REPUBLICAN RIVER AT STRATTON, NEBR.	40.141	-101.230	21238
6829500	REPUBLICAN RIVER AT TRENTON, NEBR.	40.167	-101.048	21601
6834000	FRENCHMAN CREEK AT PALISADE, NEBR.	40.352	-101.124	3367
6838000	RED WILLOW CREEK NEAR RED WILLOW, NEBR.	40.235	-100.501	2124
6841000	MEDICINE CREEK ABOVE HARRY STRUNK LAKE, NE	40.501	-100.323	1994
6841500	MITCHELL CREEK ABOVE HARRY STRUNK LAKE, NEBR.	40.472	-100.258	135
6844500	REPUBLICAN RIVER NEAR ORLEANS, NEBR.	40.132	-99.503	40352
6845000	SAPPA C NR OBERLIN, KS	39.813	-100.534	2813
6845200	SAPPA CREEK NEAR BEAVER CITY, NEBR.	40.046	-99.890	3885
6846500	BEAVER C AT CEDAR BLUFFS, KS	39.985	-100.560	4191
6847000	BEAVER CREEK NEAR BEAVER CITY, NEBR.	40.120	-99.893	5387
6847500	SAPPA CREEK NEAR STAMFORD, NEBR.	40.118	-99.517	9946
6848000	PRAIRIE DOG C AT NORTON, KS	39.810	-99.922	1772
6854000	WHITE ROCK C AT LOVEWELL, KS	39.884	-98.023	894
6854500	REPUBLICAN R AT SCANDIA, KS	39.799	-97.793	61020
6856600	REPUBLICAN R AT CLAY CENTER, KS	39.356	-97.128	63564
6866900	SALINE R NR WAKEENEY, KS	39.106	-99.870	1803
6867000	SALINE R NR RUSSELL, KS	38.966	-98.855	3890
6869500	SALINE R AT TESCOTT, KS	39.004	-97.874	7304
6870200	SMOKY HILL R AT NEW CAMBRIA, KS	38.864	-97.483	30381
6871800	NF SOLOMON R AT KIRWIN, KS	39.660	-99.116	3541

Table C.1 – continued from previous page

Station ID	Name	Latitude	Longitude	Area
6873500	SF SOLOMON R AT ALTON, KS	39.454	-98.948	4455
6876000	SOLOMON R AT BELOIT, KS	39.455	-98.110	14090
6877600	SMOKY HILL R AT ENTERPRISE, KS	38.906	-97.118	49883
6881000	BIG BLUE R NR CRETE, NE	40.596	-96.960	7034
6883000	LITTLE BLUE R NR DEWEESE, NE	40.333	-98.073	2536
6887500	KANSAS R AT WAMEGO, KS	39.198	-96.306	143175
6888000	VERMILLION C NR WAMEGO, KS	39.348	-96.217	629
6890500	DELAWARE R AT VALLEY FALLS, KS	39.351	-95.455	2388
6898000	THOMPSON RIVER AT DAVIS CITY, IA	40.640	-93.808	1816
6903400	CHARITON RIVER NEAR CHARITON, IA	40.952	-93.260	471
6903900	CHARITON RIVER NEAR RATHBUN, IA	40.822	-92.891	1422
6918070	OSAGE RIVER ABOVE SCHELL CITY, MO	38.056	-94.145	14012
6934500	MISSOURI RIVER AT HERMANN, MO	38.710	-91.439	1353275
7010000	MISSISSIPPI RIVER AT ST. LOUIS, MO	38.629	-90.180	1805230
7019000	MERAMEC RIVER NEAR EUREKA, MO	38.506	-90.592	9811
7020500	MISSISSIPPI RIVER AT CHESTER, IL	37.904	-89.836	1835274
7022000	MISSISSIPPI RIVER AT THEBES, IL	37.216	-89.468	1847188
7036100	ST. FRANCIS RIVER NEAR SACO, MO	37.385	-90.474	1720
7040100	ST. FRANCIS RIVER AT ST. FRANCIS, AR	36.456	-90.138	4584
7047810	ST. FRANCIS RIVER FLOODWAY NEAR MARKED TREE, AR	35.538	-90.485	12046
7061300	EAST FORK BLACK RIVER AT LESTERVILLE, MO	37.450	-90.827	243
7077555	CACHE RIVER NEAR COTTON PLANT, AR	35.036	-91.323	3030
7103700	FOUNTAIN CREEK NEAR COLORADO SPRINGS, CO.	38.855	-104.878	264
7103970	MONUMENT CR ABV WOODMEN RD AT COLORADO SPRINGS, CO	38.934	-104.817	466
7103990	COTTONWOOD CREEK AT MOUTH AT PIKEVIEW, CO	38.927	-104.814	49
7105500	FOUNTAIN CREEK AT COLORADO SPRINGS, CO	38.816	-104.823	1015
7105530	FOUNTAIN CR BLW JANITELL RD BLW COLO. SPRINGS, CO	38.803	-104.796	1070
7105800	FOUNTAIN CREEK AT SECURITY, CO	38.729	-104.734	1295
7106300	FOUNTAIN CREEK NEAR PINON, CO	38.429	-104.598	2240
7106500	FOUNTAIN CREEK AT PUEBLO, CO.	38.288	-104.601	2396
7124200	PURGATOIRE RIVER AT MADRID, CO.	37.129	-104.640	1308
7124410	PURGATOIRE RIVER BELOW TRINIDAD LAKE, CO.	37.144	-104.548	1743
7126300	PURGATOIRE RIVER NEAR THATCHER, CO.	37.356	-103.900	4957
7126485	PURGATOIRE RIVER AT ROCK CROSSING NR TIMPAS, CO.	37.618	-103.594	7143
7140000	ARKANSAS R NR KINSLEY, KS	37.928	-99.374	85641
7141900	WALNUT C AT ALBERT, KS	38.462	-99.015	3652
7143330	ARKANSAS R NR HUTCHINSON, KS	37.946	-97.775	100777
7144200	L ARKANSAS R AT VALLEY CENTER, KS	37.832	-97.389	3437

Table C.1 – continued from previous page

Station ID	Name	Latitude	Longitude	Area
7146500	ARKANSAS R AT ARKANSAS CITY, KS	37.038	-97.039	113217
7147800	WALNUT R AT WINFIELD, KS	37.224	-96.996	4869
7151500	CHIKASKIA R NR CORBIN, KS	37.129	-97.602	2056
7230000	LITTLE RIVER BLW LK THUNDERBIRD NR NORMAN, OK	35.222	-97.214	666
7277700	HICKAHALA CREEK NR SENATOBIA, MS	34.632	-89.924	313
7301500	NORTH FORK RED RIVER NEAR CARTER, OK	35.168	-99.507	6869
7304500	ELK CREEK NEAR HOBART, OK	34.914	-99.114	1422
7325500	WASHITA RIVER AT CARNEGIE, OK	35.117	-98.564	8070
7351750	BAYOU PIERRE NEAR LAKE END, LA	31.895	-93.342	2227
7352800	GRAND BYU NR COUSHATTA, LA	32.048	-93.302	243
8023080	BAYOU GRAND CANE NEAR STANLEY, LA	31.963	-93.941	188
8023400	BAYOU SAN PATRICIO NEAR BENSON, LA	31.875	-93.659	208
8044000	BIG SANDY CK NR BRIDGEPORT, TX	33.232	-97.695	862
8286500	RIO CHAMA ABOVE ABIQUIU RESERVOIR, NM	36.319	-106.600	4144
8287000	RIO CHAMA BELOW ABIQUIU DAM, NM	36.237	-106.417	5561
8290000	RIO CHAMA NEAR CHAMITA, NM	36.074	-106.112	8143
8313000	RIO GRANDE AT OTOWI BRIDGE, NM	35.875	-106.142	37037
8317400	RIO GRANDE BELOW COCHITI DAM, NM	35.618	-106.324	38591
8317950	GALISTEO CREEK BELOW GALISTEO DAM, NM	35.465	-106.213	1544
8318000	GALISTEO C AT DOMINGO, NM	35.512	-106.318	1658
8329500	RIO GRANDE NEAR BERNALILLO, NM	35.285	-106.596	44807
8330000	RIO GRANDE AT ALBUQUERQUE, NM	35.089	-106.681	45170
8331990	RIO GRANDE CONVEYANCE CHANNEL NEAR BERNARDO, NM	34.415	-106.804	
8332010	RIO GRANDE FLOODWAY NEAR BERNARDO, NM	34.417	-106.801	49806
8332050	BERNARDO INTERIOR DRAIN NR BERNARDO, NM	34.416	-106.821	
8334000	RIO PUERCO ABV ARROYO CHICO NR GUADALUPE, NM	35.601	-107.167	1088
8340500	ARROYO CHICO NR GUADALUPE, NM	35.592	-107.189	3600
8353000	RIO PUERCO NEAR BERNARDO, NM	34.410	-106.854	19037
8354800	RIO GRANDE CONVEYANCE CHANNEL AT SAN ACACIA, NM	34.248	-106.902	
8354900	RIO GRANDE FLOODWAY AT SAN ACACIA, NM	34.256	-106.891	69334
8358300	RIO GRANDE CONVEYANCE CHANNEL AT SAN MARCIAL, NM	33.688	-106.993	
8358400	RIO GRANDE FLOODWAY AT SAN MARCIAL, NM	33.679	-106.997	71743
8383000	PECOS RIVER AT SANTA ROSA, NM	34.943	-104.699	6864
8390500	RIO HONDO RV DIA A RH	33.349	-104.852	
8396500	PECOS RIVER NEAR ARTESIA, NM	32.841	-104.324	39627
8398500	RIO PENASCO AT DAYTON, NM	32.743	-104.414	2745
9041090	MUDDY CREEK ABOVE ANTELOPE CREEK NR. KREMMLING, CO	40.202	-106.423	376
9093700	COLORADO RIVER NEAR DE BEQUE, CO.	39.362	-108.153	19088

Table C.1 – continued from previous page

Station ID	Name	Latitude	Longitude	Area
9180000	DOLORES RIVER NEAR CISCO, UT	38.797	-109.195	11862
9180500	COLORADO RIVER NEAR CISCO, UT	38.811	-109.293	62419
9184000	MILL CREEK NEAR MOAB, UT	38.562	-109.514	194
9217000	GREEN RIVER NEAR GREEN RIVER, WY	41.516	-109.449	36260
9224700	BLACKS FORK NEAR LITTLE AMERICA, WY	41.546	-109.693	8029
9243900	FOIDEL CREEK AT MOUTH NEAR OAK CREEK, CO	40.390	-106.995	45
9251000	YAMPA RIVER NEAR MAYBELL, CO	40.503	-108.033	8762
9260000	LITTLE SNAKE RIVER NEAR LILY, CO	40.549	-108.424	10448
9261000	GREEN RIVER NEAR JENSEN, UT	40.409	-109.235	76819
9306500	WHITE RIVER NEAR WATSON, UTAH	39.979	-109.179	10412
9315000	GREEN RIVER AT GREEN RIVER, UT	38.986	-110.151	116162
9328500	SAN RAFAEL RIVER NEAR GREEN RIVER, UT	38.858	-110.370	4217
9341500	WEST FORK SAN JUAN RIVER NEAR PAGOSA SPRINGS, CO	37.392	-106.907	221
9355500	SAN JUAN RIVER NEAR ARCHULETA, NM	36.802	-107.699	8443
9356500	SAN JUAN R NR BLANCO, NM	36.730	-107.812	9220
9364500	ANIMAS RIVER AT FARMINGTON, NM	36.723	-108.202	3522
9368000	SAN JUAN RIVER AT SHIPROCK,NM	36.792	-108.732	33411
9378700	COTTONWOOD WASH NR BLANDING UTAH	37.561	-109.579	531
9379500	SAN JUAN RIVER NEAR BLUFF, UT	37.147	-109.865	59570
9380000	COLORADO RIVER AT LEES FERRY, AZ	36.865	-111.588	289562
9382000	PARIA RIVER AT LEES FERRY, AZ	36.872	-111.595	3652
9394500	LITTLE COLORADO RIVER AT WOODRUFF, AZ	34.783	-110.044	20906
9401260	MOENKOPI WASH AT MOENKOPI, AZ	36.105	-111.202	4219
9402000	LITTLE COLORADO RIVER NEAR CAMERON, AZ	35.926	-111.567	68529
9402500	COLORADO RIVER NEAR GRAND CANYON, AZ	36.101	-112.086	366744
9406000	VIRGIN RIVER AT VIRGIN, UT	37.204	-113.181	2476
9408150	VIRGIN RIVER NEAR HURRICANE, UT	37.163	-113.395	3867
9410000	SANTA CLARA RIVER AB WINSOR DAM NR SANTA CLARA, UT	37.218	-113.777	875
9415000	VIRGIN RIVER AT LITTLEFIELD, ARIZ.	36.892	-113.924	13183
9430500	GILA RIVER NR GILA, NEW MEXICO	33.061	-108.537	4828
9448500	GILA RIVER AT HEAD OF SAFFORD VALLEY, NR SOLOMON,	32.868	-109.511	20451
9471000	SAN PEDRO RIVER AT CHARLESTON, AZ.	31.626	-110.175	3196
9474000	GILA RIVER AT KELVIN, AZ.	33.103	-110.977	46648
9505350	DRY BEAVER CREEK NEAR RIMROCK, AZ	34.729	-111.776	368
10092700	BEAR RIVER AT IDAHO-UTAH STATE LINE	42.013	-111.921	12650
10104700	LITTLE BEAR R BL DAVENPORT C NR AVON UT	41.512	-111.812	160
10118000	BEAR RIVER NEAR COLLINSTON, UT	41.834	-112.055	16242
10174500	SEVIER RIVER AT HATCH, UT	37.651	-112.430	881

Table C.1 – continued from previous page

Station ID	Name	Latitude	Longitude	Area
10336610	UP TRUCKEE R A SOUTH LAKE TAHOE CA	38.922	-119.992	142
10336645	GENERAL C NR MEEKS BAY CA	39.052	-120.119	19
10336660	BLACKWOOD C NR TAHOE CITY CA	39.107	-120.162	29
10336676	WARD C AT HWY 89 NR TAHOE PINES CA	39.132	-120.158	25
10336698	THIRD CK NR CRYSTAL BAY, NV	39.240	-119.947	16
10336740	LOGAN HOUSE C NR GLENBROOK NV CA	39.067	-119.935	5
10336780	TROUT C NR TAHOE VALLEY CA	38.920	-119.972	95
11013500	TIJUANA R NR NESTOR CA	32.552	-117.084	4390
11022500	SAN DIEGO R NR SANTEE CA	32.825	-117.056	976
11042000	SAN LUIS REY R A OCEANSIDE CA	33.218	-117.360	1443
11046000	SANTA MARGARITA R A YSIDORA CA	33.311	-117.347	1873
11046500	SAN JUAN C NR SAN JUAN CAPISTRANO CA	33.519	-117.625	275
11046530	SAN JUAN C AT LA NOVIA ST BR AT SAN JUAN CAPIS CA	33.503	-117.648	282
11047000	ARROYO TRABUCO NR SAN JUAN CAPISTRANO CA	33.527	-117.670	92
11047300	ARROYO TRABUCO A SAN JUAN CAPISTRANO CA	33.498	-117.666	140
11048500	SAN DIEGO C AT CULVER DRIVE NR IRVINE CA	33.682	-117.809	108
11051500	SANTA ANA R NR MENTONE CA	34.108	-117.101	544
11057000	SAN TIMOTEO C NR REDLANDS CA	34.033	-117.209	306
11074000	SANTA ANA R BL PRADO DAM CA	33.883	-117.645	5848
11078000	SANTA ANA R A SANTA ANA CA	33.751	-117.908	4403
11105850	ARROYO SIMI NR SIMI CA	34.273	-118.788	183
11108500	SANTA CLARA RIVER AT L.A.-VENTURA CO. LINE	34.400	-118.705	
11109000	SANTA CLARA R NR PIRU CA	34.404	-118.739	1671
11110500	HOPPER CREEK NEAR PIRU	34.401	-118.826	
11113000	SESPE CREEK NEAR FILLMORE	34.451	-118.926	
11114000	SANTA CLARA RIVER AT MONTALVO	34.242	-119.190	
11117500	SAN ANTONIO CREEK AT CASITAS SPRINGS	34.380	-119.305	
11118500	VENTURA RIVER NEAR VENTURA	34.351	-119.307	
11120510	SAN JOSE C A GOLETA CA	34.430	-119.822	24
11141000	SANTA MARIA R A GUADALUPE	34.976	-120.572	4509
11141280	LOPEZ C NR ARROYO GRANDE CA	35.236	-120.472	54
11147070	SANTA RITA C NR TEMPLETON CA	35.524	-120.766	47
11148900	NACIMIENTO R BL SAPAQUE C NR BRYSON CA	35.789	-121.094	420
11149900	SAN ANTONIO R NR LOCKWOOD CA	35.897	-121.088	562
11151870	ARROYO SECO NR GREENFIELD CA	36.237	-121.482	293
11152500	SALINAS R NR SPRECKELS CA	36.631	-121.672	10764
11153900	UVAS C AB UVAS RES NR MORGAN HILL CA	37.093	-121.718	54
11160300	ZAYANTE C A ZAYANTE CA	37.086	-122.047	29

Table C.1 – continued from previous page

Station ID	Name	Latitude	Longitude	Area
11160500	SAN LORENZO R A BIG TREES CA	37.044	-122.072	275
11162720	COLMA C A SOUTH SAN FRANCISCO CA	37.654	-122.426	28
11169800	COYOTE C NR GILROY CA	37.078	-121.494	282
11176400	ARROYO VALLE BL LANG CYN NR LIVERMORE CA	37.561	-121.684	337
11176500	ARROYO VALLE NR LIVERMORE CA	37.623	-121.759	381
11176900	ARROYO DE LA LAGUNA A VERONA CA	37.627	-121.883	1044
11177000	ARROYO DE LA LAGUNA NR PLEASANTON CA	37.615	-121.882	1049
11179000	ALAMEDA C NR NILES CA	37.587	-121.961	1639
11180825	SAN LORENZO C AB DON CASTRO RES NR CASTRO V CA	37.695	-122.045	47
11180960	CULL C AB CULL C RES NR CASTRO VALLEY CA	37.718	-122.054	15
11181040	SAN LORENZO C A SAN LORENZO CA	37.684	-122.140	116
11181390	WILDCAT C A VALE RD AT RICHMOND CA	37.953	-122.338	20
11303500	SAN JOAQUIN R NR VERNALIS CA	37.676	-121.266	35066
11306000	SF CALAVERAS R NR SAN ANDREAS CA	38.144	-120.664	306
11308000	NF CALAVERAS R NR SAN ANDREAS CA	38.221	-120.699	221
11335000	COSUMNES R A MICHIGAN BAR CA	38.500	-121.045	1388
11376000	COTTONWOOD C NR COTTONWOOD CA	40.387	-122.239	2401
11377100	SACRAMENTO R AB BEND BRIDGE NR RED BLUFF CA	40.288	-122.187	23051
11382000	THOMES C A PASKENTA CA	39.888	-122.529	526
11389000	SACRAMENTO R A BUTTE CITY CA	39.458	-121.994	31274
11389470	COLUSA WEIR SPILL TO BUTTE BASIN NR COLUSA CA	39.237	-121.995	
11389500	SACRAMENTO R A COLUSA CA	39.214	-122.000	31313
11391000	SACRAMENTO R A KNIGHTS LANDING CA	38.803	-121.716	37646
11407000	FEATHER R A OROVILLE CA	39.522	-121.548	9386
11407150	FEATHER R NR GRIDLEY CA	39.367	-121.647	9521
11410000	M YUBA R NR NORTH SAN JUAN CA	39.394	-121.085	513
11417500	S YUBA R A JONES BAR NR GRASS VALLEY CA	39.292	-121.105	798
11418000	YUBA R BL ENGLEBRIGHT DAM NR SMARTSVILLE CA	39.235	-121.274	2870
11418500	DEER C NR SMARTSVILLE CA	39.224	-121.269	219
11447500	SACRAMENTO R A SACRAMENTO CA	38.587	-121.506	60883
11447650	SACRAMENTO R A FREEPORT CA	38.456	-121.501	
11452500	CACHE C A YOLO CA	38.727	-121.807	2950
11453000	YOLO BYPASS NR WOODLAND CA	38.678	-121.644	
11456000	NAPA R NR ST HELENA CA	38.511	-122.456	204
11458000	NAPA R NR NAPA CA	38.368	-122.303	565
11460000	CORTE MADERA C A ROSS CA	37.963	-122.557	47
11460400	LAGUNITAS C A SAMUEL P TAYLOR STATE PARK CA	38.027	-122.736	89
11460750	WALKER C NR MARSHALL CA	38.176	-122.818	81

Table C.1 – continued from previous page

Station ID	Name	Latitude	Longitude	Area
11461000	RUSSIAN R NR UKIAH CA	39.195	-123.195	259
11461500	EF RUSSIAN R NR CALPELLA CA	39.247	-123.130	239
11462000	EF RUSSIAN R NR UKIAH CA	39.197	-123.188	272
11463000	RUSSIAN R NR CLOVERDALE CA	38.879	-123.054	1303
11463200	BIG SULPHUR C NR CLOVERDALE CA	38.826	-122.997	221
11465200	DRY C NR GEYSERVILLE CA	38.699	-122.958	420
11467000	RUSSIAN R NR GUERNEVILLE CA	38.509	-122.928	3465
11468000	NAVARRO R NR NAVARRO CA	39.170	-123.668	785
11469000	MATTOLE R NR PETROLIA CA	40.313	-124.283	635
11471000	POTTER VALLEY PH INTAKE NR POTTER VALLEY CA	39.367	-123.128	
11472150	EEL R NR DOS RIOS CA	39.625	-123.341	1368
11472200	OUTLET C NR LONGVALE CA	39.618	-123.357	417
11473900	MF EEL R NR DOS RIOS CA	39.706	-123.325	1930
11474500	NF EEL R NR MINA CA	39.937	-123.347	642
11475000	EEL R A FORT SEWARD CA	40.218	-123.633	5457
11475500	SF EEL R NR BRANSCOMB CA	39.719	-123.653	114
11475560	ELDER C NR BRANSCOMB CA	39.730	-123.644	17
11476600	BULL C NR WEOTT CA	40.352	-124.005	73
11477000	EEL R A SCOTIA CA	40.492	-124.100	8063
11481000	MAD R NR ARCATA CA	40.910	-124.061	1256
11481500	REDWOOD C NR BLUE LAKE CA	40.906	-123.815	175
11482500	REDWOOD C A ORICK CA	41.299	-124.051	717
11523000	KLAMATH R A ORLEANS	41.303	-123.535	21950
11525600	GRASS VALLEY C A FAWN LODGE NR LEWISTON CA	40.676	-122.831	80
11525655	TRINITY R BL LIMEKILN GULCH NR DOUGLAS CITY CA	40.673	-122.921	2098
11528700	SF TRINITY R BL HYAMPOM CA	40.650	-123.494	1979
11530000	TRINITY R A HOOPA CA	41.050	-123.674	7389
11532500	SMITH R NR CRESCENT CITY CA	41.792	-124.076	1590
12026400	SKOOKUMCHUCK RIVER NEAR BUCODA, WA	46.772	-122.924	290
12031000	CHEHALIS RIVER AT PORTER, WA	46.939	-123.314	3351
12041200	HOH RIVER AT US HIGHWAY 101 NEAR FORKS, WA	47.807	-124.251	655
12097850	WHITE RIVER BELOW CLEARWATER RIVER NR BUCKLEY, WA	47.147	-121.860	971
12113350	GREEN RIVER AT TUKWILA, WA	47.465	-122.248	1140
12149000	SNOQUALMIE RIVER NEAR CARNATION, WA	47.666	-121.925	1562
12200500	SKAGIT RIVER NEAR MOUNT VERNON, WA	48.445	-122.335	8011
12301933	KOOTENAI RIVER BL LIBBY DAM NR LIBBY MT	48.401	-115.319	23307
12302055	FISHER RIVER NEAR LIBBY MT	48.356	-115.315	2181
12318500	KOOTENAI RIVER NR COPELAND ID	48.905	-116.402	34706

Table C.1 – continued from previous page

Station ID	Name	Latitude	Longitude	Area
12323600	SILVER BOW CREEK AT OPPORTUNITY MT	46.108	-112.805	888
12323750	SILVER BOW CREEK AT WARM SPRINGS MT	46.179	-112.781	1225
12324200	CLARK FORK AT DEER LODGE MT	46.398	-112.743	2593
12334550	CLARK FORK AT TURAH BRIDGE NR BONNER MT	46.826	-113.814	9472
12340000	BLACKFOOT RIVER NEAR BONNER MT	46.899	-113.756	5923
12340500	CLARK FORK ABOVE MISSOULA MT	46.877	-113.932	15594
12355000	FLATHEAD RIVER AT FLATHEAD BRITISH COLUMBIA	49.001	-114.476	1111
12355500	NORTH FORK FLATHEAD RIVER NEAR COLUMBIA FALLS, MT	48.496	-114.128	4009
12363000	FLATHEAD RIVER AT COLUMBIA FALLS, MT	48.362	-114.185	11551
12424000	HANGMAN CREEK AT SPOKANE, WA	47.653	-117.450	1785
12510500	YAKIMA RIVER AT KIONA, WA	46.253	-119.478	14543
13055198	NORTH FORK TETON RIVER AT TETON ID	43.898	-111.678	
13227000	BULLY CREEK NEAR VALE,OREG.	43.958	-117.343	1476
13344500	TUCANNON RIVER NEAR STARBUCK, WA	46.505	-118.066	1116
13351000	PALOUSE RIVER AT HOOPER, WA	46.758	-118.149	6475
14018500	WALLA WALLA RIVER NEAR TOUCHET, WA	46.028	-118.730	4292
14019200	COLUMBIA RIVER AT MCNARY DAM,NEAR UMATILLA, OR	45.933	-119.297	554260
14033500	UMATILLA RIVER NEAR UMATILLA, OR	45.903	-119.327	5931
14048000	JOHN DAY RIVER AT MCDONALD FERRY, OR	45.588	-120.409	19632
14101500	WHITE RIVER BELOW TYGH VALLEY,OREG.	45.242	-121.095	1080
14138870	FIR CREEK NEAR BRIGHTWOOD, OR	45.480	-122.026	14
14138900	NORTH FORK BULL RUN RIVER NEAR MULTNOMAH FALLS, OR	45.494	-122.036	22
14139800	SOUTH FORK BULL RUN RIVER NEAR BULL RUN, OR	45.445	-122.110	40
14242580	TOUTLE RIVER AT TOWER ROAD NEAR SILVER LAKE, WA	46.335	-122.841	1285
14306500	ALSEA RIVER NEAR TIDEWATER, OR	44.386	-123.832	865
14307620	SIUSLAW RIVER NEAR MAPLETON, OR	44.062	-123.883	1523
14330000	ROGUE RIVER BELOW PROSPECT, OR	42.730	-122.516	982
14334700	S FK ROGUE R SOUTH OF PROSPECT, OREG.	42.712	-122.507	637
15212000	COPPER R NR CHITINA AK	61.465	-144.458	53794
15241600	NINILCHIK R AT NINILCHIK AK	60.048	-151.665	350
15275100	CHESTER C AT ARCTIC BOULEVARD AT ANCHORAGE AK	61.205	-149.897	76
15281000	KNIK R NR PALMER AK	61.504	-149.033	3160
15284000	MATANUSKA R AT PALMER AK	61.609	-149.073	5335
15476000	TANANA R NR TANACROSS AK	63.388	-143.749	21808
15514000	CHENA R AT FAIRBANKS AK	64.845	-147.704	5154
15518000	NENANA R NR HEALY AK	63.845	-148.946	4947
16103000	HANALEI RIVER NR HANALEI, KAUAI, HI	22.180	-159.466	48
16200000	NF KAUKONAHUA STR ABV RB, NR WAHIAWA, OAHU, HI	21.516	-157.945	4

Table C.1 – continued from previous page

Station ID	Name	Latitude	Longitude	Area
16212800	KIPAPA STR NR WAHIAWA, OAHU, HI	21.467	-157.959	11
16213000	WAIKELE STR AT WAIPAHU, OAHU, HI	21.383	-158.011	117
16226200	N. HALAWA STR NR HONOLULU, OAHU, HI	21.382	-157.903	10
16240500	WAIAKEAKUA STR AT HONOLULU, OAHU, HI	21.328	-157.800	3
16244000	PUKELE STREAM NEAR HONOLULU, OAHU, HI	21.307	-157.788	3
16272200	KAMOOALII STR BLW LULUKU STR NR KANEOHE, OAHU, HI	21.393	-157.804	10
16275000	HEEIA STREAM AT HAIKU VALLEY NR KANEOHE, OAHU, HI	21.409	-157.823	2
16809600	LA SA FUA RIVER NEAR UMATAC, GUAM	13.307	144.664	3
16854500	UGUM RIVER ABOVE TALOFOFO FALLS, NR TALOFOFO, GUAM	13.322	144.736	15
50025155	RIO SALIENTE AT COABEY NR JAYUYA, PR	18.211	-66.563	24
50028000	RIO TANAMA NR UTUADO, PR	18.299	-66.783	48
50031200	RIO GRANDE DE MANATI NR MOROVIS, PR	18.294	-66.413	143
50034000	RIO BAUTA NR OROCOVIS, PR	18.234	-66.454	43
50035000	RIO GRANDE DE MANATI AT CIALES, PR	18.322	-66.460	332
50043800	RIO DE LA PLATA AT COMERIO, PR	18.220	-66.224	281
50045010	RIO DE LA PLATA BLW LA PLATA DAMSITE, PR	18.344	-66.238	448
50048770	RIO PIEDRAS AT EL SENORIAL, PR	18.361	-66.065	19
50050900	RIO GRANDE DE LOIZA AT QUEBRADA ARENAS, PR	18.118	-65.988	16
50051180	QUEBRADA SALVATIERRA NR SAN LORENZO, PR	18.171	-65.977	10
50051310	RIO CAYAGUAS AT CERRO GORDO, PR	18.152	-65.956	26
50051800	RIO GRANDE DE LOIZA AT HWY 183 SAN LORENZO, PR	18.184	-65.961	106
50053025	RIO TURABO ABV BORINQUEN, PR	18.160	-66.040	19
50055000	RIO GRANDE DE LOIZA AT CAGUAS, PR	18.241	-66.009	233
50055225	RIO CAGUITAS AT VILLA BLANCA AT CAGUAS, PR	18.247	-66.027	43
50055750	RIO GURABO BLW EL MANGO, PR	18.232	-65.885	58
50056400	RIO VALENCIANO NR JUNCOS, PR	18.214	-65.926	42
50057000	RIO GURABO AT GURABO, PR	18.256	-65.968	156
50058350	RIO CANAS AT RIO CANAS, PR	18.293	-66.045	20
50059050	RIO GRANDE DE LOIZA BLW LOIZA DAMSITE, PR	18.340	-66.006	541
50061800	RIO CANOVANAS NR CAMPO RICO, PR	18.316	-65.889	25
50065500	RIO MAMEYES NR SABANA, PR	18.327	-65.750	18
50071000	RIO FAJARDO NR FAJARDO, PR	18.297	-65.693	39
50075000	RIO ICACOS NR NAGUABO, PR	18.275	-65.785	3
50110900	RIO TOA VACA ABV LAGO TOA VACA, PR	18.125	-66.457	37
50115000	RIO PORTUGUES NR PONCE, PR	18.077	-66.633	23
50136400	RIO ROSARIO NR HORMIGUEROS, PR	18.158	-67.085	47
54310157	JACKSON CREEK TRIBUTARY NEAR ELKHORN, WI	42.651	-88.551	11

Appendix D

Parametric results of the US watersheds

Table D.1: Sediment yield parameters for the US stations

Station ID	$\bar{a}$	$\bar{b}$	$\hat{a}$	$\hat{b}$	RB	Sediment yield (tons/yr)	
						FDSRC	Parametric
1100000	3.67E-04	1.57	7985.5	0.98	0.14	2.2E+05	2.2E+05
1127500	1.32E-03	1.56	125.8	1.50	0.36	2.0E+03	2.2E+03
1192883	9.79E-03	1.30	49.2	1.42	0.27	8.5E+02	9.1E+02
1193500	1.34E-04	2.08	153.1	1.38	0.34	7.4E+03	7.9E+03
1197500	1.22E-03	1.49	515.5	1.08	0.20	5.9E+03	6.3E+03
1198000	6.57E-04	1.81	68.2	1.41	0.25	1.5E+03	1.6E+03
1199000	4.44E-04	1.71	1092.6	1.04	0.16	3.5E+04	3.7E+04
1200500	2.64E-04	1.75	1708.0	1.04	0.16	6.3E+04	6.6E+04
1331095	5.56E-06	1.98	7571.2	0.67	0.11	1.0E+05	1.1E+05
1357500	5.34E-04	1.63	5370.0	1.19	0.27	3.7E+05	3.9E+05
1379500	3.13E-02	1.29	148.1	1.30	0.22	9.4E+03	9.7E+03
1389500	1.88E-02	1.18	1022.9	1.22	0.16	2.7E+04	2.8E+04
1401000	2.54E-03	1.81	28.9	2.18	0.76	7.4E+03	8.4E+03
1411000	8.07E-04	1.61	95.8	0.65	0.10	4.0E+02	4.1E+02
1411500	2.66E-03	1.38	184.2	0.64	0.09	1.1E+03	1.1E+03
1434000	2.20E-06	2.13	4727.0	1.22	0.23	1.7E+05	1.8E+05
1451000	9.24E-06	2.22	1848.2	1.05	0.19	1.5E+05	1.6E+05
1464500	3.23E-03	1.64	118.6	1.23	0.34	5.0E+03	5.6E+03
1467150	1.62E-02	1.56	24.8	1.47	0.58	1.9E+03	2.2E+03
1468500	1.02E+00	1.07	275.4	1.06	0.21	1.4E+05	1.5E+05
1470500	4.11E-04	1.87	624.0	1.29	0.25	6.2E+04	6.9E+04
1470960	3.60E-04	2.00	255.2	1.22	0.24	2.3E+04	2.4E+04
1472000	4.71E-05	2.14	1844.1	1.11	0.22	4.0E+05	4.3E+05
1473000	5.42E-04	1.83	227.2	1.90	0.62	3.6E+04	4.1E+04
1473120	2.37E-03	1.89	29.0	2.31	0.81	1.8E+04	2.0E+04
1474500	3.50E-03	1.48	2449.7	1.29	0.30	2.0E+05	2.1E+05
1477120	7.01E-03	1.65	34.7	1.30	0.38	1.6E+03	1.8E+03
1481000	1.74E-04	2.05	374.5	1.20	0.35	3.3E+04	3.6E+04
1481500	1.98E-04	2.02	435.6	1.23	0.34	4.2E+04	4.4E+04
1491000	6.74E-03	1.33	94.8	1.65	0.33	2.1E+03	2.3E+03
1516500	5.41E-03	1.94	5.1	2.22	0.51	1.3E+03	1.6E+03
1517000	4.23E-03	1.97	3.8	2.36	0.54	1.4E+03	1.3E+03

Table D.1 – continued from previous page

Station ID	$\bar{a}$	$\bar{b}$	$\hat{a}$	$\hat{b}$	RB	Sediment yield (tons/yr)	
						FDSRC	Parametric
1531000	7.72E-05	1.97	1708.0	1.69	0.35	4.7E+05	5.3E+05
1531500	2.95E-05	1.89	9140.5	1.32	0.22	9.5E+05	1.0E+06
1539000	9.52E-05	1.98	363.7	1.50	0.31	2.0E+04	2.2E+04
1540500	3.67E-05	1.86	13740.5	1.25	0.18	1.5E+06	1.6E+06
1541000	8.96E-04	1.73	429.2	1.46	0.34	3.4E+04	3.7E+04
1544000	5.41E-03	1.32	313.1	1.47	0.29	6.6E+03	6.9E+03
1547200	1.25E-04	2.05	377.8	1.16	0.23	2.2E+04	2.3E+04
1547500	9.31E-05	2.06	466.1	1.03	0.19	2.1E+04	2.2E+04
1547700	9.47E-03	1.56	36.6	1.76	0.33	3.5E+03	3.8E+03
1549500	2.22E-03	1.93	37.2	1.72	0.36	6.5E+03	7.2E+03
1553500	7.05E-06	1.96	9632.7	1.24	0.19	4.4E+05	4.6E+05
1567000	3.69E-05	1.91	3588.8	1.35	0.22	2.6E+05	2.8E+05
1570500	2.44E-06	2.01	31529.2	1.19	0.17	2.4E+06	2.6E+06
1573000	1.62E-03	1.69	403.5	1.61	0.36	5.1E+04	5.9E+04
1575000	1.16E-02	1.77	63.3	1.87	0.38	4.5E+04	5.5E+04
1576500	2.56E-03	1.72	323.0	1.45	0.33	5.1E+04	6.0E+04
1578310	7.47E-04	1.42	38095.3	1.14	0.22	1.1E+06	1.2E+06
1589000	1.84E-04	2.16	110.6	1.89	0.37	5.5E+04	4.4E+04
1594440	1.50E-02	1.42	325.7	1.34	0.38	3.1E+04	3.4E+04
1597000	1.50E-03	2.01	21.0	1.53	0.31	1.4E+03	1.5E+03
1603000	1.88E-03	1.64	1060.2	1.38	0.26	1.3E+05	1.5E+05
1614500	1.60E-04	1.95	484.1	1.41	0.28	3.7E+04	3.9E+04
1631000	5.88E-06	2.27	1139.8	1.56	0.24	2.3E+05	2.0E+05
1638500	1.94E-05	1.96	7709.3	1.39	0.23	1.0E+06	1.1E+06
1639000	1.85E-02	1.36	90.1	2.17	0.72	1.5E+04	1.6E+04
1650500	1.64E-02	1.88	10.8	2.07	0.65	8.7E+03	9.8E+03
1658500	1.79E-02	1.65	2.5	2.35	0.74	4.5E+02	5.3E+02
1663500	9.40E-04	1.80	237.3	1.60	0.33	2.6E+04	3.0E+04
1664000	3.65E-03	1.56	489.3	1.58	0.35	5.0E+04	5.8E+04
1667500	1.34E-03	1.72	353.3	1.69	0.36	5.0E+04	5.9E+04
2019500	4.61E-05	1.95	1862.7	1.49	0.30	1.8E+05	1.9E+05
2029000	5.46E-06	2.17	4394.5	1.32	0.24	6.7E+05	7.2E+05
2060500	9.68E-04	1.81	1480.4	1.36	0.33	4.7E+05	5.4E+05
2066000	9.03E-04	1.71	2547.9	1.29	0.28	4.4E+05	4.9E+05
2075500	2.24E-03	1.65	2482.1	1.18	0.28	5.1E+05	5.7E+05
2083500	4.77E-03	1.39	1846.1	1.33	0.16	9.1E+04	9.6E+04
2084160	1.94E-02	1.39	17.1	2.45	0.53	2.9E+03	3.3E+03

Table D.1 – continued from previous page

Station ID	$\bar{a}$	$\bar{b}$	$\hat{a}$	$\hat{b}$	RB	Sediment yield (tons/yr)	
						FDSRC	Parametric
2116500	5.25E-04	1.83	2922.2	1.02	0.25	6.0E+05	6.5E+05
2118000	9.60E-03	1.58	286.4	1.30	0.29	4.5E+04	5.1E+04
2131000	2.35E-02	1.19	9824.5	0.89	0.12	4.6E+05	4.7E+05
2175000	8.44E-03	1.16	2462.3	0.98	0.06	2.5E+04	2.6E+04
2383500	1.19E-02	1.43	1399.1	1.06	0.22	1.6E+05	1.7E+05
2430000	1.32E-01	1.13	65.6	1.77	0.43	9.3E+03	1.0E+04
2489500	6.34E-04	1.61	8992.1	1.22	0.09	9.0E+05	9.2E+05
3015500	1.91E-04	1.84	491.8	1.39	0.33	1.9E+04	2.1E+04
3020500	2.58E-03	1.52	434.5	1.41	0.39	1.9E+04	2.0E+04
3032500	1.97E-04	1.93	729.6	1.37	0.30	8.0E+04	8.6E+04
3040000	7.21E-04	1.83	536.7	1.45	0.32	8.3E+04	9.0E+04
3061500	3.19E-03	1.82	92.9	1.89	0.62	3.8E+04	4.2E+04
3068800	4.03E-04	1.83	358.1	1.39	0.45	2.1E+04	2.3E+04
3085000	7.58E-05	1.79	12194.5	1.08	0.24	9.5E+05	9.9E+05
3111548	1.54E-02	1.71	89.4	1.41	0.35	2.9E+04	3.2E+04
3139000	1.42E-02	1.49	345.7	1.44	0.21	6.1E+04	6.7E+04
3144500	4.64E-04	1.69	6128.5	1.11	0.14	6.4E+05	6.6E+05
3150000	1.06E-03	1.61	7544.0	1.09	0.14	9.4E+05	9.7E+05
3151400	2.30E-03	1.70	160.4	1.56	0.47	1.6E+04	1.7E+04
3159500	6.04E-04	1.80	718.2	1.60	0.36	1.3E+05	1.5E+05
3195500	4.37E-04	1.56	984.3	1.30	0.33	1.3E+04	1.4E+04
3197000	1.05E-04	1.85	1739.9	1.33	0.31	1.0E+05	1.1E+05
3199000	9.37E-04	1.96	207.0	1.83	0.44	1.3E+05	1.4E+05
3200500	6.78E-04	1.86	938.1	1.47	0.33	3.1E+05	3.4E+05
3202400	1.75E-03	1.79	314.9	1.51	0.33	6.4E+04	7.2E+04
3202750	2.57E-03	1.80	125.8	1.68	0.45	3.0E+04	3.3E+04
3204000	8.56E-04	1.88	1171.7	1.56	0.31	9.0E+05	9.5E+05
3204500	1.13E-02	1.54	135.8	2.07	0.56	5.1E+04	5.5E+04
3207800	9.33E-03	1.76	255.1	1.64	0.38	2.5E+05	2.9E+05
3207965	2.81E-01	1.46	3.9	2.03	0.53	3.4E+03	3.9E+03
3209300	3.33E-03	1.55	527.5	1.56	0.37	5.1E+04	5.6E+04
3210000	5.59E-02	1.62	33.9	2.02	0.51	4.1E+04	4.6E+04
3211500	1.22E-01	1.22	137.9	1.81	0.41	3.9E+04	4.1E+04
3212500	6.03E-03	1.53	1816.6	1.54	0.30	5.1E+05	5.5E+05
3216500	7.55E-03	1.52	288.6	1.80	0.40	5.4E+04	5.8E+04
3217000	6.00E-03	1.60	149.1	2.05	0.57	4.6E+04	5.1E+04
3219500	9.59E-03	1.49	305.2	1.79	0.31	6.0E+04	6.3E+04

Table D.1 – continued from previous page

Station ID	$\bar{a}$	$\bar{b}$	$\hat{a}$	$\hat{b}$	RB	Sediment yield (tons/yr)	
						FDSRC	Parametric
3226800	8.53E-03	1.50	337.6	1.67	0.41	5.6E+04	5.8E+04
3228500	4.06E-02	1.30	120.1	1.83	0.42	1.8E+04	2.0E+04
3229000	3.90E-02	1.39	82.8	2.07	0.59	2.8E+04	3.1E+04
3230450	2.00E-02	1.51	18.3	2.07	0.57	3.4E+03	3.7E+03
3230500	7.17E-03	1.55	269.6	1.89	0.41	7.1E+04	7.8E+04
3234000	1.30E-02	1.51	510.7	1.77	0.36	2.0E+05	2.2E+05
3234500	3.21E-04	1.80	3910.9	1.42	0.23	1.1E+06	1.1E+06
3237280	1.08E-03	2.16	5.8	2.21	0.65	1.2E+03	1.3E+03
3240000	7.40E-03	1.66	82.0	1.71	0.35	1.6E+04	1.8E+04
3241500	5.86E-02	1.39	39.8	1.83	0.41	1.0E+04	1.2E+04
3244000	6.02E-02	1.37	76.6	2.37	0.67	5.7E+04	6.3E+04
3245500	1.87E-03	1.75	818.5	1.75	0.45	4.5E+05	5.0E+05
3248500	1.98E-02	1.53	88.7	1.98	0.48	3.7E+04	4.0E+04
3249500	2.69E-03	1.60	761.8	1.55	0.25	1.2E+05	1.2E+05
3251500	9.60E-03	1.48	2335.2	1.48	0.27	6.9E+05	7.1E+05
3261500	2.53E-02	1.38	331.7	1.71	0.33	7.0E+04	7.4E+04
3261950	1.22E-01	1.20	63.2	2.16	0.53	2.1E+04	2.2E+04
3265000	7.26E-03	1.56	235.8	2.00	0.50	7.6E+04	8.3E+04
3270500	9.51E-04	1.71	1761.1	1.53	0.29	4.0E+05	4.3E+05
3280600	4.04E-02	1.38	145.5	2.02	0.53	5.6E+04	6.2E+04
3281000	2.40E-04	2.08	571.8	1.51	0.31	2.8E+05	3.0E+05
3281100	1.65E-02	1.29	124.3	2.06	0.59	1.0E+04	1.1E+04
3287500	2.93E-03	1.48	5637.0	1.46	0.24	7.5E+05	7.8E+05
3291500	1.57E-02	1.54	223.7	2.31	0.82	2.4E+05	2.6E+05
3294500	1.39E-05	1.83	120099.4	0.98	0.13	1.5E+07	1.6E+07
3298500	1.68E-02	1.47	904.0	1.89	0.45	5.2E+05	5.5E+05
3308500	1.63E-03	1.64	2127.7	1.46	0.27	4.2E+05	4.4E+05
3310500	3.65E-03	1.65	518.2	1.69	0.28	1.5E+05	1.7E+05
3314500	3.08E-03	1.55	2158.9	1.33	0.23	3.0E+05	3.2E+05
3318500	2.23E-03	1.79	635.1	1.34	0.24	2.3E+05	2.4E+05
3319000	6.84E-03	1.49	881.4	1.42	0.26	1.2E+05	1.2E+05
3320000	1.40E-03	1.53	10245.0	1.18	0.12	1.1E+06	1.1E+06
3320500	1.02E-01	1.29	105.3	2.32	0.48	7.8E+04	8.4E+04
3328500	1.34E-03	1.79	643.5	1.38	0.26	1.4E+05	1.5E+05
3335500	2.88E-03	1.48	6233.2	1.22	0.18	6.5E+05	6.9E+05
3340800	1.20E-02	1.88	58.4	2.26	0.56	2.7E+05	3.0E+05
3361000	1.16E-02	1.54	154.6	1.49	0.34	2.1E+04	2.4E+04

Table D.1 – continued from previous page

Station ID	$\bar{a}$	$\bar{b}$	$\hat{a}$	$\hat{b}$	RB	Sediment yield (tons/yr)	
						FDSRC	Parametric
3365500	2.68E-03	1.59	1904.9	1.59	0.25	4.6E+05	5.1E+05
3382100	4.82E-03	1.81	71.9	2.24	0.51	8.7E+04	9.3E+04
3383000	2.29E-02	1.23	194.7	1.86	0.27	1.2E+04	1.3E+04
3384450	4.52E-03	1.65	15.9	2.63	0.89	5.2E+03	5.7E+03
3402000	1.91E-02	1.63	55.5	2.07	0.56	3.9E+04	4.4E+04
3403000	7.10E-04	1.85	851.1	1.77	0.40	4.8E+05	5.3E+05
3403500	1.45E-03	1.73	1170.7	1.67	0.37	4.8E+05	5.2E+05
3403910	4.37E-03	1.65	334.9	1.80	0.46	1.1E+05	1.2E+05
3404000	3.40E-03	1.77	2015.2	1.51	0.28	3.1E+06	3.3E+06
3404500	2.20E-04	1.91	2411.7	1.51	0.28	1.0E+06	1.1E+06
3406500	5.71E-03	1.35	483.2	1.96	0.50	2.9E+04	3.1E+04
3410500	1.29E-03	1.66	977.3	1.89	0.49	2.5E+05	2.7E+05
3455000	8.27E-04	1.85	3020.0	0.94	0.20	1.2E+06	1.2E+06
3465500	1.57E-04	2.08	1310.1	1.11	0.26	4.1E+05	4.4E+05
3467500	3.94E-04	1.92	2112.5	1.06	0.26	6.4E+05	6.8E+05
3469000	4.85E-06	2.29	7180.7	0.78	0.21	1.8E+06	1.8E+06
3487500	1.42E-04	1.91	2745.3	0.87	0.30	2.5E+05	2.7E+05
3495500	6.33E-05	2.01	5017.2	0.82	0.25	8.3E+05	8.6E+05
3497000	5.57E-05	1.96	14017.0	0.81	0.19	3.4E+06	3.6E+06
3519500	8.49E-06	2.07	6108.8	0.78	0.21	2.6E+05	2.7E+05
3520000	7.53E-06	2.08	20460.6	0.75	0.14	3.0E+06	3.1E+06
3528000	1.22E-03	1.73	1589.8	1.45	0.28	4.5E+05	4.9E+05
3532000	1.72E-03	1.73	818.5	1.53	0.29	2.1E+05	2.4E+05
3540500	1.21E-02	1.35	742.9	1.99	0.49	1.2E+05	1.3E+05
3556000	1.36E-03	2.30	54.6	0.84	0.21	8.3E+03	8.3E+03
3561000	2.96E+00	1.62	31.4	0.92	0.33	3.1E+05	3.4E+05
3566000	1.68E-04	1.91	4907.9	0.80	0.17	7.8E+05	8.2E+05
3568000	7.37E-06	2.01	39055.8	0.82	0.13	6.1E+06	6.4E+06
3571000	1.16E-02	1.46	501.4	1.67	0.30	9.8E+04	1.1E+05
3571850	2.51E-06	2.09	41792.0	0.68	0.12	4.7E+06	4.8E+06
3584500	9.21E-03	1.51	2151.5	1.59	0.30	9.0E+05	9.8E+05
3603000	7.71E-04	1.75	2952.9	1.55	0.24	1.2E+06	1.3E+06
3604500	2.26E-03	1.61	825.6	1.61	0.25	1.2E+05	1.4E+05
3609500	5.88E-04	1.52	67057.3	0.90	0.08	4.8E+06	4.9E+06
4024098	5.69E-02	1.88	2.9	2.22	0.54	3.9E+03	4.5E+03
4024430	1.33E-03	1.86	236.8	1.76	0.28	9.3E+04	1.0E+05
4058500	1.75E-03	1.38	90.3	1.30	0.14	4.4E+02	4.8E+02

Table D.1 – continued from previous page

Station ID	$\bar{a}$	$\bar{b}$	$\hat{a}$	$\hat{b}$	RB	Sediment yield (tons/yr)	
						FDSRC	Parametric
4073462	6.98E-02	1.96	2.8	1.49	0.16	9.5E+02	9.7E+02
4073468	1.27E-01	1.00	32.3	1.34	0.19	1.6E+03	1.6E+03
4086600	2.43E-02	1.18	441.0	1.15	0.13	1.2E+04	1.2E+04
4087000	9.73E-03	1.35	363.1	1.42	0.18	1.6E+04	1.7E+04
4087030	3.30E-02	1.27	22.1	1.63	0.27	1.1E+03	1.2E+03
4087088	3.28E-02	1.65	6.7	2.15	0.63	2.5E+03	3.1E+03
4087120	8.79E-03	1.61	63.3	1.84	0.48	1.2E+04	1.3E+04
4087159	5.19E-03	1.95	10.4	2.18	0.98	5.3E+03	5.8E+03
4095300	6.08E-03	1.68	72.4	1.18	0.29	4.6E+03	5.3E+03
4102700	5.88E-03	1.48	102.6	1.07	0.17	2.4E+03	2.6E+03
4142000	9.10E-05	2.19	336.3	0.88	0.15	1.8E+04	1.9E+04
4144500	3.09E-03	1.59	339.2	1.16	0.14	1.7E+04	1.8E+04
4151500	7.76E-03	1.43	331.4	1.79	0.26	3.3E+04	3.6E+04
4176500	3.10E-03	1.59	630.6	1.37	0.17	6.3E+04	6.7E+04
4182000	2.15E-02	1.47	399.2	1.77	0.29	1.6E+05	1.7E+05
4192500	2.23E-03	1.56	3189.2	1.62	0.27	7.4E+05	7.8E+05
4193500	6.99E-03	1.44	3593.6	1.62	0.26	8.1E+05	8.5E+05
4195500	2.27E-02	1.41	167.6	2.07	0.51	5.4E+04	5.7E+04
4197100	1.06E-01	1.20	70.8	2.02	0.50	1.7E+04	1.7E+04
4198000	5.35E-03	1.58	610.7	1.88	0.37	2.5E+05	2.7E+05
4199000	6.49E-03	1.64	146.7	2.16	0.61	8.5E+04	9.5E+04
4201500	5.05E-03	1.65	147.4	2.04	0.67	5.5E+04	6.1E+04
4202000	7.49E-02	0.87	199.5	1.17	0.16	2.5E+03	2.5E+03
4206000	3.89E-04	1.92	444.4	1.07	0.17	3.2E+04	3.3E+04
4207200	3.09E-03	1.87	109.3	1.43	0.45	2.5E+04	2.7E+04
4208000	4.93E-04	1.94	817.3	1.20	0.30	1.9E+05	2.0E+05
4209000	1.76E-03	1.91	231.7	1.71	0.56	1.5E+05	1.6E+05
4212100	7.13E-03	1.48	776.8	1.50	0.36	1.1E+05	1.1E+05
4221000	9.54E-04	1.80	297.1	1.49	0.34	3.2E+04	3.5E+04
4223000	1.58E-04	2.06	927.2	1.56	0.38	4.9E+05	5.4E+05
4227500	3.58E-04	1.99	1500.3	1.27	0.23	8.4E+05	8.8E+05
4232000	1.93E-04	1.93	2637.4	1.14	0.18	5.7E+05	6.0E+05
4233300	1.92E-02	1.70	45.0	1.54	0.39	1.4E+04	1.6E+04
5058700	2.39E-02	1.42	156.9	1.92	0.09	4.1E+04	4.4E+04
5059000	1.81E-02	1.52	211.6	1.73	0.07	7.5E+04	8.1E+04
5062000	2.34E-01	0.99	76.1	2.20	0.13	1.3E+04	1.4E+04
5062500	3.03E-02	1.39	139.9	1.72	0.10	2.6E+04	2.8E+04

Table D.1 – continued from previous page

Station ID	$\bar{a}$	$\bar{b}$	$\hat{a}$	$\hat{b}$	RB	Sediment yield (tons/yr)	
						FDSRC	Parametric
5099600	1.80E-01	1.33	101.2	2.34	0.12	1.8E+05	1.9E+05
5114000	4.17E-02	1.21	24.0	3.04	0.11	8.8E+03	9.5E+03
5280000	1.12E-01	1.03	676.9	1.52	0.06	4.1E+04	4.2E+04
5288500	2.40E-04	1.61	8855.8	0.90	0.05	2.3E+05	2.4E+05
5291000	9.33E-02	1.25	14.4	2.77	0.33	8.5E+03	9.5E+03
5293000	1.87E-01	1.16	21.7	2.55	0.24	1.1E+04	1.2E+04
5304500	1.94E-01	1.08	295.8	1.58	0.08	4.5E+04	4.6E+04
5317000	1.14E-01	1.31	194.2	2.09	0.16	1.5E+05	1.6E+05
5325000	4.04E-02	1.30	2756.7	1.59	0.07	8.0E+05	8.3E+05
5341500	1.03E-02	1.11	356.7	0.65	0.14	2.1E+03	2.1E+03
5357335	1.76E-03	1.36	67.3	0.80	0.05	1.8E+02	1.9E+02
5369500	9.09E-05	1.75	8001.0	0.92	0.13	2.8E+05	3.0E+05
5378500	1.26E-04	1.59	32556.4	0.80	0.05	6.8E+05	7.0E+05
5382000	6.17E-04	1.71	1363.5	1.48	0.19	1.4E+05	1.6E+05
5385000	3.63E-04	2.11	624.9	1.39	0.19	5.3E+05	5.3E+05
5387500	2.73E-03	1.89	223.2	1.82	0.24	2.3E+05	2.6E+05
5388250	2.32E-04	2.25	521.7	1.44	0.16	8.2E+05	8.3E+05
5388500	3.57E-02	2.08	3.3	2.77	0.60	5.9E+04	6.7E+04
5389400	1.15E-02	1.94	19.9	1.38	0.21	5.3E+03	5.3E+03
5389500	6.85E-03	1.24	41119.8	0.73	0.05	1.1E+06	1.1E+06
5406500	4.53E-03	1.95	41.6	0.76	0.14	2.7E+03	2.9E+03
5407000	2.03E-03	1.38	9597.4	0.71	0.09	1.9E+05	2.0E+05
5408000	2.51E-03	1.90	163.5	1.25	0.24	3.5E+04	4.0E+04
5412500	1.88E-03	1.90	768.3	1.57	0.24	9.8E+05	1.1E+06
5413500	1.54E-03	2.08	123.5	1.63	0.30	1.1E+05	1.1E+05
5418500	2.92E-03	1.78	909.4	1.40	0.23	5.1E+05	5.8E+05
5419000	7.26E-04	2.11	99.0	1.97	0.41	1.0E+05	1.1E+05
5420500	2.64E-04	1.56	54975.2	0.68	0.04	2.1E+06	2.2E+06
5421000	6.24E-03	1.46	477.4	1.70	0.20	5.3E+04	5.7E+04
5422000	4.97E-03	1.61	1545.3	1.29	0.12	4.6E+05	4.9E+05
5422470	1.53E-01	1.62	5.5	2.28	0.49	1.0E+04	1.3E+04
5426000	5.57E-01	0.80	391.8	1.31	0.08	2.2E+04	2.3E+04
5427718	2.49E-02	1.57	21.4	1.36	0.26	2.0E+03	2.3E+03
5427948	6.99E-02	1.65	1.9	2.44	0.69	1.3E+03	1.6E+03
5431017	5.06E-02	1.19	6.9	2.12	0.53	5.3E+02	5.8E+02
5431022	6.86E-02	0.96	15.4	1.61	0.24	4.1E+02	4.3E+02
5431486	1.60E-03	1.97	120.8	1.21	0.19	1.8E+04	1.9E+04

Table D.1 – continued from previous page

Station ID	$\bar{a}$	$\bar{b}$	$\hat{a}$	$\hat{b}$	RB	Sediment yield (tons/yr)	
						FDSRC	Parametric
5434500	1.73E-02	1.37	766.7	1.04	0.11	5.9E+04	6.4E+04
5436500	3.17E-03	1.58	363.8	1.08	0.16	1.7E+04	1.9E+04
5438500	1.30E-02	1.43	332.3	1.33	0.19	3.0E+04	3.2E+04
5439000	8.95E-02	1.27	40.1	1.77	0.32	7.6E+03	8.0E+03
5440000	3.93E-03	1.67	672.5	1.37	0.19	1.6E+05	1.8E+05
5446500	2.70E-04	1.81	7519.5	0.78	0.07	1.1E+06	1.2E+06
5447500	1.32E-03	1.95	599.4	1.27	0.19	3.6E+05	3.8E+05
5449500	4.23E-02	1.25	173.6	1.68	0.17	1.8E+04	1.9E+04
5451500	6.25E-03	1.66	697.3	1.54	0.17	3.6E+05	3.9E+05
5454500	1.84E-02	1.46	1741.7	1.28	0.11	5.7E+05	6.0E+05
5455000	8.67E-01	1.53	0.4	2.69	0.85	2.0E+03	2.3E+03
5464500	6.38E-04	1.75	3442.1	1.32	0.12	8.4E+05	9.1E+05
5465500	1.52E-03	1.60	7656.1	1.14	0.10	1.3E+06	1.4E+06
5466500	1.64E-02	1.75	206.1	1.71	0.28	3.3E+05	3.7E+05
5469000	2.50E-02	1.62	168.2	1.94	0.35	2.1E+05	2.4E+05
5471050	4.62E-03	1.71	456.6	1.61	0.19	2.2E+05	2.4E+05
5474000	1.80E-02	1.46	2046.9	1.52	0.19	9.8E+05	1.0E+06
5476000	1.38E-01	1.14	265.2	1.76	0.08	5.1E+04	5.2E+04
5481650	9.14E-02	1.17	2921.0	1.30	0.09	4.5E+05	4.5E+05
5482000	6.72E-03	1.60	2072.3	1.44	0.11	1.2E+06	1.2E+06
5483000	4.80E-01	0.86	4.9	2.08	0.32	9.8E+02	1.0E+03
5483450	2.77E-02	1.71	156.9	1.81	0.27	3.2E+05	3.6E+05
5483600	3.11E-02	1.30	145.7	1.87	0.31	1.9E+04	2.1E+04
5485500	1.92E-03	1.74	4481.9	1.35	0.11	3.7E+06	3.9E+06
5486490	1.68E-02	1.89	116.3	2.25	0.49	1.4E+06	1.6E+06
5487980	2.34E-01	1.42	61.0	2.63	0.67	3.8E+05	4.2E+05
5498000	5.95E-02	1.50	90.4	2.43	0.53	2.3E+05	2.4E+05
5502500	1.90E-01	1.22	96.6	2.54	0.61	1.0E+05	1.1E+05
5506000	1.50E-01	1.43	6.3	3.09	1.02	3.1E+04	3.2E+04
5506500	1.31E-01	1.28	79.9	2.49	0.55	8.7E+04	9.2E+04
5507000	1.48E-01	1.30	40.9	2.81	0.79	8.4E+04	8.7E+04
5508000	2.33E-02	1.40	931.4	1.98	0.40	4.6E+05	4.9E+05
5516500	9.24E-03	1.47	223.9	1.39	0.23	1.6E+04	1.8E+04
5520500	1.32E-03	1.65	2349.7	0.72	0.06	1.7E+05	1.8E+05
5525000	1.36E-01	1.07	502.8	1.40	0.15	4.4E+04	4.5E+04
5526000	2.41E-02	1.33	1386.0	1.48	0.17	2.2E+05	2.3E+05
5527500	3.25E-04	1.75	4511.5	1.07	0.11	4.6E+05	4.9E+05

Table D.1 – continued from previous page

Station ID	$\bar{a}$	$\bar{b}$	$\hat{a}$	$\hat{b}$	RB	Sediment yield (tons/yr)	
						FDSRC	Parametric
5532500	5.29E-03	1.50	542.8	1.22	0.21	3.6E+04	3.8E+04
5543500	5.18E-04	1.64	11810.9	0.72	0.12	8.9E+05	9.3E+05
5548280	4.29E-02	1.19	147.4	1.11	0.16	6.1E+03	6.4E+03
5552500	1.75E-03	1.71	1859.7	1.06	0.14	3.6E+05	3.8E+05
5558300	2.32E-03	1.47	16620.0	0.79	0.11	1.3E+06	1.3E+06
5568000	8.36E-03	1.61	513.5	1.67	0.23	2.5E+05	2.7E+05
5570000	1.73E-02	1.54	748.7	1.69	0.26	5.3E+05	5.8E+05
5570370	7.79E-02	1.59	25.1	1.59	0.37	1.3E+04	1.5E+04
5583000	1.57E-03	1.70	2862.1	1.43	0.12	1.2E+06	1.2E+06
5585000	2.05E-02	1.53	473.0	1.91	0.29	4.2E+05	4.5E+05
5586100	5.57E-03	1.42	25351.9	0.80	0.05	3.5E+06	3.6E+06
5587500	2.08E-03	1.46	116423.9	0.71	0.06	1.7E+07	1.7E+07
5591200	8.49E-02	1.16	299.0	1.69	0.22	4.0E+04	4.2E+04
5594100	8.38E-02	1.17	3500.3	1.23	0.11	4.9E+05	5.0E+05
5599500	3.12E-02	1.26	1346.3	1.60	0.14	1.8E+05	1.8E+05
6018500	1.22E-01	1.05	414.9	0.67	0.05	2.0E+04	2.0E+04
6025500	2.43E-04	1.72	895.3	1.38	0.08	2.6E+04	2.7E+04
6026500	4.49E-03	1.48	1776.5	0.99	0.06	1.2E+05	1.2E+05
6088300	1.10E-02	1.98	107.4	1.03	0.13	7.9E+04	8.1E+04
6088500	2.64E-02	1.91	124.4	1.00	0.12	1.6E+05	1.7E+05
6115200	2.28E-05	2.21	9780.7	0.71	0.05	6.8E+06	6.8E+06
6130500	3.42E-01	1.29	90.2	2.44	0.19	2.4E+05	2.7E+05
6185500	9.29E-04	1.81	11275.5	0.56	0.03	6.4E+06	6.6E+06
6188000	1.41E-04	2.05	546.1	1.74	0.11	2.3E+05	2.4E+05
6191500	4.89E-06	2.25	2804.0	1.21	0.06	3.8E+05	4.1E+05
6214500	2.90E-05	2.06	6358.9	1.18	0.07	1.8E+06	1.9E+06
6228000	1.02E-03	1.95	572.6	1.45	0.11	3.6E+05	3.9E+05
6236100	1.10E-02	1.63	752.8	1.60	0.10	5.9E+05	6.6E+05
6244500	3.51E+00	1.79	2.4	1.74	0.20	3.1E+04	3.7E+04
6253000	3.26E-01	1.79	174.6	0.77	0.05	1.4E+06	1.4E+06
6257000	1.04E+01	1.30	3.9	2.89	0.49	3.2E+05	3.4E+05
6258000	1.12E+00	1.92	19.3	1.19	0.18	2.6E+05	2.8E+05
6259500	9.43E-04	2.03	1584.4	1.27	0.09	3.4E+06	3.6E+06
6268500	2.21E+01	1.37	0.9	3.47	0.94	5.0E+05	5.0E+05
6279500	3.59E-02	1.65	2155.4	0.98	0.08	5.2E+06	5.6E+06
6290500	9.73E-03	1.72	188.8	1.13	0.09	4.6E+04	5.0E+04
6294000	9.82E-03	1.80	221.1	1.40	0.11	1.6E+05	1.8E+05

Table D.1 – continued from previous page

Station ID	$\bar{a}$	$\bar{b}$	$\hat{a}$	$\hat{b}$	RB	Sediment yield (tons/yr)	
						FDSRC	Parametric
6294700	1.72E-03	1.85	4352.2	0.69	0.07	3.3E+06	3.4E+06
6295000	4.04E-04	1.79	10747.0	0.92	0.05	3.2E+06	3.4E+06
6308500	2.93E-02	1.57	321.6	1.47	0.13	2.1E+05	2.2E+05
6309500	5.92E-03	2.19	63.3	1.16	0.11	5.8E+04	6.0E+04
6313000	7.67E-01	1.78	4.2	3.29	0.62	1.5E+06	1.8E+06
6313500	2.18E-01	1.73	108.4	1.88	0.25	1.7E+06	2.0E+06
6317000	4.44E+00	1.34	144.8	1.92	0.26	3.6E+06	4.1E+06
6324500	1.16E-01	1.67	292.2	1.67	0.19	2.0E+06	2.3E+06
6326500	1.03E-01	1.65	320.0	1.86	0.19	2.6E+06	2.9E+06
6329500	3.27E-04	1.88	12334.9	1.04	0.08	9.5E+06	1.0E+07
6335500	1.41E-01	1.73	69.6	2.78	0.31	5.6E+06	6.2E+06
6336000	1.87E-01	1.57	109.9	2.69	0.30	3.1E+06	3.4E+06
6337000	2.36E+02	0.74	150.4	2.59	0.27	5.9E+06	6.1E+06
6339500	1.13E-01	1.48	12.9	3.10	0.37	9.3E+04	1.0E+05
6340500	6.05E-02	1.48	29.0	2.99	0.30	1.2E+05	1.4E+05
6342500	3.63E-04	1.86	24836.9	0.59	0.04	1.8E+07	1.8E+07
6345500	8.12E-02	1.50	13.8	3.15	0.36	9.0E+04	1.0E+05
6349000	1.62E-02	1.68	60.8	2.76	0.22	3.2E+05	3.5E+05
6350000	7.83E-02	1.52	3.6	3.46	0.42	3.3E+04	3.5E+04
6352500	5.92E-02	1.44	4.0	3.83	0.35	4.0E+04	4.2E+04
6354000	2.51E-01	1.36	35.3	3.13	0.29	3.3E+05	3.9E+05
6357500	2.57E-01	1.37	10.1	3.47	0.19	1.4E+05	1.7E+05
6357800	6.72E-01	1.34	70.9	2.62	0.29	7.0E+05	7.7E+05
6359500	1.59E-01	1.58	16.8	3.29	0.41	7.0E+05	7.5E+05
6360500	8.81E-01	1.31	43.6	3.04	0.33	9.4E+05	9.9E+05
6386000	1.02E+00	1.70	2.3	3.48	0.77	8.3E+05	9.0E+05
6394000	1.74E-01	1.86	6.6	2.80	0.50	2.8E+05	3.2E+05
6400000	1.02E+00	1.38	0.9	3.86	0.55	5.8E+04	6.5E+04
6400500	2.89E-02	1.94	33.1	3.02	0.52	3.9E+06	4.6E+06
6425720	2.07E-01	1.19	0.1	4.08	0.46	2.7E+02	3.4E+02
6437000	5.17E-02	1.99	120.9	2.24	0.23	1.1E+07	1.2E+07
6439300	6.08E-02	1.71	316.4	2.25	0.27	6.7E+06	7.3E+06
6440200	3.93E+00	1.26	1.6	3.53	0.78	1.1E+05	1.2E+05
6441500	5.55E-01	1.50	19.6	3.28	0.48	1.6E+06	1.6E+06
6446000	1.65E+00	1.23	20.2	2.35	0.26	1.0E+05	1.2E+05
6447000	1.99E+00	1.47	100.8	2.33	0.48	5.7E+06	6.2E+06
6452000	1.05E+00	1.41	234.7	2.24	0.32	5.0E+06	5.6E+06

Table D.1 – continued from previous page

Station ID	$\bar{a}$	$\bar{b}$	$\hat{a}$	$\hat{b}$	RB	Sediment yield (tons/yr)	
						FDSRC	Parametric
6453500	5.07E-02	1.78	8.3	2.93	0.39	1.1E+05	1.2E+05
6457500	2.24E-02	1.88	131.7	0.56	0.11	6.8E+04	7.2E+04
6461500	8.78E-02	1.51	857.4	0.27	0.05	7.0E+05	7.1E+05
6465500	1.11E+00	1.16	1995.2	0.52	0.11	2.2E+06	2.2E+06
6477000	1.08E-02	1.57	285.5	2.18	0.05	2.5E+05	2.6E+05
6478500	3.61E-01	0.99	287.9	2.24	0.07	7.6E+04	8.0E+04
6481000	2.48E-01	1.08	220.4	2.06	0.11	6.7E+04	7.1E+04
6486000	2.85E-02	1.33	33693.9	0.61	0.04	8.8E+06	9.1E+06
6600500	6.73E-02	1.56	132.3	2.05	0.23	2.9E+05	3.4E+05
6606600	9.05E-02	1.42	711.0	1.58	0.12	8.2E+05	8.7E+05
6606700	6.39E-02	1.59	472.2	1.73	0.15	1.5E+06	1.6E+06
6610000	4.11E-02	1.42	36179.8	0.61	0.04	3.8E+07	3.9E+07
6645000	2.00E-03	1.87	1063.3	1.41	0.07	1.1E+06	1.1E+06
6650000	1.85E-03	1.85	1254.7	1.27	0.07	9.5E+05	9.4E+05
6656000	2.76E-02	1.12	1612.2	1.24	0.05	4.6E+04	4.6E+04
6758500	2.70E-02	1.48	445.0	1.73	0.13	2.3E+05	2.6E+05
6771000	3.63E-01	1.47	0.2	4.69	0.79	4.3E+04	3.7E+04
6785000	3.68E-02	1.69	1244.1	0.74	0.16	2.1E+06	2.3E+06
6790500	1.75E-03	2.04	1083.0	0.51	0.11	9.0E+05	9.4E+05
6803500	1.62E-02	1.91	81.9	2.37	0.48	1.2E+06	1.4E+06
6805500	6.35E-02	1.43	7335.5	0.99	0.14	8.2E+06	8.7E+06
6807000	5.32E-02	1.33	43517.1	0.57	0.05	2.4E+07	2.4E+07
6809000	3.43E-01	1.75	2.6	2.63	0.53	3.5E+04	3.7E+04
6809500	1.19E-02	1.85	253.8	1.97	0.35	1.4E+06	1.5E+06
6817000	6.44E-03	1.91	149.2	2.35	0.50	1.4E+06	1.6E+06
6818000	7.72E-04	1.75	49087.1	0.60	0.06	4.2E+07	4.3E+07
6821500	6.59E-01	1.48	0.7	3.97	0.60	3.9E+04	7.1E+04
6828500	1.96E+00	1.28	52.5	1.84	0.23	2.6E+05	2.9E+05
6829500	3.25E-01	1.58	24.2	2.37	0.23	2.4E+05	2.8E+05
6834000	5.28E-03	2.24	52.6	1.21	0.09	5.0E+04	5.3E+04
6838000	7.98E-02	2.22	7.3	2.38	0.33	4.3E+05	4.5E+05
6841000	3.28E-02	2.12	39.1	1.74	0.25	4.0E+05	3.8E+05
6841500	8.08E+00	1.41	0.1	4.33	1.45	4.9E+04	4.3E+04
6844500	3.18E-01	1.45	143.1	1.71	0.18	3.9E+05	4.6E+05
6845000	6.14E-01	1.45	0.6	3.92	0.65	4.0E+04	4.2E+04
6845200	7.29E+01	0.68	7.4	2.90	0.54	1.8E+05	1.8E+05
6846500	5.95E-01	1.35	0.6	3.79	0.48	1.3E+04	1.4E+04

Table D.1 – continued from previous page

Station ID	$\bar{a}$	$\bar{b}$	$\hat{a}$	$\hat{b}$	RB	Sediment yield (tons/yr)	
						FDSRC	Parametric
6847000	3.17E-01	1.45	3.0	3.07	0.39	2.2E+04	2.5E+04
6847500	2.11E-01	1.54	4.7	3.21	0.35	6.5E+04	8.5E+04
6848000	1.73E-01	1.64	0.6	4.09	0.59	7.8E+04	7.3E+04
6854000	2.34E+00	1.20	4.3	3.31	0.40	8.6E+04	1.0E+05
6854500	4.83E-03	1.90	302.9	2.10	0.28	1.8E+06	2.0E+06
6856600	1.99E-02	1.69	471.0	1.95	0.27	1.6E+06	1.9E+06
6866900	2.27E-01	1.54	0.6	4.02	0.69	3.8E+04	4.0E+04
6867000	5.45E-01	1.35	12.9	3.08	0.37	1.4E+05	1.7E+05
6869500	1.30E-01	1.50	56.8	2.59	0.29	3.1E+05	3.6E+05
6870200	1.89E-02	1.66	349.9	1.89	0.19	7.2E+05	7.8E+05
6871800	3.20E-01	1.46	2.2	3.70	0.50	6.8E+04	8.1E+04
6873500	2.71E-01	1.46	5.1	3.87	0.58	3.5E+05	3.7E+05
6876000	1.31E-01	1.44	61.0	3.07	0.45	6.6E+05	7.6E+05
6877600	1.50E-02	1.62	683.3	2.09	0.18	1.8E+06	2.0E+06
6881000	1.89E-01	1.39	165.1	2.17	0.26	4.1E+05	4.7E+05
6883000	1.08E-01	1.59	43.0	2.47	0.37	2.4E+05	3.0E+05
6887500	4.64E-03	1.69	3347.5	1.66	0.15	6.1E+06	6.7E+06
6888000	1.12E-01	1.60	13.9	3.02	0.79	2.1E+05	2.3E+05
6890500	1.11E-01	1.57	69.4	2.93	0.81	1.7E+06	1.8E+06
6898000	9.88E-02	1.55	143.5	2.37	0.49	9.2E+05	1.0E+06
6903400	3.08E-01	1.22	34.5	2.65	0.59	5.7E+04	6.1E+04
6903900	1.65E-01	1.20	281.8	1.55	0.16	8.1E+04	8.2E+04
6918070	7.04E-02	1.26	2761.6	1.80	0.22	1.3E+06	1.3E+06
6934500	1.07E-03	1.69	89039.9	0.76	0.08	8.7E+07	9.0E+07
7010000	1.68E-05	1.87	208005.4	0.68	0.05	5.6E+07	5.7E+07
7019000	2.47E-04	1.82	2014.5	1.77	0.27	6.2E+05	7.0E+05
7020500	9.72E-05	1.73	237020.6	0.64	0.05	6.2E+07	6.3E+07
7022000	6.28E-05	1.76	239638.7	0.65	0.05	6.4E+07	6.5E+07
7036100	6.69E-03	1.41	326.4	2.34	0.61	6.5E+04	7.1E+04
7040100	6.01E-02	1.34	1866.0	1.28	0.11	7.4E+05	7.5E+05
7047810	6.98E-02	1.22	3784.9	1.33	0.07	7.9E+05	8.0E+05
7061300	2.06E-02	1.39	39.2	2.45	0.66	1.0E+04	1.1E+04
7077555	1.30E-01	1.09	1367.0	1.10	0.07	1.2E+05	1.2E+05
7103700	1.93E-02	2.04	12.5	1.47	0.13	6.3E+03	6.7E+03
7103970	2.11E-02	1.93	16.6	1.88	0.22	2.0E+04	2.1E+04
7103990	3.83E-01	1.78	4.0	1.89	0.46	1.2E+04	1.5E+04
7105500	3.86E-02	1.81	40.7	1.88	0.28	8.9E+04	1.1E+05

Table D.1 – continued from previous page

Station ID	$\bar{a}$	$\bar{b}$	$\hat{a}$	$\hat{b}$	RB	Sediment yield (tons/yr)	
						FDSRC	Parametric
7105530	4.74E-03	1.95	94.8	1.56	0.25	7.6E+04	7.3E+04
7105800	1.46E-02	1.87	85.0	1.59	0.26	9.4E+04	1.1E+05
7106300	1.15E-02	1.91	82.9	1.77	0.31	1.6E+05	1.8E+05
7106500	3.16E-02	1.84	56.1	1.94	0.32	1.9E+05	2.2E+05
7124200	9.37E-03	2.33	53.5	1.51	0.17	4.0E+05	3.8E+05
7124410	8.29E-02	1.51	54.2	1.47	0.14	2.9E+04	2.8E+04
7126300	3.97E-01	1.57	14.4	2.61	0.51	2.0E+05	2.4E+05
7126485	1.79E-01	1.71	27.5	2.08	0.42	1.8E+05	2.1E+05
7140000	2.06E-02	1.64	26.3	2.76	0.15	6.2E+04	7.8E+04
7141900	5.69E-01	1.31	5.3	3.25	0.46	5.5E+04	5.8E+04
7143330	7.28E-03	1.74	284.7	1.85	0.16	3.1E+05	3.6E+05
7144200	5.95E-02	1.46	77.2	2.68	0.45	2.2E+05	2.4E+05
7146500	1.22E-02	1.62	1188.2	1.78	0.24	1.7E+06	2.0E+06
7147800	2.22E-02	1.51	277.1	2.50	0.47	5.5E+05	6.0E+05
7151500	2.37E-02	1.65	70.4	2.58	0.55	2.7E+05	3.2E+05
7230000	2.73E-01	1.48	9.4	2.99	0.39	1.1E+05	1.2E+05
7277700	1.08E-02	1.75	50.4	2.54	0.94	1.4E+05	1.7E+05
7301500	6.08E-01	1.46	22.7	2.89	0.52	5.5E+05	6.6E+05
7304500	6.33E-02	1.73	11.3	3.21	0.69	3.9E+05	4.3E+05
7325500	2.14E-01	1.50	146.8	2.23	0.32	1.0E+06	1.1E+06
7351750	4.72E-01	0.94	634.6	1.68	0.19	9.5E+04	9.7E+04
7352800	1.40E-01	0.95	28.0	2.62	0.50	3.5E+03	3.7E+03
8023080	2.09E-01	1.02	14.2	2.91	0.74	5.7E+03	6.1E+03
8023400	2.65E-01	0.95	15.7	2.90	0.74	5.1E+03	5.5E+03
8044000	2.17E-01	1.26	6.5	3.52	0.69	3.5E+04	3.7E+04
8286500	2.22E-01	1.48	384.1	1.32	0.14	8.9E+05	9.4E+05
8287000	1.05E+00	1.09	461.7	1.08	0.10	2.9E+05	2.9E+05
8290000	6.30E-01	1.40	445.3	1.31	0.12	1.8E+06	1.9E+06
8313000	1.39E-01	1.42	1290.1	1.24	0.08	1.8E+06	1.9E+06
8317400	6.23E-02	1.02	1265.9	1.00	0.07	3.1E+04	3.1E+04
8317950	5.77E+00	1.58	0.3	3.73	1.16	1.8E+05	1.9E+05
8318000	1.86E+01	1.42	0.4	4.10	1.37	7.8E+05	7.6E+05
8329500	6.12E+00	1.08	798.5	1.48	0.13	3.7E+06	3.8E+06
8330000	4.19E-01	1.29	1019.2	1.19	0.10	1.4E+06	1.4E+06
8331990	2.57E+00	1.23	147.6	1.69	0.11	8.9E+05	8.6E+05
8332010	6.26E-01	1.22	616.3	1.48	0.10	9.0E+05	9.0E+05
8332050	1.71E-02	2.11	59.6	0.75	0.09	4.4E+04	4.5E+04

Table D.1 – continued from previous page

Station ID	$\bar{a}$	$\bar{b}$	$\hat{a}$	$\hat{b}$	RB	Sediment yield (tons/yr)	
						FDSRC	Parametric
8334000	4.10E+01	1.30	2.9	2.79	0.64	7.1E+05	7.5E+05
8340500	2.05E+01	1.38	1.6	3.51	1.02	1.2E+06	1.2E+06
8353000	3.96E+01	1.28	4.2	3.32	0.77	2.8E+06	2.9E+06
8354800	1.68E+00	1.50	243.9	1.50	0.11	5.7E+06	5.4E+06
8354900	4.84E+00	1.16	592.3	1.45	0.12	4.1E+06	4.2E+06
8358300	8.01E-01	1.48	303.8	1.17	0.09	2.0E+06	2.0E+06
8358400	9.70E+00	1.11	459.3	1.57	0.12	4.7E+06	4.8E+06
8383000	4.75E-02	1.84	27.8	2.73	0.48	8.2E+05	9.0E+05
8390500	2.67E+00	1.53	2.2	3.39	0.49	4.4E+05	5.1E+05
8396500	8.33E-02	1.62	78.4	2.48	0.28	6.2E+05	7.9E+05
8398500	1.71E+00	1.49	0.0	6.17	1.47	8.3E+04	7.7E+04
9041090	6.08E-02	1.44	31.1	1.99	0.11	1.4E+04	1.5E+04
9093700	1.03E-02	1.46	3659.1	1.09	0.05	7.2E+05	7.6E+05
9180000	9.78E-03	1.90	439.8	1.78	0.11	3.2E+06	3.4E+06
9180500	7.47E-03	1.64	6580.4	1.15	0.07	8.0E+06	8.5E+06
9184000	1.85E-03	2.73	12.4	1.20	0.16	6.9E+03	5.2E+03
9217000	2.73E-03	1.58	1511.2	1.10	0.05	1.4E+05	1.6E+05
9224700	1.58E-02	1.80	181.0	1.75	0.11	4.0E+05	4.3E+05
9243900	4.24E-01	1.42	2.0	1.88	0.15	1.4E+03	1.5E+03
9251000	9.76E-03	1.53	1121.8	1.56	0.09	4.3E+05	4.3E+05
9260000	8.59E-01	1.38	362.5	1.72	0.12	2.8E+06	2.8E+06
9261000	1.10E-02	1.64	4077.8	1.06	0.07	4.5E+06	4.7E+06
9306500	1.35E-03	2.08	694.7	0.96	0.08	6.9E+05	7.2E+05
9315000	4.42E-02	1.51	5536.2	1.16	0.06	1.0E+07	1.1E+07
9328500	2.12E-01	1.78	57.6	2.09	0.20	1.4E+06	1.5E+06
9341500	1.12E-04	2.27	116.2	1.58	0.10	2.1E+04	2.3E+04
9355500	1.59E-03	1.99	1038.9	1.06	0.04	1.1E+06	1.2E+06
9356500	1.09E-02	1.74	1058.6	1.47	0.12	2.3E+06	2.4E+06
9364500	3.45E-02	1.54	700.3	1.35	0.10	5.6E+05	5.9E+05
9368000	7.77E-02	1.59	1755.8	1.22	0.11	6.9E+06	7.3E+06
9378700	3.02E+00	1.74	0.7	3.54	0.50	5.9E+05	5.7E+05
9379500	2.70E-01	1.52	1950.5	1.19	0.12	1.5E+07	1.6E+07
9380000	2.98E-03	1.80	15099.2	0.93	0.08	4.5E+07	4.9E+07
9382000	2.12E+00	1.93	5.7	2.84	0.63	5.2E+06	5.6E+06
9394500	5.66E-01	1.70	7.7	3.01	0.66	7.8E+05	8.6E+05
9401260	4.33E+00	1.79	0.5	3.92	1.14	2.1E+06	2.1E+06
9402000	3.18E+01	1.18	57.9	2.57	0.41	7.8E+06	8.1E+06

Table D.1 – continued from previous page

Station ID	$\bar{a}$	$\bar{b}$	$\hat{a}$	$\hat{b}$	RB	Sediment yield (tons/yr)	
						FDSRC	Parametric
9402500	2.04E-01	1.43	15855.2	0.89	0.08	7.8E+07	8.3E+07
9406000	1.72E-01	1.79	159.2	1.39	0.21	1.4E+06	1.6E+06
9408150	3.20E-01	1.68	133.2	1.68	0.21	1.6E+06	1.9E+06
9410000	6.37E-02	2.18	13.8	1.69	0.18	1.1E+05	1.0E+05
9415000	1.59E-02	1.96	133.4	1.87	0.24	9.4E+05	1.1E+06
9430500	1.20E-02	1.84	65.6	2.19	0.22	1.7E+05	2.1E+05
9448500	2.54E-02	1.84	135.6	2.50	0.26	3.5E+06	4.3E+06
9471000	6.74E-02	1.96	5.9	3.27	0.75	9.3E+05	1.2E+06
9474000	3.03E-01	1.66	161.1	2.41	0.21	8.3E+06	1.1E+07
9505350	2.36E+00	0.91	4.0	3.38	0.63	1.6E+04	1.8E+04
10092700	2.39E-02	1.45	1047.5	0.78	0.13	1.9E+05	2.0E+05
10104700	8.73E-03	1.74	56.5	1.08	0.10	5.5E+03	5.8E+03
10118000	2.24E-01	0.99	1527.3	0.96	0.14	1.0E+05	1.0E+05
10174500	1.70E-02	1.63	108.0	1.20	0.05	2.0E+04	2.2E+04
10336610	7.46E-03	1.41	69.1	1.54	0.14	2.2E+03	2.3E+03
10336645	5.89E-04	1.95	9.4	1.82	0.20	1.8E+02	1.9E+02
10336660	8.37E-04	2.02	22.0	1.75	0.16	1.7E+03	1.8E+03
10336676	1.51E-03	1.94	15.0	1.81	0.17	1.0E+03	1.1E+03
10336698	3.84E-03	2.20	6.0	1.35	0.09	3.6E+02	3.8E+02
10336740	1.28E-02	1.59	0.4	1.46	0.10	2.7E+00	2.9E+00
10336780	7.91E-03	1.46	32.8	1.14	0.06	5.9E+02	6.3E+02
11013500	3.37E+00	1.03	0.7	4.58	0.46	5.4E+04	5.8E+04
11022500	6.11E-02	1.44	0.8	4.21	0.54	8.9E+03	1.1E+04
11042000	6.18E-02	1.65	2.5	3.61	0.37	5.7E+04	6.5E+04
11046000	1.04E-01	1.53	1.4	4.15	0.67	7.1E+04	8.0E+04
11046500	4.71E-03	2.24	0.7	3.79	0.47	6.1E+04	7.5E+04
11046530	1.46E-01	1.78	0.5	4.22	0.63	2.3E+05	2.4E+05
11047000	1.10E-01	1.66	0.2	4.24	0.52	1.3E+04	1.2E+04
11047300	1.01E-01	1.94	1.6	3.39	0.80	1.9E+05	1.9E+05
11048500	3.37E+00	1.26	0.3	3.97	1.06	2.5E+04	2.8E+04
11051500	6.23E-03	2.04	4.6	3.25	0.29	8.5E+04	1.1E+05
11057000	2.53E+02	0.84	0.0	5.35	1.44	4.8E+04	6.2E+04
11074000	1.97E-01	1.10	127.3	1.84	0.15	2.6E+04	2.8E+04
11078000	4.93E-01	1.43	3.7	3.81	0.50	3.1E+05	2.9E+05
11105850	5.18E-01	1.83	0.1	4.41	1.15	1.1E+05	1.1E+05
11108500	1.42E-01	1.72	2.8	3.87	0.53	6.8E+05	6.8E+05
11109000	1.06E-02	2.06	8.9	3.20	0.39	7.7E+05	7.0E+05

Table D.1 – continued from previous page

Station ID	$\bar{a}$	$\bar{b}$	$\hat{a}$	$\hat{b}$	RB	Sediment yield (tons/yr)	
						FDSRC	Parametric
11110500	7.44E-02	2.14	0.2	4.14	0.92	1.9E+05	2.0E+05
11113000	1.61E-02	1.79	8.5	3.66	0.59	4.6E+05	5.0E+05
11114000	5.47E-01	1.40	4.1	4.31	0.78	9.5E+05	9.8E+05
11117500	2.09E-02	2.06	0.3	4.41	0.78	2.8E+05	2.3E+05
11118500	7.81E-02	1.60	2.7	3.98	0.64	1.7E+05	1.9E+05
11120510	7.74E-02	2.40	0.2	3.62	0.82	1.1E+05	1.5E+05
11141000	1.64E+01	1.18	0.5	4.61	0.70	6.4E+05	6.2E+05
11141280	9.62E-03	2.06	2.9	2.48	0.32	3.8E+03	4.3E+03
11147070	2.05E-02	1.89	1.8	3.16	0.64	1.4E+04	1.4E+04
11148900	1.40E-03	1.72	25.9	3.05	0.60	2.1E+04	2.2E+04
11149900	3.03E-02	1.54	19.3	2.87	0.38	4.2E+04	4.4E+04
11151870	1.80E-03	1.90	56.5	2.39	0.36	6.2E+04	6.9E+04
11152500	3.64E-02	1.65	48.5	3.22	0.31	1.5E+06	1.5E+06
11153900	1.14E-02	1.71	4.9	2.91	0.58	6.1E+03	6.7E+03
11160300	5.83E-02	1.90	1.7	3.07	0.60	2.6E+04	2.8E+04
11160500	6.28E-04	2.20	39.3	2.48	0.42	1.7E+05	1.7E+05
11162720	2.56E-01	1.91	2.4	2.48	0.97	3.4E+04	3.5E+04
11169800	7.26E-03	1.64	5.4	3.17	0.62	6.2E+03	6.3E+03
11176400	1.35E-02	1.66	4.2	3.21	0.57	9.3E+03	1.0E+04
11176500	5.77E-02	1.54	2.1	3.50	0.47	1.3E+04	1.4E+04
11176900	3.64E-02	1.59	10.9	2.92	0.58	3.1E+04	3.4E+04
11177000	7.18E-03	1.96	9.9	3.00	0.55	1.1E+05	1.2E+05
11179000	9.20E-03	1.82	20.5	3.00	0.49	1.8E+05	1.9E+05
11180825	1.61E-01	1.83	1.2	2.96	0.61	1.8E+04	1.8E+04
11180960	4.24E-01	1.79	0.4	3.16	0.66	9.3E+03	1.0E+04
11181040	2.92E-02	1.80	5.7	2.66	0.69	1.6E+04	1.8E+04
11181390	5.16E-02	2.14	0.6	3.22	0.73	2.2E+04	2.6E+04
11303500	1.27E-01	1.06	3507.8	1.40	0.05	3.1E+05	3.2E+05
11306000	1.69E-03	1.64	20.8	2.60	0.47	2.6E+03	2.9E+03
11308000	2.41E-03	1.68	12.8	2.54	0.47	2.0E+03	2.1E+03
11335000	3.64E-04	1.84	211.6	2.14	0.28	4.7E+04	5.3E+04
11376000	1.07E-04	2.15	394.7	2.09	0.31	6.1E+05	6.8E+05
11377100	2.03E-06	2.18	11543.8	1.06	0.12	1.2E+06	1.3E+06
11382000	4.34E-04	2.24	131.0	2.10	0.30	5.5E+05	5.7E+05
11389000	2.15E-06	2.22	11742.9	1.20	0.11	3.0E+06	3.1E+06
11389470	2.41E-01	1.18	159.9	3.22	0.39	6.2E+05	5.8E+05
11389500	1.17E-05	2.10	12308.9	0.76	0.06	2.0E+06	2.1E+06

Table D.1 – continued from previous page

Station ID	$\bar{a}$	$\bar{b}$	$\hat{a}$	$\hat{b}$	RB	Sediment yield (tons/yr)	
						FDSRC	Parametric
11391000	7.33E-06	2.16	12138.0	0.56	0.04	1.8E+06	1.8E+06
11407000	5.03E-06	2.14	2386.8	1.75	0.15	4.1E+05	4.6E+05
11407150	3.72E-04	1.61	3700.0	1.49	0.09	1.8E+05	2.1E+05
11410000	2.82E-05	2.34	222.7	1.83	0.24	1.2E+05	1.1E+05
11417500	6.06E-05	2.05	225.7	1.98	0.27	3.4E+04	3.6E+04
11418000	6.70E-03	1.04	1694.7	1.57	0.15	7.0E+03	7.3E+03
11418500	4.67E-03	1.54	42.5	2.35	0.49	6.1E+03	6.6E+03
11447500	3.36E-05	1.87	25767.7	0.77	0.05	2.5E+06	2.5E+06
11447650	3.24E-05	1.85	24947.5	0.78	0.05	1.8E+06	1.9E+06
11452500	3.84E-02	1.56	153.2	2.50	0.28	6.6E+05	6.8E+05
11453000	6.13E-02	1.21	575.2	3.06	0.25	6.8E+05	6.8E+05
11456000	2.53E-03	1.90	18.7	2.83	0.56	4.5E+04	5.0E+04
11458000	3.99E-03	1.72	39.7	2.85	0.50	6.9E+04	7.5E+04
11460000	4.48E-03	1.89	4.9	2.89	0.66	7.3E+03	7.8E+03
11460400	3.82E-04	2.07	15.1	2.41	0.41	4.0E+03	4.2E+03
11460750	1.61E-03	2.05	5.4	2.99	0.50	1.4E+04	1.6E+04
11461000	2.01E-03	1.94	52.4	2.48	0.54	1.2E+05	1.3E+05
11461500	3.66E-04	2.07	248.9	1.38	0.27	5.0E+04	5.4E+04
11462000	1.00E-01	1.13	259.8	1.40	0.22	2.4E+04	2.5E+04
11463000	1.15E-04	2.12	453.1	2.00	0.32	5.3E+05	5.9E+05
11463200	8.16E-04	2.08	37.9	2.62	0.47	1.2E+05	1.4E+05
11465200	6.92E-03	1.69	119.4	2.24	0.31	1.2E+05	1.3E+05
11467000	1.29E-02	1.42	869.8	2.24	0.32	4.6E+05	5.0E+05
11468000	1.16E-03	1.84	144.5	2.52	0.45	2.0E+05	2.3E+05
11469000	5.33E-05	2.24	606.9	2.04	0.37	1.5E+06	1.7E+06
11471000	3.35E-01	0.74	214.2	0.48	0.05	5.2E+03	5.2E+03
11472150	7.87E-04	1.85	252.5	2.50	0.39	4.5E+05	4.8E+05
11472200	3.31E-03	1.58	117.8	2.51	0.49	4.7E+04	4.8E+04
11473900	1.97E-04	2.08	754.0	2.00	0.35	1.8E+06	2.0E+06
11474500	5.78E-04	1.92	206.3	2.45	0.49	4.3E+05	4.0E+05
11475000	8.14E-05	2.04	1790.4	2.23	0.35	6.3E+06	6.9E+06
11475500	1.74E-03	1.87	59.9	2.37	0.42	5.2E+04	5.6E+04
11475560	1.46E-03	1.87	11.9	2.05	0.29	8.5E+02	9.1E+02
11476600	3.34E-03	2.10	55.1	2.03	0.29	1.7E+05	1.9E+05
11477000	4.53E-05	2.08	3138.8	2.15	0.34	1.2E+07	1.4E+07
11481000	2.07E-03	1.83	773.8	1.87	0.32	1.3E+06	1.4E+06
11481500	2.88E-04	2.24	139.7	1.71	0.30	1.1E+05	1.2E+05

Table D.1 – continued from previous page

Station ID	$\bar{a}$	$\bar{b}$	$\hat{a}$	$\hat{b}$	RB	Sediment yield (tons/yr)	
						FDSRC	Parametric
11482500	3.83E-04	2.00	598.0	1.78	0.29	5.0E+05	5.5E+05
11523000	6.64E-07	2.37	7182.2	1.22	0.13	1.7E+06	1.6E+06
11525600	3.56E-04	2.48	32.4	1.64	0.15	2.1E+04	1.7E+04
11525655	3.64E-06	2.35	738.0	1.33	0.07	4.5E+04	4.6E+04
11528700	1.39E-04	2.07	747.1	1.86	0.22	6.8E+05	7.6E+05
11530000	5.62E-06	2.33	3989.3	1.45	0.16	4.5E+06	4.6E+06
11532500	2.31E-06	2.13	2413.0	1.70	0.32	1.6E+05	1.8E+05
12026400	3.66E-04	1.79	294.9	1.37	0.21	9.2E+03	1.0E+04
12031000	8.14E-05	1.76	3522.5	1.29	0.16	1.1E+05	1.2E+05
12041200	4.01E-08	2.90	2494.4	1.06	0.27	7.6E+05	6.0E+05
12097850	2.53E-05	2.35	1501.9	0.82	0.15	4.6E+05	4.4E+05
12113350	2.99E-04	1.90	1519.0	0.98	0.14	1.9E+05	2.0E+05
12149000	5.61E-07	2.42	3810.1	0.95	0.21	2.3E+05	2.3E+05
12200500	6.51E-07	2.36	18734.6	0.54	0.12	3.0E+06	3.1E+06
12301933	5.60E-03	1.14	12097.5	0.68	0.09	7.6E+04	7.6E+04
12302055	2.81E-05	2.35	404.3	1.28	0.10	7.2E+04	7.6E+04
12318500	1.79E-07	2.32	15481.7	1.01	0.07	7.9E+05	8.4E+05
12323600	5.89E-03	1.71	52.3	1.03	0.08	2.5E+03	2.7E+03
12323750	1.37E-03	1.68	98.1	1.06	0.07	1.5E+03	1.6E+03
12324200	5.45E-03	1.52	278.0	0.75	0.06	9.5E+03	1.0E+04
12334550	2.74E-05	2.08	1285.1	0.94	0.06	5.0E+04	5.2E+04
12340000	7.86E-06	2.13	1388.1	1.24	0.06	4.7E+04	5.0E+04
12340500	5.11E-05	1.92	2799.0	1.09	0.06	1.5E+05	1.6E+05
12355000	1.48E-05	2.20	661.5	1.51	0.10	6.6E+04	7.2E+04
12355500	2.54E-06	2.26	2531.5	1.31	0.08	2.1E+05	2.3E+05
12363000	4.15E-08	2.58	9417.7	1.05	0.10	1.0E+06	1.1E+06
12424000	9.37E-04	1.94	98.9	2.17	0.34	6.6E+04	7.4E+04
12510500	1.71E-04	1.90	3754.2	0.85	0.08	5.0E+05	5.2E+05
13055198	7.83E-04	1.77	327.4	0.98	0.07	1.1E+04	1.2E+04
13227000	8.52E-03	2.22	17.0	2.22	0.22	1.5E+05	1.6E+05
13344500	1.61E-04	2.68	170.0	1.00	0.09	2.8E+05	2.0E+05
13351000	3.25E-02	1.55	357.0	1.79	0.19	3.9E+05	4.2E+05
14018500	1.04E-02	1.83	467.1	1.40	0.17	8.7E+05	9.1E+05
14019200	5.95E-07	1.91	204124.3	0.61	0.06	2.9E+06	3.0E+06
14033500	1.24E-02	1.67	343.3	1.63	0.19	2.9E+05	3.1E+05
14048000	2.59E-03	1.77	1716.4	1.33	0.11	1.3E+06	1.3E+06
14101500	1.17E-03	1.97	417.9	1.03	0.11	1.1E+05	1.2E+05

Table D.1 – continued from previous page

Station ID	$\bar{a}$	$\bar{b}$	$\hat{a}$	$\hat{b}$	RB	Sediment yield (tons/yr)	
						FDSRC	Parametric
14138870	2.17E-04	1.85	29.6	1.31	0.32	1.1E+02	1.1E+02
14138900	4.76E-05	2.19	64.5	1.28	0.32	6.7E+02	6.8E+02
14139800	7.95E-04	1.60	98.8	1.27	0.30	7.7E+02	8.3E+02
14242580	4.30E-04	2.21	2108.2	1.02	0.17	7.9E+06	8.0E+06
14306500	6.67E-05	1.93	1104.5	1.50	0.24	7.8E+04	8.5E+04
14307620	1.93E-04	1.78	1456.4	1.53	0.24	1.1E+05	1.2E+05
14330000	2.87E-11	3.84	1472.3	0.51	0.07	3.6E+04	2.6E+04
14334700	1.30E-05	2.36	361.4	1.09	0.13	1.8E+04	1.7E+04
15212000	2.45E-07	2.48	35162.7	1.16	0.05	7.0E+07	7.9E+07
15241600	1.50E-03	1.74	106.4	1.04	0.11	2.6E+03	2.8E+03
15275100	8.13E-03	2.10	24.4	0.61	0.11	2.5E+03	2.6E+03
15281000	2.92E-03	1.67	5246.5	1.49	0.09	5.0E+06	5.3E+06
15284000	1.41E-04	2.14	3547.2	1.22	0.09	6.6E+06	6.9E+06
15476000	9.25E-07	2.56	8226.3	0.96	0.04	9.3E+06	9.9E+06
15514000	2.34E-04	1.82	1189.5	1.27	0.09	7.7E+04	8.2E+04
15518000	1.18E-05	2.35	3250.1	1.17	0.08	2.8E+06	3.0E+06
16103000	2.03E-05	2.39	163.3	1.56	0.54	2.3E+04	2.2E+04
16200000	2.68E-03	2.07	9.0	1.86	0.79	1.5E+03	1.6E+03
16212800	4.86E-03	2.15	3.5	2.39	0.92	3.1E+03	3.5E+03
16213000	1.96E-02	1.81	18.8	2.05	0.53	1.7E+04	2.1E+04
16226200	1.33E-01	1.57	1.2	2.71	0.96	1.9E+03	2.0E+03
16240500	2.49E-03	2.94	4.2	1.26	0.42	1.4E+03	8.6E+02
16244000	1.33E-02	2.59	0.7	2.32	0.64	1.3E+03	1.3E+03
16272200	2.14E-02	1.71	7.3	1.57	0.34	7.6E+02	8.6E+02
16275000	1.38E-02	2.60	1.0	2.24	0.39	3.2E+03	2.4E+03
16809600	3.32E-02	2.18	1.8	2.22	0.78	3.3E+03	3.5E+03
16854500	2.27E-03	2.28	16.5	1.67	0.47	8.3E+03	8.1E+03
50025155	1.70E-03	2.12	12.7	2.20	0.45	1.1E+04	8.5E+03
50028000	2.39E-03	2.36	45.3	1.26	0.36	3.8E+04	3.6E+04
50031200	4.30E-03	2.05	39.1	2.22	0.45	1.4E+05	1.5E+05
50034000	8.07E-04	2.51	4.1	3.35	0.55	1.6E+06	8.6E+05
50035000	2.15E-04	2.27	97.2	2.26	0.48	3.4E+05	3.4E+05
50043800	2.96E-03	1.90	30.5	3.06	0.77	2.8E+05	3.3E+05
50045010	3.74E-02	1.44	5.6	4.29	0.97	1.4E+05	1.5E+05
50048770	4.82E-02	2.15	10.7	1.98	0.77	8.8E+04	9.2E+04
50050900	5.79E-04	2.63	11.1	2.39	0.72	2.2E+05	1.3E+05
50051180	3.79E-02	1.94	1.0	3.08	0.86	9.4E+03	9.0E+03

Table D.1 – continued from previous page

Station ID	$\bar{a}$	$\bar{b}$	$\hat{a}$	$\hat{b}$	RB	Sediment yield (tons/yr)	
						FDSRC	Parametric
50051310	1.54E-03	2.31	18.4	2.21	0.57	6.8E+04	6.0E+04
50051800	9.45E-03	1.86	62.7	1.84	0.49	6.5E+04	7.1E+04
50053025	2.10E-03	2.40	13.7	1.84	0.54	2.3E+04	1.7E+04
50055000	5.60E-03	1.88	91.1	2.22	0.59	2.4E+05	2.8E+05
50055225	3.03E-02	1.76	8.4	2.74	0.72	3.5E+04	3.7E+04
50055750	3.50E-02	1.69	13.5	2.43	0.78	2.2E+04	2.6E+04
50056400	1.40E-02	1.94	9.8	2.85	0.82	1.1E+05	1.2E+05
50057000	9.05E-03	1.79	26.6	2.85	0.76	1.2E+05	1.5E+05
50058350	3.54E-02	2.04	7.0	2.09	0.65	2.2E+04	2.2E+04
50059050	3.30E-02	1.48	28.3	3.50	1.17	2.3E+05	2.5E+05
50061800	1.70E-02	1.78	9.3	2.41	0.63	9.7E+03	1.1E+04
50065500	2.59E-04	2.31	43.0	1.49	0.58	5.9E+03	5.3E+03
50071000	7.76E-03	1.84	33.7	1.99	0.72	2.0E+04	2.4E+04
50075000	3.74E-03	2.46	12.1	1.36	0.60	6.3E+03	5.3E+03
50110900	2.43E-02	2.01	5.3	2.45	0.53	2.5E+04	2.5E+04
50115000	2.75E-02	2.13	7.5	2.22	0.53	5.6E+04	5.2E+04
50136400	2.04E-03	2.31	43.8	1.33	0.33	4.7E+04	2.8E+04
54310157	1.15E-01	1.36	1.8	1.89	0.64	2.7E+02	3.0E+02

Appendix E

Arikaree River at Haigler, Nebraska

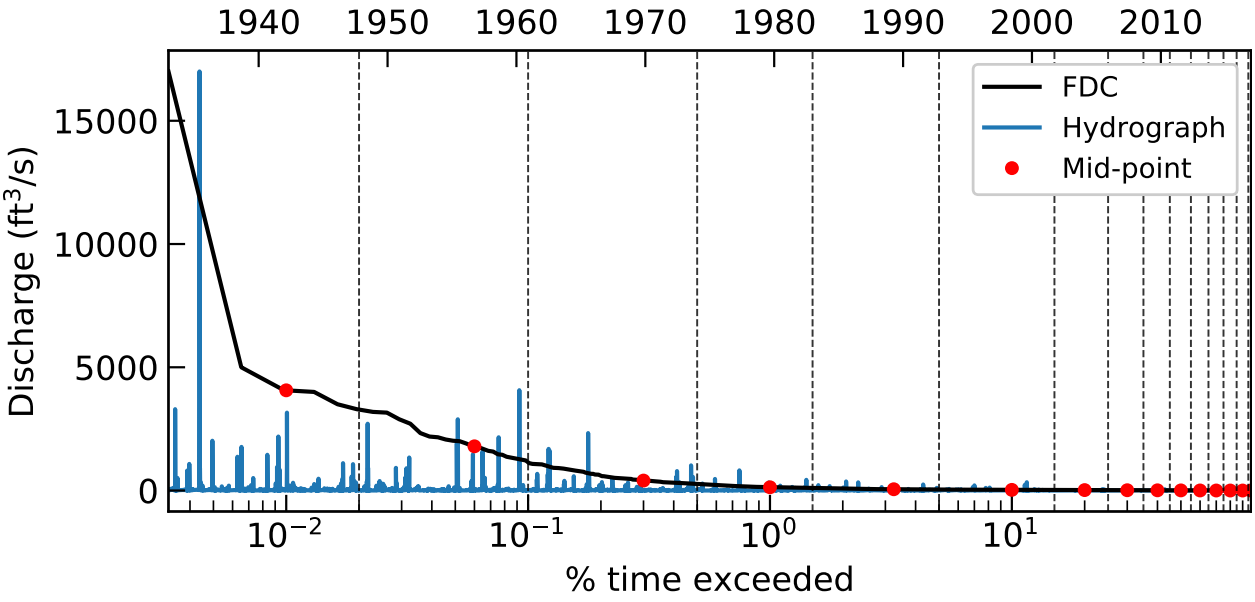

Figure E.1: Hydrograph and the flow duration curve of the Arikaree River at Haigler in Nebraska (USGS 06821500)

Figure E.1 presents a example where the difference of sediment discharge by the flow-duration sediment-rating-curve (FDSRC) method and the parametric method is 82%. The FDSRC method gives the mean annual sediment discharge to be 39,000 tons/year but the parametric method computes to be 71,000 tons/year. The cause of difference is because the FDSRC takes the median value as the represented discharge of each bin (red dots). The extreme event is therefore not included in the calculation.